

# Seismic Response Control of Structures Using a Novel Adaptive Passive Negative Stiffness Device

by  
**Dharma Theja R. Pasala, Apostolos A. Sarlis,  
Satish Nagarajaiah, Andrei M. Reinhorn,  
Michael C. Constantinou and Douglas P. Taylor**

**Technical Report MCEER-13-0004**

**June 10, 2013**

## NOTICE

This report was prepared by Rice University and the University at Buffalo, State University of New York as a result of research supported primarily by the George E. Brown, Jr. Network for Earthquake Engineering Simulation (NEES) Program of the National Science Foundation, NEESR award number CMMI-0830391. Neither MCEER, associates of MCEER, its sponsors, Rice University, the University at Buffalo, State University of New York, nor any person acting on their behalf:

- a. makes any warranty, express or implied, with respect to the use of any information, apparatus, method, or process disclosed in this report or that such use may not infringe upon privately owned rights; or
- b. assumes any liabilities of whatsoever kind with respect to the use of, or the damage resulting from the use of, any information, apparatus, method, or process disclosed in this report.

Any opinions, findings, and conclusions or recommendations expressed in this publication are those of the author(s) and do not necessarily reflect the views of MCEER, the National Science Foundation, or other sponsors.

---

## Seismic Response Control of Structures Using a Novel Adaptive Passive Negative Stiffness Device

by

Dharma-Theja R. Pasala,<sup>1</sup> Apostolos A. Sarlis,<sup>2</sup> Satish Nagarajaiah,<sup>3</sup>  
Andrei M. Reinhorn,<sup>4</sup> Michael C. Constantinou<sup>5</sup> and Douglas P. Taylor<sup>6</sup>

Publication Date: June 10, 2013

Submittal Date: December 19, 2012

Technical Report MCEER-13-0004

NSF Grant Number CMMI-NEESR-0830391

- 1 Senior Riser Engineer, Intecsea; former Graduate Student, Department of Civil and Environmental Engineering, Rice University
- 2 Ph.D. Candidate, Department of Civil, Structural and Environmental Engineering, University of Buffalo, State University of New York
- 3 Professor, Department of Civil and Environmental Engineering & Mechanical Engineering and Material Science, Rice University
- 4 Clifford C. Furnas Professor, Department of Civil, Structural and Environmental Engineering, University at Buffalo, State University of New York
- 5 Professor, Department of Civil, Structural and Environmental Engineering, University at Buffalo, State University of New York
- 6 President, Taylor Devices, Inc.

MCEER  
University at Buffalo, State University of New York  
133A Ketter Hall, Buffalo, NY 14260  
Phone: (716) 645-3391; Fax (716) 645-3399  
E-mail: [mceer@buffalo.edu](mailto:mceer@buffalo.edu); Website: <http://mceer.buffalo.edu>

---



# Project Overview

## Development of Next Generation Adaptive Seismic Protection Systems

Design of conventional structures specified by the codes is based on the philosophy that the structure should withstand seismic loads while sustaining an acceptable level of damage. Structures are designed to prevent collapse but their serviceability and functionality in the aftermath of strong earthquake ground motion are not taken into consideration. This is achieved by designing structures to be ductile and letting them yield when subjected to strong earthquake ground motions. Yielding leads to stiffness and strength degradation, increased interstory drifts, and damage with permanent drifts, which render the structure non-functional.

Alternatively, the yielding can be emulated in a structural system by adding an adaptive “negative stiffness device” (NSD) and shifting the yielding away from the main structural system, leading to the new idea of “apparent weakening” that occurs to ensure structural stability at all displacement amplitudes. This is achieved through an adaptive negative stiffness system, a combination of NSD and a fluid damper. By engaging the NSD at an appropriate displacement (apparent yield displacement that is well below the actual yield displacement of the primary structural system), the composite structure-device assembly behaves like a yielding structure (while the primary structure remains mostly elastic). The concept and the NSD have been developed by the project team. The feasibility of this new concept has been experimentally verified at the University at Buffalo-NEES facility on different structures.

Structural weakening and the addition of damping is an approach previously proposed to reduce seismic forces and drifts in the retrofit of structures. It is also used in the design of new buildings with damping systems. While this approach is efficient, it does not significantly reduce and may even amplify inelastic excursions and permanent deformations of the structural system during a seismic event. A novel negative stiffness device (NSD) is developed in this project that can emulate weakening of the structural system without inelastic excursions and permanent deformations. The NSD produces yielding by engaging at a prescribed displacement and generating negative stiffness, thus reducing the stiffness of the combined primary structure and NSD system, and leading to a bilinear inelastic system.

The new transformative ideas of “Negative Stiffness Device” and “apparent weakening” have been demonstrated in this project by means of experimental and analytical study. The new concept results in significant damage and response reduction. The system can be used in new buildings as well as for retrofit situations. NSD is the first practical negative stiffness device implementable in large structures; such a device did not exist prior to this project. The NSD is adaptive but passive, and exhibits true negative stiffness behavior by possessing predesigned variations of stiffness as a function of structural displacement amplitude. The NSD properties can be easily adapted by changing the lever arm to ac-

commodate any change in the properties of the structure observed over time. It is likely to impact the state of practice of supplemental devices in earthquake protection. Extensive analytical modeling has also been developed and validated using the shake table test results. The nonlinear analytical models have been incorporated into 3D-BASIS, IDARC and Opensees computer programs, thus enabling technology transfer.

The concept of negative stiffness and apparent yielding/weakening has been experimentally verified in a three-story base-isolated structure and base isolated bridge with the NSD at the isolation level and also in a three-story fixed-base steel structure (moment frame) with the NSD in the first story. To accentuate the advantages of incorporating the NSD in structures, the responses of different systems including (1) base structure; (2) base structure with damper; (3) base structure with NSD; and (4) base structure with NSD and damper; are compared for a suite of ground motions. The behavior of all four systems are predicted analytically and the predicted results are in excellent agreement with the experiments. Shake table tests confirmed that by adding the NSD and damper, acceleration, base shear and deformations of the structure can be significantly reduced. In bilinear inelastic structures, the addition of the NSD and damper will prevent collapse as well as reduce its response during severe earthquakes.

*The primary focus of this research is to analyze and experimentally verify the response reduction attributes of an NSD in (a) elastic structural systems, (b) yielding systems, and (3) multistory structures. The results presented in this report demonstrate that by placing an NSD in a particular story, the superstructure above that story can be isolated from the effects of ground motion. Since the NSDs in the bottom floors will undergo large deformations, a generalized scheme to incorporate NSDs with different force deformation behavior in each story is proposed.*

## **Project Management Committee**

Satish Nagarajaiah, Principal Investigator, Rice University, Department of Civil and Environmental Engineering and Mechanical Engineering and Material Science, Houston, TX 77005; *Satish.Nagarajaiah@rice.edu*.

Andrei M. Reinhorn, Co-Principal Investigator, Department of Civil and Environmental Engineering, University at Buffalo, State University of New York, Buffalo, NY 14260; *reinhorn@buffalo.edu*.

Michael C. Constantinou, Co-Principal Investigator, Department of Civil and Environmental Engineering, University at Buffalo, State University of New York, Buffalo, NY 14260; *constan1@buffalo.edu*.

Michael Symans, Co-Principal Investigator, Department of Civil and Environmental Engineering, Rensselaer Polytechnic Institute, Troy, NY 12180; *symans@rpi.edu*.

Jian Zhang, Co-Principal Investigator, Department of Civil and Environmental Engineering, University of California, Los Angeles, CA 90095; *zhangj@ucla.edu*.

Douglas P. Taylor, Co-Principal Investigator, Taylor Devices Inc., North Tonawanda, NY 14120; *taylordevi@aol.com*.

# Abstract

Current seismic design practice promotes inelastic response in order to reduce the design forces. By allowing the structure to yield while increasing its ductility, the global forces can be kept within the limited bounds dictated by the yield strength. However, during severe earthquakes, the structures undergo significant inelastic deformations leading to stiffness and strength degradation, increased interstory drifts, and damage with residual drift. The research presented in this report seeks to address these challenges.

To prevent the inelastic effects observed in yielding systems, a new concept of “apparent weakening” is proposed and verified through shake table studies in this project. “Apparent weakening” is introduced in the structural system using a complementary “adaptive negative stiffness device” (NSD) that mimics “yielding” of the global system thus attracting it away from the main structural system. Unlike the concept of weakening and damping, where the main structural system strength is reduced, the new system does not alter the original structural system, but instead produces effects compatible with an early yielding. Response reduction using NSD is achieved in a two step sequence. First the NSD, which is capable of exhibiting nonlinear elastic stiffness, is developed based on the properties of the structure. This NSD is added to the structure resulting in reduction of the stiffness of the structure and NSD assembly or “apparent weakening” - thereby resulting in the reduction of the base shear of the assembly. Then a passive damper, designed for the assembly to reduce the displacements that are caused due to the “apparent weakening”, is added to the structure - thereby reducing the base shear, acceleration and displacement in a two step process.

The primary focus of this report is to analyze and experimentally verify the response reduction attributes of the NSD in (a) elastic structural systems (b) yielding systems and (3) multistory structures. Experimental studies on 1:3 scale three-story frame structure have confirmed that consistent reductions in displacements, accelerations and base shear can be achieved in an elastic structure and bilinear inelastic structure by adding the NSD and viscous fluid damper. It has also been demonstrated that the stiffening in the NSD will prevent the structure from collapsing. Analogous to the inelastic design, the acceleration and base shear and deformation of the structure and NSD assembly can be reduced by more than 20% for moderate ground motions and the collapse of the structure can be prevented for severe ground motions.

Simulation studies have been carried out on an inelastic multistory shear building to demonstrate the effectiveness of placing NSDs and dampers at multiple locations along the height of the building; referred to as “distributed isolation”. The results reported in this study have demonstrated that by placing a NSD in a particular story, the superstructure above that story can be isolated from the effects of ground motion. Since the NSDs in the bottom floors will undergo large deformations, a generalized scheme to incorporate NSDs with different force deformation behavior in each story is proposed. The properties of the NSD

are varied to minimize the localized inter-story deformation and distribute it evenly along the height of the building.

# Acknowledgements

This research is supported by National Science Foundation, grant number NSF-CMMI-0830391, and by Taylor Devices, Inc. of North Tonawanda, NY. This support is gratefully acknowledged.

The authors would like to thank the Structural Engineering and Earthquake Simulation Laboratory (SEESL) staff at the University at Buffalo for their assistance during the experimental testing of the three story frame structure, and Mr. John Metzger of Taylor Devices, Inc. for detailing the NSD.



# TABLE OF CONTENTS

Section	Title	Page
1	<b>Introduction .....</b>	1
1.1	Adaptive Systems .....	2
1.2	Importance of Negative Stiffness Device: Alternate Explanation .....	4
1.3	Weakening and Damping of Structural Systems .....	5
1.4	Adaptive Negative Stiffness System .....	6
1.4.1	Working Principle .....	6
1.4.2	Challenges in Inelastic Structures .....	7
1.5	Simulation Studies .....	9
1.5.1	Periodic Ground Motion .....	11
1.6	Summary .....	21
2	<b>Negative Stiffness Device .....</b>	23
2.1	NSD Description .....	24
2.2	Analytical Model .....	24
2.2.1	Gap spring Assembly .....	28
2.2.2	Significance of Dual Amplification .....	30
2.3	Experimental Study .....	34
2.3.1	Experimental Setup .....	34
2.3.2	Experimental Results .....	37
2.3.3	Analytical Results .....	41
2.4	Summary .....	42
3	<b>Experimental Setup and Component Testing .....</b>	45
3.1	Three-story Frame Structure (3SFS) .....	46
3.1.1	Moment Resisting System .....	47
3.1.2	Vertical Support System .....	49
3.1.3	Floor System. ....	52
3.2	NSD and Damper Installation in 3SFS .....	53
3.2.1	Negative Stiffness Device .....	53
3.2.2	Viscous Damper .....	58
3.3	Instrumentation .....	59
3.4	Experimental Results .....	61
3.4.1	3SFS Analytical Model .....	65
3.5	Summary .....	68
4	<b>Apparent-Weakening in SDOF Structures: Experimental Study .....</b>	71
4.1	Elastic Structures .....	72
4.1.1	3SFS and NSD Assembly .....	73
4.1.2	3SFS, NSD and Damper Assembly .....	74
4.1.3	Comparative Study .....	76
4.2	Yielding Structures .....	81
4.2.1	Mild-Yielding Structures .....	86
4.2.2	Heavy-yielding Structures .....	87

# TABLE OF CONTENTS

Section	Title	Page
4.3	Summary .....	95
<b>5</b>	<b>Apparent-Weakening in MDOF Structures .....</b>	<b>99</b>
5.1	Unbraced 3SFS Response to Moderate Ground Motion .....	100
5.2	Unbraced 3SFS Response to Severe Ground Motion .....	104
5.3	Analytical Modeling of Nine-story Frame .....	109
5.4	Vertically Distributed Isolation .....	119
5.5	Summary .....	130
<b>6</b>	<b>Conclusions .....</b>	<b>137</b>
6.1	“Apparent Weakening” in Elastic SDOF Structure .....	137
6.2	“Apparent Weakening” in Yielding SDOF Structure .....	138
6.3	Distributed Isolation in MDOF Structure using NSD .....	138
<b>7</b>	<b>References .....</b>	<b>141</b>
 <b>Appendices (provided on CD)</b>		
A	Dynamic Equation of Motion for the NSD.....	173
A.1	Derivations. ....	173
A.2	Numerical Simulations .....	179
B	Component Drawings of 3SFS .....	185
C	Experimental Data .....	195

# LIST OF FIGURES

Figure	Title	Page
1.1	Schematic diagram showing the components in AS and NS .....	6
1.2	Schematic force-deformation plots of (a) components (b) components and assembly of NS (c) components and assembly of AS .....	7
1.3	Working principle of adaptive system (a) schematic representation of components (b) component F-D plots (c) assembly behavior.....	8
1.4	Different feasible force-displacements of structure-device assembly for yielding systems (a) no constraints on the force exerted by NSD (b) keeping the force exerted by NSD constant beyond $u_y$ (c) stiffening the NSD beyond $u_y$ .....	9
1.5	Instability in nonlinear systems with added negative stiffness. (a) Schematic representation (b) component F-D plots (c) assembly behavior .....	9
1.6	Force deformation behavior of structure, NSD and assembly .....	11
1.7	Response of AS and BS for periodic input in elastic structure .....	12
1.8	F-D behavior of columns and dampers in elastic structure .....	13
1.9	F-D behavior of the (a) components of AS and (b) assembly forces.....	13
1.10	Response of AS and BS for periodic input in yielding structure .....	14
1.11	F-D behavior of columns and dampers in yielding structure .....	15
1.12	F-D behavior of the components of PS and AS .....	15
1.13	Comparison of the assembly F-D behavior in yielding structures .....	16
1.14	Response of AS and BS for Kobe ground motion .....	18
1.15	F-D behavior of columns and dampers for Kobe ground motion .....	18
1.16	F-D behavior of the components of PS and AS for Kobe ground motion .....	19
1.17	Comparison of the assembly F-D behavior for Kobe ground motion .....	19
1.18	Comparison of response spectra for C <sub>1</sub> type cycloidal pulse .....	20
1.19	Comparison of response spectra for Sylmar ground motion .....	21
2.1	Schematic diagram and photograph of NSD .....	25
2.2	Fabrication drawings of GSA showing the coil-springs .....	26
2.3	Undeformed shape, deformed shape and free body diagrams of components in NSD	28
2.4	Schematic of the equivalent system of GSA .....	29
2.5	Schematic diagram of the force displacement plots of NSD.....	31
2.6	The behavior of NSD with the change in $K_{sc}$ value .....	31
2.7	The behavior of NSD with the change in $P_{in}$ value .....	32
2.8	Schematic diagram of the NSD-3. .....	33
2.9	Comparing the F-D behavior of NSDs with different configuration .....	35
2.10	Schematic diagram and the photograph of NSD test setup.....	36
2.11	NSD connection with the top frame using end-angle assembly and the miniature ball transfer plates used to transfer the NSD load to top of frame .....	37
2.12	Force-deformation behavior of the test-rig .....	38
2.13	Observed experimental F-D behavior of NSD-West .....	39
2.14	Comparison of the displacements of various points on NSD-West .....	40
2.15	Observed experimental F-D behavior of NSD-East .....	40
2.16	Comparison of the displacements of various points of NSD-East .....	41
2.17	Comparison of the experimental and analytical F-D behavior of NSD-West .....	42

## LIST OF FIGURES (CONT'D)

Figure	Title	Page
2.18	Comparison of the experimental and analytical F-D behavior of NSD-East .....	43
3.1	3SFS installed on the shake table at NEES equipment site, University at Buffalo, SUNY .....	47
3.2	Schematic diagram showing the components in 3SFS .....	48
3.3	Photograph and schematic diagram of 3SFS (Elevation) .....	50
3.4	Photograph and schematic diagram of 3SFS (Isometric view) .....	51
3.5	Beam-column block showing the connections .....	52
3.6	Photograph of gravity frames in the second floor of 3SFS .....	53
3.7	Predicted behavior of 3SFS and NSD assembly w/ and w/o GSA-2 .....	54
3.8	GSA-2 connected to the CB2 of NSD .....	54
3.9	Photograph and schematic diagram of 3SFS (Elevation) .....	56
3.10	Observed experimental force-deformation behavior of NSD-East .....	57
3.11	End angle assembly to connect the NSDs to floor slab .....	58
3.12	Experimental and predicted behavior of NSD-West .....	58
3.13	Experimental and predicted behavior of NSD-East .....	59
3.14	Experimental and predicted behavior of viscous damper .....	60
3.15	Force deformation loops of the load-cells and accelerometers [BS] .....	63
3.16	Force deformation loops of the load-cells and accelerometers [AS] .....	63
3.17	Torsion and rocking in the test structure [BS] .....	64
3.18	Torsion and rocking in the test structure [AS] .....	65
3.19	F-D behavior of 3SFS with braces in second and third floor .....	67
3.20	Displacement and acceleration of the first floor of braced-3SFS .....	68
3.21	F-D behavior of all the floors in 3SFS .....	69
3.22	Displacement and acceleration of the first floor of 3SFS .....	69
3.23	Displacement and acceleration of the roof of 3SFS .....	70
4.1	Schematic diagram depicting “apparent-weakening” in elastic systems .....	73
4.2	F-D behavior of 3SFS and assembly in NS (Kobe GM; PGA=0.29g) .....	74
4.3	F-D behavior of NSDs in NS (Kobe GM; PGA=0.29g) .....	74
4.4	First-floor response and base shear of NS (Kobe GM; PGA=0.29g) .....	75
4.5	F-D behavior of NS with components (Kobe GM; PGA=0.29g) .....	75
4.6	F-D behavior of 3SFS and damper in AS (Kobe GM; PGA=0.29g) .....	76
4.7	F-D behavior of NSDs in AS (Kobe GM; PGA=0.29g) .....	77
4.8	F-D behavior of AS with components in elastic structure (Kobe GM; PGA=0.29g) ....	77
4.9	First-floor displacement, acceleration and base shear of AS in elastic structure (Kobe GM; PGA=0.29g) .....	78
4.10	Comparison of F-D behavior of AS (Kobe GM; PGA=0.29g) .....	79
4.11	F-D behavior of BS, PS, NS and AS with components in elastic structure (Kobe GM; PGA=0.29g) .....	81
4.12	Comparison of assembly force in SDOF elastic structure (Kobe GM; PGA=0.29g) ....	82
4.13	Comparison of first-floor displacement, acceleration and base-shear in elastic structure (Kobe GM; PGA=0.29g) .....	83

## LIST OF FIGURES (CONT'D)

Figure	Title	Page
4.14	Summary of peak responses in elastic systems .....	84
4.15	Schematic diagram depicting “apparent-weakening” in yielding systems .....	85
4.16	Recoverable drift and residual drift in NSD and bilinear inelastic structure assembly ....	86
4.17	F-D behavior of 3SFS and assembly in NS (Pacoima GM; PGA=0.57g) .....	87
4.18	F-D behavior of NSDs in NS (Pacoima GM; PGA=0.57g). ....	88
4.19	F-D behavior of NS with components in mild-yielding structure (Pacoima GM; PGA=0.57g) .....	88
4.20	First-floor response and base shear of NS in mild-yielding structure (Pacoima GM; PGA=0.57g) .....	89
4.21	Trace of F-D behavior of NS with components in mild-yielding structure (Pacoima GM; PGA=0.57g) .....	89
4.22	F-D behavior of 3SFS and assembly in NS (Pacoima GM; PGA=0.81g). ....	90
4.23	F-D behavior of NSDs in NS (Pacoima GM; PGA=0.81g) .....	91
4.24	F-D behavior of NS with components in heavy-yielding structure (Pacoima GM; PGA=0.81g) .....	91
4.25	First-floor response and base shear of NS in heavy-yielding structure (Pacoima GM; PGA=0.81g) . ....	92
4.26	Trace of F-D behavior of NS with components in heavy-yielding structure (Pacoima GM; PGA=0.81g) .....	92
4.27	F-D behavior of BS, PS, NS and AS with components (Kobe GM; PGA=0.65g) .....	93
4.28	Comparison of first-floor displacement, acceleration and base-shear (Kobe GM; PGA=0.65g) .....	94
4.29	Comparison of assembly forces in SDOF structure (Kobe GM; PGA=0.65g). ....	95
4.30	Summary of peak responses in yielding systems .....	97
5.1	Schematic diagram and picture of unbraced 3SFS .....	101
5.2	F-D behavior of individual floor in AS for Pacoima ground motion (PGA= 0.62g) ....	101
5.3	F-D behavior of NSD-East, NSD-West and damper in AS for Pacoima ground motion (PGA= 0.62g) .....	102
5.4	First floor response and base shear of AS (Pacoima GM; PGA=0.62g) .....	102
5.5	Comparison of F-D behavior of AS with components (Pacoima GM; PGA=0.62g) ...	103
5.6	F-D behavior of all the floors in AS, BS, PS and AS with components (Pacoima GM; PGA=0.62g) .....	104
5.7	Comparison of F-D behavior of all the systems in first-floor (Pacoima GM; PGA=0.62g) .....	105
5.8	Comparison of the time-history of first floor response in all systems (Pacoima GM; PGA=0.62g) .....	106
5.9	Comparison of response profile of all the systems in unbraced 3SFS (Pacoima GM; PGA=0.62g) .....	107
5.10	F-D behavior of individual floor in NS for Pacoima ground motion (PGA=0.78g) ....	108
5.11	F-D behavior of NSD-East and NSD-West in NS for Pacoima ground motion (PGA=0.78g) .....	108
5.12	First floor response and base shear of NS (Pacoima GM; PGA=0.78g) .....	109

## LIST OF FIGURES (CONT'D)

Figure	Title	Page
5.13	Comparison of F-D behavior of NS with components (Pacoima GM; PGA=0.78g) .....	110
5.14	F-D behavior of all the floors in AS, BS, PS and AS with components (Pacoima GM; PGA=0.78g) .....	111
5.15	Comparison of F-D behavior of all the systems in first-floor (Pacoima GM; PGA=0.78g) .....	112
5.16	Comparison of the time-history of first floor response in all systems (Pacoima GM; PGA=0.78g) .....	113
5.17	F-D behavior of all the systems and components shown separately (Pacoima GM; PGA=0.78g) .....	114
5.18	Comparison of response profile of all the systems in unbraced 3SFS (Pacoima GM; PGA=0.78g) .....	115
5.19	Bar graphs summarizing the shake-table results of unbraced 3SFS .....	116
5.20	Schematic diagram of multi-story building with NSDs in every floor .....	117
5.21	F-D plots depicting the strength reduction factor in single story .....	118
5.22	Schematic F-D plots depicting the strength reduction factor .....	118
5.23	Comparison of the maximum response profile of the structure for periodic input.....	120
5.24	Comparison roof acceleration and base shear experienced by the BS, PS-3 and AS-3 for periodic input.....	121
5.25	F-D behavior of third-floor for periodic input .....	122
5.26	Comparison of the maximum response profile of the structure for periodic input.....	123
5.27	Comparison of roof acceleration and base shear experienced by the BS, PS and AS for periodic input .....	124
5.28	F-D behavior of first-floor for periodic input .....	125
5.29	Comparison of the maximum response profile of the structure for Kobe-NS ground motion [PGA=0.84g] .....	127
5.30	F-D behavior of the 1 <sup>st</sup> floor in BS, PS and AS-optimal for Kobe-NS ground motion [PGA=0.84g] .....	128
5.31	Comparison of roof acceleration and base shear experienced by the BS, PS and AS-optimal for Kobe-NS ground motion [PGA=0.84g] .....	130
5.32	Comparison of the story drift profiles of BS, PS and AS .....	131
5.33	Comparison of the story acceleration profiles of BS, PS and AS .....	132
5.34	Comparison of the inter-story deformation profiles of BS, PS and AS .....	133
5.35	Bar graphs summarizing the normalized response of BS, PS and AS for six ground motions .....	134

## LIST OF TABLES

Table	Title	Page
1.1	Performance indices used to evaluate different systems .....	17
1.2	Summary of simulation results for recorded ground motions .....	17
1.3	Summary of response spectra for cycloidal pulses .....	22
2.1	Summary of the values used for different configurations of NSDs .....	34
2.2	Values of the parameters used in NSDs. ....	43
3.1	List of all the sensors used for data acquisition .....	62
3.2	Summarized list of torsion and differential response for BS and AS .....	66
4.1	Summary of the peak responses from the shake table tests on braced structure [elastic tests] .....	80
4.2	Summary of the peak responses from the shake table tests on braced structure [yielding tests] .....	96
5.1	Summary of the peak responses from the shake table tests on unbraced structure [elastic tests].....	117
5.2	Optimized apparent yield displacements (normalized) in each story for all ground motions .....	126
5.3	Summary of the peak responses from the shake table tests on unbraced structure [yielding tests].....	129



# Chapter 1

## Introduction

Experience from the past demonstrated that the earthquakes have a tremendous socioeconomic impact, a huge loss of life and property damage on the endured communities. The recent, Haiti earthquake that occurred on January 12, 2010 resulted in an estimated death toll of 316,000 and property damage of about 14 billion dollars (USGS). In the 21st century, the worldwide death toll due to earthquakes is over 815,000 and the property damage is about 150 billion dollars (USGS). The damage due to the earthquake disasters cannot be completely avoided but the effects can be significantly subdued by exercising the proper design practices. The field of earthquake engineering has stemmed to tackle the issues involved in seismic resistant structural design. The objective of earthquake engineering is to design, construct and maintain structures to perform during earthquakes.

Designing structures to withstand seismic loads has been well-explored in the structural design community since the 1920s (NEES). Based on the experiences from past earthquakes, shake-table tests and analytical studies several specification and guidelines have been incorporated in the design codes. The philosophy of earthquake design for structures, as used in the design codes, is to minimize the structural damage for moderate ground motions and to avoid collapse or serious damage in strong ground motions. In other words, the building should survive a rare, very severe earthquake by sustaining significant damage without collapsing and it should remain safe and serviceable for more frequent, but less severe earthquakes. This is achieved by inelastic design of structures.

Conventional structures designed for loads specified by codes undergo significant inelastic deformations during severe earthquakes, leading to stiffness and strength degradation, increased interstory drifts, and damage with residual drift. These yielding structures however keep the global forces within limited bounds dictated by the yield strength (Reinhorn et al., 2002). Passive seismic protection systems in the form of supplemental damping devices have been used in many civil engineering infrastructure to mitigate wind and seismic loads (Constantinou and Symans, 1993; Spencer and Nagarajaiah, 2003; Viti et al., 2006; Cimellaro et al., 2009). This approach has emerged as an efficient way to reduce response and limit damage by shifting the inelastic energy dissipation from the framing system to the dampers. Examples of

few such passive systems are base isolation systems (Nagarajaiah et al., 1991), fluid dampers (Constantinou and Symans, 1993), tuned mass dampers (Nagarajaiah, 2009), friction dampers (Fenz and Constantinou, 2007).

Active-control of structures, wherein the excessive structural response can be attenuated using actuators, can also be used to reduce inelastic behavior. The force exerted by the actuator is calculated in real-time using a control algorithm and feedback from sensors. Measured feedback signal could be the excitation and/or response of structure. Although this approach is more efficient than passive-control, high power requirement and continuous measurement of feedback signal limit its applications. Semiactive control strategies combine the best features of both passive and active control systems. Semiactive control devices offer the adaptability of active control devices without requiring the associated large power sources (Spencer and Nagarajaiah, 2003). Thus, semiactive systems have received considerable attention in the recent past. Semiactive systems operate on battery power, which is critical during seismic events when the main power source to the structure may fail. Even in semi-active control local feedback is unavoidable.

Despite the progress in advancing the field of structural control for the past five decades there is still a need to develop new devices to overcome the limitations of the existing approaches. The research carried in this study attempts to bridge this gap.

## 1.1 Adaptive Systems

In this study, a new concept - “apparent weakening”, an adaptive structural system - “Adaptive Negative Stiffness System” (AS) and a novel “Negative Stiffness Device” (NSD) are proposed and developed in detail. Adaptive systems belong to the category of passive seismic protection systems but they are more sophisticated than the regular passive systems. An adaptive system consists of adaptive stiffness and/or damping devices which are capable of changing the stiffness and/or damping of the device depending on the displacement amplitude (Fenz and Constantinou, 2008; Nagarajaiah, 2009). These devices are designed to exhibit a force-displacement behavior which upon the addition of structure properties will result in an adaptive system having superior characteristics compared to the original structure.

Recently, Iemura and Pradono (Iemura and Pradono, 2009) proposed pseudo-negative-stiffness dampers (PNSD) that are hydraulic or semiactive or active devices capable of producing negative-stiffness hysteretic loops. It has been shown in their investigations that by adding negative-stiffness hysteretic loops, the total force would be lowered significantly. Common passive dampers that act in parallel with the stiffness of structure add to the total force rendering the shear force larger than that due to stiffness of the base-structure alone. It must be noted that the passive hydraulic dampers cannot “push” the structure in the same direction as the structural displacement; the adaptive NSD proposed in this study can. A hydraulic device that is fully active or semiactive as in the case of PNSD can generate a pseudo-negative stiffness in which case feedback control would be needed to generate the negative stiffness. The passive negative stiffness friction damper-a convex frictional interface or bearing, opposite of the well known frictional

pendulum base isolation bearing, that is essentially an unstable friction bearing—proposed by Imeura and Pradono (Imura and Pradono, 2009) can generate the pseudo negative stiffness. The pseudo negative stiffness is by virtue of the fact that horizontal force at the convex frictional bearing assists the motion in either direction; however, this type of a system is primarily applicable to base isolated structures, wherein such frictional bearings are used. An additional complication of the pseudo negative stiffness friction bearing is that the structure to which it is attached has to accommodate significant vertical motion in addition to the horizontal displacement.

Soong (Soong, 1998) proposed an active control approach to experimentally simulate yielding structure. An active control algorithm has been proposed to reduce the stiffness of structure in real time without any damage to the structure. Different types of active control methods and possible configurations of the actuator to implement the proposed approach has been suggested. The only objective of Soong's approach is to develop an yielding structure out of an elastic structure without any damage to the structure. Essentially, a closed loop system that behaves like an nonlinear-inelastic system is generated. The NSD proposed in this work is an adaptive device with out any external power supply or feedback signal and the main objective of the device is to reduce the response characteristics of the assembly. Structure and the NSD assembly simulates a nonlinear-elastic system (not a hysteretic system).

In this study, a new passive device is developed, as it does not need any feedback signal or external power supply to generate the desired force. Detailed analytical and experimental study on the NSD is presented in Chapter 2. In brief, The NSD consists of (a) a self contained highly compressed spring in a double negative stiffness magnification mechanism and (b) a “gap spring assembly” (GSA) mechanism which delays the engagement of negative stiffness until the structural system undergoes a prescribed displacement. The NSD employs double chevron braces that self-contain the large vertical forces needed for the development of the horizontal negative stiffness without transferring these forces to the structure.

By adding the NSD, yielding is emulated in a structural system and “yielding” is shifted away from the main structural system-leading to the new idea of “apparent weakening” that occurs ensuring structural stability at all displacement amplitudes. This is achieved through an adaptive negative stiffness system (AS), combination of NSD and a nonlinear damper. By engaging the NSD at an appropriate displacement (simulated yield displacement), which is well below the actual yield displacement of the structural system, a composite structure-device assembly, behaves like a yielding structure (Pasala et al., April, 2012b). The NSD has a re-centering mechanism thereby avoiding permanent deformation in the composite structure-device assembly unless the main structure itself yields. Essentially, a yielding-structure is “mimicked” without any, or with minimal permanent deformation or yielding in the main structure. In summary, the main structural system suffers less accelerations, less displacements and less base shear, while the AS “absorbs” them. This report presents comprehensive details on development and study of the AS/NSD. Through numerical simulations, the effectiveness and the superior performance of the AS/NSD as compared to a structural system with supplemental passive dampers is presented.

Combination of adaptive negative stiffness and damping device can result in reduction in base shear

and displacement response of the structure. However, to date truly negative stiffness systems have received relatively little attention as compared to aforementioned semiactive or pseudo negative stiffness systems and thus represent a significant gap. Hence, development of new true negative stiffness devices is necessary to shift the yielding behavior from the structural system to AS/NSD. AS/NSD can reduce damage in frames by reducing the base shears and deformations and they can also eliminate residual inter-storey drifts. An alternate explanation on the need for negative stiffness in adaptive systems to reduce the acceleration is discussed next. Working principle of AS is explained with schematic diagrams in section-1.4 and simulation studies demonstrating the concept of “apparent-weakening” are presented in section-1.5.

## 1.2 Importance of Negative Stiffness Device: Alternate Explanation

Analytically, active control is the most effective, robust way for reducing the response of structure. But, from practical implementation point of view it suffers with two limitations:

1. large external power to drive the actuator and
2. dependency on the structural-response feedback.

Recently, researchers have developed algorithms to break down the control force, calculated from any active control algorithm, into a combination of passive forces and the remaining marginal amount as an active force—a concept termed as “integrated design of inelastic controlled structural systems” by Reinhorn et al. (Reinhorn et al., 2009) using the concept “weakening” introduced by Reinhorn et al. (Reinhorn et al., 2002), Viti et al. (Viti et al., 2006), and Cimellaro et al. (Cimellaro et al., 2009). Due to the limitations and unreliability of the active control devices during extreme events, the objective was to let the passive components take the maximum amount of force, which are more reliable, leaving very little for the actuators that impart active control force.

Consider a linear multi degree of freedom system with mass  $M$ , stiffness  $K$  and damping  $C$  subjected to a ground motion  $\ddot{x}_g$ . The equation of motion is shown in Eq. 1.1.  $x$  is the relative displacement vector of the structure and  $F_a$  is the desired active control force required to control the structure.  $F_a$  can be calculated easily using standard LQR control algorithms. Active control force can be represented as shown in Eq. 1.2.  $G_2$  and  $G_2$  are constant gain matrices. Using optimization, the gain matrices  $H_1$  and  $H_2$  can be found such that the error between  $F_a$  and  $F_p$  is minimized.  $H_1$  and  $H_2$  are the gain matrices that are directly associated to the additional damping and stiffness forces that need to be add to the structure using passive devices. The remaining force  $F_a - F_p$  is implemented through an active device (Cimellaro et al., 2009).

$$M\ddot{x} + C\dot{x} + Kx = -M\ddot{x}_g + F_a \quad (1.1)$$

$$F_a = G_1x + G_2\dot{x} \quad (1.2)$$

$$F_p = H_1x + H_2\dot{x} \quad (1.3)$$

The control force  $F_p$  is exerted through four passive components, namely: (i) Positive damping device ( $C_1\dot{x}$ ), (ii) Negative damping device ( $C_2\ddot{x}$ ), (iii) Positive stiffness device ( $C_3x$ ) and (iv) Negative stiffness device ( $C_4x$ ).

The constants  $C_1$ ,  $C_2$ ,  $C_3$  and  $C_4$  are representative of properties of the devices. Positive and negative damping force can be implemented using fluid dampers. Positive stiffness can be easily implemented by adding supplemental braces; the only force that is hard to incorporate is the true negative stiffness. In this study a new concept of “apparent softening and weakening” is introduced wherein the “yielding” is shifted to the AS/NSD. A mechanism is proposed to develop the true negative stiffness to simulate global yielding.

### 1.3 Weakening and Damping of Structural Systems

Reinhorn et al. (Reinhorn et al., 2005) and Viti et al. (Viti et al., 2006) introduced the concept of weakening structures (reducing strength), while introducing supplementary viscous damping to reduce simultaneously total accelerations and inter-story drifts. Design methodologies for changing the stiffness of structures and adding damping devices using control theory have been proposed by Gluck et al. (Gluck et al., 1996) to determine the magnitude and the locations of changed structural elements (often requiring softening rather than stiffening) and the added damping, while insuring structural stability. More recently, the design of weakened (reduced strength) structures with supplemental damping was introduced by Reinhorn et al. (Reinhorn et al., 2009), using principles of structural control. In the latter approach, a two-stage design procedure was suggested:

1. first using a nonlinear active control algorithm, to determine the new structural parameters while insuring stability, then
2. determine the properties of equivalent structural parameters of passive system, which can be implemented by removing, or weakening, some structural elements, or connections, reducing the yield capacity of the structure and by addition of energy dissipation systems.

Passive dampers and weakened elements are designed using an optimization algorithm to obtain a response as close as possible to an actively controlled system. The weakening of structures leads to an early yielding of the structural system resulting in damage and permanent deformation. The adaptive negative stiffness system AS/NSD, developed in this study is designed to prevent such damage due to inelastic excursions and permanent deformation, but still exhibit the yielding desirable for reduction of base shear.

## 1.4 Adaptive Negative Stiffness System

### 1.4.1 Working principle

Assume a perfectly-linear single degree of freedom structure with stiffness,  $K_e$ , and no damping, a NSD with stiffness  $K_{NSD}$  and a passive damper with damping coefficient  $C$ . All the three elements are shown in Figure 1.1(a) and the force displacement plots are shown in Figure 1.2(a). By adding NSD to the structure, schematically shown in Figure 1.1(b), the assembly stiffness reduces to  $K_a = K_e - K_{NSD}$  beyond the displacement  $u'_y$  (shown in Figure 1.2(b)). If,  $F_2$  and  $u_2$  are the maximum restoring force and maximum displacement of a perfectly-linear system (green line in Figure 1.2(b)) then for the same load the maximum restoring force and maximum displacement of the assembly are  $F_3$  and  $x_3$  (blue line in Figure 1.2(b)), respectively.  $K_{NSD}$  is designed to achieve the desired reduction in base shear. Force exerted by the NSD is shown as red line in Figure 1.2(b). Although the reduction in base shear is achieved the maximum deformation of adaptive system is substantially increased in the process when compared with an elastic system.

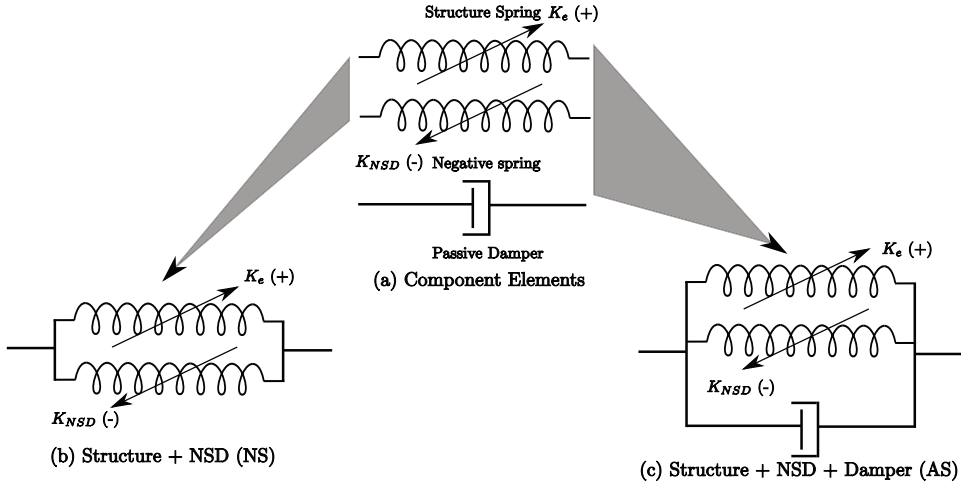


Figure 1.1: Schematic diagram showing the components in AS and NS

Deformation of this assembly can be reduced by adding a passive damping device in parallel to the NSD, schematically shown in Figure 1.1(c). A linear viscous damper is used as a passive damping device. By adding the viscous damper to the structure along with NSD, maximum displacement is reduced resulting in  $x'_3 < x_2$  shown in Figure 1.2(c). Since the assembly of structure and NSD acts like a nonlinear elastic system, viscous damper even with a very small damping coefficient can be effective. It should be noted that by adding a damper to structure and NSD assembly base shear of the assembly is not significantly increased.

At this stage, there is one important constraint that is imposed on the NSD. From Figure 1.1(a,b,c)

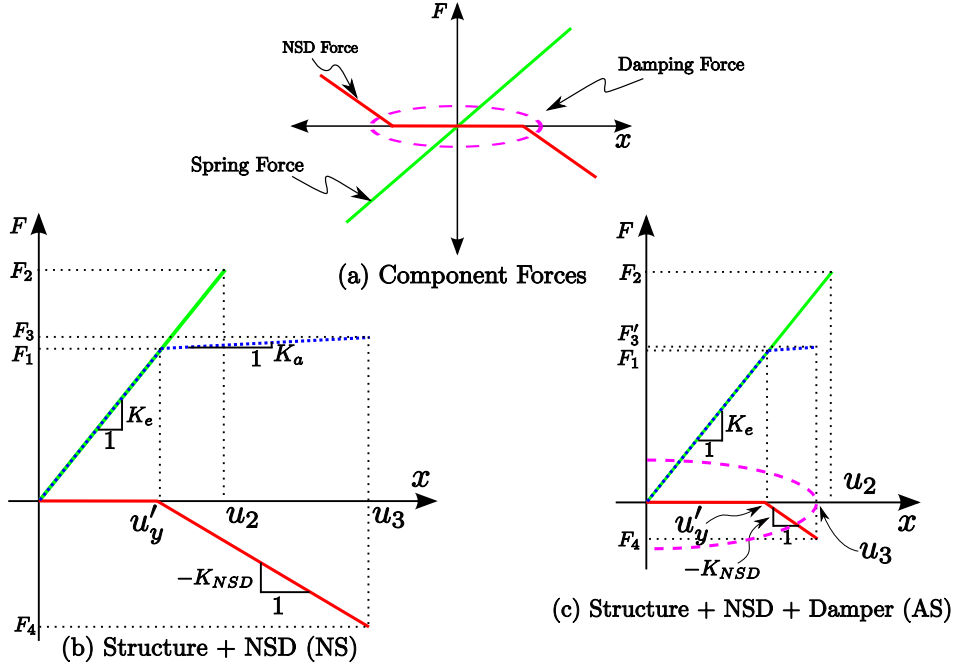


Figure 1.2: Schematic force-deformation plots of (a) components (b) components and assembly of NS (c) components and assembly of AS

it can be seen that there is an offset displacement,  $u'_y$ , called as “apparent yield-displacement”, before the negative stiffness device is engaged. This is to avoid excessive response at relatively small external excitations. For displacements  $u$  such that  $|u| < u'_y$  the structure and NSD assembly behaves like the actual structure. This initial gap is provided by the horizontal spring with elastic-bilinear behavior that has been implemented using a pair of mechanical springs (Sarlis, 2012).

#### 1.4.2 Challenges in inelastic structures

Another important constraint on NSD comes into picture when the structural system starts yielding. Assume an elastic-purely-plastic structure and NSD assembly, schematically shown in Figure 1.3(a). Force displacement plots of the base structure and NSD are shown separately in Figure 1.3(b). If the structure is subjected to loads that will take it beyond the yield displacement,  $u_y$ , there are two limitations (refer to Figure 1.3(c)).  $F_y$  is the yield force of the structure. First, the tangential stiffness of the adaptive system becomes negative i.e., for displacements greater than  $u_y$ , the slope is negative, as shown in Figure 1.3(c). This signifies an unstable condition and this behavior is not desired as it would result in the collapse of structure. Fortunately, an NSD that has constant negative stiffness is physically not realizable (Pasala et al., April, 2012a). The stiffness of the NSD changes at large displacements to positive stiffness, which provides the desired hardening effects.

The second limitation is the increased base shear. In Figure 1.3(c), the structure yields first in the positive direction then after the first load reversal, when the structure yields in the negative direction, the peak base shear of the structure and NSD assembly,  $F_b$ , is greater than the base shear that is targeted,  $F_t$ , i.e.  $|F_b| > |F_t|$ . So the negative stiffness of the NSD has to be modified, once the structure starts yielding, to avoid this condition. Similar behavior is observed in the case of a bilinear system if the post-elastic stiffness of the base structure is less than the negative stiffness of the NSD.

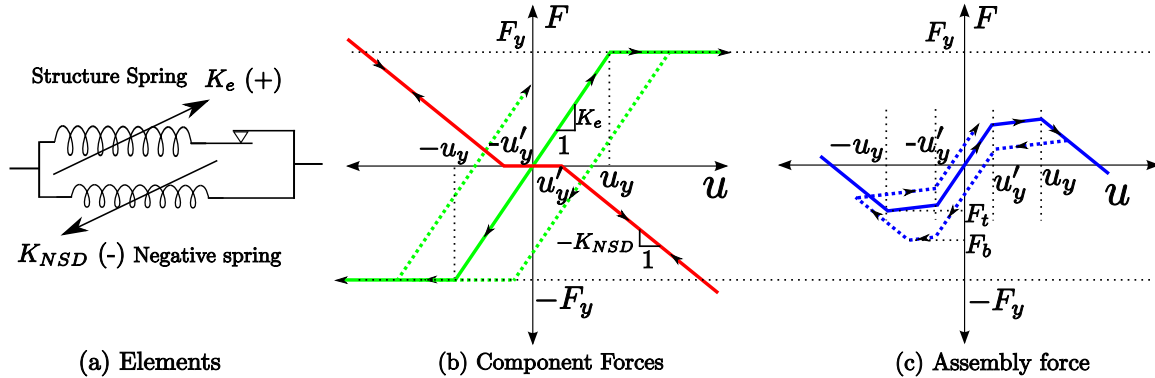


Figure 1.3: Working principle of Adaptive system. (a) Schematic representation of components (b) component F-D plots (c) assembly behavior [(Green line) : Base-structure, (Red line) : NSD, (Blue line) : Assembly]

The three possible ways of exerting the negative stiffness are:

1. Having a constant negative stiffness for all displacements beyond  $u'_y$ , shown in Figure 1.4(a)
2. Keeping the force exerted by the NSD constant beyond  $u_y$  (shown in Figure 1.4(b))
3. Stiffening the NSD beyond  $u_y$  (shown in Figure 1.4(c))

Three curves, shown in Figure 1.4, are for the base-structure (SF), NSD (NF) and the structure with NSD (TF). Figure 1.4(a) is the response of an NSD with constant negative stiffness,  $K_{NSD}$ , and without any constraints on the negative force generated, which is not possible as described earlier. Figure 1.4(b and c) is for second and third approaches respectively.

From Figure 1.4, clearly both the second and third approaches i.e., saturating or stiffening of the NSD after the structure undergoes deformation beyond yield point, will definitely work. Impact of the second approach is shown more clearly in Figure 1.5. Schematic diagram of an elastic-purely-plastic structure and NSD assembly is shown in Figure 1.5(a). Force-displacement behavior of the base structure and NSD are shown separately in Figure 1.5(b). Force-displacement behavior of the structure with NSD is shown in Figure 1.5(c). The second approach is an idealistic case and is hard to develop a passive device that is capable of exhibiting this force-displacement behavior.

The NSD developed and tested in this work is based on the third approach that is capable of exhibiting the hardening behavior beyond a certain displacement.

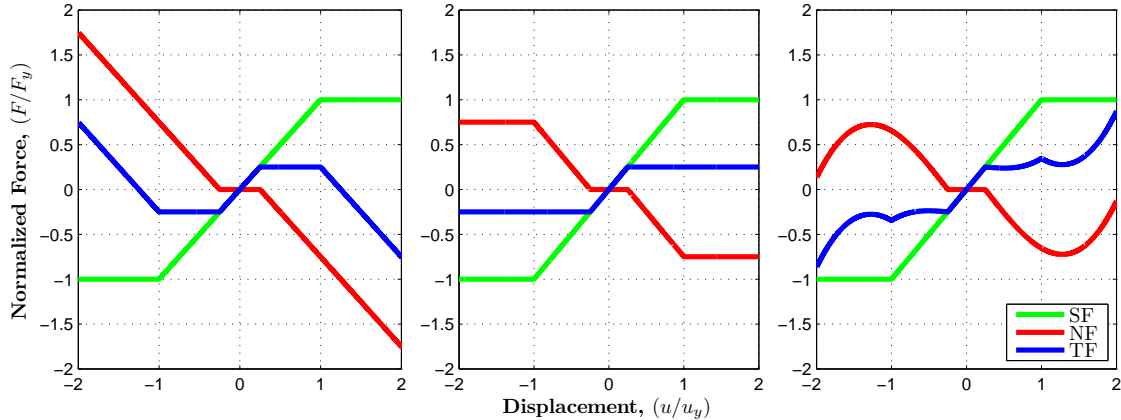


Figure 1.4: Different feasible force-displacements of structure-device assembly for yielding systems (a) no constraints on the force exerted by NSD (b) keeping the force exerted by the NSD constant beyond  $u_y$  (c) stiffening the NSD beyond  $u_y$  [SF: Spring Force; NF: NSD Force; TF: Total Force]

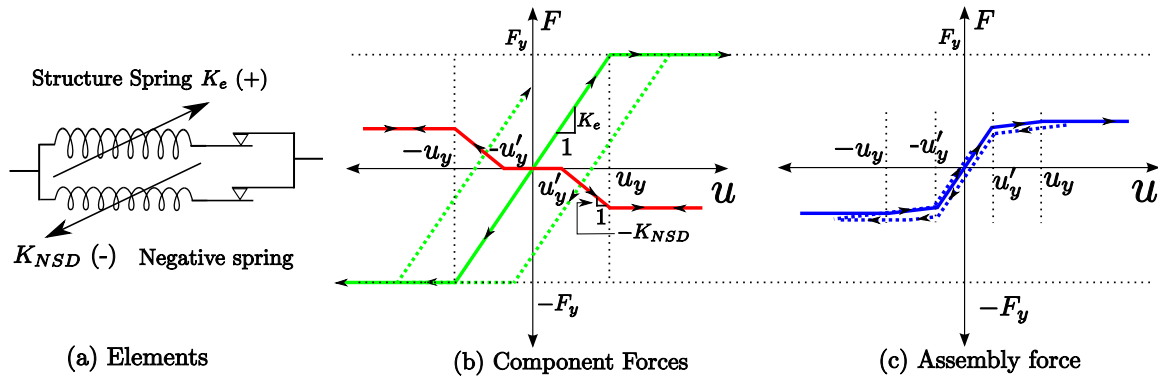


Figure 1.5: Instability in nonlinear systems with added negative stiffness. (a) Schematic representation (b) component F-D plots (c) assembly behavior [(Green line) : Base-structure, (Red line) : NSD, (Blue line) : Assembly]

## 1.5 Simulation studies

The main objective of the adaptive system is to reduce the base shear (foundation force) of the structure and at the same time limit the maximum displacement and acceleration of structure. It will be uneconomical and unrealistic to design devices that will retain the structure in elastic state, without any yielding,

after a major earthquake. So, all the cases considered in this chapter involve structure whose properties are representative of a real building and the loading cases for which there is yielding in the structure.

The model used as the test structure in the simulations is calculated from the capacity curve of the test-setup presented in chapter 3, obtained using the commercial softwares with the exact detailing. The strength reduction factor of the three-story frame,  $R_{oy} = F_o/F_y = 1.25$ , which is a conservative design.  $F_o$  is the maximum force in the elastic system for the suite of the ground motions used in this simulation study and  $F_y$  is the yield force of the three-story structure. As per the seismic code, ASCE-07, the desired strength reduction factor for moment resisting steel structures should be 4. The NSD is designed such that the strength reduction factor,  $R'_{yy} = F_y/F'_y = 4$ , where,  $F'_y$  is the apparent-yield-strength (force in the NSD and structure assembly at  $u'_y$ ). Hence, the NSD and structure assembly has a strength reduction factor,  $R'_{oy} = F_o/F'_y$  of 5. The strength reduction factor  $R'_{yy}$  should not be greater than 4 due to safety considerations. Sivaselvan-Reinhorn model (Sivaselvan and Reinhorn, 2000) is used to capture the hysteretic behavior. The Governing equation of motion for the structure is

$$m\ddot{u} + \left(2\xi\sqrt{K_e m}\right)\dot{u} + \alpha K_e u + (1 - \alpha)K_e u_y z = -m\ddot{u}_g \quad (1.4)$$

$$\dot{z} = (1 - |z|^\eta(\gamma \operatorname{sgn}(z\dot{u}) + \beta))\dot{u}/u_y \quad (1.5)$$

Eq. 1.5 can be represented in the displacement differential form as

$$\frac{dz}{du} = \frac{(1 - |z|^\eta(\gamma \operatorname{sgn}(z\dot{u}) + \beta))}{u_y} \quad (1.6)$$

where,  $m$  is the mass of structure,  $\xi$  is the damping ratio,  $\alpha$  is the post-yield stiffness ratio.  $\gamma$ ,  $\eta$  and  $\beta$  are constant parameters that determine the shape of bilinear hysteretic loops.  $z = F_{hys}/F_y$ , is the ratio of hysteretic force to the yield force. The tangential stiffness of the hysteretic part is proportional to  $\frac{dz}{du}$ .  $K_e$  is the initial elastic stiffness and  $\alpha K_e$  is the post-yielding stiffness of the structure obtained from the push over curve. The tangent stiffness of the system can be then represented by the following relation; shows low stiffness after yielding ( $z \rightarrow 1$ ):

$$K_{tangent} = K_e (\alpha + (1 - \alpha)[1 - |z|^\eta(\gamma \operatorname{sgn}(z\dot{u}) + \beta)]) \quad (1.7)$$

The values for remaining parameters are obtained using nonlinear interior-point optimization algorithm by minimizing the error between the capacity curve and the analytical model. The force deformation behavior of the structure, NSD and the assembly are shown in Figure 1.6. The displacement and forces in Figure 1.6 are normalized with the yield displacement and yield force. Viscous damper is used as the supplemental passive damper in the simulations. Equations to calculate the force exerted by the NSD are presented in chapter 2.

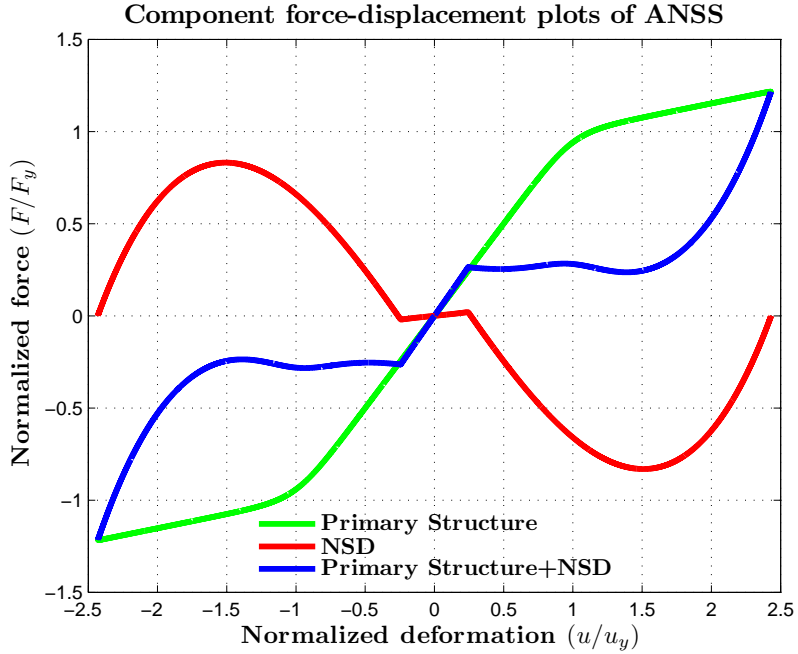


Figure 1.6: Force deformation behavior of structure, NSD and assembly

### 1.5.1 Periodic ground motion

A periodic input consisting of five cycles sine function is used as an excitation with a frequency identical to the natural frequency of the base structure,  $\omega_n = \sqrt{K_e/m}$ .

#### Elastic systems

For those systems that will remain in elastic region for the design ground motion. NSD is found to be very effective. NSD will reduce the base shear of the structure substantially. To demonstrate this point, a periodic ground motion is applied to the structure. Amplitude of the ground motion is chosen such that the structure and NSD assembly will remain in elastic region. Response time histories comparing the actual structure and adaptive system are shown in Figure 1.7. Adaptive system (AS) here refers to the structure, NSD and viscous damper with 0% damping. BS refers to base-structure (bilinear system). It can be seen from the plots in Figure 1.7 that all the response characteristics i.e., displacement, velocity and acceleration of the BS case have higher amplitude compared to the AS case. Comparison of the column forces and damper forces in BS and AS are shown in Figure 1.8. The component forces acting in the AS are shown in Figure 1.9(a) and F-D behavior of the assembly forces are shown in Figure 1.9(b). “Apparent yield displacement” for the NSD is at a normalized displacement of 0.25, since  $R'_{yy} = 4$ . It is evident from the results in Figure 1.8 and 1.9 that in the case of AS the primary structure remains in the elastic region

(displacement of the AS is less than the yield displacement of the primary structure,  $u_y$ ), whereas in the case of base structure the primary structure yields. It should be noted that passive damper is not yet included for the results shown in Figure 1.7, 1.8 and 1.9. NSD alone is effective for reducing base shear, without any increased deformations, in elastic structures. A passive damper can be added to reduce the deformation of structure along with the base shear, which is considered next.

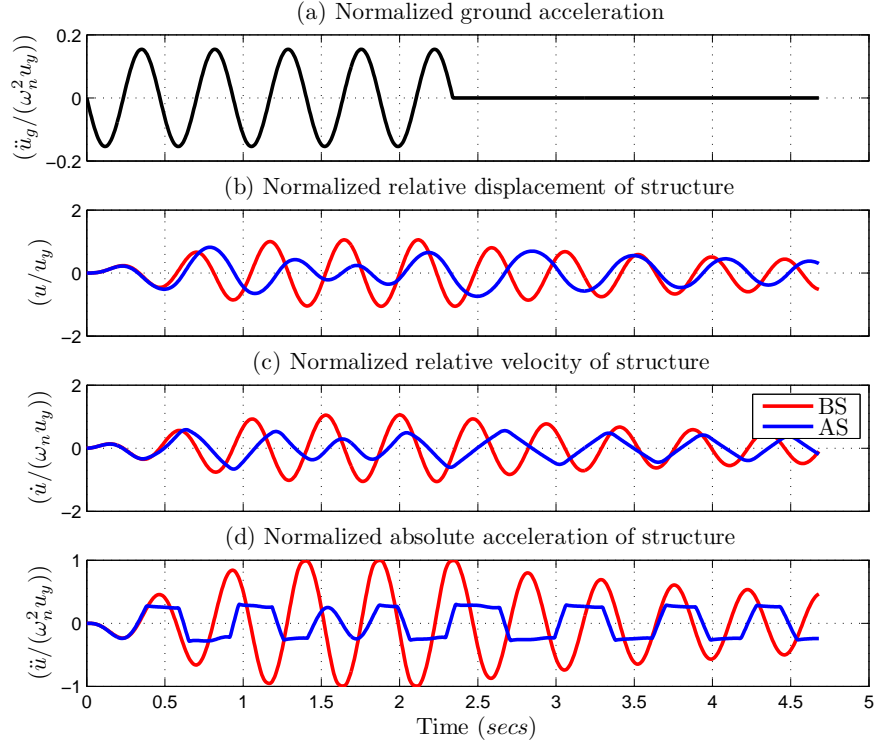


Figure 1.7: Response of AS and BS for periodic input in elastic structure

### Inelastic systems

The performance of the NSD is further verified for higher input amplitudes. Amplitude of input periodic ground motion is increased so that the adaptive system starts yielding. As discussed earlier with NSD alone the deformation of the adaptive system will increase due to reduction of stiffness. Passive viscous damper with 20% damping ratio is used to contain the increased displacements that occur in the AS due to reduction in total stiffness of the system. Simulation results for three systems are compared in Figure 1.10-1.13 after the addition of passive viscous damper: (i) Bilinear system (referred to as BS), (ii) Bilinear system with passive damper (referred to as PS) and (iii) Bilinear system with passive damper and NSD (referred to as AS).

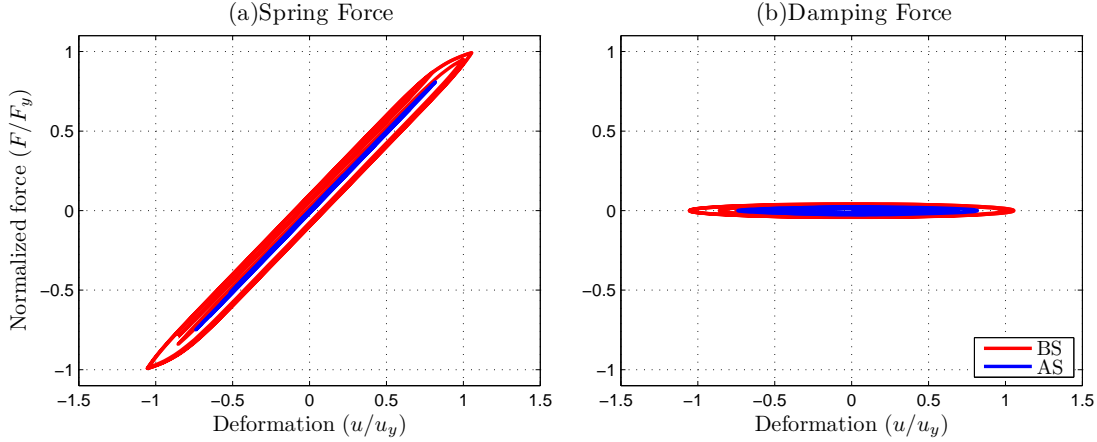


Figure 1.8: F-D behavior of columns and dampers in elastic structure

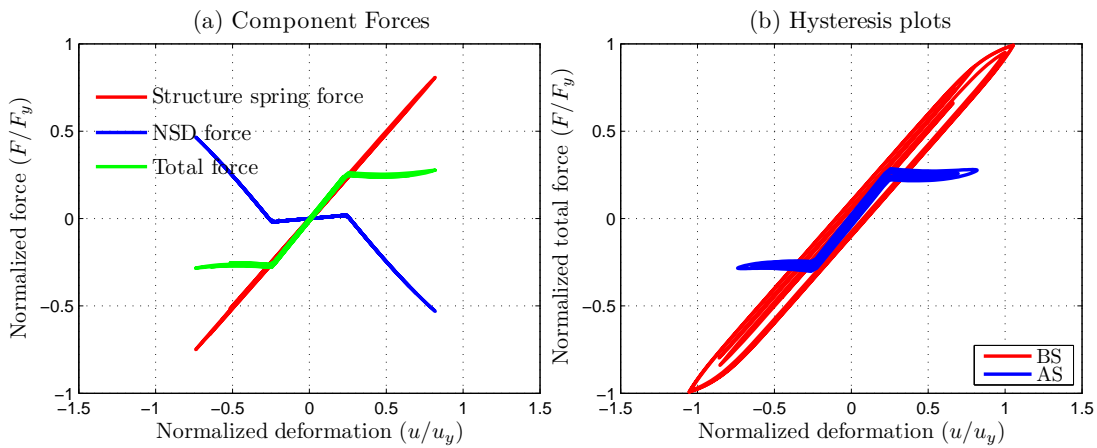


Figure 1.9: F-D behavior of the (a)components of AS and (b)assembly forces

For all these systems response time histories are shown in Figure 1.10, column forces and damper forces are compared in Figure 1.11, hysteresis loops of components of PS and AS are shown in Figure 1.12 and the assembly forces are shown in Figure 1.13. For the periodic input with input-frequency,  $\omega_n$ , and five cycles, the structure yields; the addition of passive damper results in the deformation of the structure being reduced substantially with a higher base shear. Figure 1.10 shows the reduction in all the responses of an adaptive system (base-structure with NSD and passive damper). Maximum deformation of adaptive system and passive system are comparable in Figure 1.10 and Figure 1.13, but the acceleration of adaptive system is 40% less-compared to passive system and base-structure. Forces exerted by the passive damper in case of both adaptive and passive system, shown in Figure 1.11(b), are comparable. The shear forces experienced by the columns in the two cases of AS and PS is approximately the same, shown in Figure

1.11(a).

In the AS, the base shear (force transferred to the structure's base) is reduced substantially, whereas in the PS case the base shear is larger than the BS case, shown in Figure 1.13. Also, the accelerations reduce substantially in AS case, as compared to both BS and PS cases, which is a significant benefit as the secondary systems can be protected preventing severe post earthquake losses. From Figure 1.10-1.13, it can be concluded that the three main objectives of the adaptive system are clearly achieved.

1. Base shear of the structural system has been reduced substantially. In case of passively damped system the base shear is greater than the base structure, the column shears remain approximately the same in AS and PS as both experience approximately the same displacement
2. The accelerations are substantially reduced in the case of AS as compared to BS and PS
3. Deformation of the AS is also reduced when compared to the BS and is of similar magnitude as the PS

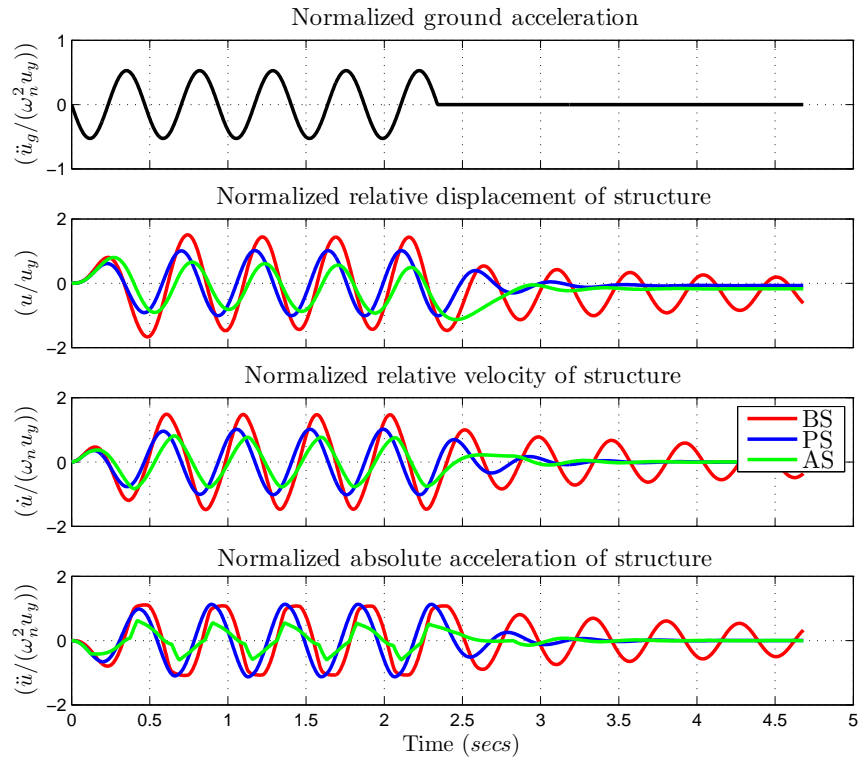


Figure 1.10: Response of AS and BS for periodic input in yielding structure

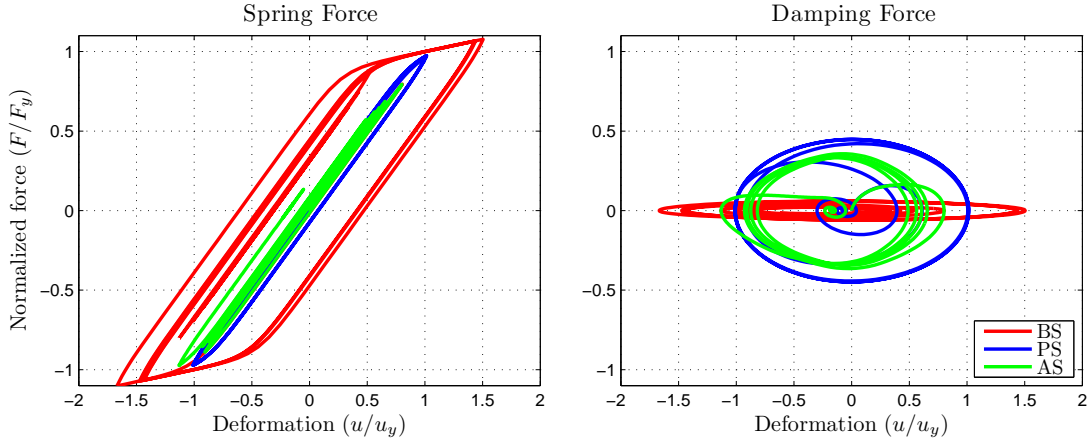


Figure 1.11: F-D behavior of columns and dampers in yielding structure

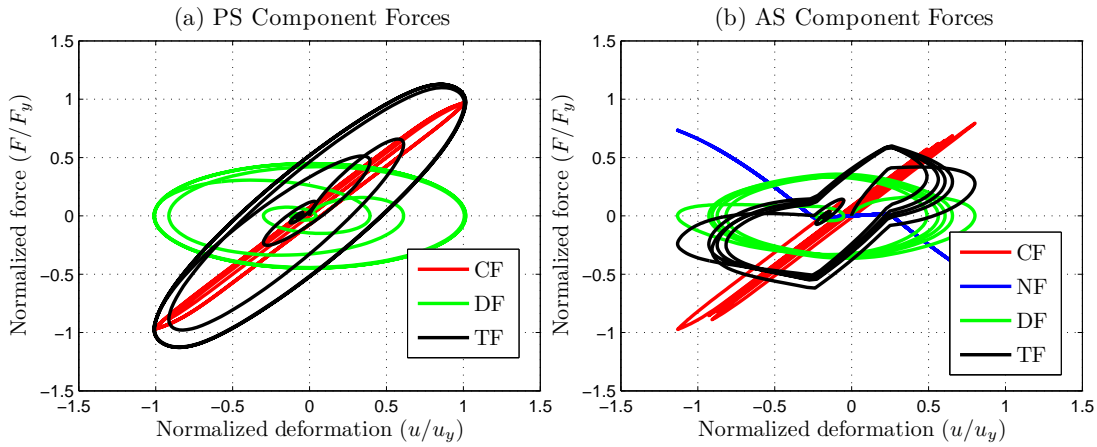


Figure 1.12: F-D behavior of the components of PS and AS

### Response to ground motion

To demonstrate the efficiency of the AS for earthquake ground motions, four standard performance criteria suggested for nonlinear benchmark structures (Ohtori et al., 2004), are used to evaluate and compare the performance of AS with passively-controlled-structure and original structure. Performance functions are shown in Table 1.1. There are minor modifications in the indices used in this study compared to the benchmark indices; formulae for all the indices are listed in Table 1.1. In Table 1.1,  $u_y$  is the yield displacement,  $K_e$  is elastic stiffness of the structure,  $F_{TF}$  is the base shear (structure force with NSD force and PD force),  $F_{col}$  is the force experienced by the columns. Seven standard ground motions are used to evaluate the performance of the AS/NSD developed in this study. The ground motions chosen are representative of both the far field and near-fault earthquakes. The performance indices of all the three systems for seven

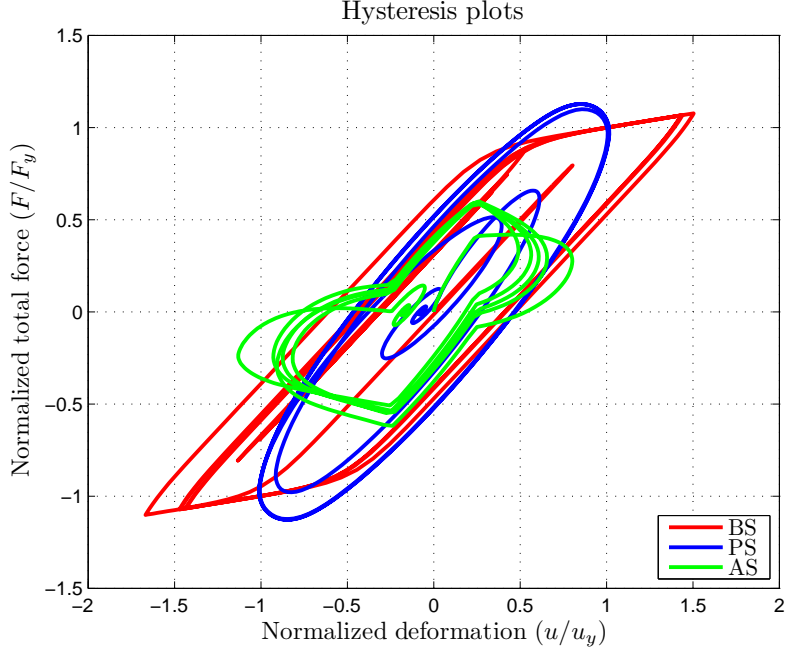


Figure 1.13: Comparison of the assembly F-D behavior in yielding structures

ground motions are listed in Table 1.2. From the results in Table 1.2, it can be seen that absolute accelerations ( $J_2$ ) of AS is lower than BS by 40% to 60% and it is lower than PS by 16% to 45%. Base shear ( $J_3$ ) of AS is lower than the BS by 55% to 70% and it is lower than PS by 40% to 65%. Inter-storey displacements ( $J_1$ ) of AS in some cases are 30% more than the PS but they are consistently less than BS by 20% or more. It should be noted that a simple viscous damper is adopted in these simulations. Although the base shear ( $J_3$ ) of the AS is lower than the PS by 55% or more, the force experienced by the columns ( $J_4$ ) follows the same trend as the inter-story displacement (shown in Table 1.2).

Response characteristics of all the three systems (BS, PS and AS) for Kobe #5 fault-normal (FN) ground motion are shown in Figure 1.14. Column forces and damper forces of different systems for Kobe ground motion are shown in Figure 1.15. AS and PS have slightly yielded but the BS has significantly yielded and undergone permanent deformation, shown in Figure 1.15(a,b). The shear forces and damper forces in AS and PS are similar. Hysteresis loops and component forces of AS and PS are shown in Figure 1.16. “Apparent-weakening” is evident from the component plots in Figure 1.16(b). In the AS, when compared with PS, peak acceleration and base shear have been reduced by 40%, shown in Figure 1.17. Peak inter-storey deformation in the case of AS is 30% more than the PS and the peak damping force of AS is 35% less than the PS, shown in Figure 1.17. Adding NSD to the base structure reduced the base shear significantly and the deformations of the assembly are contained with the addition of damper.

To demonstrate that the proposed adaptive negative stiffness device is effective for a range of structural

Table 1.1: Performance indices used to evaluate different systems

Name	Evaluation Parameter	Formula
$J_1$	Inter-storey drift	$\max_t \left( u(t) / u_y \right)$
$J_2$	Abs. acceleration	$\max_t \left(  \ddot{u}(t) + \ddot{u}_g(t)  / \max( \ddot{u}_g(t) ) \right)$
$J_3$	base shear	$\max_t \left(  F_{TF}  / K_e u_y \right)$
$J_4$	Column force	$\max_t \left(  F_{col}  / K_e u_y \right)$

Table 1.2: Summary of simulation results for recorded ground motions

PI	System	ElCentro #5 FN	Lucerne Valley FN	Rinaldi FN	Erzincan NS	Newhall FN	Sylmar FN	Pacoima
$J_1$	BS	0.72	0.98	1.00	0.68	1.66	1.24	0.61
	PS	0.48	0.47	0.64	0.45	0.93	0.65	0.45
	AS	0.64	0.69	0.83	0.56	0.93	0.78	0.55
$J_2$	BS	4.01	7.86	2.90	3.42	1.81	6.46	2.30
	PS	2.83	4.19	2.05	2.41	1.63	4.79	1.81
	AS	2.30	3.52	1.36	1.96	0.99	2.66	1.40
$J_3$	BS	0.72	0.93	0.97	0.68	1.10	1.03	0.61
	PS	0.48	0.47	0.64	0.45	0.90	0.65	0.45
	AS	0.29	0.28	0.30	0.27	0.31	0.30	0.27
$J_4$	BS	0.72	0.93	0.97	0.68	1.10	1.03	0.61
	PS	0.48	0.47	0.64	0.45	0.90	0.65	0.45
	AS	0.64	0.69	0.82	0.56	0.90	0.78	0.55

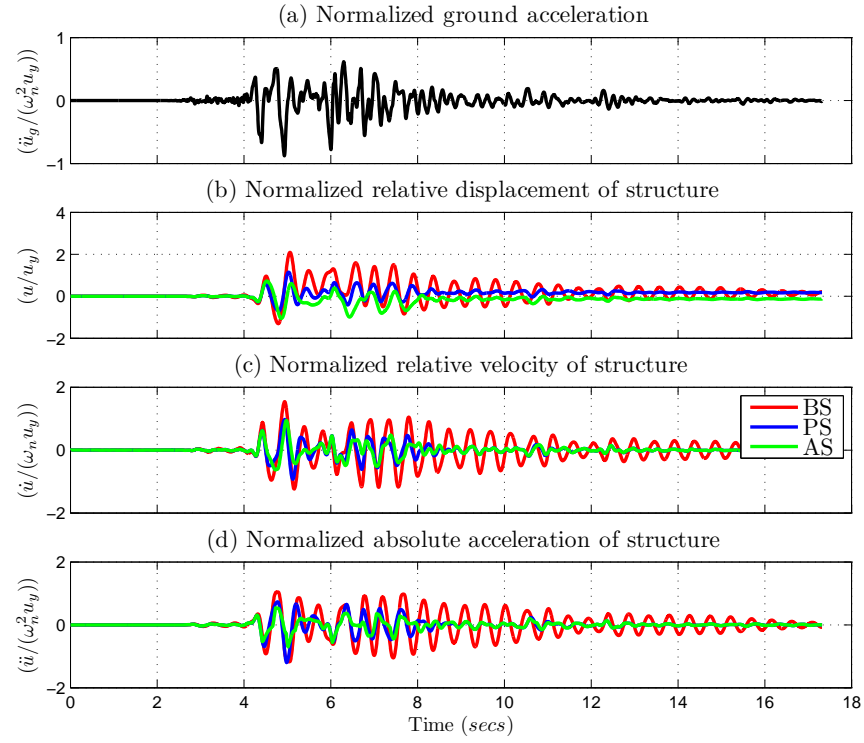


Figure 1.14: Response of AS and BS for Kobe ground motion

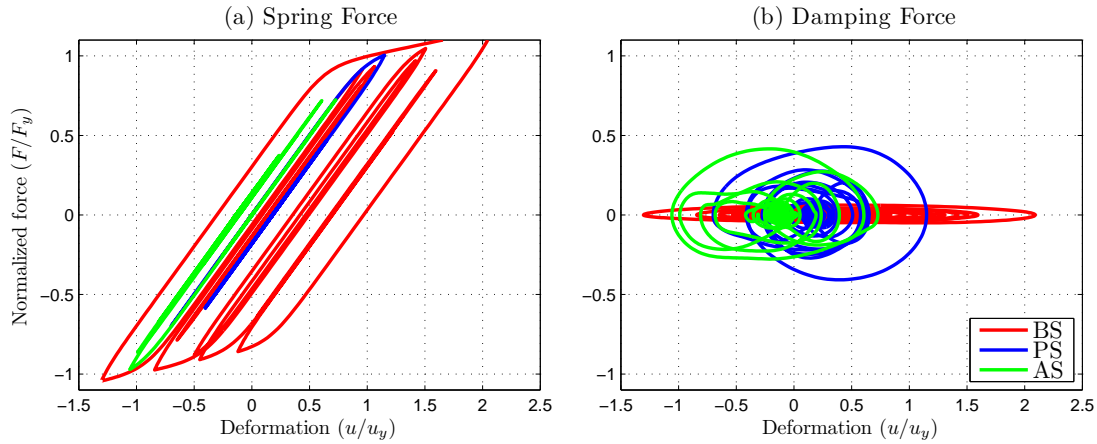


Figure 1.15: F-D behavior of columns and dampers for Kobe ground motion

systems (systems with different natural frequencies) response spectra are generated for BS, PS and AS. Responses are presented in dimensionless  $\pi$ -terms, displacement  $u\omega_p^2/a_p$ , base shear- $F_{shear}/ma_p$ , acceleration-

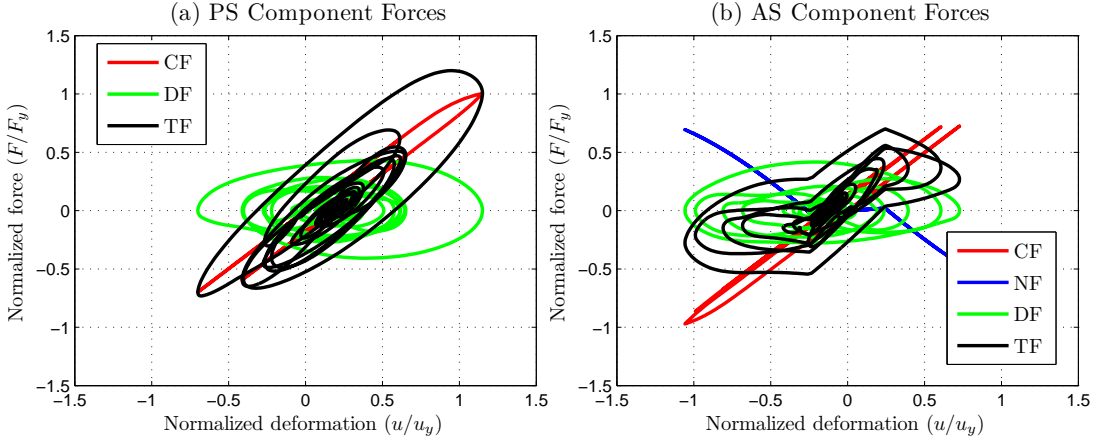


Figure 1.16: F-D behavior of the components of PS and AS for Kobe ground motion

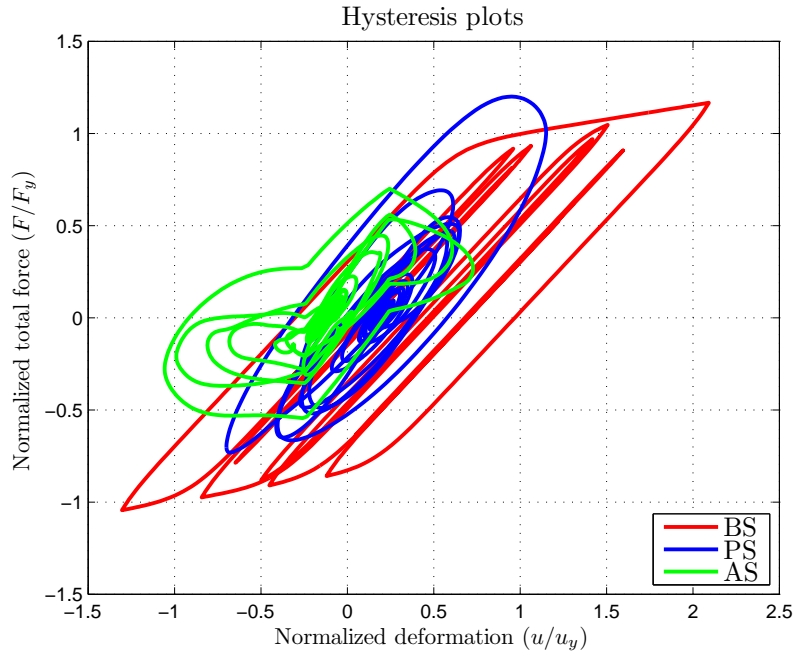


Figure 1.17: Comparison of the assembly F-D behavior for Kobe ground motion

$\ddot{u}/\alpha_p$  and frequency- $T_s/T_p$ . Where,  $\alpha_p$  is the pulse-amplitude of the acceleration,  $\omega_p$  is the frequency of the pulse,  $T_s$  and  $T_p$  are the time-periods of structure and pulse, respectively. Makris and Black (Makris and Black, 2004a,0) have developed cycloidal pulses that are representative of the actual recorded ground motions. These cycloidal pulses and recorded ground motion data are used to test the performance of the AS. Response spectra is generated for both cycloidal pulses and recorded ground motions. Response-spectra

plots are represented in dimensionless  $\pi$ -terms proposed by Makris and Black (Makris and Black, 2004b). All the earthquake motions responses are represented by equivalent pulses and the corresponding amplitudes and time-periods for normalization. Response spectra of  $C_1$  pulse type ground motion and Sylmar FN ground motion are shown in Figure 1.18 and Figure 1.19, respectively. For  $C_1$  ground motion, the pulse-period,  $T_p = 0.5$  seconds is used to generate spectra in Figure 1.18. The Sylmar FN ground motion can be approximated by a  $C_2$  pulse with a period ( $T_p$ ) of 2.3 seconds and an acceleration peak ( $a_p$ ) of  $64.6 \text{ in/sec}^2$ , which is used to normalize the spectra in Figure 1.19.

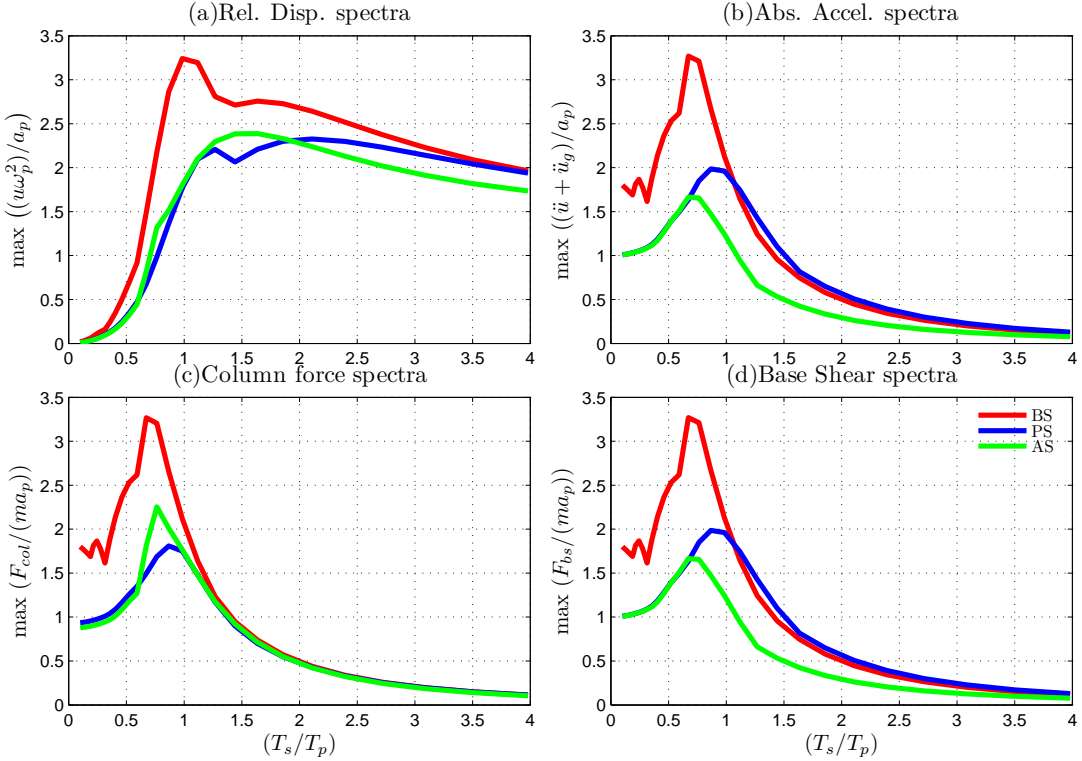


Figure 1.18: Comparison of response spectra for  $C_1$  type cycloidal pulse

For highly stiff structures  $T_s/T_p < 0.5$ , the response of the PS and AS are similar because the normalized displacement of the structure remains less than  $u'_y$ , shown in Figure 1.18(a), 1.19(a). For  $0.5 < T_s/T_p < 1.5$  peak acceleration and base shear of the AS is more than 30% lower than BS and PS because of the NSD, shown in Figure 1.18(b,c), 1.19(b,c). The peak displacement of AS in the same region is 20% higher than the PS but 50% less than BS. For  $T_s/T_p > 3$ , all the three systems (BS, PS and AS) start yielding and the NSD starts stiffening so the peak acceleration and base shear of all the systems are same, shown in Figure 1.18(b,d), 1.19(b,d). Column force in the AS is slightly higher than the PS around the peak in the spectra plots and it is almost identical for all other time-periods. Peak relative displacement of BS is always greater than the PS and AS. Key observations based on the response spectra plots of pulses and ground motion

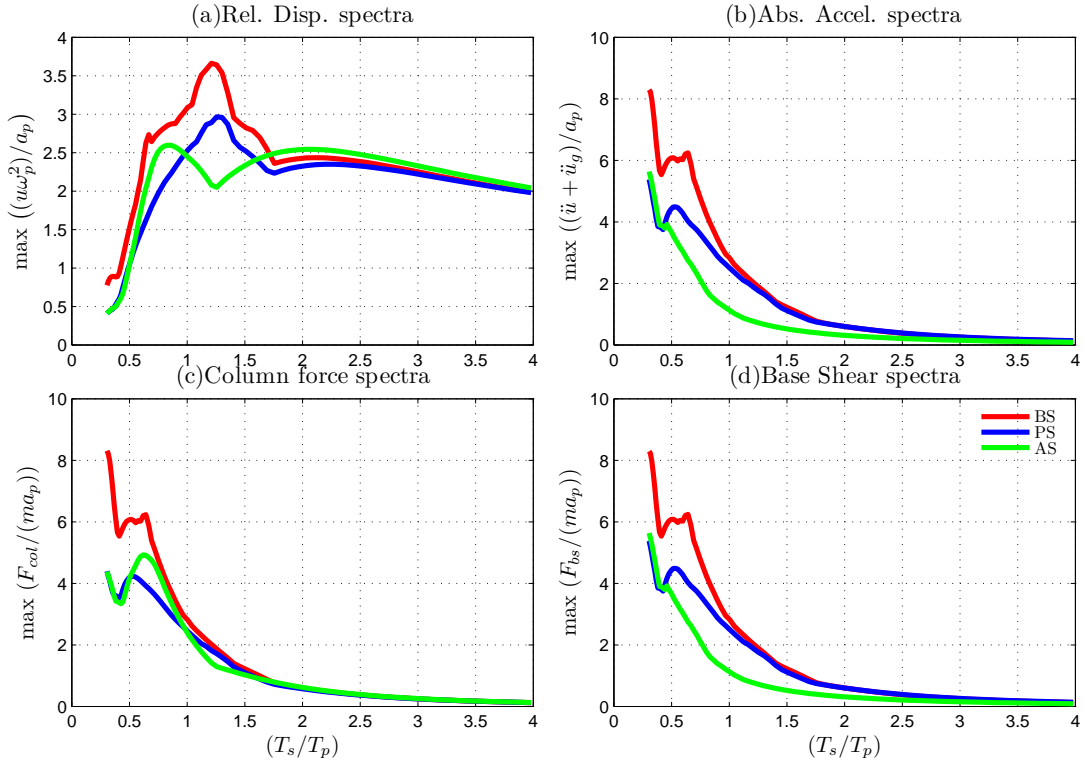


Figure 1.19: Comparison of response spectra for Sylmar ground motion

data are listed in Table 1.3.

## 1.6 Summary

The new idea of an “apparent weakening” is a novel concept that is proposed in this study. An “apparent weakening” is introduced in the structural system using a complementary negative stiffness device (NSD) that mimics “yielding” of the global system thus attracting it away from the main structural system. Unlike the concept of weakening proposed earlier (summarized by Reinhorn et al., (Reinhorn et al., 2009)), where the main structural system strength is reduced, the new system does not alter the original structural system, but produces effects compatible with an early yielding.

Adaptive negative stiffness system (AS) is an assembly of primary structure, NSD and passive damper (PD). AS is referred as adaptive system or adaptive stiffness system. The main objective of the adaptive system is to shift the yielding behavior of the structure to the NSD and reduce the base shear (foundation force) of the structure and at the same time limit the maximum displacement and acceleration of structure. Adaptive systems belong to the category of passive seismic protection systems but they are more sophisticated than the regular passive systems. The adaptive system that is developed in this work consists of

Table 1.3: Summary of response spectra for cycloidal pulses

$T_s/T_p$ Range	Description
$T_s/T_p < 0.5$	PS and AS have same response characteristics but they have a superior spectral characteristics compared to BS due to the passive damper
$0.5 < T_s/T_p < 1.5$	PS and AS have same response characteristics but they have a superior spectral characteristics compared to BS due to the passive damper Peak column force of AS is higher than PS Displacement has mixed behavior for PS and AS
$1.5 < T_s/T_p < 3.0$	AS has superior characteristics compared to PS and BS in peak acceleration and base shear And the column force of AS is same as PS Displacement has mixed behavior for PS and AS
$3.0 < T_s/T_p$	All the three systems yield in this region NSD starts stiffening resulting in increased peak acceleration and base shear responses All the systems exhibit same spectral characteristics

two components that are designed in a two step sequence, similar to the approach developed by Reinhorn et al. (Reinhorn et al., 2009). First an adaptive negative stiffness device, which is capable of changing its stiffness during lateral displacement, is developed based on the properties of the structure. This NSD is designed to exhibit negative stiffness behavior which upon the addition of structure properties will result in reduction of the stiffness of the structure and NSD assembly or “apparent weakening” thereby resulting in the reduction of the base shear of the assembly. Then a passive damper is designed for the assembly to reduce the displacements that are caused due to the “apparent weakening”-thereby reducing the base shear and displacement in a two step process.

This report presents comprehensive details of principles and the study of the behavior of the AS. The NSD is described in detail in the next chapter. Through numerical simulations and simulation studies it is shown that the concept of AS is very effective in elastic and some inelastic structural systems. The effectiveness and the superior performance of the AS as compared to a structural system with supplemental passive dampers when subjected to periodic and random input ground motions is demonstrated by numerical results.

## Chapter 2

# Negative Stiffness Device

True negative stiffness means that the force must assist motion, not oppose it as in the case of a positive stiffness spring. A passive device capable of exhibiting true negative stiffness, negative stiffness device (NSD), without external power supply is developed and studied in this work. The approach used to generate the negative stiffness is similar to the idea proposed by Nagarajaiah and Reinhorn (Nagarajaiah and Reinhorn, 1994). A precompressed spring is used to generate the force to push the structure and a lever-mechanism is adapted to amplify the generated force. The concept of using springs to achieve a low stiffness system was first introduced by Molyneaux (Molyneaux, 1957) for vibration isolation in aircraft systems. More recently, Platus (Platus, 1992, 2004) developed ultra sensitive vibration isolation devices to isolate the the structure from horizontal-vibrations using pre-compressed springs. Thus far the application of negative stiffness devices has been limited to vibration isolation of small scale systems. Due to the large compression forces (usually of the order of self weight of structure) required to generate the desired negative stiffness, in the case of large structural systems, using pre-compressed springs was not perceived. So, a dual amplification mechanism is adapted along with the pre-compressed spring idea to achieve the desired level of forces to emulate a yielding system (“apparent weakening”).

This chapter is organized as follows: Section-2.1 contains the detailed description of various components in the NSD and their connections. Working principle of NSD and the derivations pertaining to the development of equation of motion of NSD is presented in section-2.2. More detailed model including the inertial terms and other nonlinear terms are presented in section-A. Description of the test setup used to characterize the behavior of NSD and the experimental results are summarized in section-2.3. Conclusions based on the comparisons between the observed experimental and predicted results are discussed in section-2.4.

## 2.1 NSD Description

The NSD is fabricated by Taylor Device Inc., Tonawanda. All the elements of NSD are made with mild steel. Schematic diagram and photograph of the NSD with labeled components is shown in Figure 2.1. NSD consists of (1) pre-compressed spring (2) two chevrons (CB1 and CB2) (3) two channel sections (4) pivot plate (5) lever-arm (6) two double pinned columns and (6) two gap spring assemblies (GSA).

Each channel section is welded to the loose ends of chevrons; bottom channel is welded to the bottom chevron (CB1) and the top channel is welded to the top chevron (CB2). One leg of each chevron is made out of steel-flats and the other leg is made of hollow square section (HSS). The two chevrons are coupled such that the steel flats of CB1 engulf the HSS of CB2 and viceversa. Pre-compressed spring (CS), made out of cylindrical steel tube by machining a helical groove along the axis of the cylinder, is placed vertically between the two chevron braces CB1 and CB2, as shown in Figure 2.1. Since the CS is pre-loaded, it will exert force to push the chevrons closer. To retain the chevrons at certain spacing, two double pinned columns (DPC) are connected to the channels of chevrons braces at either ends. Essentially, the pre-load force stored in the CS is balanced by the tension in DPCs; hence, NSD is self-contained for the vertical forces.

As mentioned earlier, an amplification mechanism is also incorporated using a simple lever principle. To achieve this, pivot-plate and lever-arm are added to the device. Pivot-plate is connected to the top of CB1 using 1 *in.* diameter pins. Instead of connecting the top of CS directly to the CB1, it is connected to the bottom of pivot-plate. The top of pivot plate is connected to the lever-arm which in turn is connected to the top channel of NSD. Two elastic-bilinear springs, referred as gap-spring assemblies (GSA), are placed horizontally, connecting CB2 and the bottom channel of NSD.

GSA has three coil-spring and is equivalent to series connection of two coil-springs, two soft springs ( $S'_1, S''_1$ ) and a stiff spring ( $S_2$ ), as shown in Figure 2.2.  $S_2$  sits inside the cup and flushes against the CB2. GSA has a circular plate on one end and it is bolted horizontally to the bottom channel. The circular plate is connected to the rest of the assembly with a steel rod that can apply force and compress  $S'_1$  and  $S''_1$ . The working principle of NSD and GSA are explained in the next section.

## 2.2 Analytical Model

Consider a floor in the structure in which “apparent-weakening” is desired, the NSD should be bolted to the bottom of floor and the top of NSD is connected to the ceiling of the floor using a end-angle assembly that will transfer only the horizontal forces, described in detail in the next chapter. Five crucial points (pin-joints in the device) are marked in Figure 2.1 to explain the working principle of the device. Any inter-story structural deformation will result in the deformation of the top channel, CB2 and the lever-arm. Since the lever-arm is connected to the pivot plate (point-B) and the pivot plate is fixed at point-C, any deformation of point-B will result in rotation of pivot-plate about point-C. As a result, point-D will displace in the opposite direction to that of point-B. Also, the bottom of CS is connected to CB2, so,

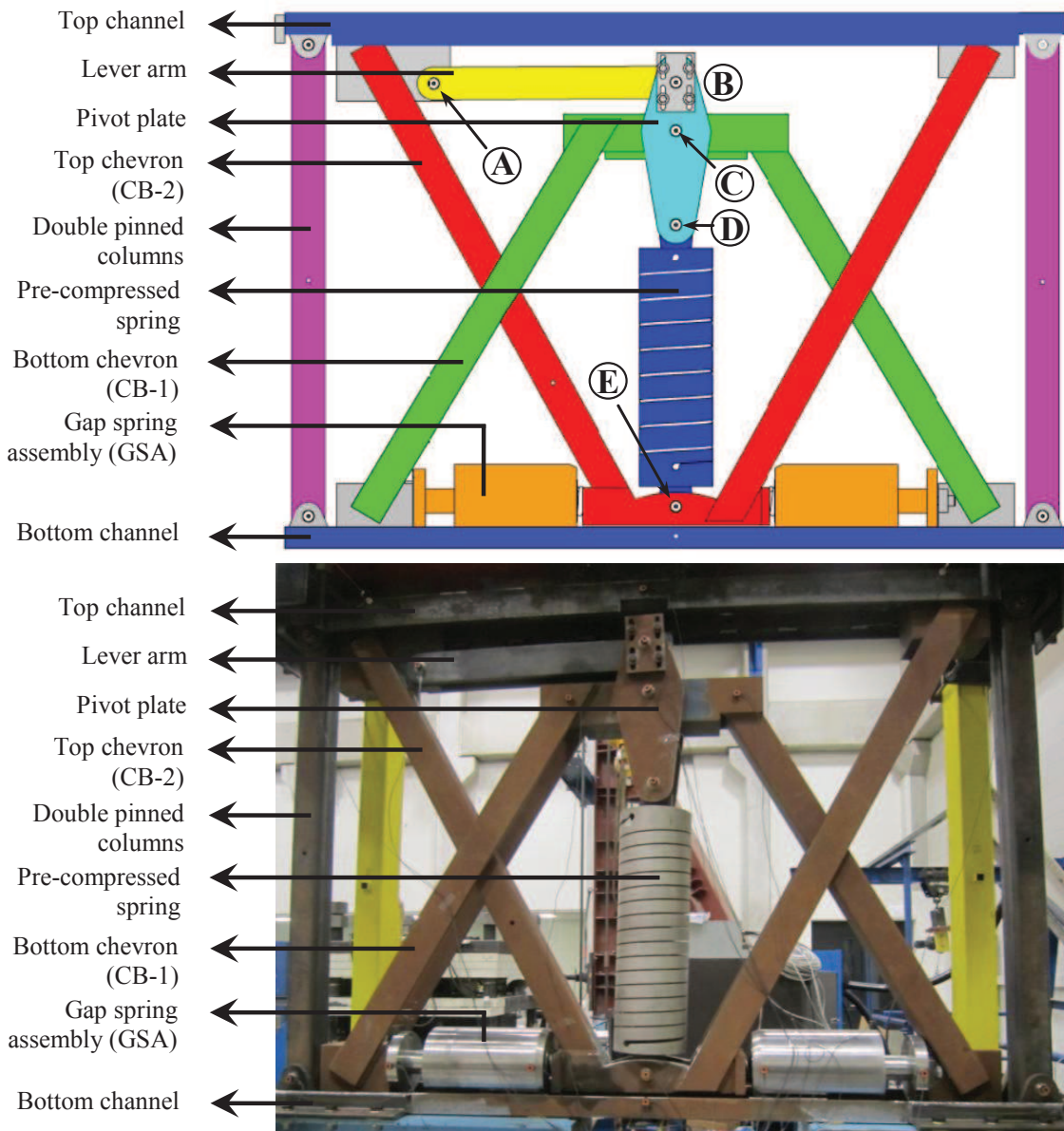


Figure 2.1: Schematic diagram and photograph of NSD

point-E will undergo same deformation as point-B. The total lateral deformation of the CS is magnified by comparison to the displacement of point A (a) by the ratio CD to BC and (b) due to the movement of point E in the opposite direction to D. Essentially, any deformation at the top of NSD will result in the horizontal deformation of CS both at the top and bottom; this is the dual amplification mentioned previously.

Assuming all the elements are rigid, deformed shape, undeformed shape and free body diagram of

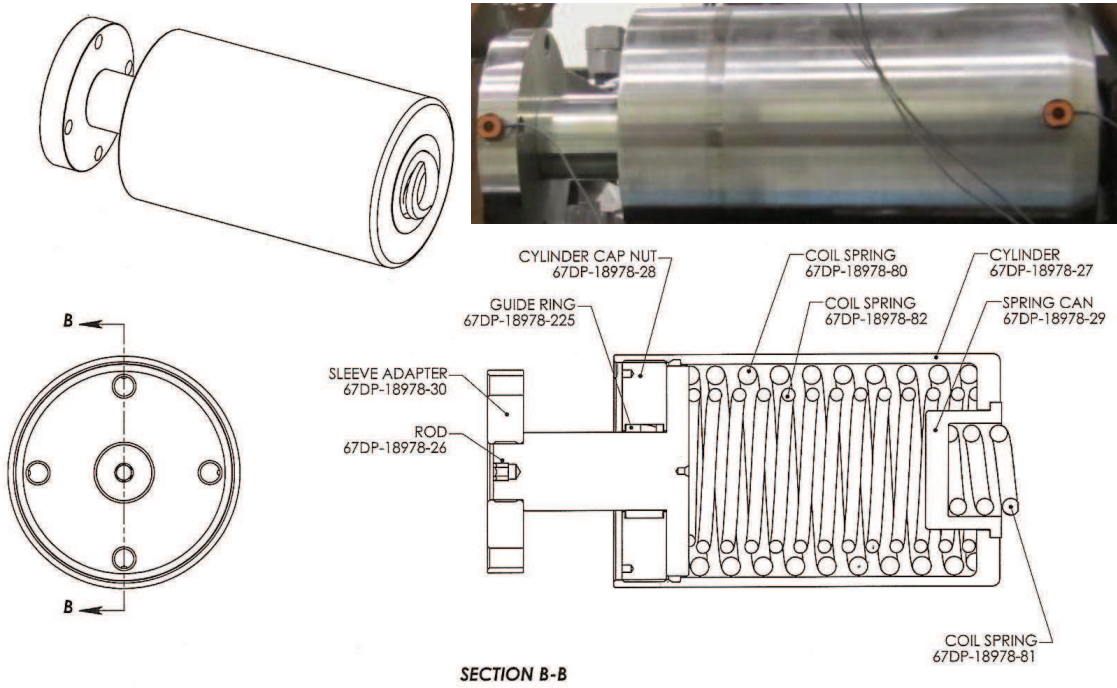


Figure 2.2: Fabrication drawings of GSA showing the coil-springs. Inset: Photograph of GSA

NSD for an arbitrary horizontal displacement of the structure,  $u$ , is shown in Figure 2.3. The pivot plate rotates by angle  $\psi$ , the CS rotates by an angle of  $\theta$  and the lever-arm rotates by an angle of  $\theta_{lv}$ . When the top of NSD moves horizontally, the DPCs rotate and all the elements connected to the top channel and CB2 undergo a vertical displacement  $b'$ , given in Eq. 2.1

$$b' = b \left( 1 - \sqrt{1 - \left( \frac{u}{b} \right)^2} \right) \quad (2.1)$$

where,  $b$  is the height of DPCs. Points A and E displace horizontally by a distance  $u$ , same as the structure displacement, shown in Figure 2.3(b). Point-B moves by a  $u' < u$  due to the rotation of the lever-arm.  $\theta_{lv}$  and  $u'$  are coupled together by the compatibility equation given by Eq. 2.2-2.3

$$u' = u + l_{lv} (\cos(\theta_{lv}) - 1) \quad (2.2)$$

$$\theta_{lv} = \sin^{-1} \left( \frac{l_2 - b' - \sqrt{l_2^2 - (u')^2}}{l_{lv}} \right) \quad (2.3)$$

The simultaneous equations, Eq. 2.2 and 2.3, are transcendental equations. The solution is calculated

numerically at each time step using Newton-Raphson iteration. From the numerical study, it has been found that the solution converges in 6 to 10 iterations. However, since the maximum rotation of  $\theta_{lv}$  is less than  $3^\circ$ , so  $\theta_{lv}$  is assumed to be zero and  $b = b'$ . Since  $u' \ll l_2$  and  $b' \approx 0$ ,  $\theta_{lv}$  only depends on the ratio  $l_2/l_{sv}$ . The angles  $\psi$  and  $\theta$  are calculated using Eq. 2.4-2.5

$$\psi = \sin^{-1} \left( \frac{u'}{l_2} \right) \quad (2.4)$$

$$\theta = \tan^{-1} \left( \frac{\left[ u + u' \frac{l_1}{l_2} \right]}{\left[ l_p + l_1 (1 - \cos(\psi)) + b' \right]} \right) \quad (2.5)$$

where,  $l_1$  and  $l_2$  are the lengths of pivot-plate CD and BC, respectively.  $l_p$  is the initial length of compressed spring, when  $u = 0$ . Once the points D and E move in opposite direction, length of the CS increases. Length of the CS in deformed configuration,  $l_{extd}$ , is calculated using Eq. 2.6

$$l_{extd} = \sqrt{\left( l_p + l_1 (1 - \cos(\psi)) + b' \right)^2 + (l_1 \sin(\psi) + u)^2} \quad (2.6)$$

In the deformed configuration, the axial force exerted by CS,  $F_{sc}$ , is calculated using Eq. 2.7

$$F_{sc} = P_{in} + K_{sc} (l_{extd} - l_p) \quad (2.7)$$

where,  $P_{in}$  is the initial compressive force in the spring and  $K_{sc}$  is the stiffness of compressed spring. The axial force in lever arm,  $F_{lv}$ , is given by Eq. 2.8

$$F_{lv} = F_{sc} \frac{l_1 \sin(\psi + \theta)}{l_2 \cos(\psi - \theta_{lv})} \quad (2.8)$$

The total lateral force exerted by the NSD at the top of the device (without GSA),  $F_{vs}$ , is equal to the sum of horizontal forces at point-B and point-D (Eq. 2.9).

$$F_{vs} = F_{sc} \sin(\theta) + F_{lv} \cos(\theta_{lv}) \quad (2.9)$$

Assuming  $\theta_{lv} = 0$  and  $b = b'$ , lateral force exerted by the NSD (without GSA) is given by

$$F_{vs} = F_{sc} \left[ \sin \theta + \frac{l_1 \sin(\theta + \psi)}{l_2 \cos \psi} \right] \quad (2.10)$$

Since the NSD consists of many moving elements, equation of motion for the NSD including the inertial terms is also developed. However, in the operating frequency range, the contribution of inertial terms is insignificant. These derivations are presented in Appendix A.

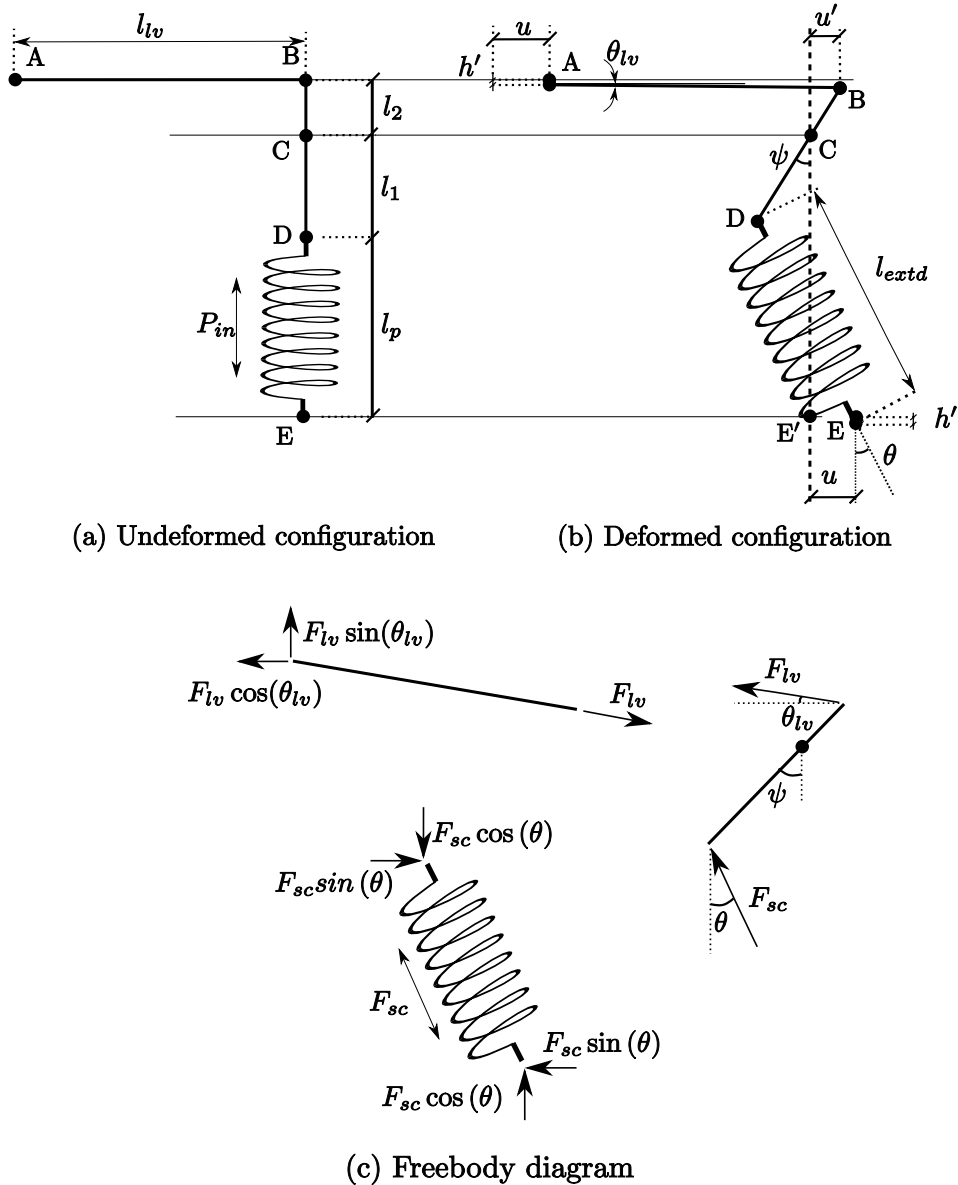


Figure 2.3: Undefomed shape, deformed shape and free body diagrams of components in NSD

Next, the working principle and the analytical model for the GSA is presented.

### 2.2.1 Gap spring assembly

“Apparent yield-displacement”, described in section-1.4.1, is achieved using the the GSA. Two GSAs are present in each NSD and each GSA exhibits bilinear elastic behavior. They are designed in such a way that one GSA engages for positive displacements and the other for negative displacements. Equivalent

system for the GSA is shown in Figure 2.4. GSA consists of (1) soft spring ( $S_1$ ) with a stiffness of,  $K_{S1}$ , and a pre-load,  $P_{S1}$  (2) stiff spring ( $S_2$ ) with a stiffness,  $K_{S2}$ , in series to achieve bilinear-elastic structure. Free length of  $S_1$  is  $L_{S1}$  and the installed length is  $L'_{S1}$ . Pre-load in  $S_1$  is calculated using Eq. 2.11

$$P_{S1} = K_{S1} (L_{S1} - L'_{S1}) \quad (2.11)$$

When a load,  $F_g$ , is applied on the GSA, since spring- $S_1$  is pre-loaded, spring- $S_2$  deforms until the compression-force in  $S_2$  reaches  $P_{S1}$ . Once the external load is greater than  $P_{S1}$ , both  $S_1$  and  $S_2$  deform. The force exerted by GSA is given in Eq. 2.12

$$F_g = \begin{cases} K_{S2}u & \text{if } |u| \leq \frac{P_{S1}}{K_{S2}}, \\ P_{S1} + \frac{K_{S1}K_{S2}}{K_{S1}+K_{S2}} & \text{if } |u| > \frac{P_{S1}}{K_{S2}} \end{cases} \quad (2.12)$$

For the GSA used in this study, the desired stiffness of the soft spring is 0.15 *kip/in.* A coiled-spring with 0.15 *kip/in.* was not available so two soft-springs,  $S'_1$  and  $S''_1$ , with stiffness of 0.11 *kip/in.* and 0.04 *kip/in.*, respectively and they have a free length of 25.9 *in.*. They are compressed to 9.7 *in.* (a pre-load of 2.25 kips, together) and placed inside the cylindrical case. The spring  $S_3$ , has a stiffness of 7.5 *kip/in.* and is placed in a cup outside the cylindrical case. The correlation between the spring stiffness and the desired NSD properties is explained next.

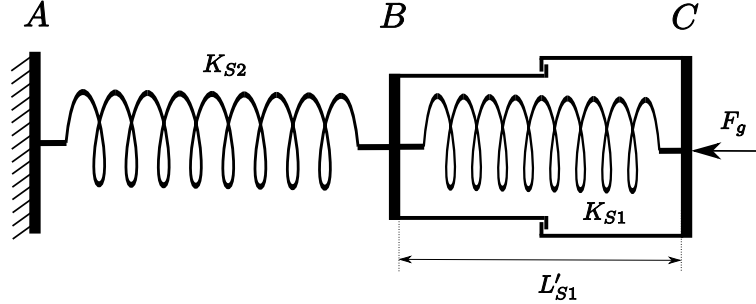


Figure 2.4: Schematic of the equivalent system of GSA

Force displacement characteristics of the pre-compressed spring, GSA and the NSD are shown in Figure 2.5(a),(b) and (c) respectively. Five distinct points are shown in Figure 2.5(a). Point “0” is the initial position and lateral force exerted by the vertical spring,  $F_{vs}$ , is zero. When the precompressed vertical spring is displaced to an inclined position at angle  $\theta$  from the vertical, the axial force in the pre-compressed spring,  $F_{sc}$ , is given by Eq. 2.7. At point-“1” in Figure 2.5(a) the secant stiffness ( $-F_{vs1}/u'_1$ ) and tangential stiffness (slope at point-“1”) are both negative. At point-“2” the secant stiffness ( $-F_{vs2}/u_2$ ) is still negative and tangential stiffness reaches zero. At point-“3” the secant stiffness ( $-F_{vs3}/u_3$ ) is still

negative but the tangential stiffness becomes positive. At point-“4” secant stiffness becomes zero and the tangential stiffness remains positive. At point-“4”,  $l_{extd} = l_p + P_{in}/K_{sc}$ , hence the net axial force in the inclined spring becomes zero,  $F_{sc} = 0$ , or all the pre-compression force is lost; thus  $F_{vs} = 0$ . At point-“5” both the secant stiffness and tangential stiffness are positive.

The horizontal spring exhibits elastic-bilinear behavior, the transition in stiffness occurs at displacement  $u'_y$  and stiffness of the spring is zero for  $|u| > u'_y$ , as shown in Figure 2.5(b). Since it is not possible to achieve zero stiffness beyond  $u'_y$ , a soft spring is used in the GSA used in this study. The total force-displacement characteristics of the NSD is shown in Figure 2.5(c). The initial stiffness of the horizontal spring,  $F_{g1}/u'_y$ , is designed to match (or be greater than) the initial negative stiffness of the inclined spring resulting in zero stiffness for the NSD till  $|u| \leq u'_y$  i.e.,  $F_{g1} - F_{v1} = 0$ . The stiffness of the horizontal spring,  $K_g$ , beyond  $u'_y$  is chosen to be zero (or a very low value); hence, essentially the behavior of vertical spring is reflected in the NSD for displacements beyond  $u'_y$ . NSD exhibits positive secant and tangential stiffness beyond point-“3”, as shown in Figure 2.5(c). The total lateral force,  $F_{NSD}$ , combination of pre-compressed spring and GSA, is given by Eq.

$$F_{NSD} = F_{vs} + F_g \quad (2.13)$$

The NSD behaves like a nonlinear-elastic spring with variable stiffness as described above. All the equations developed so far in this chapter are based on the assumption that all the elements are rigid. Assuming that CB1, CB2 and the top channel are flexible, the force exerted by NSD on the structure is given by,

$$F_{NSD} = F_{vs} + F_g + K_f u_f \quad (2.14)$$

where,  $K_f$  stands for the equivalent stiffness due to the flexibility of CB1, CB2 and top channel.  $u_f$  is the equivalent deformation due to the flexing of the chevron braces.

The impact of preload in the CS,  $P_{in}$ , and the stiffness of CS,  $K_{sc}$ , on the overall behavior of NSD is studied next. F-D behavior of NSD with different  $K_{sc}$  and  $P_{in} = 3.7$  kip is shown in Figure 2.6 and the behavior of NSD with  $K_{sc} = 1$  kip/in and different  $P_{in}$  are shown in Figure 2.7. For the plots shown in Figure 2.6 and 2.7,  $l_1 = 10$ ,  $l_2 = 5$  and  $l_p = 30$  are used and GSA is not added. By changing the  $K_{sc}$  value, keeping  $P_{in}$  same, initial stiffness of NSD remains the same but the rate at which NSD loses the preload increases as a result the NSD stiffens faster with higher stiffness of CS. By keeping the stiffness of CS same and increasing the preload, initial stiffness and stiffening point are proportional to the amount of pre-load but the stiffness beyond the stiffening point remains the same.

## 2.2.2 Significance of dual amplification

Using a pre-compressed spring to achieve negative stiffness has already been implemented in aerospace and automobile industry, but the real advantage of NSD comes from the dual amplification adapted in the device. The two amplification approaches are (1) double brace mechanism, wherein the point-E moves

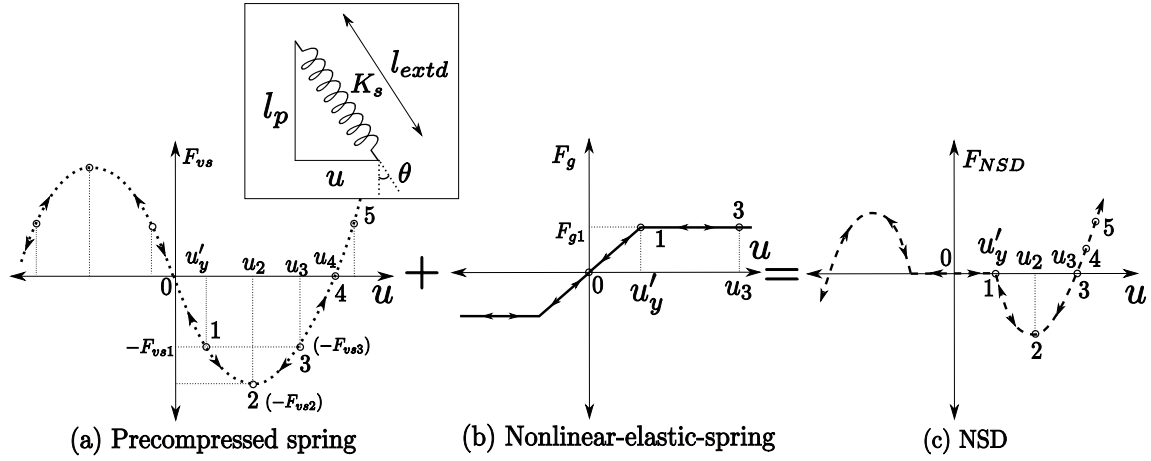


Figure 2.5: Schematic diagram of the force displacement plots of NSD

Force deformation plots for same  $P_{in}$  and different  $K_{sc}$

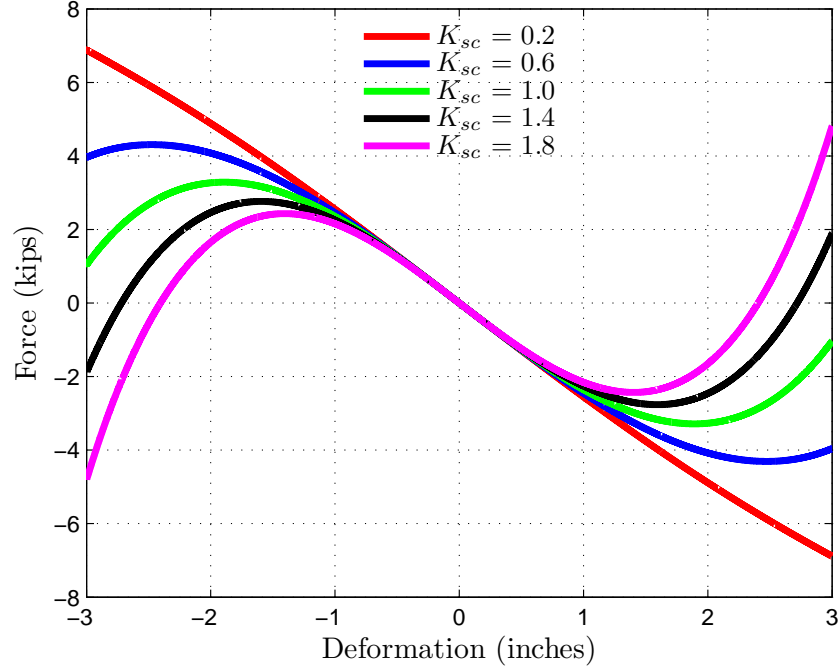


Figure 2.6: The behavior of NSD with the change in  $K_{sc}$  value

with the structure and (2) lever mechanism to amplify the deformation of point-D. To elucidate the advantage of the NSD developed in this study, three NSDs with different configurations are compared. The three systems are (1) the actual NSD (NSD-1), equivalent schematic diagram shown in Figure 2.8(a) (2)

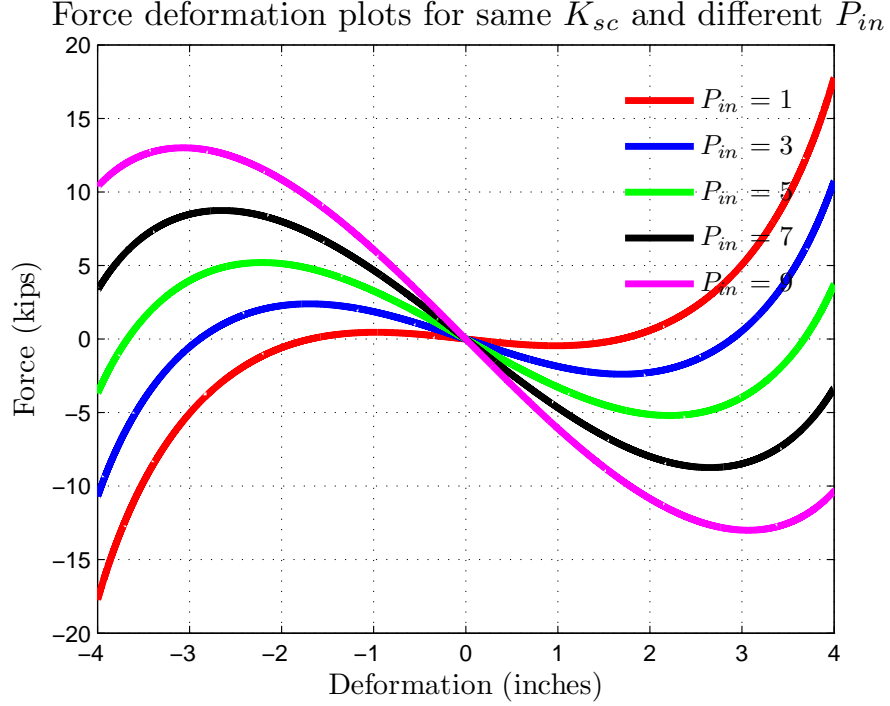


Figure 2.7: The behavior of NSD with the change in  $P_{in}$  value

NSD without the double chevron connection (NSD-2), schematic diagram shown in Figure 2.8(b) and (3) NSD without double chevron brace and the lever arm (NSD-3), schematic diagram shown in Figure 2.8(c). Although double chevrons are used in NSD-3, they do not amplify the deformation of NSD; it is just a provision to reduce the length of CS instead of spanning the floor height. In NSD-2, the point-E is directly connected to the bottom of NSD, so only the lever-mechanism amplify the deformation of point-D.

Since the connections and the geometry of the system has changed, the force exerted by NSD-2 is calculated using Eq. 2.15-2.19

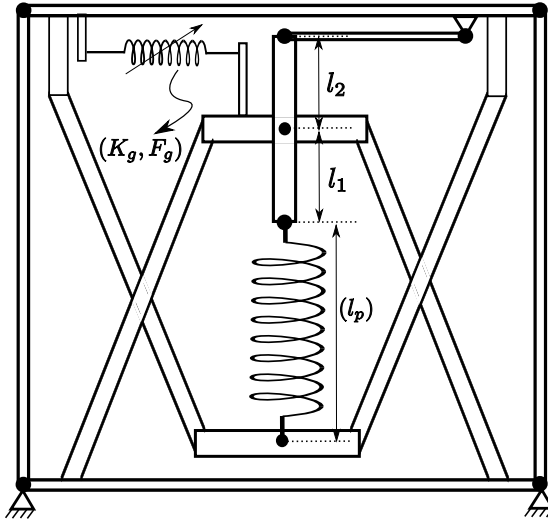
$$F_{NSD2} = F_{sc} \frac{\sin(\theta + \psi)}{\cos(\psi)} \quad (2.15)$$

$$F_{sc} = ((l_{extd} - l_p) - P_{in}/K_{sc}) K_{sc} \quad (2.16)$$

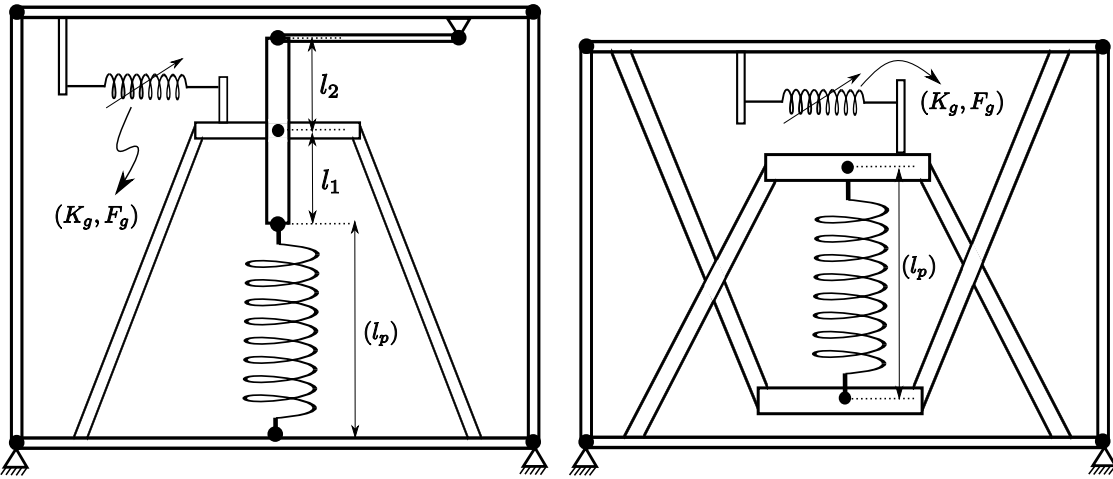
$$\sin(\psi) = \frac{u}{l_2} \quad (2.17)$$

$$\tan(\theta) = \frac{u l_1 / l_2}{l_{extd}} \quad (2.18)$$

$$l_{extd} = \sqrt{(u l_1 / l_2)^2 + (l_p + l_1 (1 - \cos(\phi)))^2} \quad (2.19)$$



(a) Equivalent schematic diagram of the NSD



(b) Schematic diagram of the NSD-1 without double chevron connection (c) Schematic diagram of the NSD-2 without lever and double chevron connection

Figure 2.8: Schematic diagram of the NSD-3

The force exerted by NSD-3 is given by Eq. 2.20-2.23

$$F_{NSD3} = F_{sc} \sin(\theta) \quad (2.20)$$

$$F_{sc} = ((l_{extd} - l_p) - P_{in}/K_{sc}) K_{sc} \quad (2.21)$$

$$\sin(\theta) = \frac{u}{l_{extd}} \quad (2.22)$$

$$l_{extd} = \sqrt{u^2 + l_p^2} \quad (2.23)$$

Assuming the dimensions  $l_p$ ,  $l_1$  and  $l_2$  are constant, the values of  $P_{in}$  and  $K_{sc}$  desired to achieve the same force-displacement behavior in all the three case is shown in Table 2.1. For NSD-1 and NSD-2 two cases are presented with different lever ratio,  $\epsilon = 1$  and  $\epsilon = 2$ . The force-deformation behavior of all the five systems is shown in Figure 2.9. In Table 2.1, the values of  $P_{in}$  and  $K_{sc}$  are scaled with the yield-strength and the stiffness of the structure for which they are designed and shown in parenthesis. Increasing the lever ratio will reduce the required stiffness of the CS by more than nine folds and the desired preload is reduced by more than three folds (compare the data of  $\epsilon = 1$  and  $\epsilon = 2$  in Table 2.1). The double chevron connection will reduce the demand on the stiffness and preload of the CS by 50%. With just the CS (NSD-3), the value of  $K_{sc}$  is two orders more than the NSD-1 and  $P_{in}$  is one order more than NSD-1. The preload and stiffness of CS in the case of NSD-1 ( $\epsilon = 2$ ) shows that “apparent weakening” is practically feasible even in structures with large mass. Next, the experimental setup used to test the NSD and the observed experimental results are compared with simulation results using the analytical models used in this chapter.

Table 2.1: Summary of the values used for different configurations of NSDs

Variable	NSD-1 ( $\epsilon = 2$ )	NSD-1 ( $\epsilon = 1$ )	NSD-2 ( $\epsilon = 2$ )	NSD-2 ( $\epsilon = 1$ )	NSD-3
$l_p$ (in)	30	30	30	30	30
$l_1$ (in)	10	10	10	10	-
$l_2$ (in)	5	10	5	10	-
$K_{sc}$ (kip/in)	2.7 (0.23)	25 (2.1)	4.5 (0.4)	76 (6.3)	1220 (101.7)
$P_{in}$ (kip)	8.9 (0.74)	27.2 (2.3)	11.5 (1)	47 (3.9)	15.83 (15.8)

## 2.3 Experimental Study

The force-deformation behavior of the NSD is very crucial for “apparent weakening” in yielding systems. So, characterizing the behavior of NSD is very crucial before the installation in the test structure. The experimental setup used to test the NSDs is briefed next.

### 2.3.1 Experimental setup

The setup used for testing the NSD is shown in Figure 2.10. The setup has a steel girder (bottom frame) and a support frame bolted to the concrete floor along North-South direction. Two spacers (also, steel girders shown in cyan color in Figure 2.10) are placed on the bottom frame and the bottom-channel of NSD is bolted to the top of spacers. Another steel girder (top frame) is placed on top of the device and two vertical actuators are connected to either ends of top frame to carry the weight of the frame. Lateral swaying of the frame is prevented by the lateral restraint frame (LRF). LRF has “U”-shaped hollow square

F-D plots of NSDs with different configuration

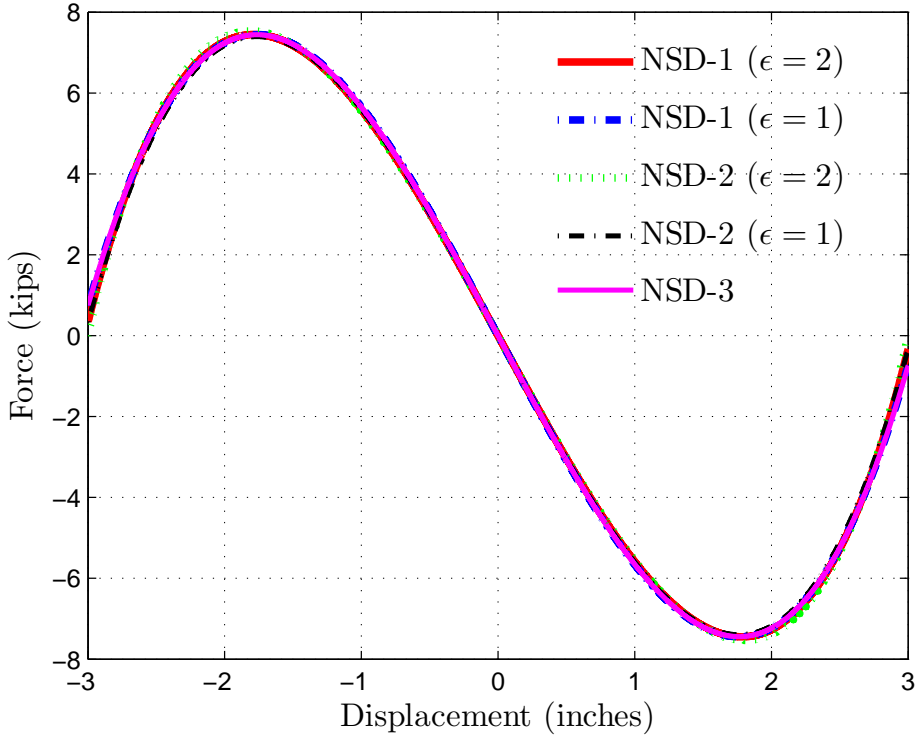


Figure 2.9: Comparing the F-D behavior of NSDs with different configuration

sections (HSS), shown in yellow color in Figure 2.10, bolted to the bottom frame and the free ends of the frame has steel plate assembly with bearings to avoid friction force between the top frame and LRFs. A horizontal actuator is connected to one end of the top frame and the support frame as shown in Figure 2.10. End angle assembly is used to connect the top of the NSD to the top frame. End angle assembly has “L”-shaped section with gussets and slotted holes, shown in Figure 2.11. One leg of the end angle assembly is bolted to the top-frame and the other leg is polished and flushed against the ball-transfer plate of NSD. The miniature ball transfer plate (BTP) is a  $3/16$  in. thick plate with 18 ball bearings ( $3/8$  in. diameter) embedded in the steel plate as shown in Figure 2.11. BTPs are bolted to the ends of NSD with two counter-sunk bolts. Bearings of BTP sit against the polished surface of end angle assembly and they prevent transfer of any vertical load from the NSD to the structure.

Two accelerometers and five string potentiometers are installed on the device to measure the acceleration and deformation of various points on the device. The deformations and force exerted by the NSD are measured using the in-built load cells and linear variable displacement transducers (LVDTs) of actuators. Data from all the sensors mentioned above is recorded in the Flex-test data acquisition system. Krypton K600 camera system is also used to measure the deformation of all the elements in NSD. Light emitting diode (LED) sensors are placed at 17 points on the NSD and the deformation of the device is captured

for all the tests. All the three actuators are operated in the displacement control mode. The two vertical actuators are programmed to maintain a specific distance between the bottom and top frames and the horizontal actuator is programmed to track a periodic signal with definite time-period and amplitude. The experimental results from these tests are discussed next.

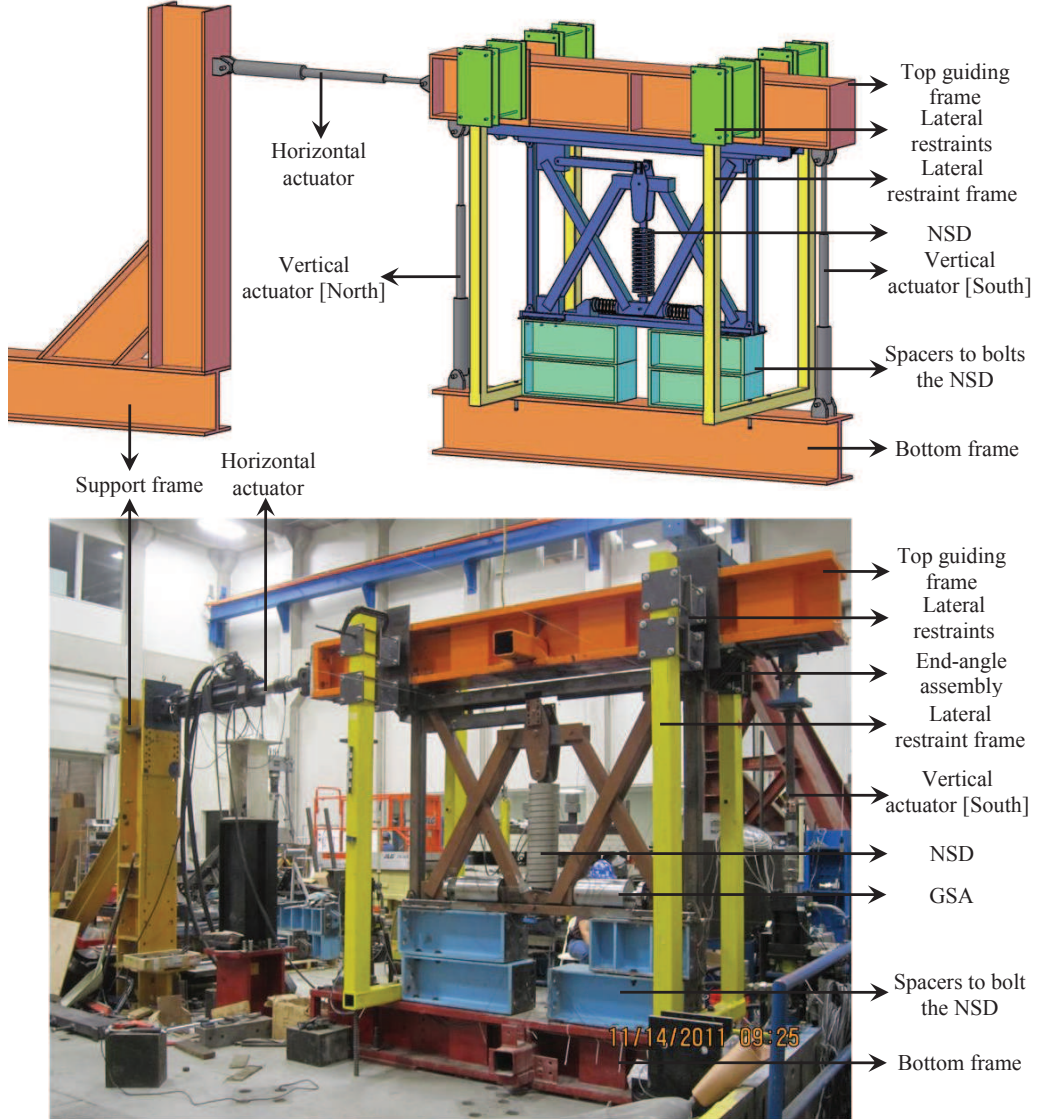


Figure 2.10: Schematic diagram and the photograph of NSD test setup

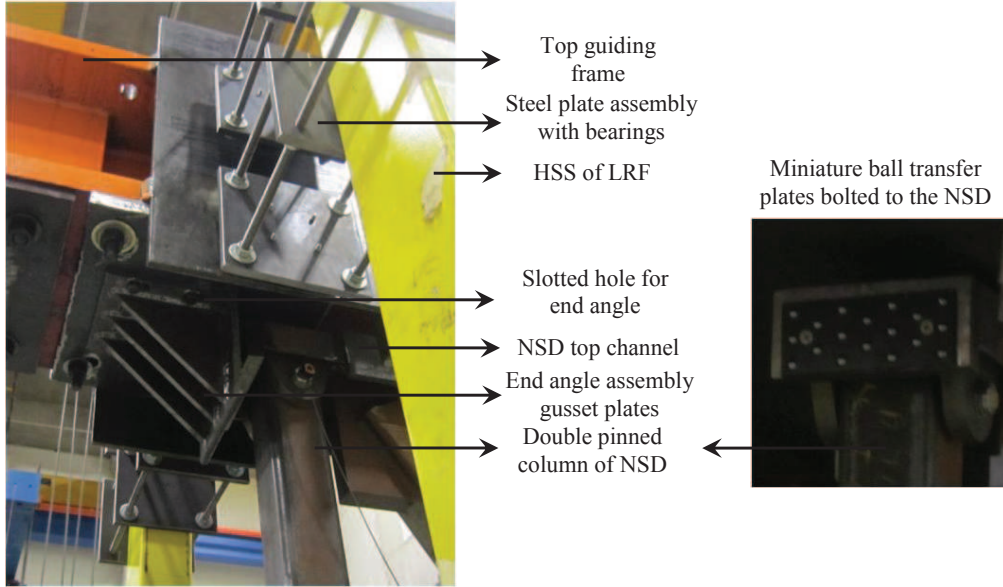


Figure 2.11: NSD connection with the top frame using end-angle assembly and the miniature ball transfer plates used to transfer the NSD load to topo frame

### 2.3.2 Experimental results

Two NSDs (NSD-East and NSD-West) are tested with this setup. Response of both the NSDs is calculated for three cycles of sinusoidal input at two different frequencies ( $0.1\text{ Hz}$  and  $0.01\text{ Hz}$ ). To obtain the dynamic properties of the NSD, the device has to be tested at frequencies higher than  $0.1\text{ Hz}$ . However, the tests couldn't be carried at higher frequencies because of the flexing in the restraining-frames. Each device is tested at  $1.5\text{ in.}$  amplitude first and then the amplitude is increased in steps of  $0.5\text{ in.}$  First step in testing the NSD is to characterize the behavior of test-rig and use that information to compensate the NSD test data.

Since the top-frame sitting on the two vertical actuators is like an inverted pendulum, the setup itself exhibits negative stiffness. The test rig is subjected to periodic displacement of  $3\text{ in.}$  amplitude and  $0.01\text{ Hz}$  frequency. The force deformation behavior of the NSD test rig is shown in Figure 2.12(a) and the measured actuator displacement and actuator force is shown in Figure 2.12(b,c). Test-rig has a negative stiffness of  $67\text{ lb/in.}$  and a consistent friction loop width of  $200\text{ lb.}$ , as shown in Figure 2.12(a). The force-displacement loops of the NSDs obtained from the test data should be compensated for the inverse-pendulum action of the test-rig. The actuator force measured using the load-cell is noisy so a low-pass butterworth filter is used to obtain clear data. Similar test has been performed at  $0.1\text{ Hz}$  frequency but the obtained data is inconsistent due to slipping and vibration of the LRF. Since the top frame is held in position using the side-restraining frames the friction significantly increased at high frequencies.

After calculating the slope and loop width of the test-rig from the F-D plots, NSD-West is placed in

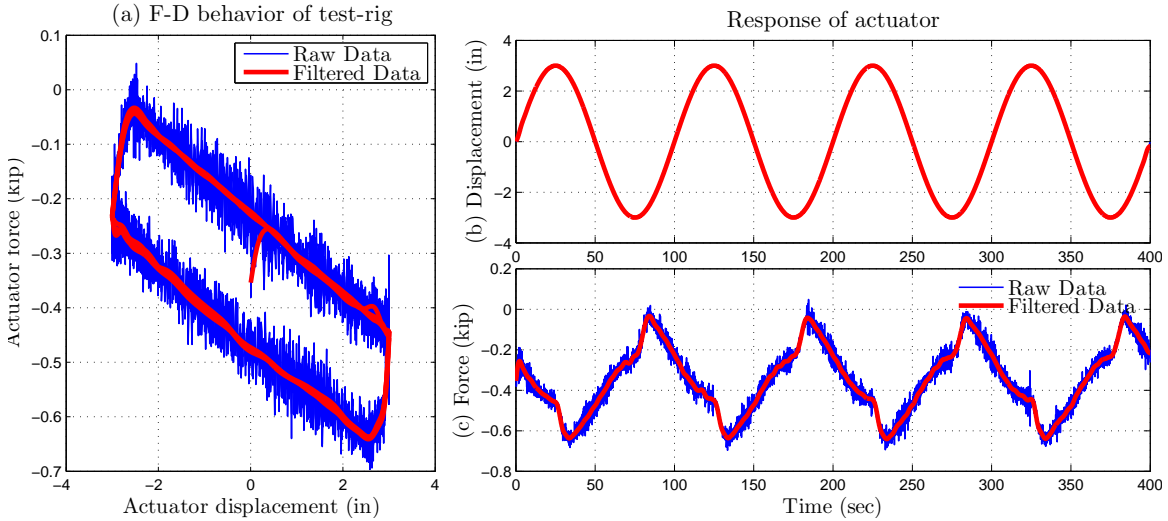


Figure 2.12: Force-deformation behavior of the test-rig

the test rig and tested at a displacement of 2.5 *in.* amplitude and 0.01 *Hz* frequency for three cycles of sinusoidal input. The choice of the displacement amplitude is based on the estimated maximum deformation of the device in the 3SFS tests. The F-D behavior measured from the load-cell and LVDT data is shown in Figure 2.13(a). The hysteresis loop in Figure 2.13(a) is due to the friction in the test setup and also the friction in the joints of NSD. As mentioned previously, the observed behavior of the NSD has to be corrected for the inverted pendulum action and the F-D loop of the device has to be centered. The compensated behavior of the NSD-West is shown in Figure 2.13(b). For the three cycles of the test, forward loop and the reverse loop are separated and averaged, shown in Figure 2.13(b). F-D behavior of individual loops (average of the forward and reverse loops) and mean of all the loops is also shown in Figure 2.13(b). It is clear from Figure 2.13 that the the NSD-West exhibits symmetric and retraceable force-deformation behavior. “Apparent yield-displacement” of the NSD-West is equal to 0.2 *in.*, peak negative force exerted is 7 *kip* at a displacement of 1.5 *in.* and the CS loses all the compression force at 2.5 *in.* displacement.

For the same test, using the experimental data from the Krypton camera system, the flexibilities of all the elements can be studied. The points A, B and E of the NSD (Figure 2.1) have the same displacement as shown in Figure 2.14(a). This confirms that (1) lever-arm undergoes very small rotations ( $u = u'$ ) and (2) CB2 is not flexible for NSD-West. The deformation of point-C and point-D are compared with point-A in Figure 2.14(b) for the NSD-West. The ratio of the deformations of point-D and point-A, shown in Figure 2.14(b), is equal to the lever ratio of the device and this confirms that there is no flexing in the pivot plate. The point-C of NSD-West has undergone little or no deformation (<0.03 *in.*) which means the CB1 is also not flexible for NSD-West. Two LEDs are also placed on the steel casing of the GSAs and the measured deformation is shown in Figure 2.14(c). Since the LEDs are on the steel casing the deformation shown in Figure 2.14(c) is only the deformation of the softer springs ( $S'_1$  and  $S''_1$ ). Each GSA deforms on

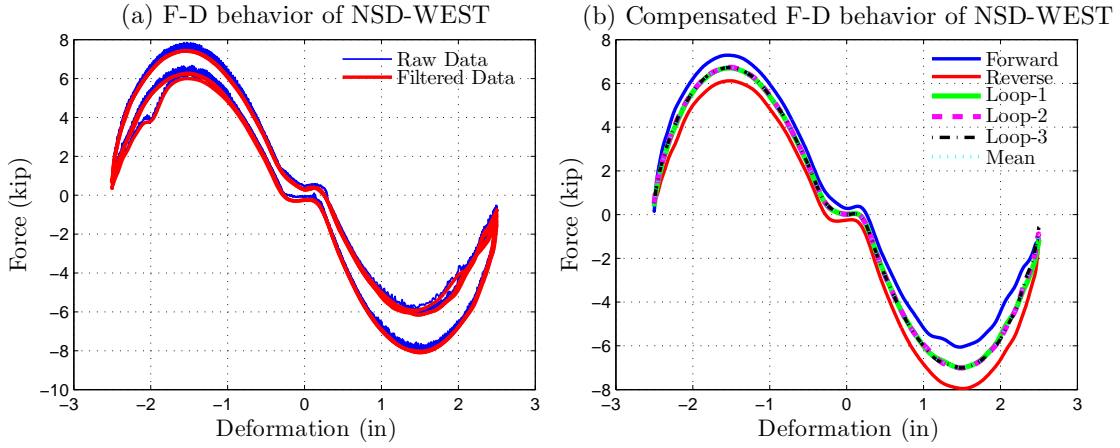


Figure 2.13: Observed experimental force-deformation behavior of NSD-West

one side as shown in Figure 2.14(c). The gap in which the GSA-left and GSA-right remain undeformed, shown in Figure 2.14(c), is equal to 0.4 in. This confirms with the force-deformation plots or NSD-West, shown in Figure 2.13, that the “apparent yield-displacement” is 0.2 in. which means that the stiff springs of both GSAs ( $S_2$ ) deforms for the first 0.2 in. on either side.

NSD-East is also tested in same setup to ensure that both the devices exhibit the desired behavior. NSD-East is also tested at a displacement of 2.5 in. amplitude and 0.01 Hz frequency for three cycles of sinusoidal input. The F-D behavior measured from the load-cell and LVDT data is shown in Figure 2.15(a) and the compensated behavior of the NSD-West is shown in Figure 2.15(b). For the three cycles of the test, averaged individual loops are shown in Figure 2.15(b). Unlike NSD-West, the F-D behavior of NSD-East is asymmetric but the loops are retraceable. The peak force in the positive direction is 7 kip at 1.3 in. and the peak force for negative displacements is 9.5 kip at 1.7 in. Also, the stiffness of the stiff spring in GSAs is significantly larger than the negative stiffness of the CS; hence the NSD-East exhibit positive stiffness for deformations  $|u| < 0.2$ . “Apparent yield-displacement” of the NSD-East is also equal to 0.2 in.

The displacement of points A, B and E of NSD-East are similar and they are symmetric about zero displacement as shown in Figure 2.16(a). The deformation of point-C and point-D are compared with point-A in Figure 2.16(b). The deformations of point-D is not symmetric about the zeros-axis, shown in Figure 2.14(b). This could be because of the differential flexibilities of chevron braces CB1 and CB2. The point-C of NSD-East has undergone a deformation of 0.06 in.) which means that CB1 of NSD-East is also more flexible than the NSD-West. The deformation of the GSAs is shown in Figure 2.14(c). GSA-left has undergone 0.3 in. more deformation than the GSA-right, shown in Figure 2.14(c). This also confirms the differential flexibilities of chevron braces in NSD-East. Next, the analytical models presented in this chapter are used to capture the observed experimental behavior.

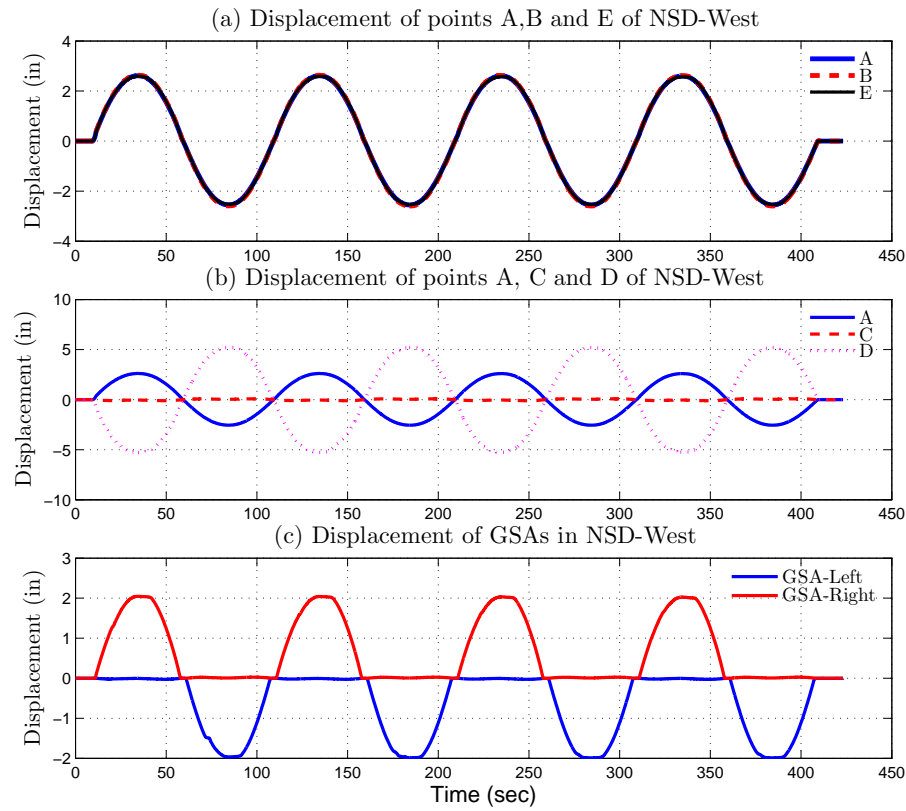


Figure 2.14: Comparison of the displacements of various points on NSD-West

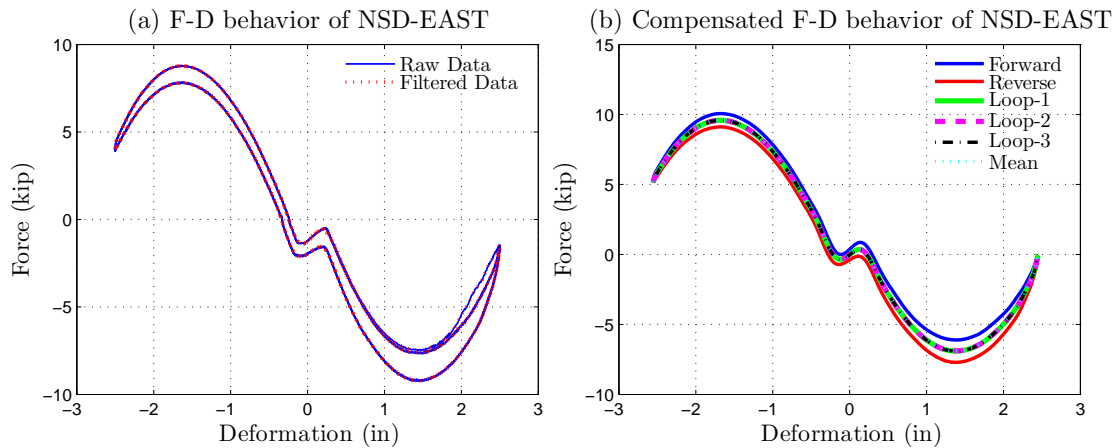


Figure 2.15: Observed experimental force-deformation behavior of NSD-East

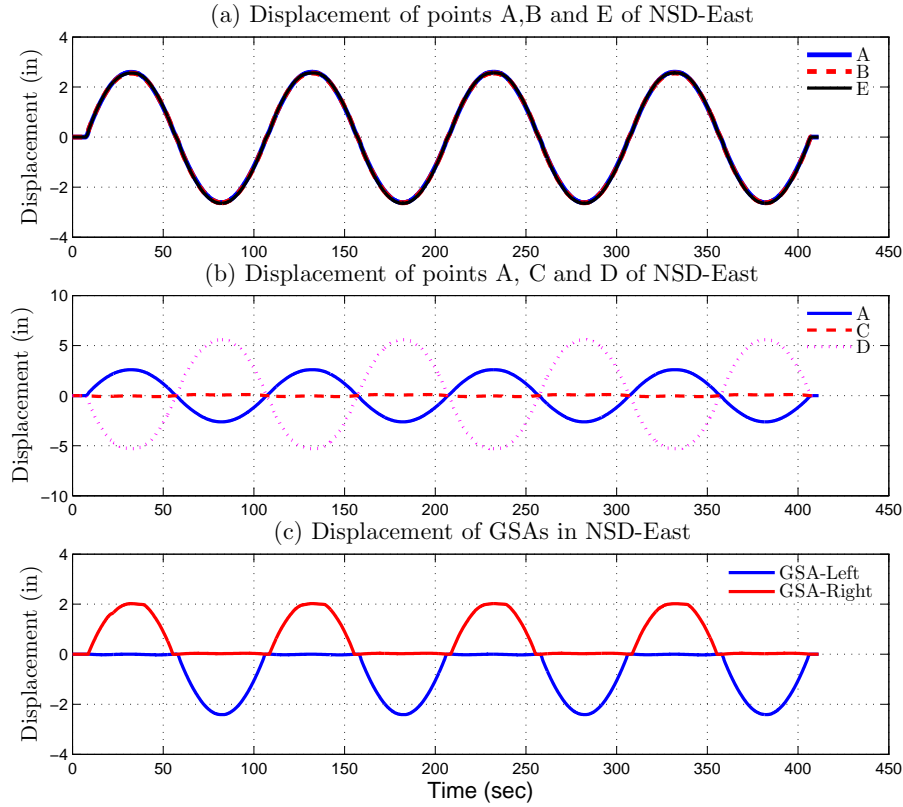


Figure 2.16: Comparison of the displacements of various points on NSD-East

### 2.3.3 Analytical results

NDS-West and NSD-East designed to exhibit identical properties, however, because of the uncertainty in the material properties and the connections different F-D behavior has been observed in the experimental results. Some of the variables in the analytical are measured ( $L_1$ ,  $L_2$  and  $L_p$ ) and the feasible range for the remaining variables is also known. Set of feasible values for these variables are determined by calibrating the analytical model with the observed experimental results. Comparison of the experimental and predicted F-D loops of the NSD-West are shown in Figure 2.17(a) and the components of the analytical model are shown in Figure 2.17(b). Since the observed behavior of NSD-West is symmetric, the analytical model developed in this chapter can capture the observed behavior very accurately. Calibrated values of all the variables used for the analytical model of NSD-West are shown in Table 2.2. From Figure 2.17, it is clear that all the key features including, “apparent yield-displacement”, peak NSD force and the initial stiffness of NSD for both experimental data and the analytical model are in good agreement. Bilinear-elastic behavior of the GSAs in NSD-West and the lateral force exerted by the CS are shown in Figure 2.17.

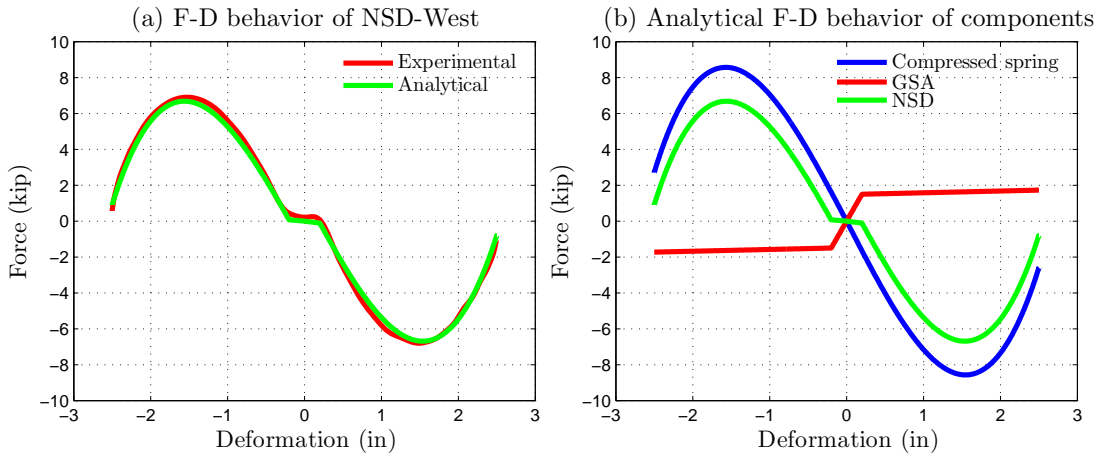


Figure 2.17: Comparison of the experimental and analytical F-D behavior of NSD-West

Since the NSD-East tend to exhibit asymmetric loops, this behavior can be captured analytically by writing Eq. 2.14 as

$$F_{NSD}(u) = F_{vs}(\tilde{u}) + F_g(u) + K_f(u) + P_o \quad (2.24)$$

where,  $\tilde{u} = u - u_o$  is the linear transformation of  $u$  and it is introduced to shift the F-D curve of CS along the displacement-axis and  $P_o$  is the constant force added to shift the F-D curve along the force-axis. It should be noted that the shift is created only for the CS and not for the GSA or the chevrons. The need for creating this shift in the NSD equation of motion is explained next.

GSAs, shown in Figure 2.2, have a through threaded-rod that maintains the pre-compression load in the soft-spring. The same threaded-rod is used to bolt the GSAs to the bottom-angle of NSD. The stiff-spring is just placed in the cup and flushed against the bottom of CB2. The GSAs are designed to not exert any force on the CB2 in the undeformed configuration  $u = 0$ . However, due to the misalignment and tolerances in springs and the threaded-rod of GSAs, there will be a net force acting on CB2 even when the NSD (and structure) is in undeformed position. This residual force is addressed through an artificial shift as given in Eq. 2.24. Using the modified equation, the experimental and analytical F-D loops of NSD-East are compared in Figure 2.18(a). The F-D behavior of components shown in Figure 2.18(b) clearly shows the translation of the displacement and force of CS. The values of all the variables used to capture the behavior of NSD-East are shown in Table 2.2.

## 2.4 Summary

In this chapter, detailed description of the working principle and the analytical models of the NSD are presented. The key feature of the device, the dual amplification achieved from the double chevron and the lever-arm mechanism, is highlighted with a numerical study. From the practical point of view, it has been

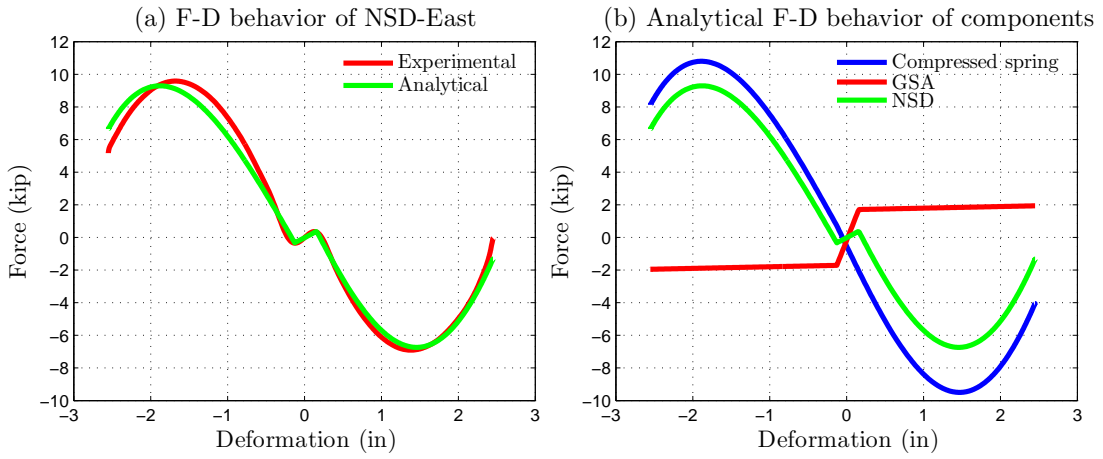


Figure 2.18: Comparison of the experimental and analytical F-D behavior of NSD-East

Table 2.2: Values of the parameters used in NSDs

Variable	Unit	NSD-West	NSD-East
$l_1$	inch	10	40
$l_2$	inch	5.13	4.99
$l_p$	inch	30	30
$K_{sc}$	kip/in	3.8	3.8
$P_{in}$	kip	2.8	3.25
$K_{S1}$	kip/in	0.1	0.1
$K_{S2}$	kip/in	7.5	12
$P_{S1}$	kip	1.5	1.6
$K_{CB1}$	kip/in	122	65.4
$K_{CB2}$	kip/in	400	400
$P_o$	kip	-	0.75
$u_o$	inch	-	0.14

shown that the demand on the preload requirements to achieve the desired negative stiffness in real life structures can be significantly reduced using the NSD. The fact that the device is completely passive and still has the adaptability to change the device properties offline makes it a very powerful tool in structural control.

An experimental study carried to characterize and evaluate the behavior of NSDs has also been reported. The force-deformation loops obtained from the experiments have confirmed that the NSDs exhibits elastic behavior. The behavior of NSDs predicted using the analytical models is in excellent agreement with the observed experimental results.



## Chapter 3

# Experimental Setup and Component Testing

The goal of the experimental study is to

1. show the effectiveness of “apparent weakening” in elastic and mild-yielding single degree of freedom (SDOF) systems
2. study the behavior of structure and NSD assembly in heavy-yielding systems
3. study the impact of NSDs in multi-story structures

It has been found from the preliminary analytical study that for the heavy-yielding tests, all the four columns in first story will yield after every ground motion test. Since it is extremely time consuming and uneconomical to disassemble the entire structure to replace the columns, a versatile and generic test structure is needed that can be used to achieve all the three goals with minimum cost and effort. The three-story frame structure (3SFS) built and tested in this study posses all these attributes.

3SFS was first developed by Kusumastuti et al. (Kusumastuti et al., 2005) to study the behavior of structural systems near collapse. The first structural model developed was a one-third scale, three-story three-bay steel structure. 3SFS is designed to have sacrificial elements (components that will be severely damaged for strong ground motions) that can be readily replaced upon damage and the structure can be further tested without disassembling the entire frame. Using the versatility of the model, Kusumastuti et al. (Kusumastuti et al., 2005) also tested and characterized the behavior of irregular-structures for a suite of ground motions. 3SFS has two independent support systems: moment resisting frames or simply the moment frames (MFs) to bear the lateral inertial forces exerted on the structure and gravity frames (GFs) to carry the gravity load of the entire structure. Since the two frames are completely decoupled and the entire gravity load is borne by the GFs, the sacrificial elements in the MFs can be replaced easily without disassembling the entire structure.

In this study, the experiments on the 3SFS were carried at the NEES equipment site at University at Buffalo, SUNY. Two NSDs and a viscous damper are installed in the first floor. The experiments on the 3SFS have been performed in two phases. In the first phase, the top two floors of the 3SFS are braced, essentially making the 3SFS a SDOF system. The SDOF system is subjected to a series of ground motion with increasing peak-ground-acceleration (PGA) to demonstrate the concept of “apparent weakening” in elastic and yielding structures. In the second phase, the braces in the top two floors are removed and the behavior of NSDs in MDOF systems is studied. Three different types of systems are tested in both the phases for five ground motions from PEER database:

1. 3SFS or the base structure (BS): NSDs and the damper are disconnected
2. 3SFS and the NSD assembly (NS): NSDs are connected and the damper is disconnected
3. 3SFS, NSDs and damper assembly (AS): both NSDs and the damper connected

Since replacing columns after every heavy-yielding test was expensive, only NS and(or) AS are tested for all the ground motions. To compare all the three systems, response of the missing system is simulated using the calibrated analytical models.

The contents in this chapter are organized as follows: Section-3.1 presents the details of all the components in 3SFS and their connections. In section-3.2, the analytical models of NSD and dampers and the installation in the 3SFS is presented. A brief discussion on the instrumentation of the test setup and data acquisition is given in section-3.3. Section-3.4 presents the experimental results of the testing of 3SFS and the analytical model used to capture the experimental behavior. The key observations from these test results and comparisons are summarized in section-3.5

### **3.1 Three-story frame structure (3SFS)**

The 3SFS is also a one-third scale three-story fixed base structure, similar to the structure developed by Kusumastuti et al. (Kusumastuti et al., 2005), but it only has one-bay. 3SFS is installed on a single-axis shake table is shown in Figure 3.1, the picture is taken from the East. The shake table is aligned to move the structure in north-south direction (longitudinal direction). A support frame (orange color in Figure 3.1), located to the south of the shake table, is used for the installation of string-potentiometers to measure the displacement at various heights of 3SFS. Megadac data acquisition system, located at the foot of support frame, is used to record the experimental data. Overhead crane is used to install the 3SFS on shake-table and also to hold the 3SFS as a precautionary measure, in case if the 3SFS collapse during the tests.

3SFS has three components, shown separately in Figure 3.2 (1) moment resisting system, designed to resist the inertial forces of the floor system (2) vertical support system, designed to carry the gravity load of the floor system (3) floor system containing three 3.5 *in.* thick steel plates that form the floor slabs. The damageable lateral load resisting system and the undamageable vertical load system are completely

disjoint and they are connected to the floor system separately. Details of these components and their assembly is discussed next.

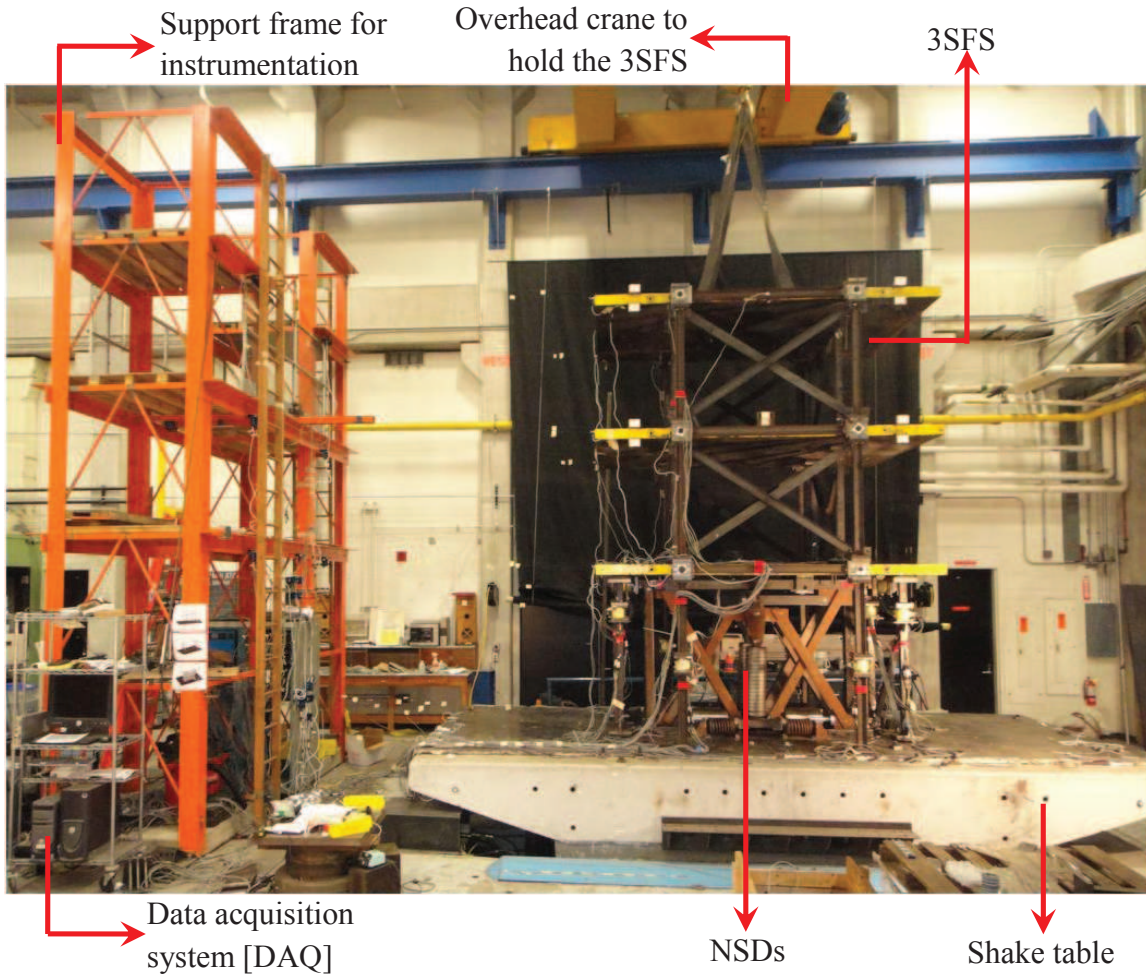


Figure 3.1: 3SFS installed on the shake table at NEES equipment site, University at Buffalo, SUNY

### 3.1.1 Moment resisting system

The moment resisting system has two moment frames (MF), MF-east and MF-west, aligned along the north-south direction as shown in Figure 3.2(a) (also shown as red colored frames in Figure 3.3 and Figure 3.4). Each moment frame has five components: columns, beams, beam-column blocks, cross-braces and load-cells; all the components are marked in Figure 3.2(a), 3.3 and 3.4. Columns and beams in all the three stories are made of standard steel section S3×5.7 and they have 1 *in.* thick steel plates with through holes welded on either sides. Schematic drawings of all the elements, with dimensions are shown in Appendix-B.

The columns and beams are connected to the beam-column block, shown in Figure 3.5. Beam-column

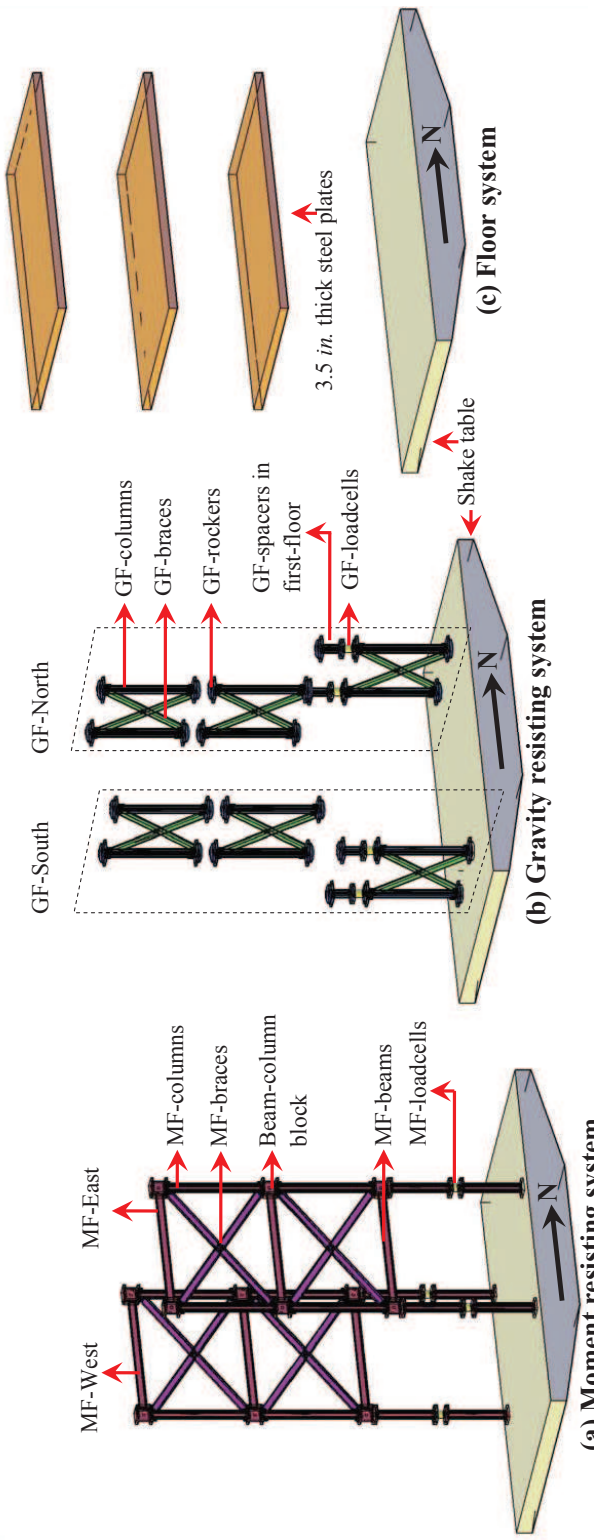


Figure 3.2: Schematic diagram showing the components in 3SFS

block is a machined steel block (“I”-shaped cross-section) with threaded holes in the vertical direction to connect the columns and through holes along longitudinal direction to connect the beams. It also has a slotted hole ( $1\frac{1}{16}$  in. diameter and 2 in. long) in east-west direction to connect the moment frames to the steel-slabs as shown in Figure 3.5. The MFs are connected to the steel slabs with a one inch bolt that passes through the vertical slotted hole of beam-column block and is threaded into the steel slab. The bolt can freely move in the vertical slot of the beam-column block so the gravity load of slabs cannot be exerted on the moment frame. The entire gravity load is carried by the gravity frame. When the MF sways in the longitudinal direction, the inertial forces of the steel slabs are transferred to the MFs through the one inch bolt and the slack in the vertical slot will prevent the transfer of gravity load to MF columns. To avoid the frictional forces between the beam-column block and the bolt a teflon washer is placed on either side of the block. Accelerometer and the string-pot holder placed on the beam-column block can be seen in Figure 3.5.

For the tests in the first two phase of this study, the behavior of AS in SDOF system has been studied. So, the top two stories of the moment frame are braced using steel sections C3x4.1 making the structure essentially a SDOF system as shown in Figure 3.2(a), 3.3 and 3.4. The diagonal braces are also bolted at the center. The columns and braces of the second and third floor of MF have the same configuration and dimensions. In the first floor since the floor height is taller than the other two and also the load-cells are added the configuration is different. To measure the base shear experienced by the columns in first story one load-cell is added to each column. Since the shear in the middle of the columns in first story is very low, load-cells are strategically placed at this point. The clear spacing between the two MFs is equal to 78.75 in (same as the width of steel slab, details in Appendix-B).

### 3.1.2 Vertical support system

Vertical support system is designed to carry the gravity load and it cannot provide any resistance to the lateral load. This is achieved by creating a hinge-hinge end connection for all the gravity columns. Each story has two gravity frames (GFs), GF-North and GF-South, aligned in the east-west direction (perpendicular to the plane of motion) symmetrically on either side of the center line of steel slabs as shown in Figure 3.2(b). Gravity frame consists of two S3x5.7 columns and each column has hinge connections at either end. Opposite corners of the gravity columns in each gravity frame are connected with L2x2x0.25 braces to prevent torsion in the 3SFS, shown in Figure 3.2(b), 3.4 and 3.6. Gravity column hinges are made out of a steel plate having a convex surface with a 10 in. radius on one side, and a flat surface on the other side, shown in Figure 3.6. The convex side of the hinge-plate sits against the steel slabs or base plate to provide axial support and the flat surface faces the gravity column end plate. Four oversize holes were provided in the hinge-plate, gravity column end-plate, and steel slab. Steel pins are used to connect the end plate of the gravity column to the hinge-plate and the steel slab, preventing any possible slip as shown in Figure 3.6. The steel pins are used just to hold the gravity frames but not to rigidly connect it to the floor. Since the gravity frame has hinge-plates with a convex surface in all the four corners, the gravity

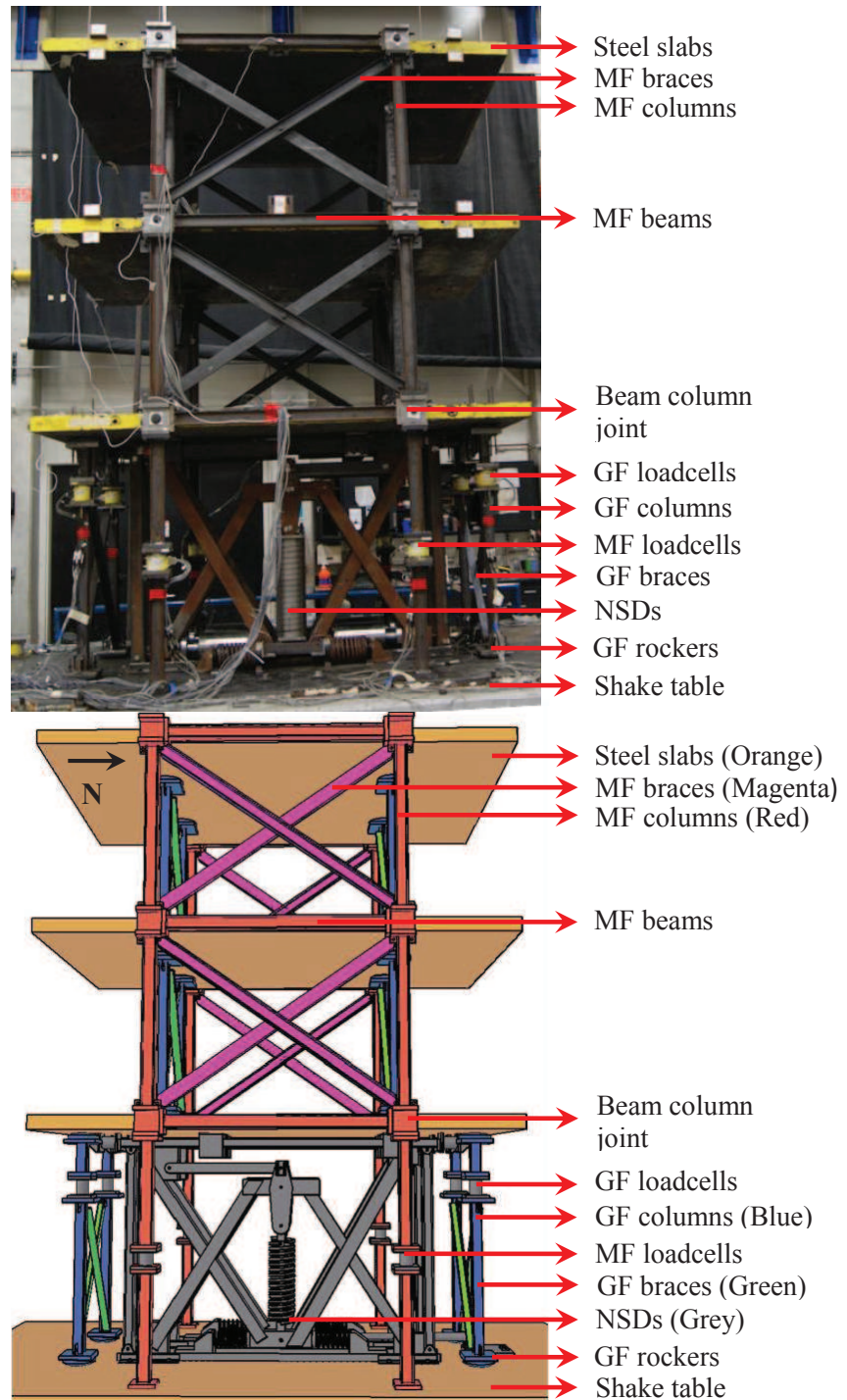


Figure 3.3: Photograph and schematic diagram of 3SFS (Elevation)

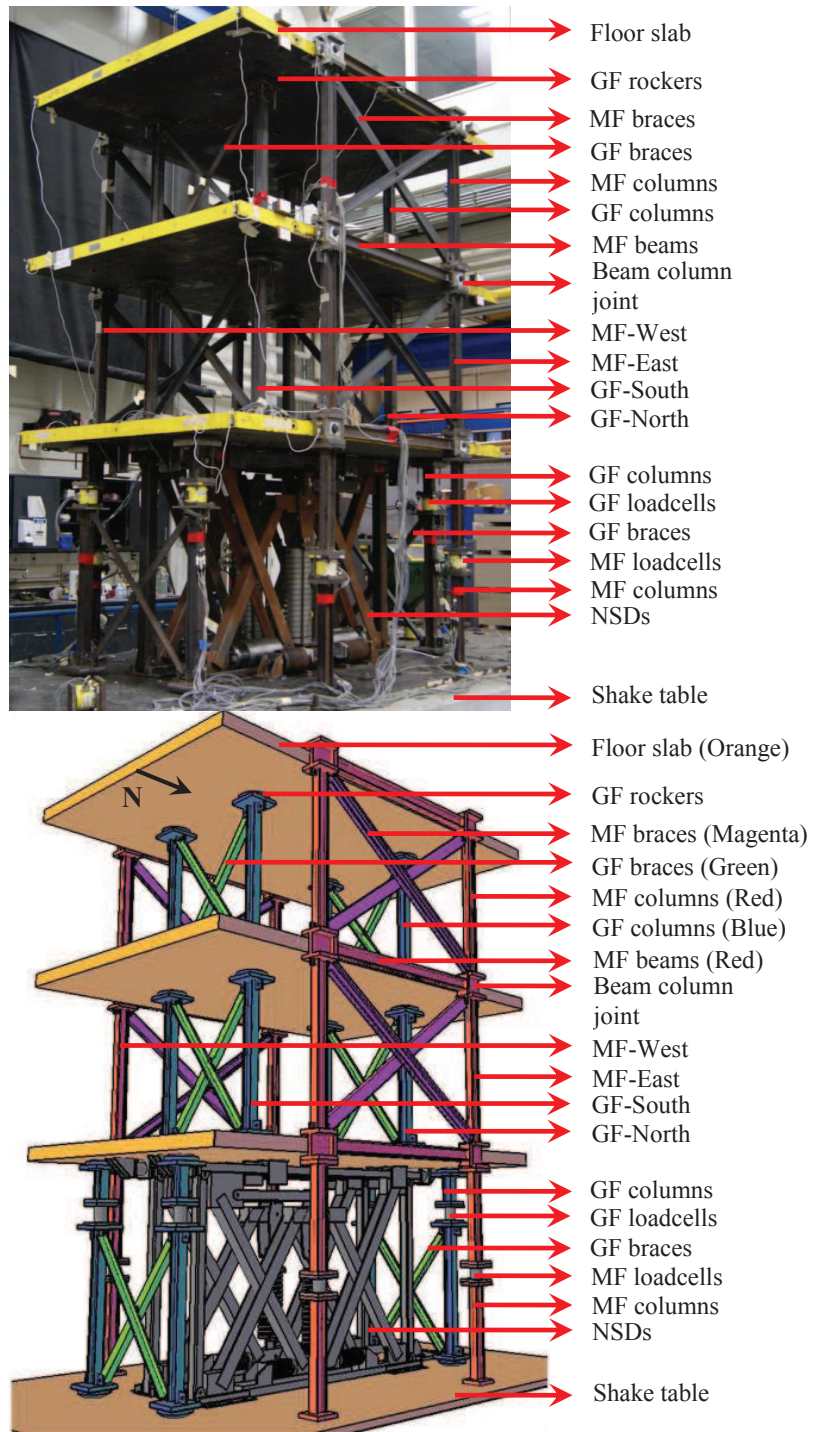


Figure 3.4: Photograph and schematic diagram of 3SFS (Isometric view)

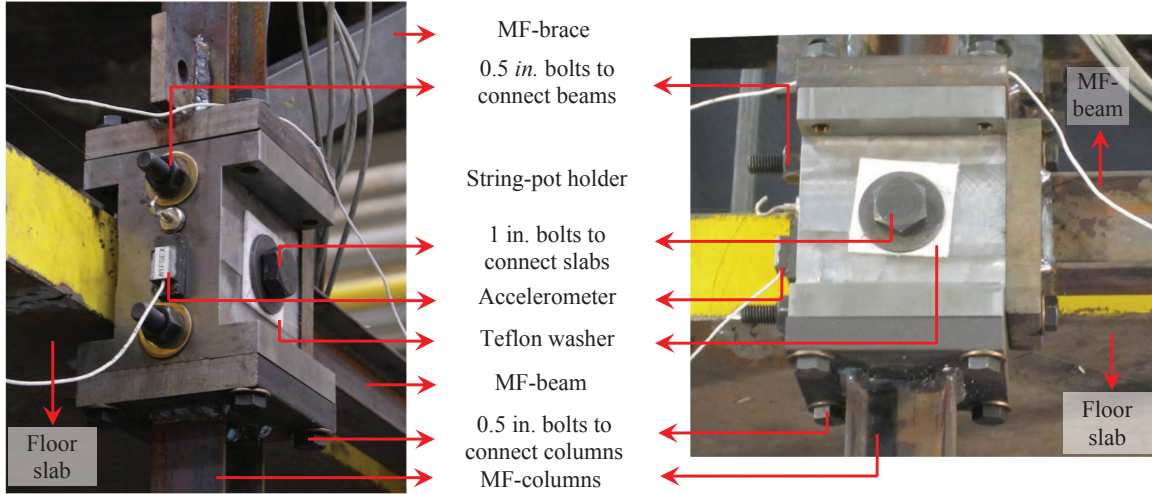


Figure 3.5: Beam-column block showing the connections

frame can rock freely under lateral loads without changing the vertical geometry of the model.

The gravity frames in second and third story are placed between the adjacent columns of MF-east and MF-west as shown in Figure 3.4. In Figure 3.3, the gravity frames in second and third floor cannot be seen clearly because they are right behind the moment frame columns. In the model developed by Kusumastuti et al. (Kusumastuti et al., 2005), gravity frames in all the three stories were aligned. In this study, since the NSDs are placed in the first story and they cannot be accommodated in the clear space available between the gravity frames, they are moved towards the edge in the first story. Similar to the MFs, the gravity columns in first story have load cells to measure the gravity load of the structure and also the shear force in case if the gravity frame provides any lateral resistance. Although the height of first-floor is 13.25 in. more than the other two floors, to avoid confusion and to maintain uniformity, six identical gravity frames are fabricated. To span the entire floor, load cells and spacers are added on top of the GFs in first floor as shown in Figure 3.2(b) and 3.4.

### 3.1.3 Floor system

The floor system is required in 3SFS to generate inertia forces. It comprises of three 3.5 in. thick steel plates located at a height of 60.5 in., 107.75 in. and 155 in. from the top of the shake table, shown in Figure 3.2(c), 3.4 and 3.6. Weight of each plate is 8.5 kip. The gravity load exerted by the floor system will be of a huge concern during the yielding tests of 3SFS. In case if the columns of the frame has a huge permanent drift, the gravity load of the floor system is sufficient to collapse the structure due to P- $\Delta$  effect. To prevent the collapse of structure, two separate support systems (MF and GF) are developed. The weight of all the plates is transferred to the shake table through the gravity frame. The inertial forces of the floor system are transferred only to the moment frame through the 1 in. bolts. The hinges will

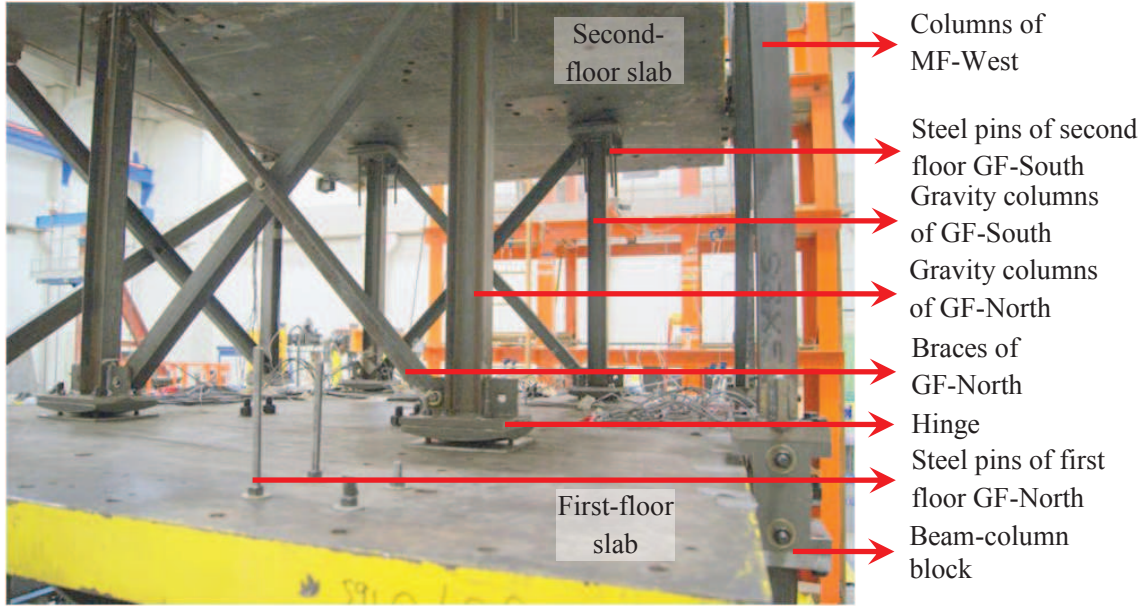


Figure 3.6: Photograph of gravity frames in the second floor of 3SFS

prevent the transfer of inertial forces to the gravity frame.

## 3.2 NSD and Damper Installation in 3SFS

To study the role of NSD and damper in AS and also to demonstrate the effectiveness of “apparent-weakening”, response of three different systems have to be studied experimentally for each ground motion data. In order to prevent the delays in connecting and disconnecting the NSDs and damper special connections are provided between the 3SFS, NSD and damper. These connection details are presented in this section.

### 3.2.1 Negative stiffness device

Detailed description of NSD, working principle and the experimental studies to characterize the behavior of NSD are presented in chapter 2. From the preliminary analysis, based on the observed experimental behavior of NSD, it has been found that the negative stiffness of NSDs is more than what is required and the predicted behavior of 3SFS and NSD assembly was not complying with the desired behavior (assembly force should always be in first and third quadrant of F-D plot), shown in Figure 3.7(a). The discrepancy in the stiffness is due to fabrication tolerances and flexibilities of chevron braces in NSD.

The behavior of the assembly can be improved by either reducing the negative stiffness of NSD or adding positive stiffness externally. The negative stiffness can only be reduced by changing the pre-loaded

spring (explained in section-2.2) and since it is expensive to replaced the machined spring, two additional GSAs (GSA-2) are added to the NSDs to reduce the negative stiffness of NSD, as shown in Figure 3.8. GSA-2 is tested separately and using the experimental data, the predicted force deformation behavior of 3SFS and NSD assembly with the addition of GSA-2 is shown in Figure 3.7(b). The behavior shown in Figure 3.7(b) is very close to the desired behavior. Readers should note that the actual NSD has only one GSA (GSA-1) but in this study an extra GSA (GSA-2) is added to the system.

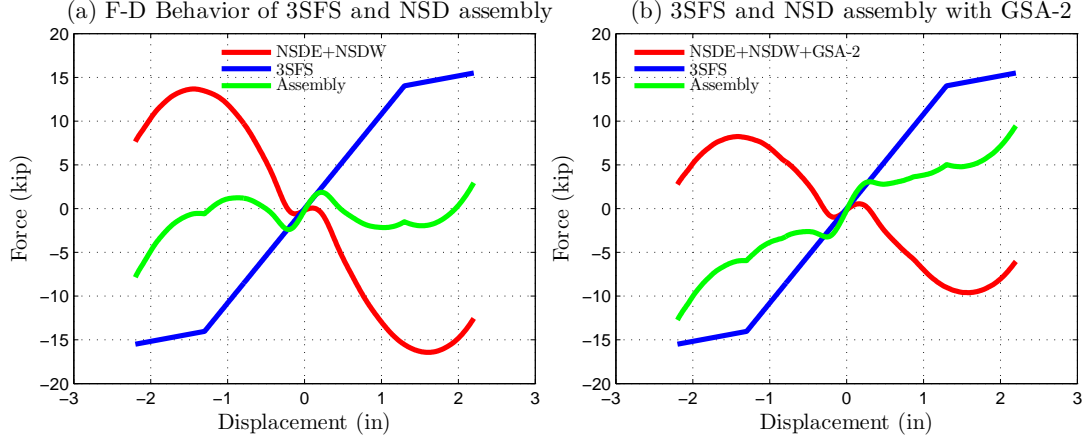


Figure 3.7: Predicted behavior of 3SFS and NSD assembly w/ and w/o GSA-2

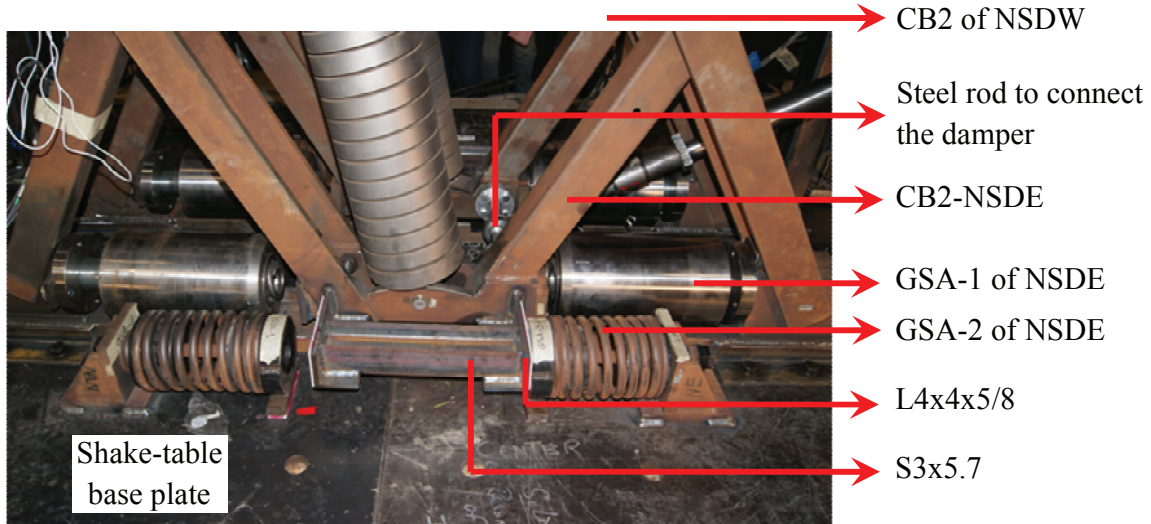


Figure 3.8: GSA-2 connected to the CB2 of NSD

Side view and front view of the NSDs installed in the first floor of 3SFS is shown in Figure 3.9 and

3.10. The bottom of the NSDs is bolted down to the shake table. A clear space of 2 *in.* is provided at the top between the NSD and the first floor slab. Two restrainers are placed around the top channel of NSD and bolted to the first floor slab to prevent any out of plane motion, shown in Figure 3.9. An “L” shaped assembly with gussets referred as end-angle assembly is designed as an interface to connect the NSD to the first story slab, shown in Figure 3.11. One flange of the end-angle assembly is bolted to the first story slab and a load-cell is fastened on the other flange facing the NSD, shown in Figure 3.11. Miniature ball transfer plates are fixed to both the ends of NSD (explained in section 2.3.1) and they are flushed against the load-cell connected to the end-angle assembly. The ball transfer plates have very low friction and they can only transmit lateral load and will not exert any vertical force on the structure.

The flange of the end-angle assembly that is connected to the floor-slab has slotted holes (1.5 *in.* long) for eight 1/2 *in.* bolts, shown in Figure 3.11. The slotted holes along with a 1 *in.* spacer, facilitate connecting and disconnecting the NSDS. By moving the end-angle assembly towards the edge of the floor slab and removing the spacer, a clear space of 2.5 *in.* is provided between the end angle assembly and the NSD. Since the maximum deformation of the floor is less than 2 *in.*, the NSDs can be easily connected and disconnected from the 3SFS just with the end angle assembly. Before disconnecting or connecting the end-angle assembly, the preloaded springs of the NSDs are compressed using four 3/4 clamp bolts until the NSD is in the undeformed configuration. Although the initial stiffness of NSD is positive for this particular NSDs, the preloaded spring is clamped as a safety measure. The role of load-cells placed between the NSD and end-angle assembly is to measure the force exerted by each NSD separately.

Force exerted by the NSD with the additional GSA and all the flexibilities, derived in chapter 2, is given by Eq. 3.1

$$F_{NSD} = - \left( \frac{P_{in} + K_{sc} l_p}{l_{extd}} - K_{sc} \right) \frac{l_1}{l_2} \left( 2 + \frac{l_2}{l_1} + \frac{l_p + l_1}{\sqrt{(l_2^2 - u^2)}} \right) u + F_{g1} + F_{g2} + F_f \quad (3.1)$$

where,  $F_{g1}$ ,  $F_{g2}$  and  $F_f$  are the forces exerted by GSA-1, GSA-2 and chevron flexing, respectively.

$$F_{g1} = \begin{cases} K_{S2}^1 u & \text{if } |u| \leq \frac{P_{S1}^1}{K_{S2}^1}, \\ P_{S1}^1 + \frac{K_{S1}^1 K_{S2}^1}{K_{S1}^1 + K_{S2}^1} & \text{if } |u| > \frac{P_{S1}^1}{K_{S2}^1} \end{cases} \quad (3.2)$$

$$F_{g2} = \begin{cases} K_{S2}^2 u & \text{if } |u| \leq \frac{P_{S1}^2}{K_{S2}^2}, \\ P_{S1}^2 + \frac{K_{S1}^2 K_{S2}^2}{K_{S1}^2 + K_{S2}^2} & \text{if } |u| > \frac{P_{S1}^2}{K_{S2}^2} \end{cases} \quad (3.3)$$

$$F_f = \begin{cases} K_{f1} u_f & \text{if } u \leq 0, \\ K_{f2} u_f & \text{if } u > 0 \end{cases} \quad (3.4)$$

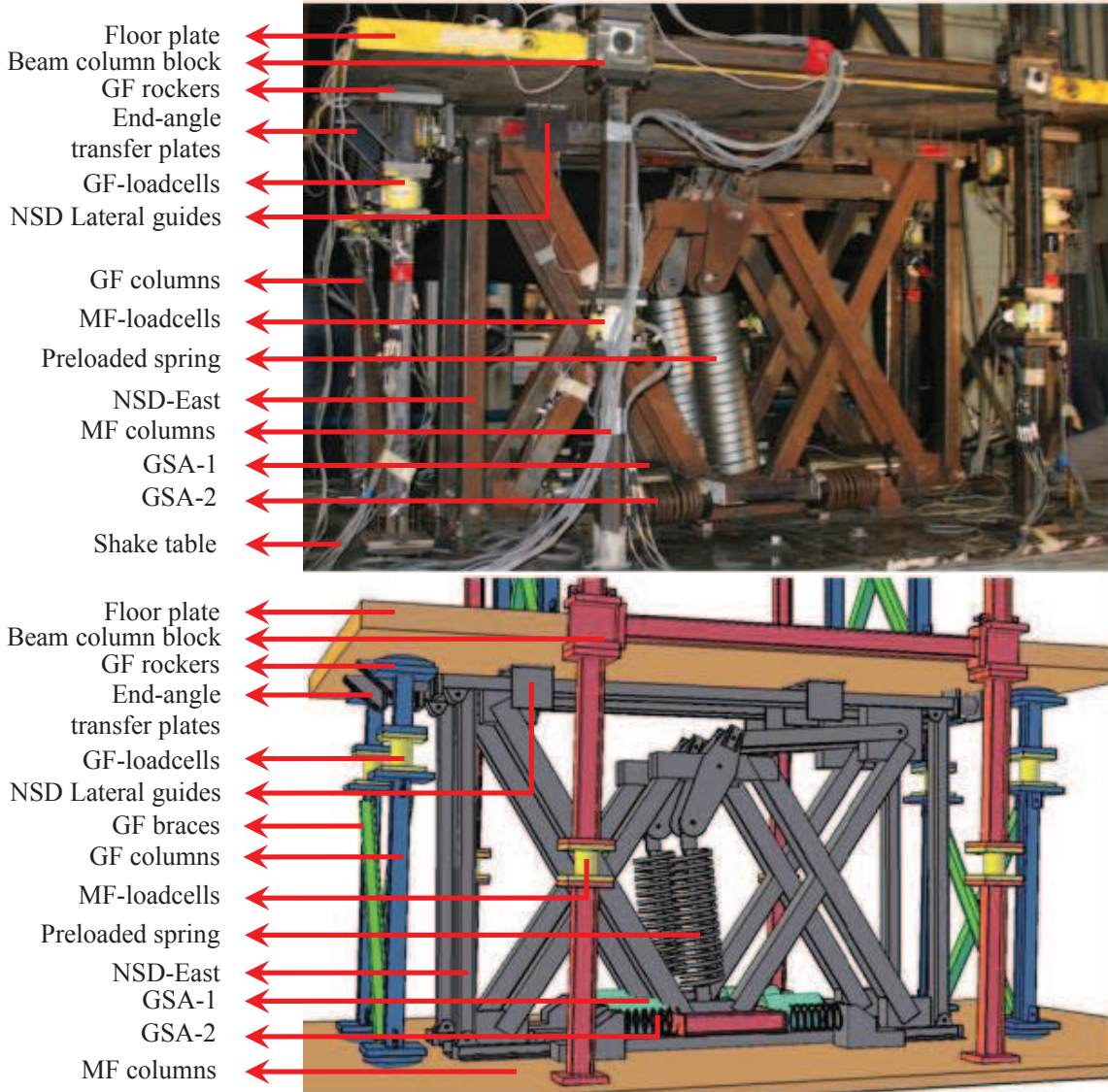


Figure 3.9: Photograph and schematic diagram of 3SFS (Elevation)

Due to the imperfections in NSD fabrication, chevrons exhibit different stiffness for positive and negative deformations as shown in Eq. 3.4.  $u_f$  is the deformation of point-C and point-E due to the flexing of chevron braces. Using these equations, the predicted and experimental force deformation behavior of NSD-West and NSD-East are shown in Figure 3.12(a) and 3.13(a), respectively. The predicted behavior is in very close agreement with the observed experimental behavior for both the NSDs. Due to the addition of GSA-2, both the devices exhibit high positive stiffness till  $|u| < 0.2 \text{ in}$ . The F-D loop of NSD-East is asymmetric, shown in Figure 3.13(a), this is captured in the analytical model through linear transformation explained in Eq. 2.24. The force-deformation behavior of the components, GSA-1, GSA-2

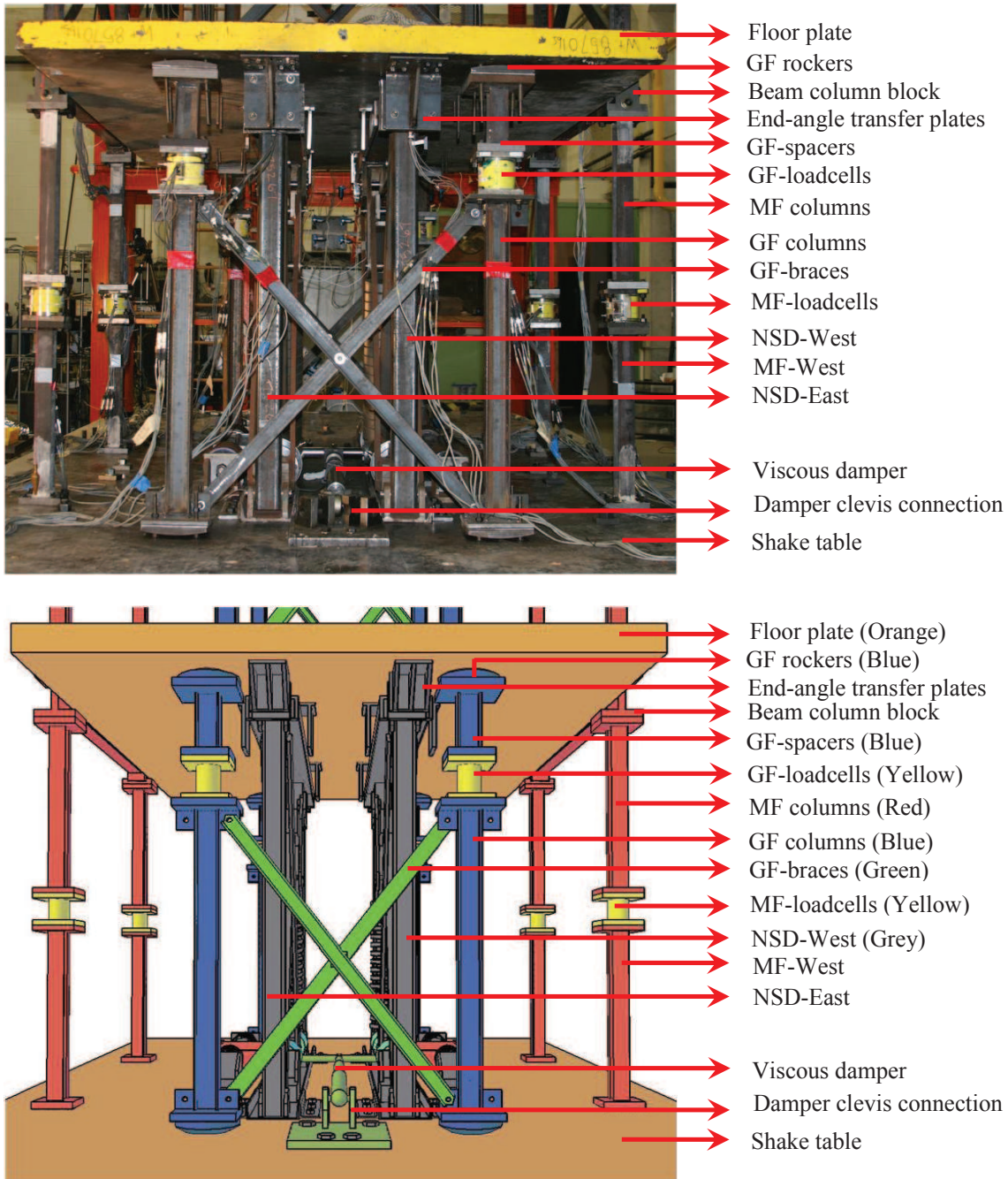


Figure 3.10: Observed experimental force-deformation behavior of NSD-East

and lateral force due to CS, of both the NSDs are shown in Figure 3.12(b) and 3.13(b). Next, the damper connection in the first floor of 3SFS and the analytical model for the damper is detailed.

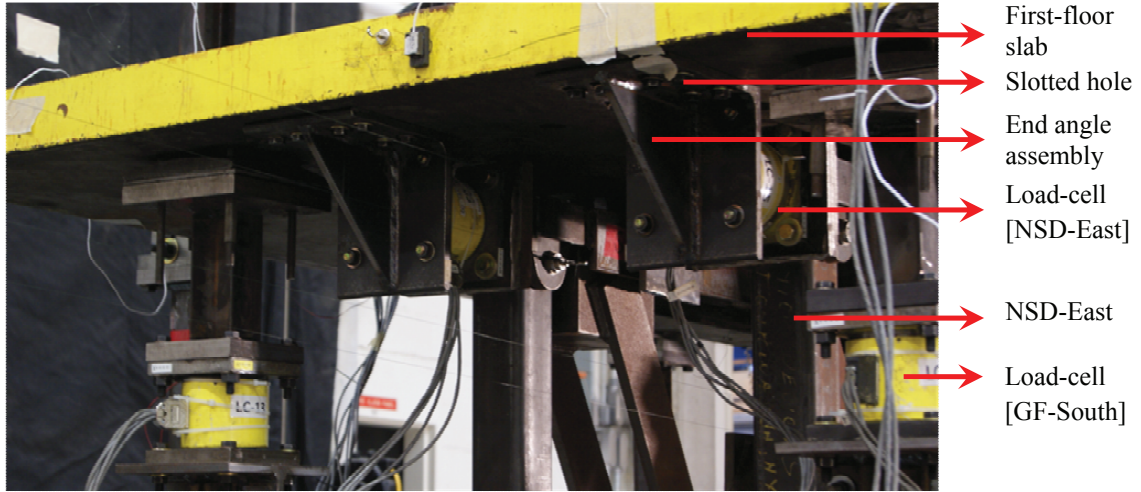


Figure 3.11: End angle assembly to connect the NSDs to floor slab

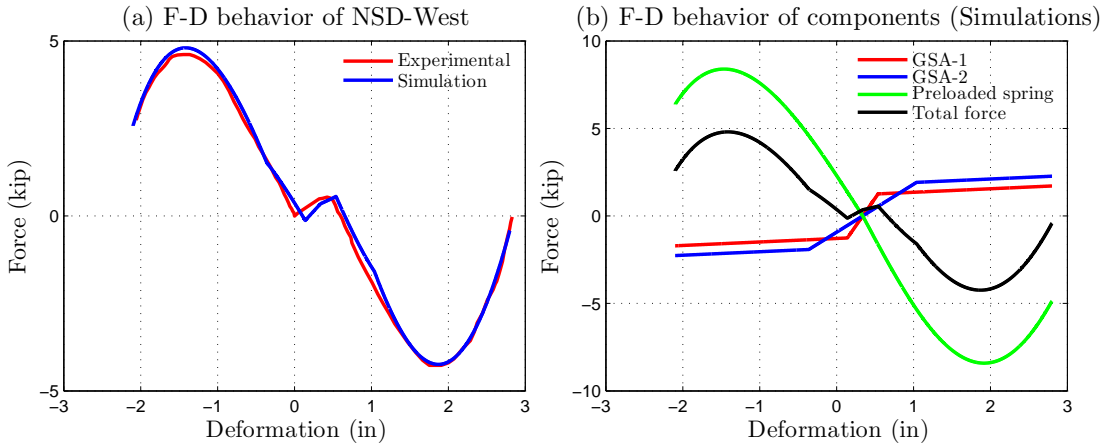


Figure 3.12: Experimental and predicted behavior of NSD-West

### 3.2.2 Viscous damper

Viscous damper developed by the Taylor Devices Inc. is used in this experimental study. The damper exhibits linear force-velocity behavior and has a damping coefficient of  $0.3769 \text{ kips}\cdot\text{sec/in}$ . A load-cell is attached to the damper to measure the force exerted by the damper. Length of the damper is  $20 \text{ in}$ . and the clear space in the first story is  $58.75 \text{ in}$ . so the damper could not be connected directly in the first-floor. Also, to achieve the desired damping the damper has to be connected horizontally aligning along north-south direction. When the end-angle assembly is connected to the NSD, the bottom of the chevron CB2 will undergo the same deformation as the first story slab as explained in section-2.3.2. So, one end of the damper is connected to a rod that is fixed to the bottom of the CB-2s of NSD-east and NSD-west, shown

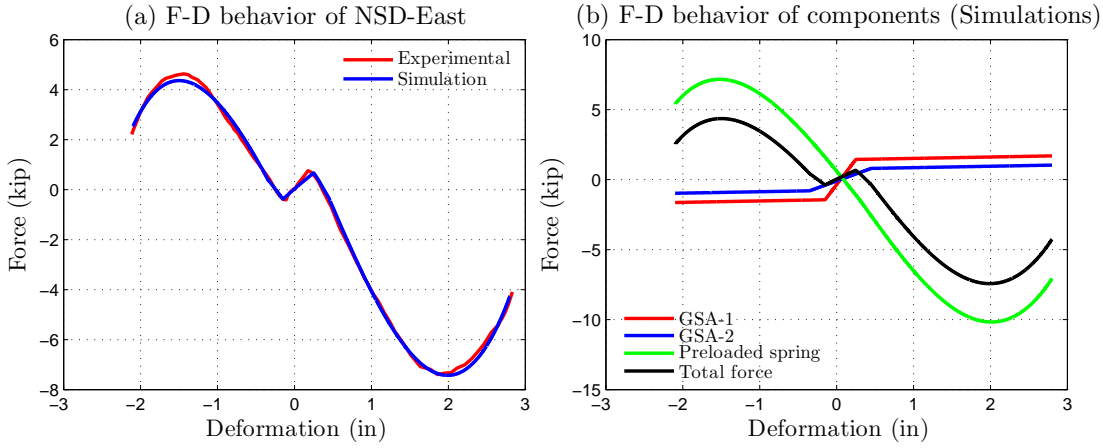


Figure 3.13: Experimental and predicted behavior of NSD-East

in Figure 3.10 and the other end of the damper is fixed to the shake table using a clevis connection. To test the structure only with NSD, the damper end that is connected to the shake table is disconnected and is held up using a rope.

Preliminary tests on The viscous damper has revealed that the force-velocity behavior of the viscous damper is linear if the velocity is less than 12.5 *in/sec*, but for larger velocities the force-velocity behavior observed was nonlinear as shown in Figure 3.14(a). To capture the behavior of damper for all amplitudes, a higher order term is added to the linear term as shown in Eq. 3.5. The force exerted by the damper,  $F_{PD}$ , is given by

$$F_{PD} = 0.312\dot{u} + 1.17 \times 10^{-6}\dot{u}^5 \quad (3.5)$$

Force-velocity behavior of the damper comparing the experimental results with the analytical results (Eq. 3.5) is shown in Figure 3.14(a). The force-deformation of analytical model and experimental results is shown in Figure 3.14(b). The predicted behavior of the damper shown in Figure 3.14 is in very good agreement with the experimental results.

### 3.3 Instrumentation

Thus far location of 12 multi-axis load-cells (in NSDs, moment-frame columns and gravity columns of first floor) and a uniaxial load-cell (in damper) to measure the force of various components in the structure is presented. Each load-cell measures axial force, shear force (shear-X and shear-Y) and moment (moment-X and moment-Y) at the installed location. Apart from these load-cells, the structure is heavily instrumented with string-potentiometers, strain-gages and accelerometers. Summary of all the instruments and location is summarized in Table 3.1.

In plane displacements and accelerations of the structure at floor level is measured at four different

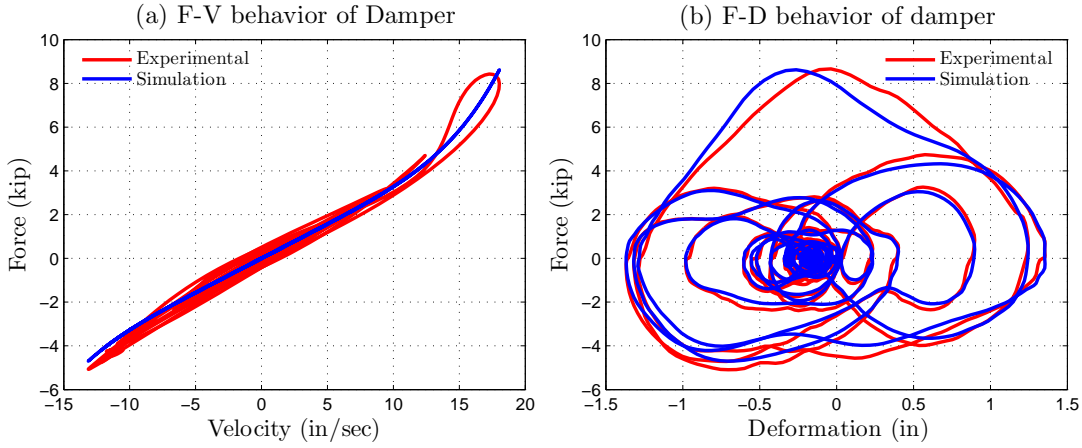


Figure 3.14: Experimental and predicted behavior of viscous damper

points (one on each moment frame and two on the floor slab) along the transverse direction. Eight accelerometers are placed on the shake-table to measure the in-plane motion, out of plane motion, and rocking of the shake-table. String potentiometers and accelerometers are also placed at all the pin connections in both the NSDs to capture the complete behavior of NSD. Strain gages are attached to the columns and beams of the MF-West, in the first story, to monitor the yielding status of the beams and columns in moment frame. In total, 28 string potentiometers, 24 accelerometers and 12 strain gages are used in this test. String-pots are installed on the support frame, located to the south of shake-table, shown in Figure 3.1. Fishing lines with magnetic holders are used to connect the string pots to the structure, glue-stick is used to attach the accelerometers and epoxy-adhesive is used to attach the strain gages. More than two sensors are used to measure the same response at each floor level to avoid data loss in the case of the sensor malfunctioning.

Megadac data acquisition with 112 channels and in-built signal conditioner is used to record the experimental data. The data is acquired at a rate of 256 samples per second. All the force transducers are calibrated with respect to NIST traceable 20 *kip* reference load cell. From the calibration tests, it has been found that the moment measured using the multi-axis load-cells exhibit a nonlinear behavior with significant hysteresis. So, the moments recorded in these tests has not been used in the analysis. Data from some of the load cell channels keeps drifting due to the joule-effect in the cables, so all the channels, except the strain-gage channels, are tore before every test.

The shake table used in this study is a five-axis shake table, but in this study it is only used as a single-axis shake table. The shake table has four vertical actuators and two horizontal actuators (25 *kN* capacity). Plan of the table has 12 *ft.* by 12 *ft.* steel base with a payload capacity of 85 kips (specimen load) and an operating frequency range of 0 to 50 *Hz*. The table is furnished with a reinforced concrete platform of 20 *ft.* by 12 *ft.*. The 3SFS tested on the shake-table exerts a lot of overturning moment for large

accelerations. So, the shake table controller is tuned to compensate for the actuator structure interaction. With the addition of NSD, the assembly exhibits bilinear elastic stiffness and the shake table has to be retuned again to achieve the target ground motion. Essentially, two sets of controller properties (tuned parameters) are calculated and used subsequently for all the tests. Despite all the best efforts, it has been observed in the experimental results that shake table was rocking. The observed shake table response for commanded ground motion is slightly different.

In the next section, the experimental results from the preliminary tests, the data processing adapted and the channels used for analyzing the data are discussed.

### 3.4 Experimental Results

All the elements in 3SFS are connected through bolts, except the end plates of GF and floor slabs. After the installation of structure the shake table is subjected to white noise tests to loosen the elements that were held by friction in the GFs. Then the structure is subjected to Newhall (1994) ground motion and the performance of the sensors and the functionality of the components in 3SFS is verified for BS and AS separately.

The shear force in the columns of first floor can be calculated from the accelerometers installed at the floor level and also from the load-cells installed in the MF. To ensure that the data measured from different sensors is consistent, first the F-D behavior of first-floor measured using load-cells and the accelerometers is compared in Figure 3.15. The base shear measured with the load-cells is 14% more than the shear calculated from acceleration. Since the accelerometers are more reliable than load-cells and moreover the channels in load-cell are coupled, the load-cell data is scaled to match the shear calculated from acceleration data, shown in Figure 3.15. The base shear in AS can be calculated from accelerometers or by adding the NSD load-cell and MF load-cell data (compensated). For Newhall ground motion the base shear calculated from both the approaches is compared in Figure 3.16. The response calculated from different sensors, shown in Figure 3.16, for AS is accurately matching and this justifies the need for compensating the load-cell data.

The next step is to ensure that there is no torque in the 3SFS and also no relative deformation between the MF and the floor-slabs. Two terms are defined here:  $\Delta_1$ , a measure of torsion, refers to the difference in the recorded data between two sensors, one in East and one in West, located at the same height;  $\Delta_2$  refers to the difference in the recorded data between two adjacent sensors, one on the moment frame and one on the floor-slab. Since the MFs are not bolted tightly to the floor-slabs, the relative motion between the MF and floor-slabs has to be verified to ensure that there is no slack in the 1 in. bolts. The shake-table rocking ( $M_y$ ) for Newhall GM in the case of BS is shown in Figure 3.17(a). The PGA of the ground motion is 0.18 g and the peak acceleration due to rocking is 0.04 g (20 % of PGA), so it is important to consider the measured shake-table rocking in the simulation studies. The acceleration of the roof measured on MF-East and MF-West is shown in Figure 3.17(b) and the data measured from both the sensors is very

Table 3.1: List of all the sensors used for data acquisition

Sensor	Location	Direction <sup>#</sup>	Remarks
Uni-axial load-cell	damper	F-X	Measures the damper force
	MF columns	F-X,F-Y	In-plane and out of plane shears
	GF columns	F-X,F-Y,F-Z	Dead load of floor slabs and shears due to inertial forces
Multi-axis load-cell	NSDs	F-X,F-Y,F-Z	Normal load exerted by the NSDs and friction in vertical direction
	MF	D-X	One string-pot on each frame (floor level) to measure the displacement and torsion
	Floor slabs	D-X	Two string-pots (SW and SE corner)
	Shake table	D-X	Two string-pots (SW and SE corner)
String-pots	NSD-pins	D-X	Located at points-A, B, C, D and E
	MF	A-X,A-Y	Two per floor for in-plane motion and one each in the first and third floor for out of plane motion
	Floor slabs	A-X,A-Y	Two per floor for in-plane motion and one per floor for out of plane motion
	Shake table	A-X,A-Y,A-Z	Two for in-plane, two for out of plane and 4 to measure rocking
Accelero-meters	NSD-pins	A-X	Located at points A,C and E
	MF-West columns	S-Z	Four SGs on the flanges of columns (2 in. from top and bottom)
	MF-West beam	S-X	Eight SGs on top and bottom flanges of the beam at 1/3 distance from both ends
† F: force; D:Displacement; A: Accelerometer; S: strain			
‡ X: North-South; Y: East-West; Z: Vertical direction			

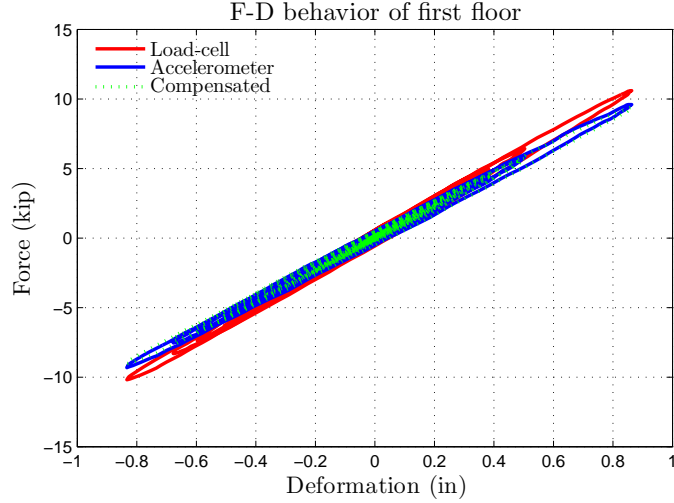


Figure 3.15: Force deformation loops of the load-cells and accelerometers [BS]

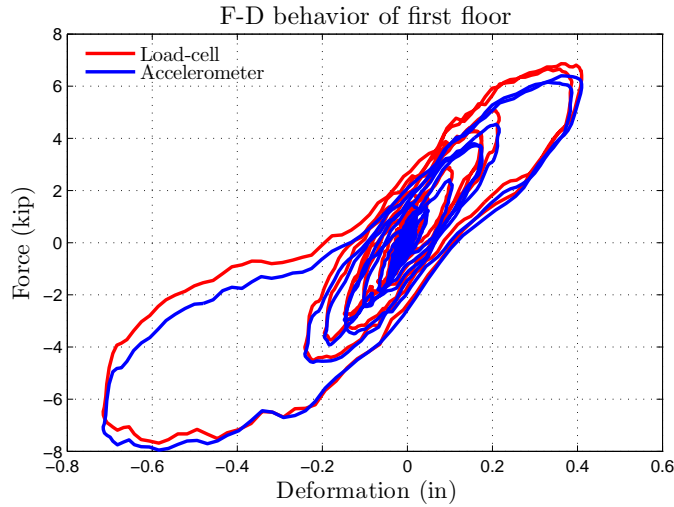


Figure 3.16: Force deformation loops of the load-cells and accelerometers [AS]

close confirming that there is no torsion in the case of BS. The percentage difference in the displacement of the roof measured on MF-East and MF-West,  $\Delta_1 u$ , is shown in Figure 3.17(c). The peak difference in displacement is less than 1.5% which is a sign that the displacements of both the MFs are synchronous. It should be noted that observed 1.5%, shown in Figure 3.17(c), also contains the measurement noise.

The same analysis is carried on the AS and the response plots are shown in Figure 3.18. Although the commanded PGA is same in the case of BS and AS, the PGA achieved in the case of AS is 0.2 g due to the structure and actuator interaction. This difference is much more evident for higher amplitudes. The

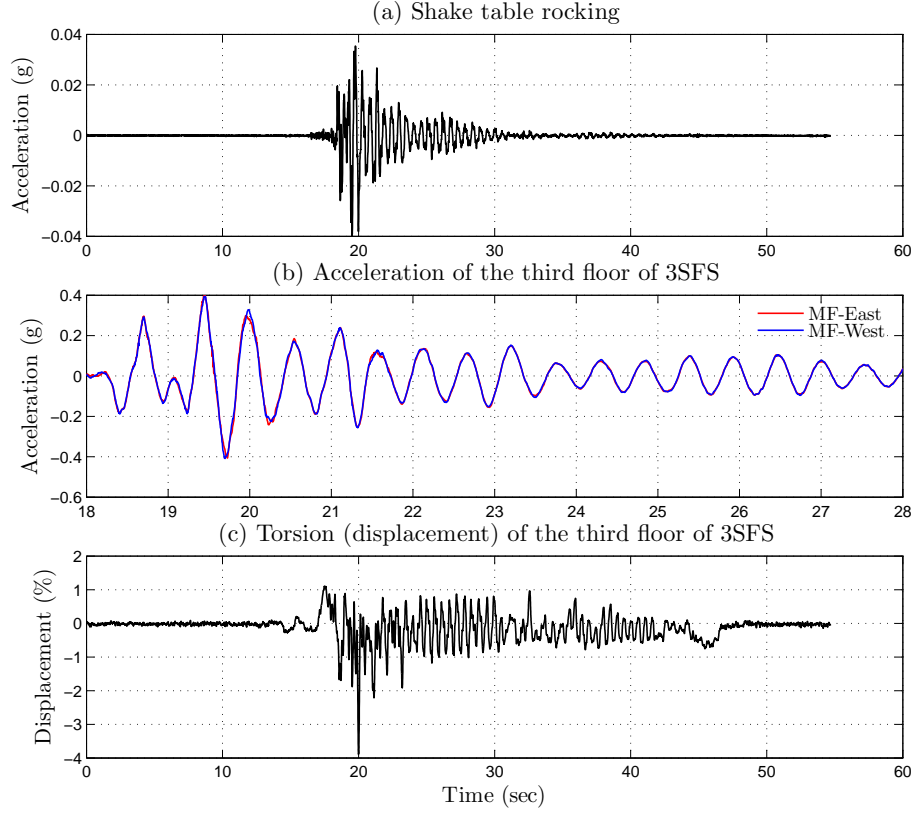


Figure 3.17: Torsion and rocking in the test structure [BS]

peak acceleration of shake-table rocking is 0.1 g (50% of PGA). The acceleration of MF-West and MF-East, shown in Figure 3.17(b), shows that the acceleration of both the MFs are close except at the peaks when the NSDs engage. The  $\Delta_1 u$  at the roof is less than 1.5% similar to the case of BS.

The response of BS and AS for Newhall ground motion is summarized in Table 3.2. The difference in response ( $\Delta_2 u$  and  $\Delta_2 \ddot{u}$ ) columns 5 through 8 of Table 3.2 is less than 5% confirming that there is no slack in the connecting bolt between MF and floor-slab. The torsion-displacement,  $\Delta_1 u$ , is also less than 3% at all floors. However, the torsion-acceleration  $\Delta_1 \ddot{u}$  is close to 10% in the case of both BS and AS. If this difference is completely due to the torsion, the values of  $\Delta_1 u$  and  $\Delta_1 \ddot{u}$  of second and third floors should be higher than the first-floor. Since the structure is vibrating in the first-mode and still the torsion values are same in all the floors this could be due to the measurement noise in the accelerometers. Next, the analytical model used to capture the behavior of 3SFS is presented.

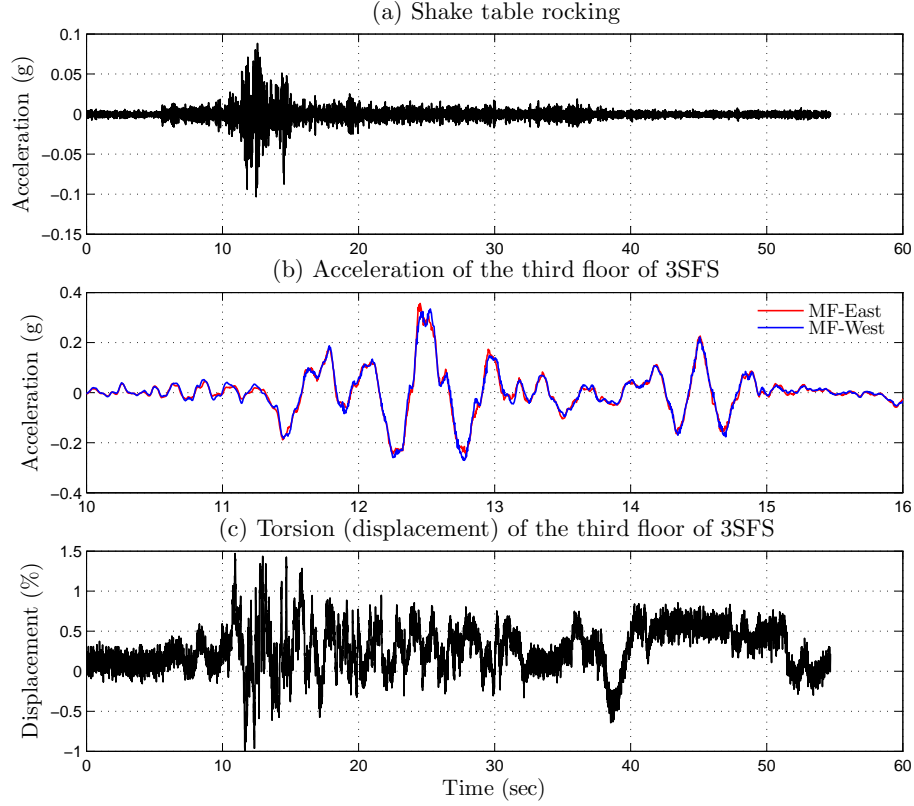


Figure 3.18: Torsion and rocking in the test structure [AS]

### 3.4.1 3SFS Analytical Model

Since the primary structure will be yielding in the experiments carried in this study, the columns are modeled using Sivaselvan-Reinhorn model (Sivaselvan and Reinhorn, 2000). The structure also has contact forces at three connections (1) NSDs and floor-plates (2) gravity frames and floor-plates (3) beam-column blocks and floor-plates. Due to these connections, a lot of frictional-damping has been observed in the experiments, this is also captured using Sivaselvan-Reinhorn model. First, a set of shake-table tests have been performed with sine-sweep input to estimate the stiffness and damping of three modes of 3SFS. Essentially, the analytical model of each-floor in 3SFS has viscous damping, friction damping and hysteretic model to capture the column behavior. The values various parameters used in the models is different for the 3SFS with braces in the second and third floor, acting as a SDOF structure, and the 3SFS without braces. Governing equation of motion for the 3SFS is given in Eq. 3.6

$$\mathbf{M}\ddot{\mathbf{u}} + \mathbf{C}\dot{\mathbf{u}} + \mathbf{F}_s(\mathbf{u}) + \mathbf{F}_f(\mathbf{u}) = -\mathbf{M}\mathbf{I}\ddot{\mathbf{u}}_g - \mathbf{M}\mathbf{L}\ddot{\theta}_g \quad (3.6)$$

$$F_{si}(u_{ri}) = \alpha_{si}K_{si}u_{ri} + (1 - \alpha_{si})K_{si}u_{syi}z_{si} \quad (3.7)$$

Table 3.2: Summarized list of torsion and differential response for BS and AS

Location	BS				AS			
	$\Delta_1 \ddot{u}$	$\Delta_1 u$	$\Delta_2 \ddot{u}$	$\Delta_2 u$	$\Delta_1 \ddot{u}$	$\Delta_1 u$	$\Delta_2 \ddot{u}$	$\Delta_2 u$
Shake table	3.22	3.41	-	-	2.95	2.46	-	-
First floor	12.85	1.82	1.59	1.99	9.08	2.35	2.65	1.45
Second floor	9.95	3.82	1.57	7.36	9.33	1.71	2.61	4.64
Third floor	9.35	3.89	0.86	1.20	12.70	1.23	2.40	1.09

$$\frac{dz_{si}}{du_{ri}} = \left( \frac{1 - |z_{si}|^{\eta_{si}} (\gamma_{si} \operatorname{sgn}(z_{si}) du_{ri}) + \beta_{si}}{u_{syi}} \right) \quad (3.8)$$

where,  $u$  is the displacement vector of the structure relative to the ground.  $\ddot{u}_g$  and  $\ddot{\theta}_g$  are the shake table horizontal acceleration and rotation due to shake table rocking.  $\mathbf{M}$  and  $\mathbf{C}$  are the mass and damping matrices of the structure.  $\mathbf{I}$  and  $\mathbf{L}$  are the influence coefficient vectors for shake table acceleration and rotation.  $\mathbf{F}_s(\mathbf{u})$  and  $\mathbf{F}_f(\mathbf{u})$  are the force vectors containing the force due to friction in each floor and the story-columns. The nonlinear stiffness force in each story is calculated using Eqs. 3.7, 3.8. Subscript- $i$  stands for  $i^{th}$  story,  $F_{si}$  is the nonlinear spring force in  $i^{th}$  story,  $u_{ri} = u_i - u_{i-1}$  is the inter story deformation of  $i^{th}$  story and  $u_{syi}$  is the yield displacement. The parameters  $\alpha_{si}$ ,  $K_{si}$ ,  $\eta_{si}$ ,  $\gamma_{si}$  and  $\beta_{si}$  are the constants in Sivaselvan-Reinhorn model for  $i^{th}$  story. The friction force,  $\mathbf{F}_f(\mathbf{u})$ , is calculated using the equations similar to Eqs. 3.7, 3.8.

Weight of steel slabs in each story is measured ( $M_1=M_2=M_3=8.6$  kips) and used to calculate the mass matrix,  $\mathbf{M}$ , elastic stiffness of the columns is calculated from individual story stiffness ( $K_{s1}=10.9$  kip/in;  $K_{s2}=56.0$  kip/in;  $K_{s3}=35.0$  kip/in), damping matrix,  $\mathbf{C}$ , is calculated assuming 1% damping ( $\xi = 0.01$ ) in each floor ( $C_1 = 2\xi \sqrt{M_1 K_{s1}}$ ,  $C_2 = 2\xi \sqrt{M_2 K_{s2}}$  and  $C_3 = 2\xi \sqrt{M_3 K_{s3}}$ ). The matrices and the components are shown below

$$\mathbf{M} = \begin{bmatrix} M_1 & 0 & 0 \\ 0 & M_2 & 0 \\ 0 & 0 & M_3 \end{bmatrix}; \mathbf{C} = \begin{bmatrix} C_1 + C_2 & -C_2 & 0 \\ -C_2 & C_2 + C_3 & -C_3 \\ 0 & -C_3 & C_3 \end{bmatrix}; \mathbf{I} = \begin{bmatrix} 1 & 1 & 1 \end{bmatrix}$$

$$\begin{aligned}
\mathbf{L} &= \begin{bmatrix} 60.5 & 107.75 & 155 \end{bmatrix} \\
\mathbf{F}_s(\mathbf{u}) &= \begin{bmatrix} F_{s1}(u_{r1}) + F_{s2}(u_{r2}) & -F_{s2}(u_{r2}) & 0 \\ -F_{s2}(u_{r2}) & F_{s2}(u_{r2}) + F_{s3}(u_{r3}) & -F_{s3}(u_{r3}) \\ 0 & -F_{s3}(u_{r3}) & F_{s3}(u_{r3}) \end{bmatrix} \\
\mathbf{F}_f(\mathbf{u}) &= \begin{bmatrix} F_{f1}(u_{r1}) + F_{f2}(u_{r2}) & -F_{f2}(u_{r2}) & 0 \\ -F_{f2}(u_{r2}) & F_{f2}(u_{r2}) + F_{f3}(u_{r3}) & -F_{f3}(u_{r3}) \\ 0 & -F_{f3}(u_{r3}) & F_{f3}(u_{r3}) \end{bmatrix}
\end{aligned}$$

The constants in Sivaselvan-Reinhorn model are estimated by minimizing the error between experimental and analytical hysteresis loop. From the optimization study,  $\alpha_{si} = 0.2$ ,  $\eta_{si} = 12$ ,  $\gamma_{si} = 0.84$  and  $\beta_{si} = 0.16$ . Predicted and the observed experimental force-deformation behavior of all the floors in 3SFS for San Fernando earthquake ground motion [Recorded at Pacoima dam, 164 (CDMG station 279)] (PGA = 0.75g) is shown in Figure 3.19. The analytical predictions are matching with the experimental results very accurately in the first-floor. The experimental force-deformation behavior of the second and third floors is more noisy compared to the first-floor because the shear in first-floor is measured using the load-cells whereas in the second and third floors it is calculated from the floor acceleration. The maximum deformation of second and third floor is less than 0.15 in. and the peak deformation of first-floor is 1.95 in. First floor deformation and acceleration is shown in Figure 3.20 for the same ground motion. From the comparisons in Figure 3.20, the peak response characteristics and also the frequency-information obtained from the analytical model of 3SFS can capture the observed experimental behavior very accurately. The permanent drift observed in the experiments is 0.21 in. and the permanent deformation in the simulations is 0.25 in.

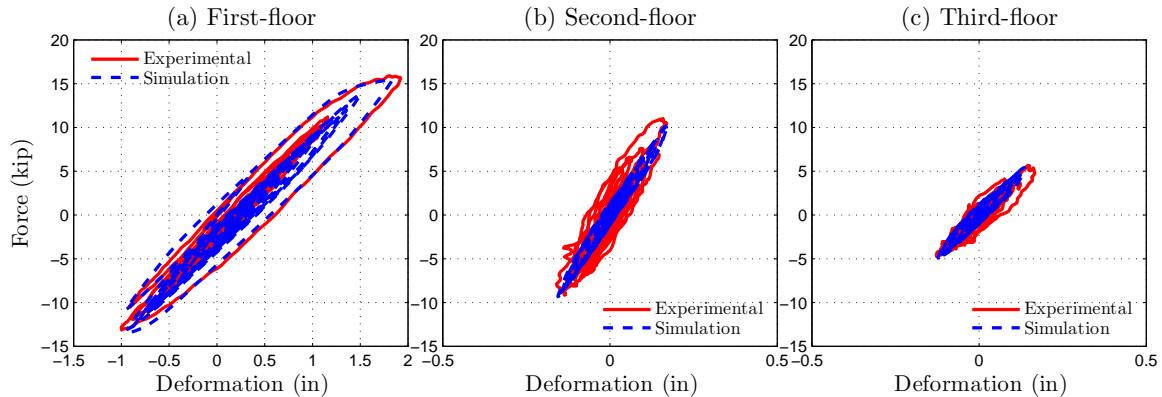


Figure 3.19: F-D behavior of 3SFS with braces in second and third floor

Next, the behavior of 3SFS without the braces is verified for Kobe ground motion (1995). The experimental force-deformation behavior of all the floors is shown in Figure 3.21. The analytical predictions are

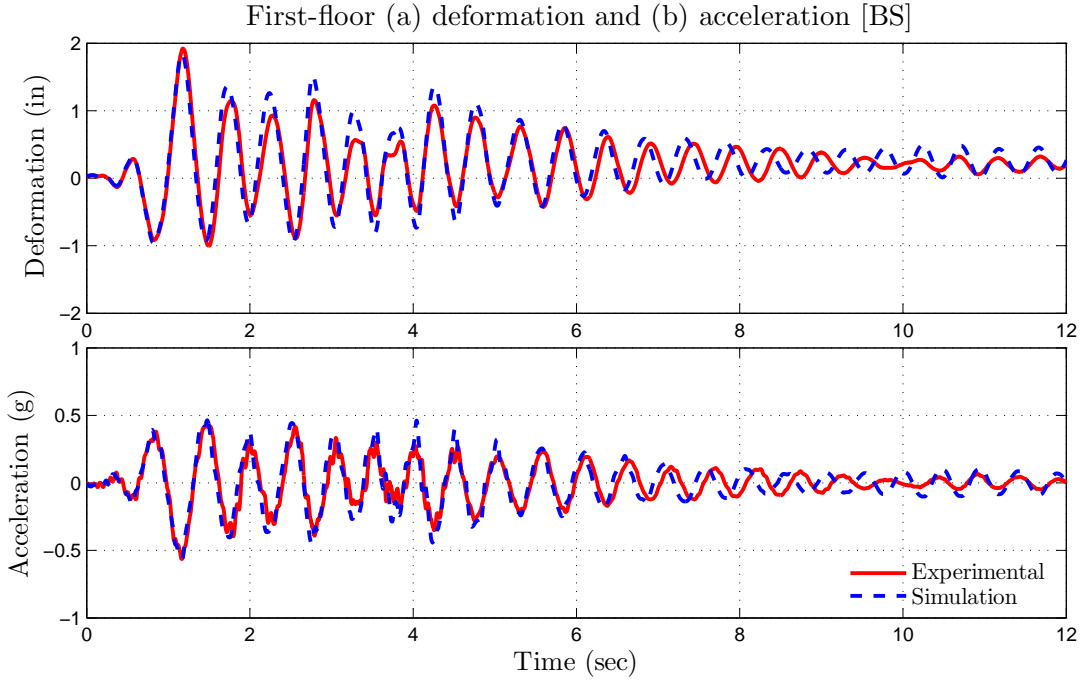


Figure 3.20: Displacement and acceleration of the first floor of braced-3SFS

matching with the experimental results very accurately in all the first-floor unlike the braced structure, shown in Figure 3.21. The maximum deformation of the second and third floors (Figure 3.21) is 0.75 in. and 0.5 in. respectively. The elastic stiffness of the columns in each floor is  $K_{s1}=8.9 \text{ kip/in}$ ,  $K_{s2}=11.2 \text{ kip/in}$  and  $K_{s3}=9.2 \text{ kip/in}$ . Sivaselvan-Reinhorn model constants are  $\alpha_{si} = 0.17$ ,  $\eta_{si} = 6$ ,  $\gamma_{si} = 0.84$  and  $\beta_{si} = 0.16$ . First floor deformation and acceleration is shown in Figure 3.22; roof deformation and acceleration is shown in Figure 3.23. Similar to the braced structure, the comparisons in Figure 3.22 and 3.23, the peak response characteristics are matching accurately but the frequency-information is slightly off because of the dynamics of the second and third floors. The friction in the second and third floors is also highly nonlinear because of the slipping in the gravity columns.

### 3.5 Summary

In this chapter, the experimental setup of the three-story frame structure, the connections between the 3SFS, NSD and damper is presented in detail. The analytical models for each of the components is also presented and the models are calibrated using the experimental data from the component testing.

It has been found from the shake-table studies that the 3SFS will undergo very little torsion and can be ignored in the analysis. The data measured from various sensors (many of them redundant) is verified and is found to be consistent. The experimental data has confirmed that the two support systems (lateral

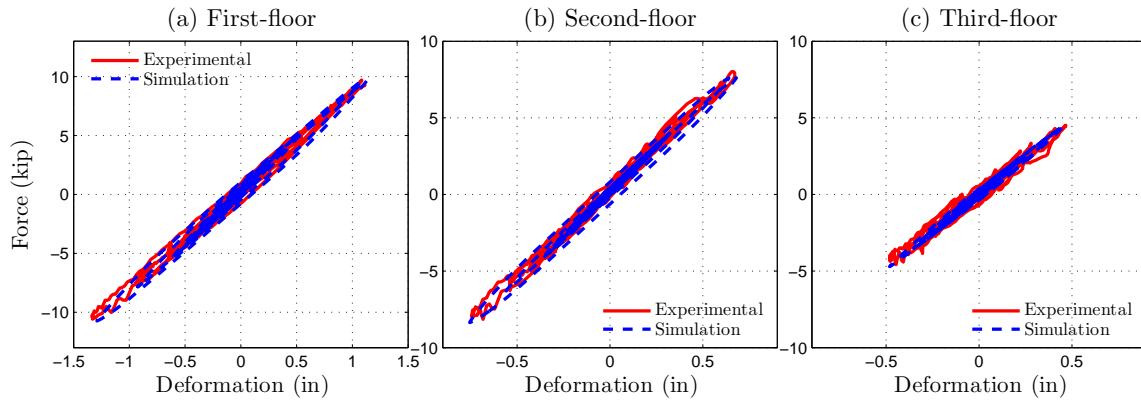


Figure 3.21: F-D behavior of all the floors in 3SFS

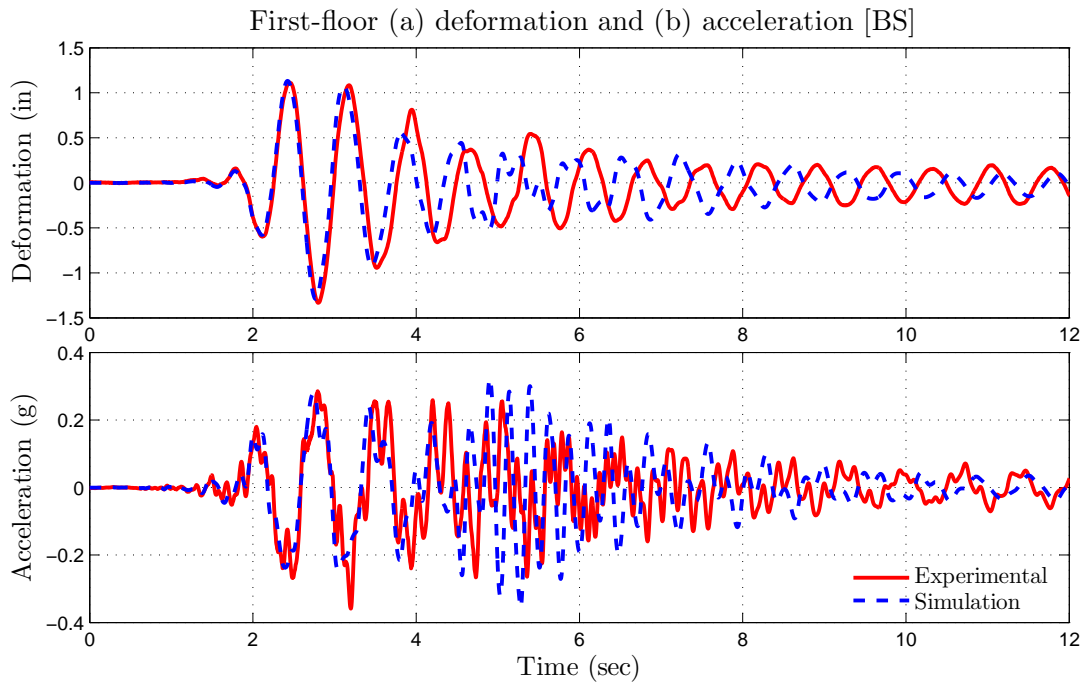


Figure 3.22: Displacement and acceleration of the first floor of 3SFS

force resisting system and vertical load carrying system) are completely independent and stable; hence it is an ideal test structure to perform yielding tests with NSD. The behavior of the NSD, damper and 3SFS can be modeled and can be very accurately predicted using the analytical models presented in this chapter. The comparisons between the numerical predictions and experimental data is in very close agreement and these component models can also be used to predict the behavior of 3SFS and assembly, which is presented in the next chapter.

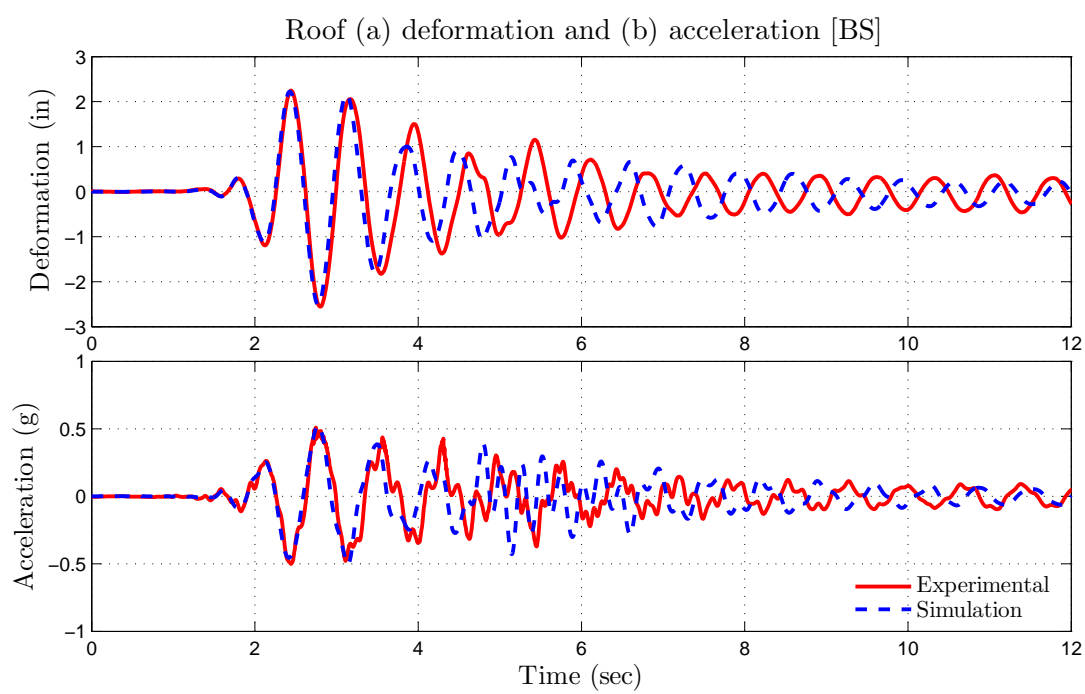


Figure 3.23: Displacement and acceleration of the roof of 3SFS

## Chapter 4

# Apparent-Weakening in SDOF Structures: Experimental Study

This chapter presents the results from the experimental study on three-story fixed-base structure (3SFS) that demonstrates the concept of “apparent weakening” in SDOF structural systems. The top two floors of 3SFS are braced making the 3SFS a SDOF structure. First, the effectiveness of “apparent-weakening” in reducing the response of elastic systems is demonstrated. Then the performance of structure and NSD assembly when the primary structure has yielded is evaluated and the issues involved in such systems are presented in detail.

To accentuate the advantages of “apparent-weakening” in structures over the existing passive energy dissipation devices, experimental results of three different systems: 3SFS (BS); 3SFS with NSD (NS); 3SFS with NSD and damper (AS); and analytical results of 3SFS with damper (PS) are compared for a suite of ground motions. Five standard ground motions (see Table 4.1) from the PEER database have been used for the shake-table tests. The ground motions chosen are representative of both the far field and near-fault earthquakes. Analytical models, based on principles of mechanics, describing the behavior of each and all of the three systems (presented in chapter 3) are used to reproduce the experimental results. Also, these models are further used to estimate the response of PS and the missing tests. Since the damper is connected to the structure through the NSD, as explained in section-3.2, 3SFS with the damper (PS) could not be tested experimentally without connecting the NSD. In order to emphasize the significance of NSD in AS, the response of 3SFS with viscous damper (PS) is simulated and compared with the experimental results of the BS, NS and AS.

Due to the braces in the second and third floors of 3SFS, the columns in the first story will yield first when the frame is subjected to severe ground motion. The strain in the columns of the first-floor is monitored during the tests and they are replaced after they yield. Since replacing the columns after every test is expensive and time consuming, shake-table tests at higher PGA values (tests in which the first floor columns of 3SFS yield) have only been conducted on: 3SFS with NSD and; 3SFS with NSD and damper

assembly for different PGA values. For comparisons, the behavior of other systems is predicted using the calibrated analytical models.

The rest of the chapter is organized as follows: “Apparent-weakening” in elastic structures is verified using the experimental results (BS, NS and AS) and simulation studies (PS) in section 4.1. In section 4.2 the issues involved when the primary structure undergoes plastic deformation are addressed. Experimental results (response and hysteresis loops) of 3SFS and comparisons with 3SFS assembly equipped with (i) NSD (ii) damper (iii) NSD and damper are also discussed in section 4.2. Section 4.3 contains the conclusions based on the experimental and simulation studies on SDOF structures.

## 4.1 Elastic structures

The concept of “apparent-weakening” in elastic and inelastic systems is explained in chapter 1. The main objective of the adaptive negative stiffness system is to shift the yielding behavior from the structure to the NSD and reduce the base shear (foundation) force of the structure while limiting its maximum response displacement and acceleration. The negative stiffness device (NSD), used in this study, exhibits nonlinear-elastic negative stiffness behavior; by adding NSD to the elastic structure the resulting structure-device assembly behaves like a bilinear-elastic structure (Pasala et al., 2012c). Peak acceleration and base shear experienced by the structures can be reduced by adding the negative stiffness device and the additional deformations caused due to the reduced stiffness can be contained by adding the viscous damper. A short description of the working principle of adaptive negative stiffness system in reference to the 3SFS and NSD developed in this study is presented next.

Assume a single degree of freedom linear elastic structure with stiffness  $K_e$  and no damping, the force deformation (F-D) behavior ( $F_s(u)$ ) is shown in Figure 4.1(a,b). At displacements  $u_1$  and  $u_2$ , the force in the structure are  $F_{s1}$  and  $F_{s2}$  respectively, shown in Figure 4.1(b). The F-D behavior of NSD ( $F_{NSD}(u)$ ) is shown in Figure 4.1(a,b); NSD has zero stiffness until  $|u| < u_1$  and beyond this displacement it exerts negative nonlinear-elastic stiffness. The displacement at which the NSD engages,  $u_1$ , called as “apparent yield-displacement” and the force exerted by the NSD at displacement  $u_2$  is  $-F_{NSD2}$  ( $F_{NSD2} > 0$ ), shown in Figure 4.1(b). Although the NSD exhibits nonlinear stiffness beyond  $u_1$ , the stiffness of NSD between  $u_1$  and  $u_2$  remains almost constant,  $K_{NSD}$ , so the NSD can be assumed to be linear in this region. This argument is also justified using the F-D curves obtained from the experimental results shown in the forthcoming sections. The F-D behavior of the structure and NSD assembly is shown in Figure 4.1(c). At displacement  $u_1$ , the assembly force,  $F_{n1}$ , is same as the force in the primary structure ( $F_{n1} = F_{s1}$ ) because the NSD does not exert any force until  $|u| > u_1$ . At displacement,  $u_2$ , the force in the assembly is  $F_{n2} = F_{s2} - F_{NSD2}$ . The stiffness of the structure and NSD assembly,  $K_n$ , is equal to  $K_e$  for  $|u| < u_1$  and  $K_n = K_e - K_{NSD}$  for  $u_1 \leq |u| < u_2$ . Since the structure and device assembly is elastic and exhibits two stiffness,  $K_e$  and  $K_n$ , it is called “bilinear elastic” system.

In chapter 3, it has been shown that the behavior of the components: 3SFS (BS), NSD-East, NSD-

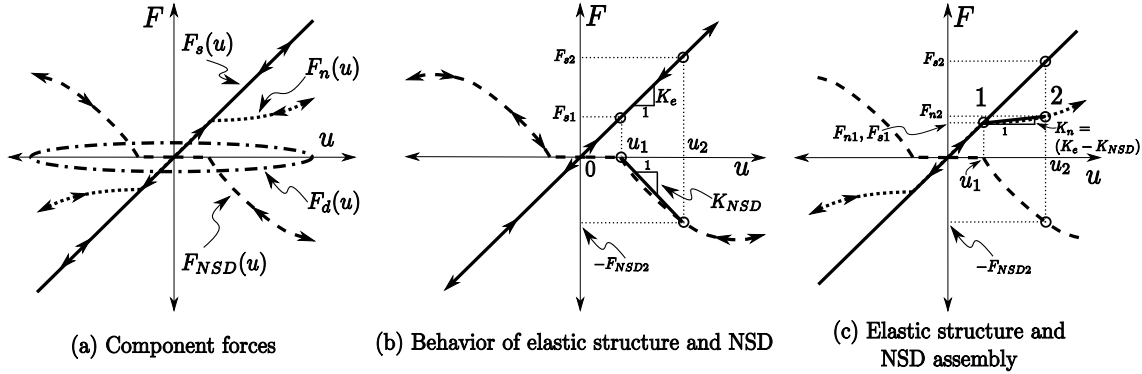


Figure 4.1: Schematic diagram depicting “apparent-weakening” in elastic systems

West and the viscous damper; can be captured accurately. Next, the predicted behavior of NS and AS is compared with experimental results to show that the analytical models used in this study are consistent in capturing the observed experimental behavior. The measured ground acceleration and shake-table rocking is used as the ground excitation in the simulation studies. Shear force in the columns is measured using the MF-load-cells, base shear is calculated using the acceleration of all the three floors, force exerted by the NSDs and damper are also measured using the load-cells. Kobe fault-normal ground motion with PGA of 0.29g is used to test the performance of all the four systems in elastic region.

#### 4.1.1 3SFS and NSD assembly

The role of NSD in NS and AS is to reduce the base shear of the structure and as a result reduce the acceleration experienced by the structure. This is depicted in the results shown in Figure 4.2-4.5. Force-deformation curves of the columns in the first-floor of 3SFS and the assembly (3SFS, NSD-East and NSD-West) in NS for the Kobe FN ground motion is shown in Figure 4.2. The reduction in assembly stiffness with the addition of NSD is evident from Figure 4.2. Force-deformation behavior of the NSD-East and NSD-West is shown in Figure 4.3. Please note that the F-D loops of NSD in Figure 4.3 have significant friction hysteresis, but the models developed previously in section-3.2.1 do not take this into account. Sivaselvan-Reinhorn model is used to account for the friction hysteresis of NSDs.

First-floor deformation, acceleration and base shear are shown in Figure 4.4. The predicted first-floor deformation and base shear is matching the experimental behavior very accurately. The acceleration predicted using the analytical model has high frequency information due to the inclusion of shake table rocking. The experimental and predicted force-deformation loops of all the components in NS are separately shown in Figure 4.5. From Figure 4.5, it is evident that by adding NSDs to the 3SFS the peak assembly force in the first-floor is reduced by 45%. The peak acceleration of the first-floor is also reduced by 25% compared to BS (refer to Table 4.1 and Figure 4.14) but the peak deformation of the first story has increased by 10% in the case of NS. This increase in inter-story deformation is due to the reduction

in story stiffness. From Figure 4.5, it is evident that the addition of NSD to 3SFS will result in bilinear elastic behavior of the assembly. It is also clear from all the subplots in Figure 4.2-4.5 that the observed experimental behavior of all the components and the assembly in the NS can be captured very precisely with the analytical model used in this study. Next, the role of viscous damper in AS is demonstrated.

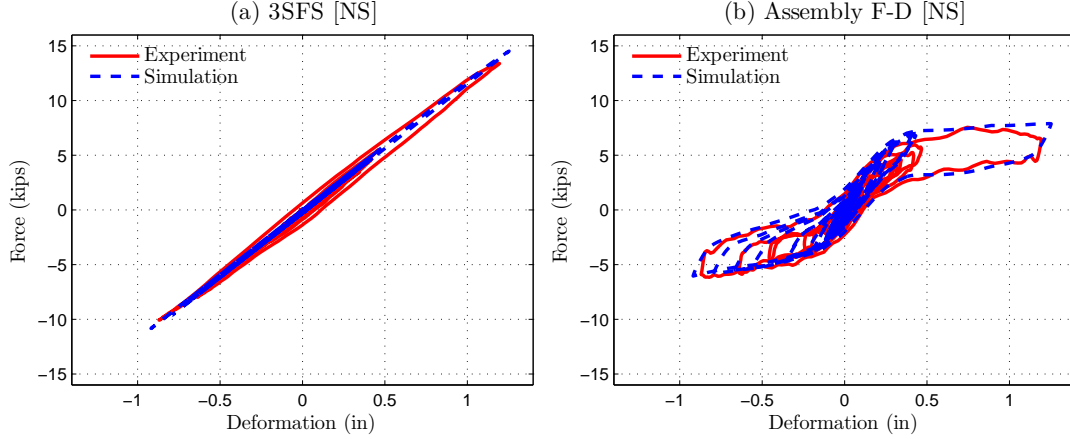


Figure 4.2: F-D behavior of 3SFS and assembly in NS (Kobe GM; PGA=0.29g)

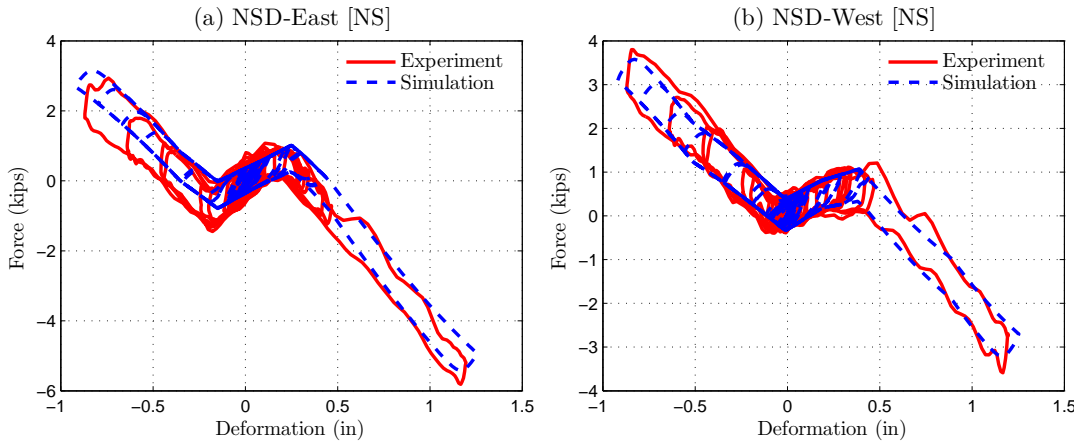


Figure 4.3: F-D behavior of NSDs in NS (Kobe GM; PGA=0.29g)

#### 4.1.2 3SFS, NSD and damper assembly

For the same system described previously (3SFS and NSD assembly), by adding the viscous damper the deformation of the assembly is reduced along with the base shear and acceleration. The Experimental and predicted force-deformation loops of the first-floor of 3SFS and damper are compared in Figure 4.6.

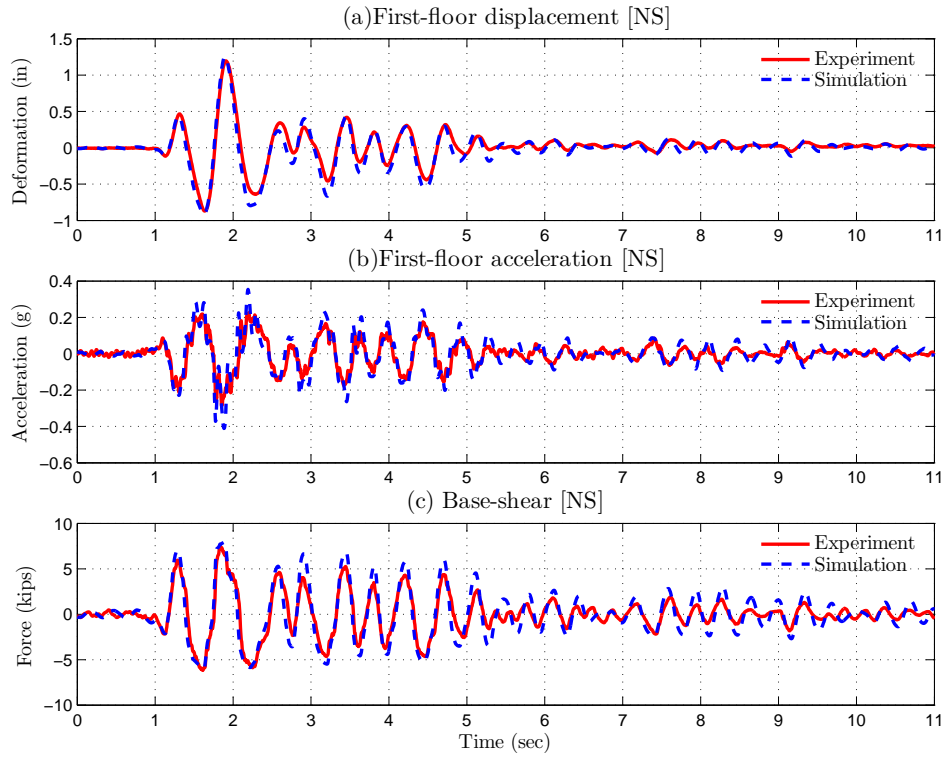


Figure 4.4: First-floor response and base shear of NS (Kobe GM; PGA=0.29g)

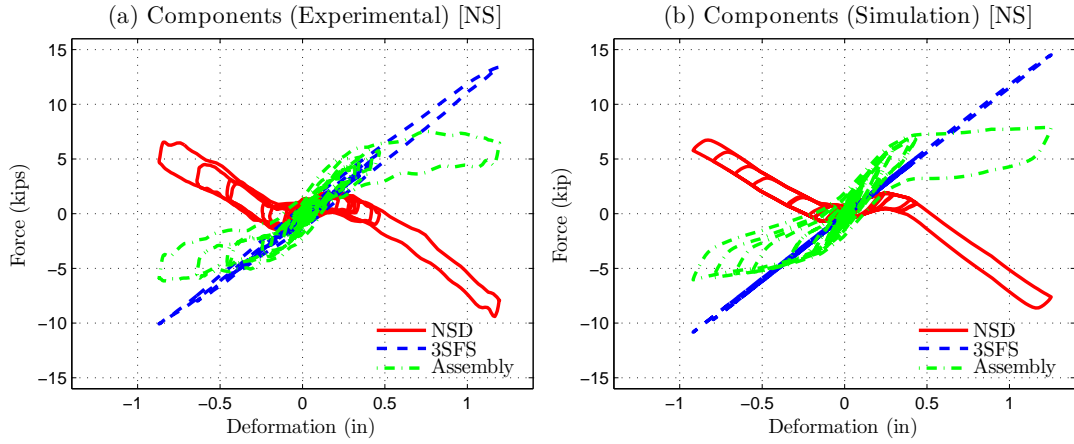


Figure 4.5: F-D behavior of NS with components (Kobe GM; PGA=0.29g)

The stiffness of 3SFS in Figure 4.6(a) is 5% higher than the simulations and also Figure 4.2(a) due to the additional connections of NSD. Force-deformation behavior of NSD-East and NSD-West is shown in Figure 4.7. The maximum deformation of NSD has decreased to 0.8 in. from 1.2 in. (Figure 4.3) with

the addition of viscous damper. The F-D behavior of all the components of AS are shown separately for experiments and simulations in Figure 4.8. The first-floor deformation, acceleration and base shear of AS are shown in Figure 4.8. Unlike the case of NS, the acceleration response of simulations and experiments is matching very accurately in the case of AS. The experimental and predicted F-D behavior of AS is compared in Figure 4.10. The analytical hysteresis loop is bigger than the experimental but the overall trend is matching very well.

By adding the viscous damper, the additional damper force exerted on the structure will increase the base shear of the structure by 15% compared to NS but it is still 30% less than the BS (refer to Figure 4.4, 4.9, 4.14 and Table 4.1). The peak acceleration of the AS is same as the NS but the peak deformation of AS is 20% less than the BS this reduction is significant compared to the 10% increase as in the case of NS. By adding the viscous damper the base shear is slightly increased but the significant reduction in inter-story deformation achieved outperforms the increase in base shear.

The observed experimental behavior of all the components and the assembly in the AS is very accurately captured with the analytical model. This confirms that the response of PS predicted using the analytical model should be a very good estimate of the actual response of PS. Next, the response of all the systems is compared to show the effectiveness of AS.

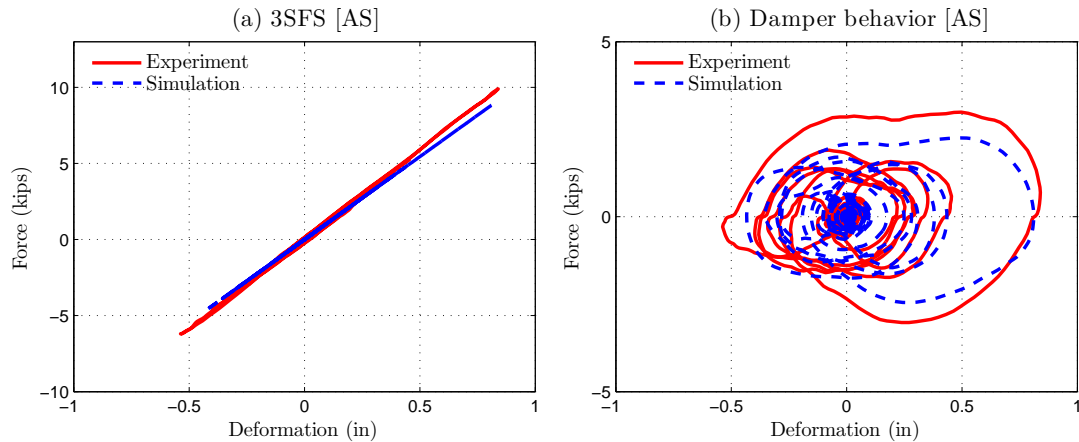


Figure 4.6: F-D behavior of 3SFS and damper in AS (Kobe GM; PGA=0.29g)

#### 4.1.3 Comparative study

By adding NSD to an elastic structure, the structure and NSD assembly will emulate a bilinear elastic system. Although addition of NSD will result in reduction of base shear and acceleration, it will also result in increased deformations. A viscous damper in conjunction with the NSD will attenuate base shear, accelerations and displacements. In order to justify the usage of the NSD with the damper (AS), the response of AS is compared with PS next. The force-deformation loops of the first-floor in all the systems

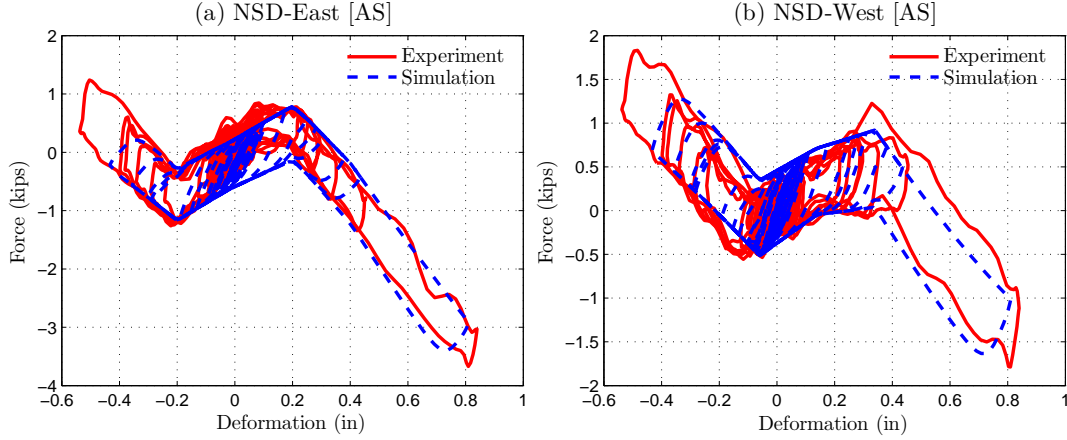


Figure 4.7: F-D behavior of NSDs in AS (Kobe GM; PGA=0.29g)

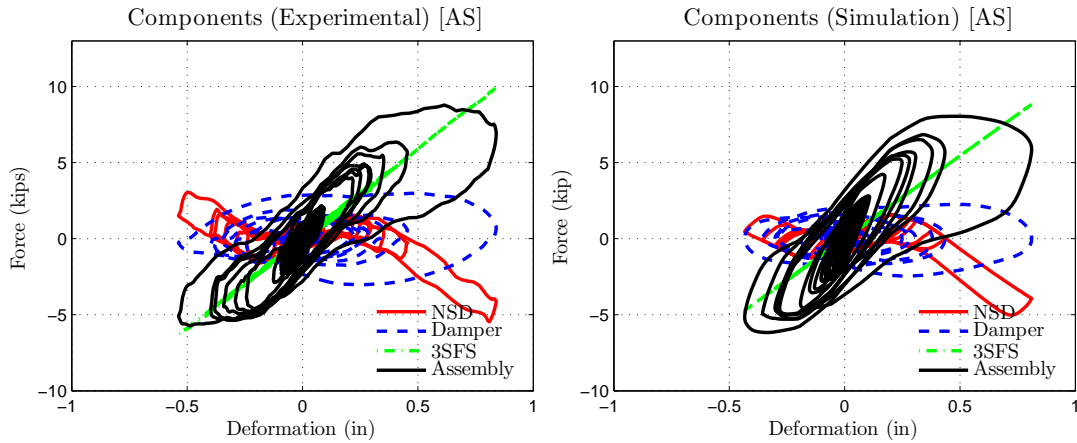


Figure 4.8: F-D behavior of AS with components in elastic structure (Kobe GM; PGA=0.29g)

with the components is shown in Figure 4.11. The assembly F-D behavior is compared in Figure 4.12, first floor deformation, acceleration and base shear are compared in Figure 4.13. The asterisk mark on PS in the figures and tables indicates that the results are predicted and not from the shake-table tests.

In the case of PS, although the peak first-floor deformation of PS is reduced by 20% compared to BS, there is no reduction in the base shear and the acceleration and this underlines the need of NSD in AS, shown in Figure 4.13. From Figure 4.11 and Figure 4.12, it is clear that with the addition of NSD, the assembly exhibits elastic bilinear behavior and as a result the base shear is reduced by more than 45% in the case of NS and 30% in the case of AS when compared to the BS and PS. From Figure 4.13(a), it can be seen that there is no permanent drift in the structure. Due to the presence of viscous damper in the AS, the displacements are reduced by 20% compared to BS and NS, the base shear and acceleration

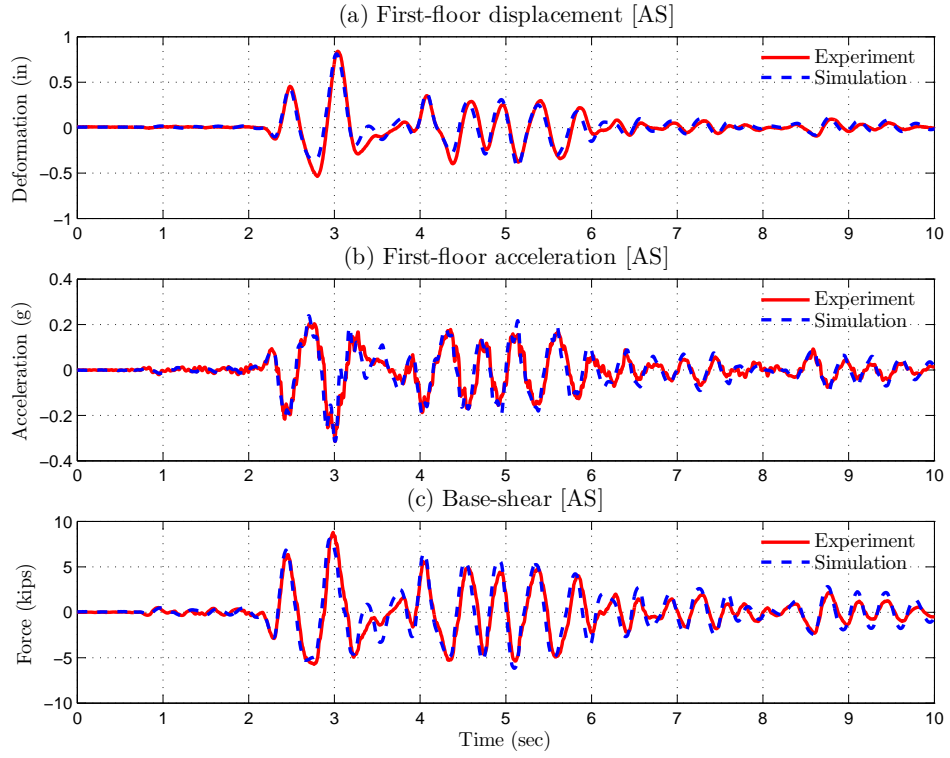


Figure 4.9: First-floor displacement, acceleration and base shear of AS in elastic structure (Kobe GM; PGA=0.29g)

are reduced by 30% and 20% respectively, compared to BS and PS. Addition of viscous damper (PS) will reduce the peak deformation by more than 20% compared to BS, but the structure will experience almost the same acceleration and base shear as the uncontrolled structure, shown in 4.13(b,c). The NSD in conjunction with a viscous damper is capable of simultaneously reducing the base shear, the acceleration and the displacement of the structure.

Similar study has been carried out for four other ground motions from PEER database and the peak response are tabulated in Table 4.1 and shown as bar-graphs in Figure 4.14. As stated previously, the ground motions are chosen to cover both the near-fault and far-field earthquakes. Since the NSD and structure assembly is a highly nonlinear system, NSD designed to reduce response for a structure and specific design ground motion has to be verified through analytical studies. The analytical models developed in this research are representative of the real life structures and can be used to verify the performance of AS for any ground motion data.

All the experimental results of BS, NS, AS and the simulation results of PS, shown in Table 4.1 and Figure 4.14 are summarized below. The key observations from the results presented in Table 2 are:

- Base shear of the NS and AS is consistently reduced by more than 20% compared to BS and in some

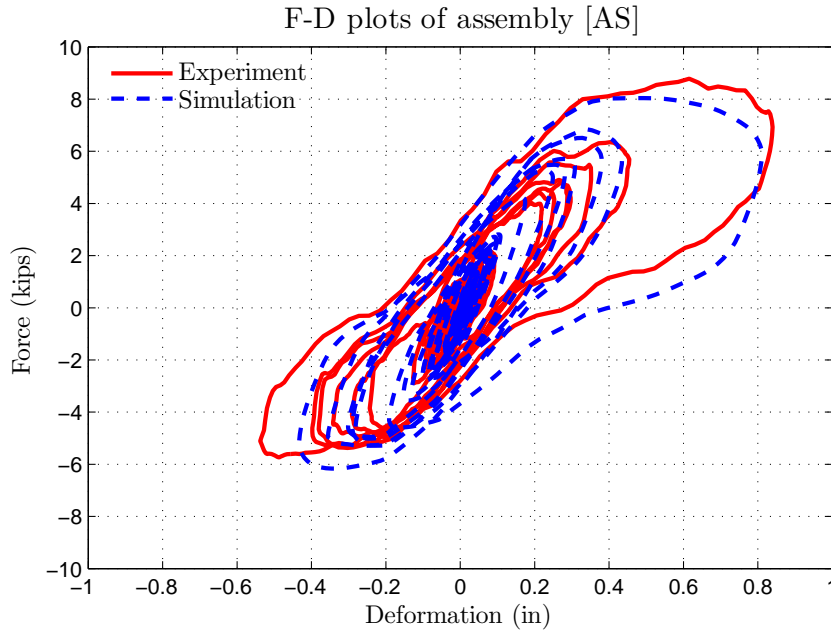


Figure 4.10: Comparison of F-D behavior of AS (Kobe GM; PGA=0.29g)

cases up to 35% (Pacoima, Chi-Chi and Newhall). Base shear of PS is only reduced by 5% in the case of Kobe and Newhall when compared to the BS and for the other ground motions it is reduced only by 15%.

- In the case of NS the peak deformation of the first-floor has a mixed response when compared with BS. Since there is no damper in the NS, the peak deformations can be larger than BS. For Kobe, Pacoima and Sylmar the peak deformation of NS is 5% more than the BS and for Chi-Chi and Newhall it is 20% less than BS. However, when the viscous damper is connected (PS and AS), the peak deformation is consistently reduced by more than 20%.
- Addition of damper reduces displacements consistently for all the ground motions both in the case of PS and AS. Among the AS and PS the response has mixed behavior; for Pacoima and Sylmar, PS has 10% lesser displacements than AS and for the other three ground motions AS has 5% lesser deformations than PS.
- Peak acceleration of the first-floor in the case of PS is very similar to BS for Kobe and Newhall ground motions and it is reduced by 20% for the other ground motions. With the addition of NSD to the 3SFS along with the damper (AS) these accelerations are reduced by more than 20% and in the case of Pacoima it is reduced by 40%.

Essentially, adding NSD to the elastic structure, a bilinear elastic system can be emulated and as a result the base shear demands on the main structure during strong earthquakes can be reduced by more

Table 4.1: Summary of the peak responses from the shake table tests on braced structure [Elastic-tests]

Serial number	Ground motion	System	Cmd. PGA (g)	First-floor response		Base shear (kip)
				Deform. (in)	Accel. (g)	
1	Kobe, 1995	BS	0.29	1.08	0.39	12.21
2		PS*	0.29	0.87 (19%)	0.39 (1%)	11.39 (7%)
3		NS	0.29	1.20 (-11%)	0.29 (27%)	7.55 (38%)
4		AS	0.29	0.84 (22%)	0.31 (20%)	8.78 (28%)
5	Pacoima, 1971	BS	0.56	1.20	0.45	13.05
6		PS*	0.56	0.67 (44%)	0.32 (29%)	8.89 (32%)
7		NS	0.56	1.25 (-4%)	0.29 (37%)	7.05 (46%)
8		AS	0.56	0.82 (32%)	0.27 (41%)	7.70 (41%)
9	Sylmar, 1994	BS	0.48	0.89	0.35	10.23
10		PS*	0.48	0.63 (29%)	0.26 (26%)	8.72 (15%)
11		NS	0.48	0.99 (-12%)	0.30 (15%)	6.84 (33%)
12		AS	0.48	0.74 (17%)	0.28 (21%)	8.08 (21%)
13	Chi-Chi, 1999	BS	0.76	1.07	0.44	11.97
14		PS*	0.76	0.70 (35%)	0.34 (23%)	9.48 (21%)
15		NS	0.76	0.86 (19%)	0.33 (24%)	6.43 (46%)
16		AS	0.76	0.59 (45%)	0.35 (21%)	7.88 (34%)
17	Newhall, 1994	BS	0.32	1.32	0.45	13.93
18		PS*	0.32	1.05 (21%)	0.46 (-1%)	13.53 (3%)
19		NS	0.32	1.01 (24%)	0.34 (25%)	8.77 (37%)
20		AS	0.32	1.00 (25%)	0.36 (21%)	9.15 (34%)

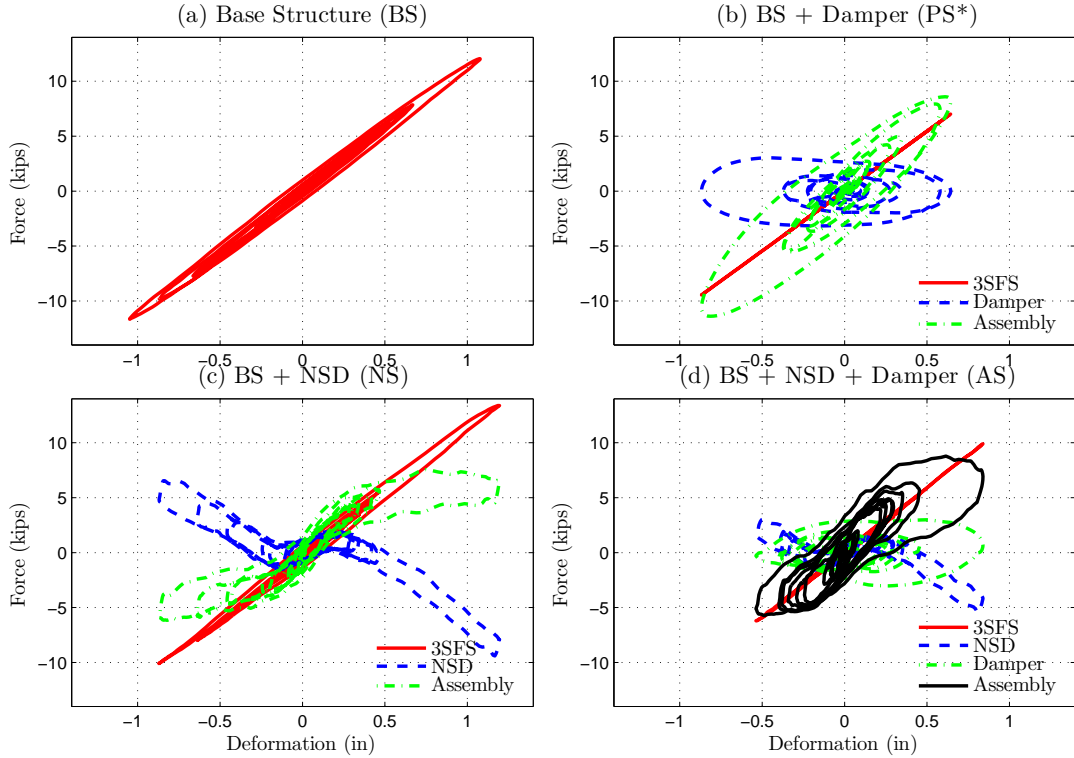


Figure 4.11: F-D behavior of BS, PS, NS and AS with components in elastic structure (Kobe GM; PGA=0.29g)

than 30%, the peak acceleration experienced by the structure is also reduced by more than 20%. However, the peak displacement of the NSD and structure assembly is increased due to the reduction in stiffness induced by the NSD. These increased deformations are controlled by adding a viscous damper. Consistent response reductions are observed for a suite of ground motions by the addition of the viscous fluid damper. The observed experimental behavior can be reproduced by the presented analytical models at the component level and also for the structure and device assembly. Next the concept is extended to yielding systems and the complications involved when the primary structure undergo inelastic deformation are discussed.

## 4.2 Yielding structures

The objective of the adaptive negative stiffness system is to shift the yielding behavior from the structure to the NSD and reduce the base shear (foundation) force of the structure while limiting its maximum response displacement and acceleration using the passive damper. In this chapter, two terms: (1) apparent yield-displacement and (2) yield displacement will be repeatedly used. To differentiate the two terms the

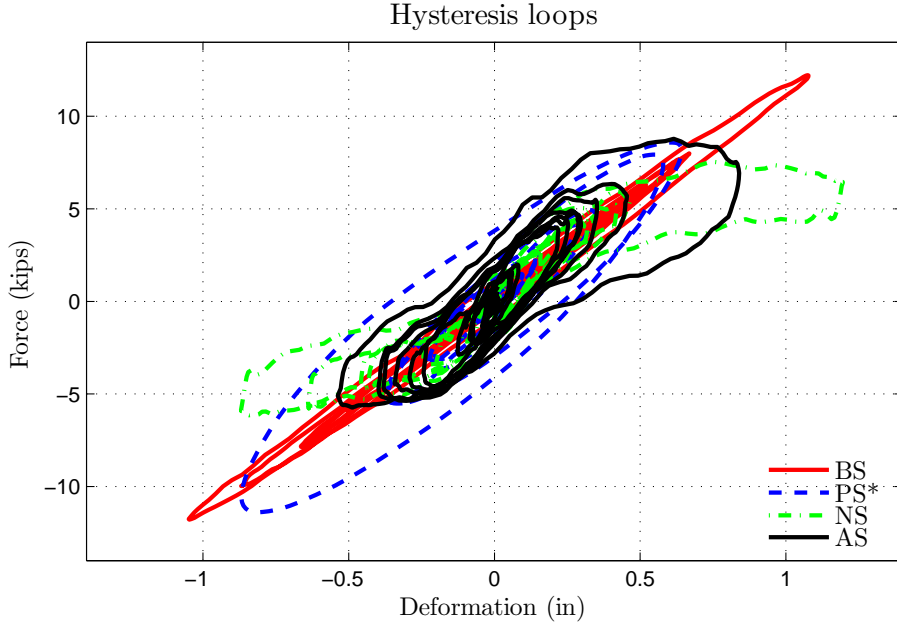


Figure 4.12: Comparison of assembly force in SDOF elastic structure (Kobe GM; PGA=0.29g)

idea of apparent weakening in bilinear inelastic structures is described next.

The force displacement characteristics of the bilinear inelastic structure, NSD and the structure with NSD assembly are shown in Figure 4.15(a), (b) and (c) respectively. Primary structure has a yield displacement  $u_y$  and the yield force is  $F_y$ , shown in Figure 4.15(a). Three crucial points are marked on the force deformation behavior of the NSD, shown in Figure 4.15(b). Point-1 is the displacement at which NSD engages (also referred as apparent yield-displacement), point-3 is when the NSD starts stiffening (stiffness becomes positive beyond point-3) and point-4 is when the NSD loses all the compression force. Readers should refer to section 2.2 for more details on the behavior of NSD.

By adding the NSD to the primary structure, the resulting force-displacement behavior of the combined system is shown in Figure 4.15(c). The behavior of the structure with NSD will not be altered for  $|u| < u'_y$ . Beyond  $u'_y$ , the stiffness of the combined system reduces until  $u_3$ . The structure and NSD assembly behaves like a nonlinear elastic structure for displacements  $|u| < u_y$ . For displacements larger than  $u_3$ , the stiffness of the structure and NSD assembly again increases and the magnitude will be higher than the elastic stiffness. At displacement  $u_4$ , the structure and the assembly (primary structure with NSD) will experience the same amount of force, shown in Figure 4.15(c). Beyond  $u_4$ , the structure with NSD will have a very high stiffness and also has higher force compared to the primary structure. The stiffening point of NSD,  $u_3$ , should be close to the yield displacement of the primary structure,  $u_y$ .

From the force deformation behavior of structure and NSD assembly shown in Figure 4.15(c): (1) the assembly exhibits the same behavior as the primary structure for  $|u| < u'_y$  (2) the shear force experienced

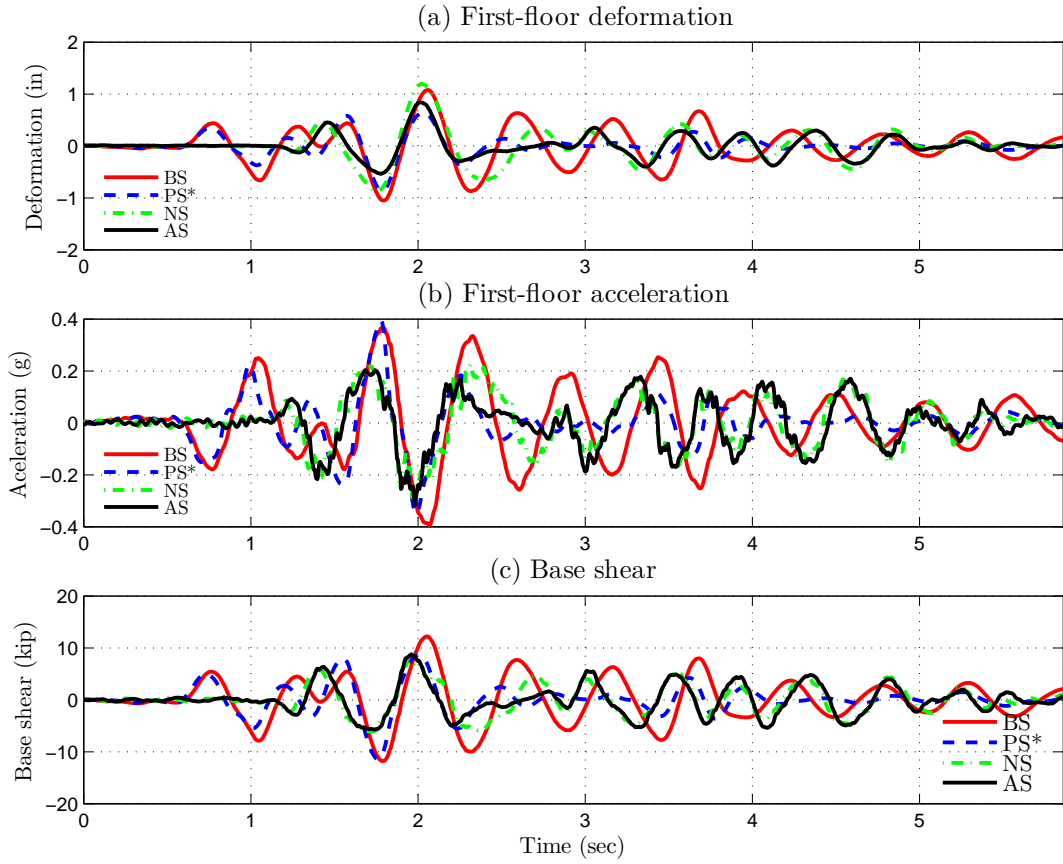


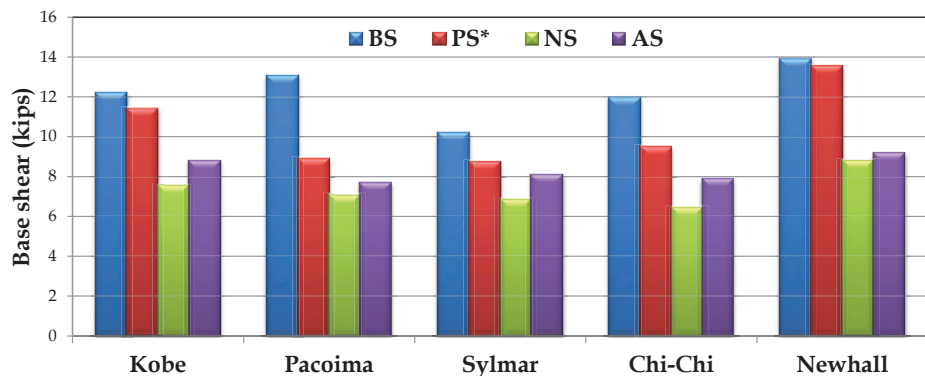
Figure 4.13: Comparison of first-floor displacement, acceleration and base-shear in elastic structure (Kobe GM; PGA=0.29g)

by the assembly is significantly less than the primary structure for  $u'_y < |u| < u_4$ . (3) the stiffness of the assembly is very high for  $|u| > u_4$ , so the assembly can be prevented from collapsing due to large plastic deformations. Since the primary structure itself is yielding, the permanent deformation of the structure and NSD assembly after a ground motion is discussed next in detail.

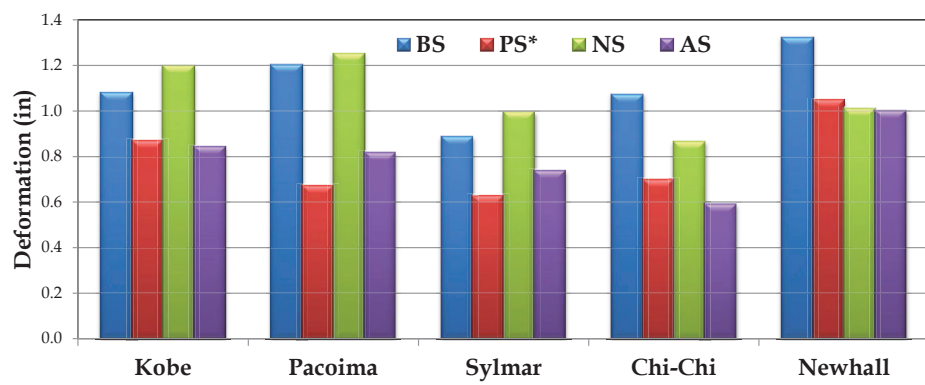
The behavior of primary structure itself is inelastic; adding a nonlinear-elastic device to the yielding structure will result in a more involved system. To understand the permanent deformations in the structure and NSD assembly, it is studied in two different regimes: (1) mild yielding systems (2) heavily yielding systems (Pasala et al., 2012d). Mild yielding systems:

The response of the structure and NSD assembly in mild yielding case is shown in Figure 4.16(a). Say, for a given ground motion, the assembly first deforms in the negative direction but the deformation is less than  $u_y$  (shown in Figure 4.16(a)); so the assembly will remain nonlinear elastic and retraces its path. Next, the assembly deforms in the positive direction and reaches a peak deformation at point-5,  $u_5 > u_y$  (shown in Figure 4.16(a)). Since the peak deformation is greater than  $u_y$ , the primary structure will undergo

### Base shear in the 3SFS



### Deformation of first-floor in the 3SFS



### Acceleration of first-floor in the 3SFS

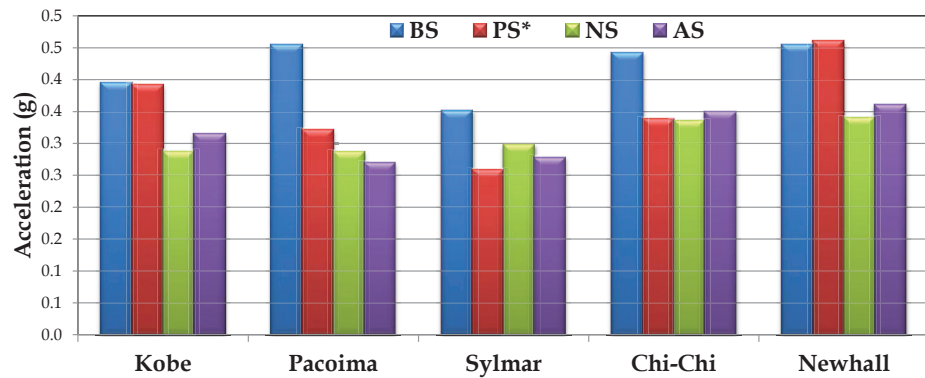


Figure 4.14: Summary of peak responses in elastic systems

a permanent inelastic deformation and will have a residual drift (plastic deformation). If there are no significant peaks in the subsequent load, the assembly will oscillate at low amplitudes and reaches point-6 (shown in Figure 4.16(a)) at the end of loading cycle. The plastic deformation in the primary structure

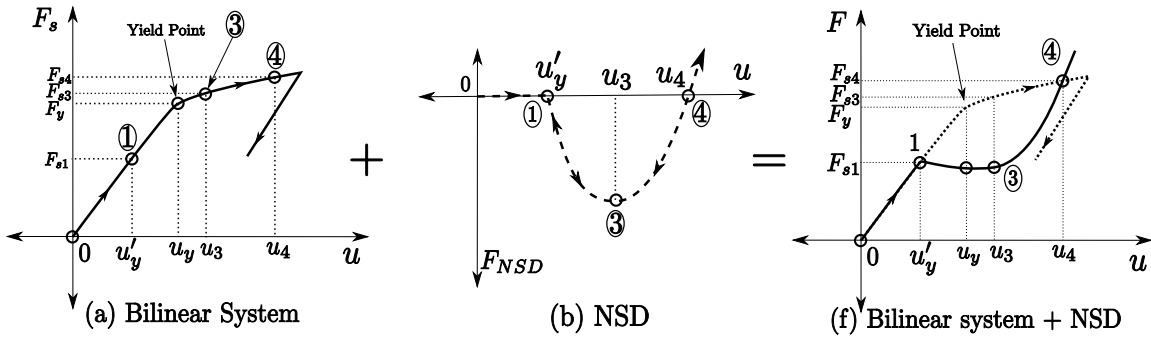


Figure 4.15: Schematic diagram depicting “apparent-weakening” in yielding systems

is  $u_{d6} = u_5 - u_y$ ; subscript-“d” refers to permanent drift. Since the NSD exerts no stiffness for  $|u| < u'_y$ , the permanent deformation in the assembly is same as the plastic deformation in the primary structure if  $|u_{d6}| < u'_y$  as shown in Figure 4.16(a). If the permanent yield deformation in the structure,  $u_d$ , is less than  $u'_y$ , then the structure is assumed to have undergone mild yielding. The assembly always reaches the point where the assembly force is zero, following a loading cycle. Next, the condition in which,  $|u_d| > u'_y$ , is studied.

#### Heavily yielding systems:

Assume a particular load in which there are two dominant half-pulses, one in the positive direction and the other in negative direction. For the first pulse, say, the assembly deforms in negative direction with mild yielding as shown in Figure 4.16(b). Then for the next pulse, the assembly deforms in positive direction and reaches a peak deformation  $u_7$ . Since there are no other dominant pulses, the assembly oscillates at low amplitudes and reaches point-9, where the assembly force is zero as shown in Figure 4.16(b). The permanent deformation in the assembly is  $u_{d9}$ . It should be noted that the assembly force is zero at point-9, but the force in the primary structure is  $F_{s9}$  and the force in NSD is  $F_{NSD9}$  as shown in Figure 4.16(b). The forces in structure and NSD have save magnitude but with different sign so they nullify each other to result in zero assembly force. The actual plastic deformation in the primary structure is  $u'_{d9}$ ; which is less than  $u_{d9}$  as shown in Figure 4.16(b). By disconnecting the NSD, the primary structure will move to the displacement  $u'_{d9}$ . The difference of the displacements  $u_{d9}$  and  $u'_{d9}$  is called recoverable permanent-drift or simply recoverable-drift,  $u_{rd}$ .

In brief, for heavily yielded systems, the permanent drift in the assembly ( $u_{d9}$ ) is larger than the plastic deformation in the primary structure ( $u'_{d9}$ ). Deformation,  $u_{rd}$  can be recovered from the assembly to reach  $u'_{d9}$ . In the experiments carried on the 3SFS, the connectors between the NSD and primary structure have a slotted hole to disengage the NSD easily and recover  $u_{rd}$ . The trend in the permanent deformation of the primary structure and assembly will again be different for deformation larger than  $u_4$  (shown in Figure 4.15(b)). Due to the very high assembly stiffness for displacement greater than  $u_3$ , the assembly deformation will never reach  $u_4$ . The concept explained using schematic diagrams shown in

Figure 4.16 can be extended to multiple loading cycles. Next the experimental results of NS in which the primary structure had yielding is presented. The results are overlapped with predicted results obtained from the analytical models.

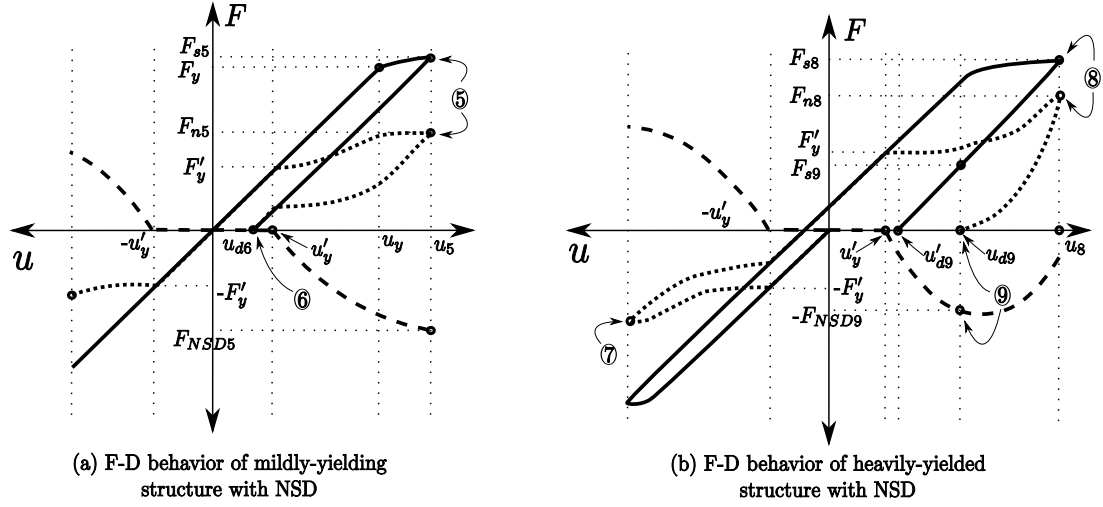


Figure 4.16: Recoverable drift and residual drift in NSD and bilinear inelastic structure assembly

#### 4.2.1 Mild-yielding structures

In this section “apparent weakening” in mild and heavily yielding systems is analyzed through shake-table studies on 3SFS and NSD assembly (NS). Since the damper has a maximum stroke of only two inches and the yield displacement is 1.5 inches, the heavy yielding tests could not be carried on the 3SFS, NSD and damper assembly. In elastic systems, experimental results for Kobe FN ground motion are presented in section 4.1. In the case of mild yielding and heavy yielding, 3SFS and NSD assembly is subjected to Pacoima ground motion at two different amplitudes (peak ground acceleration (PGA) of 0.57g and 0.81g).

When the assembly is subjected to the ground motion at PGA of 0.57g there is mild yielding in the primary structure. The force-deformation behavior of the primary structure (3SFS), and the assembly is shown in Figure 4.17; the F-D loops of NDS-East and NSD-West are shown in 4.18. The experimental and analytical force-deformation behavior of the assembly with the components is shown separately in Figure 4.19. First-floor displacement, acceleration and base shear response are shown in Figure 4.20. From force-deformation behavior of primary structure, shown in Figure 4.17(a) and displacement response shown in Figure 4.20(a), it is clear that the 3SFS has yielded at 1.8 seconds when the peak deformation in the structure is 1.7 inches. The structure has undergone plastic deformation and it subsequently vibrates about 0.11 inch displacement. Although the primary structure has yielded, since the plastic deformation is less than the simulated yield displacement, the permanent drift in the assembly is same as the permanent drift in

the primary structure. Force-deformation behavior shown in Figure 4.17(a) and Figure 4.19 confirms that the base shear of the assembly is reduced by more than 50% by adding the NSD to the primary structure. This behavior is consistent in both the predicted analytical results and observed experimental results.

The trace of the force-deformation plots of 3SFS, NSD and assembly (similar to the schematic plots shown in Figure 4.16(a)) is shown in Figure 4.21 for both experimental and analytical results. The trace of force-deformation plots is obtained by removing the friction in the NSDs (Figure 4.18), assembly (Figure 4.17(b)) and discarding the vibrations after 2.5 seconds. From the experimental results in Figure 4.21(a), the permanent drift in the assembly and the plastic deformation in the primary structure are same, 0.11 in. and in the case of simulation results, shown in Figure 4.21(b), it is equal to 0.09 in. The plastic deformation in 3SFS and the permanent drift in assembly are same because the simulated yield displacement in NSD is 0.25 in. and the permanent drift in the primary structure is less than 0.25 in..

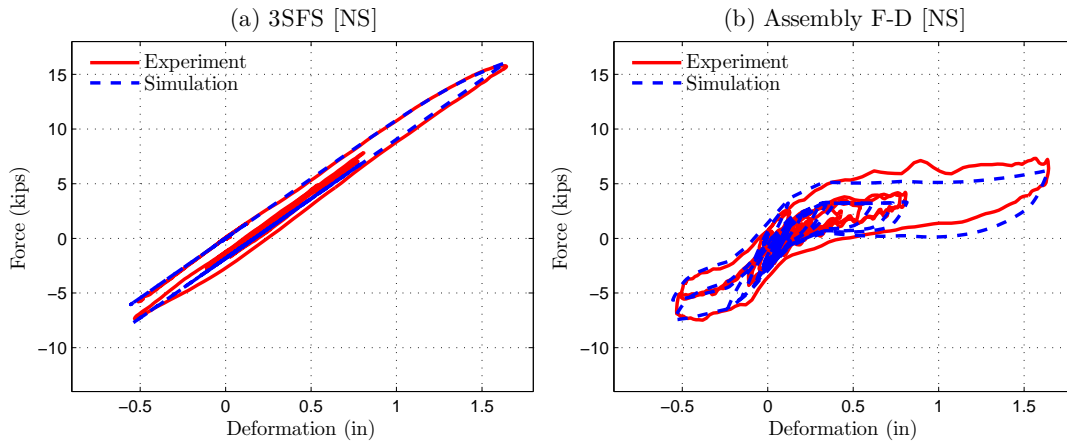


Figure 4.17: F-D behavior of 3SFS and assembly in NS (Pacoima GM; PGA=0.57g)

#### 4.2.2 Heavy-yielding structures

When the structure is subject to the ground motion with PGA of 0.81g, the primary structure in NS has yielded significantly. The force-deformation behavior of the primary structure (3SFS) and the assembly are shown in Figure 4.22, and NSDs (NSD-East and NSD-West) are shown in Figure 4.23. The experimental and analytical force-deformation behavior of the assembly with the components is shown separately in Figure 4.24 for the heavy yielding case. First floor displacement and acceleration response of the first-floor are shown in Figure 4.25(a,b), and base shear is shown in Figure 4.25(c). The overall trend in the analytical and experimental behavior depicted in Figure 4.22 and Figure 4.23 is similar, but the peak deformation in the experiments is 2.83 in. and the peak deformation in analytical studies is 2.51 in.

From the experimental force-deformation behavior of primary structure shown in Figure 4.22(a) and displacement response shown in Figure 4.25(a), 3SFS has yielded at 2.3 seconds when the peak deforma-

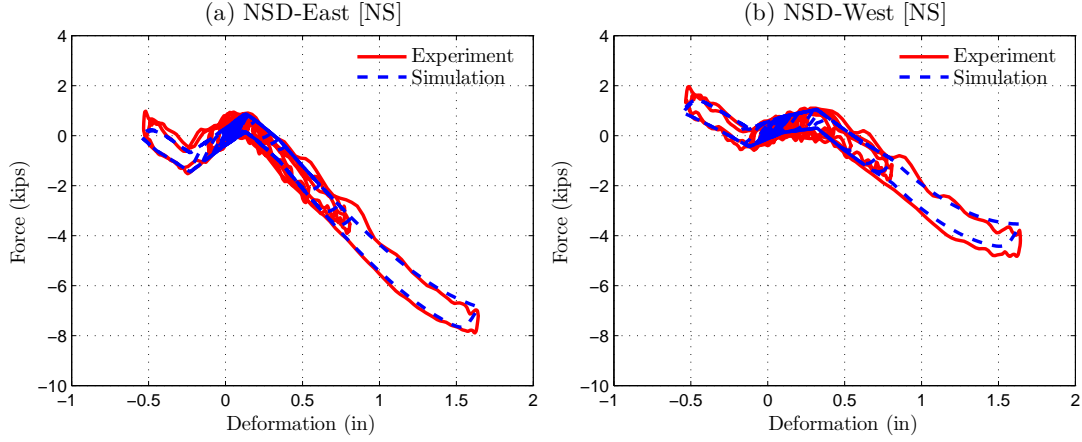


Figure 4.18: F-D behavior of NSDs in NS (Pacoima GM; PGA=0.57g)

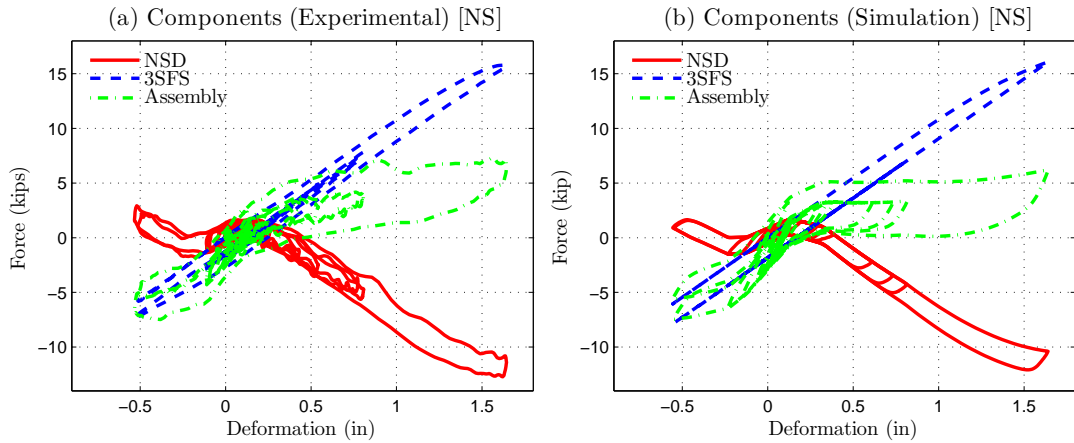


Figure 4.19: F-D behavior of NS with components in mild-yielding structure (Pacoima GM; PGA=0.57g)

tion in the structure is 2.83 *in.* The plastic deformation of the primary structure is 1.14 *in.* as shown in Figure 4.25(a). Since the simulated yield displacement (0.25 *in.*) is significantly less than the plastic deformation in the 3SFS, the permanent deformation of the assembly will be higher than the plastic deformation of the 3SFS due to the presence of NSD as explained in the previous section. The assembly starts stiffening at 2 in displacement resulting in the increase in base shear as shown in Figure 4.24. Once the assembly starts stiffening, the excessive deformation caused due to the initial reduction in stiffness is contained and the structure is prevented from collapsing. Essentially, the accelerations and base shear of the assembly are reduced between the displacements, 0.5 *in.* and 3 *in.* by removing a segment of the force deformation loop of primary structure.

The trace of the force-deformation plots of 3SFS, NSD and assembly (similar to the schematic plots

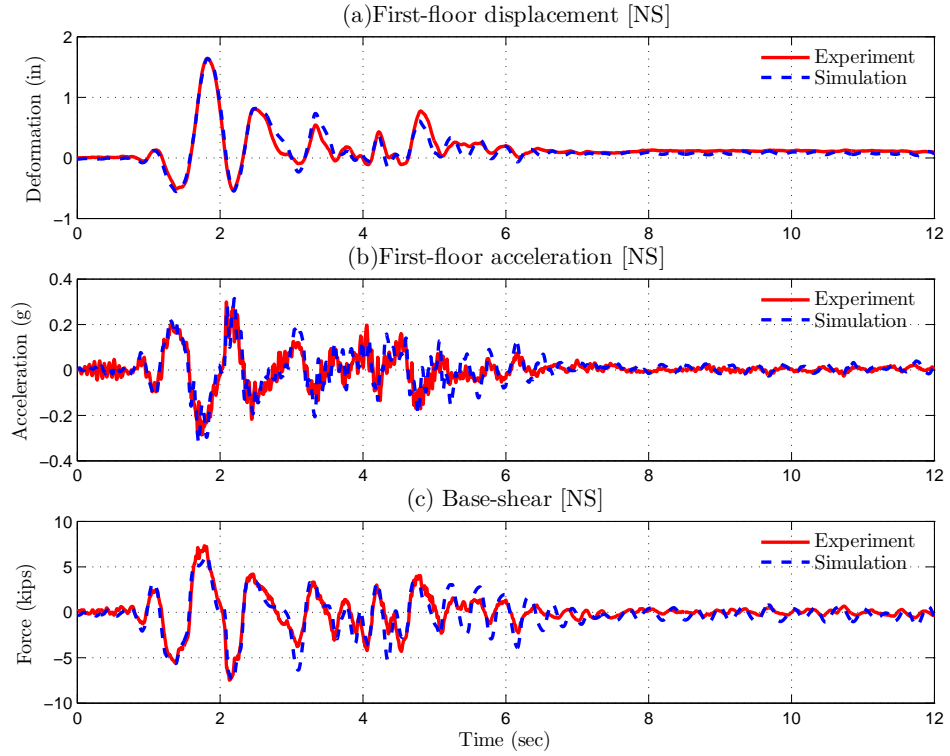


Figure 4.20: First-floor response and base shear of NS in mild-yielding structure (Pacoima GM; PGA=0.57g)

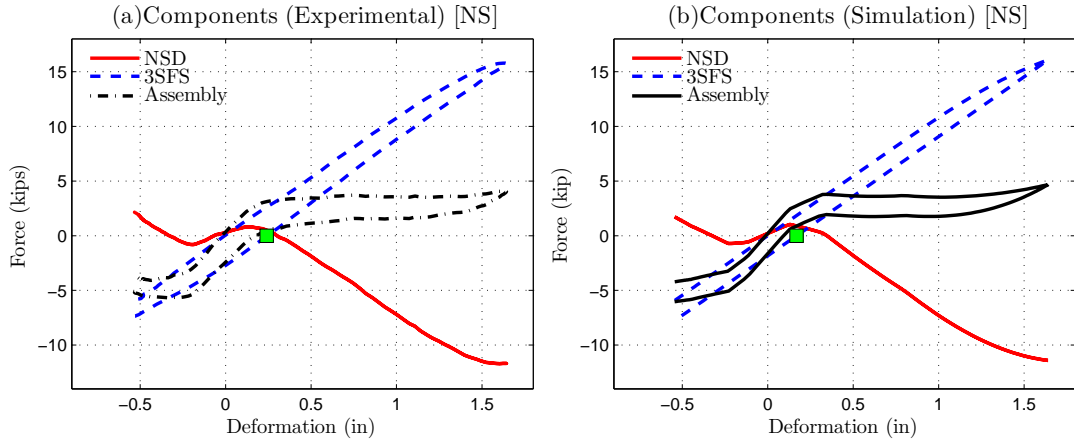


Figure 4.21: Trace of F-D behavior of NS with components in mild-yielding structure (Pacoima GM; PGA=0.57g)

shown in Figure 4.16(b)) is shown in Figure 4.26 for both experimental and analytical results. The trace of force-deformation plots is obtained by removing the friction in the NSDs (Figure 4.23), assembly (Figure

4.22(b)) and discarding the vibrations after 2.5 seconds. From the experimental results in Figure 4.26(a), the permanent drift in the assembly is 2.1 *in.* and the plastic deformation in the primary structure, shown in Figure 4.25(a) is 1.14 *in.* In the case of simulation results, shown in Figure 4.26(b), the permanent drift in the assembly is 2 *in.* and the plastic deformation in the primary structure, shown in Figure 4.25(a), is 0.89 *in.* Since the plastic deformation in the primary structure is much larger than the simulated yield displacement, the permanent drift in the assembly will be higher than the plastic deformation in the primary structure. So, in the experimental results, the residual drift in the NS will be *in.* *in* and the recoverable drift is 0.97 *in.* In the deformation plot shown in Figure 4.26(b), the NSD is disengaged from the structure at 9 seconds so the drift in the structure has reduced to 1.14 *in.*

In the next section, the advantages of using NSD in conjunction with the damper to attenuate the acceleration, displacement, base shear and permanent drift response is demonstrated by comparing with three other systems.

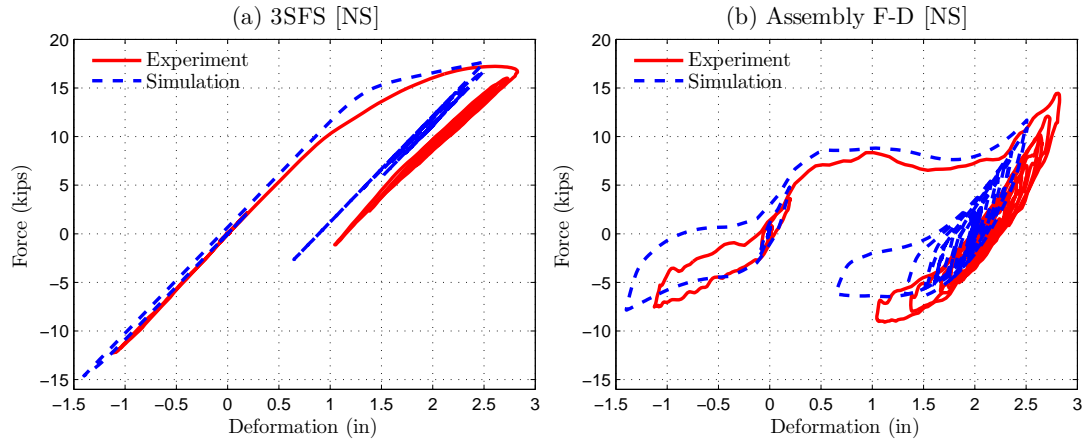


Figure 4.22: F-D behavior of 3SFS and assembly in NS (Pacoima GM; PGA=0.81g)

Since the columns were yielding significantly after a strong ground motion, only one yielding experiment for each ground motion has been conducted. For Newhall, Pacoima and Sylmar ground motions, the NS is tested and for Kobe ground motion, the AS is tested. In this section the experimental results of AS and the simulation results of BS, PS and NS are compared to demonstrate the effectiveness of apparent-weakening and damping in yielding structures. The results from other shake table tests are summarized in Table 4.2 and Figure 4.30.

Force-deformation loops of all the four systems with components are shown in Figure 4.27 for Kobe-FN ground motion with PGA of 0.65g. Superscript-“\*” denotes that the results are simulated using the analytical model. The accelerations, deformations (showing the drifts) and base shears of all the four systems are compared in Figure 4.28. From Figure 4.27(a) and Figure 4.28(a), the BS has undergone plastic deformation in the negative direction first and then in the positive direction. The peak deformation,

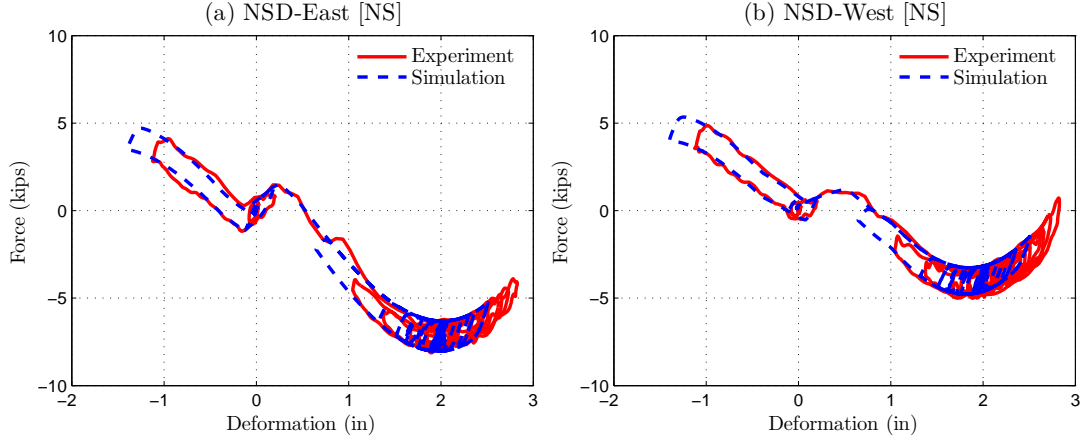


Figure 4.23: F-D behavior of NSDs in NS (Pacoima GM; PGA=0.81g)

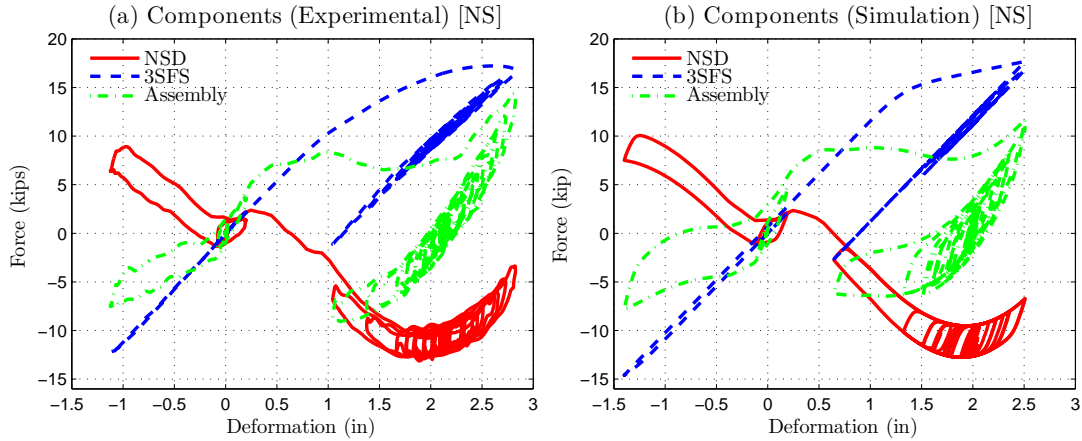


Figure 4.24: F-D behavior of NS with components in heavy-yielding structure (Pacoima GM; PGA=0.81g)

acceleration and base shear of the first story in the BS are 2.84 *in.*, 0.79g and 17.7 *kips*, respectively, shown in Table 4.2. By adding NSD to the 3SFS (NS) due to the reduction in assembly stiffness beyond 0.5 *in.*, the assembly has undergone significant deformation until it gets into the stiffening region, shown in Figure 4.27(c). Once the assembly enters the stiffening region, due to the high assembly stiffness and large plastic deformation of the 3SFS, the assembly will remain in the stiffening region. Permanent drift in the assembly after the ground motion is 1.67 *in.* (shown in Figure 4.28(a)) and the plastic deformation in the 3SFS is 0.87 *in.* as shown in Figure 4.27(c). The permanent drift in the NS after disconnecting the NSD at 6 seconds is shown in Figure 4.28(a). So, by adding the NSD, the accelerations and base shears can be reduced and the structure can be prevented from collapsing for large deformations. Although the peak

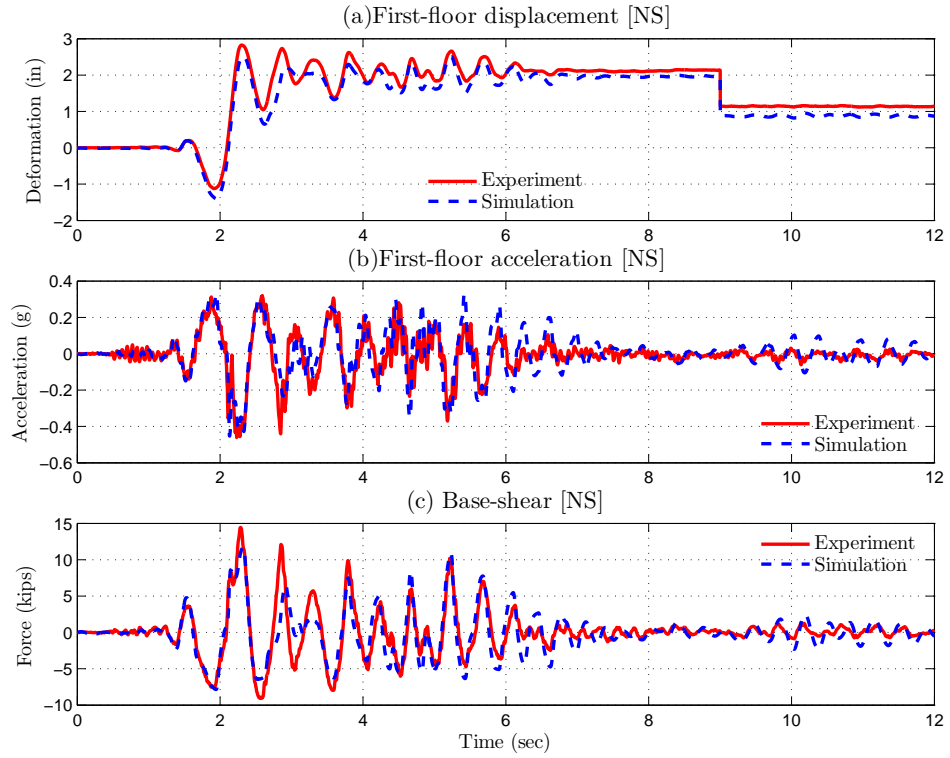


Figure 4.25: First-floor response and base shear of NS in heavy-yielding structure (Pacoima GM; PGA=0.81g)

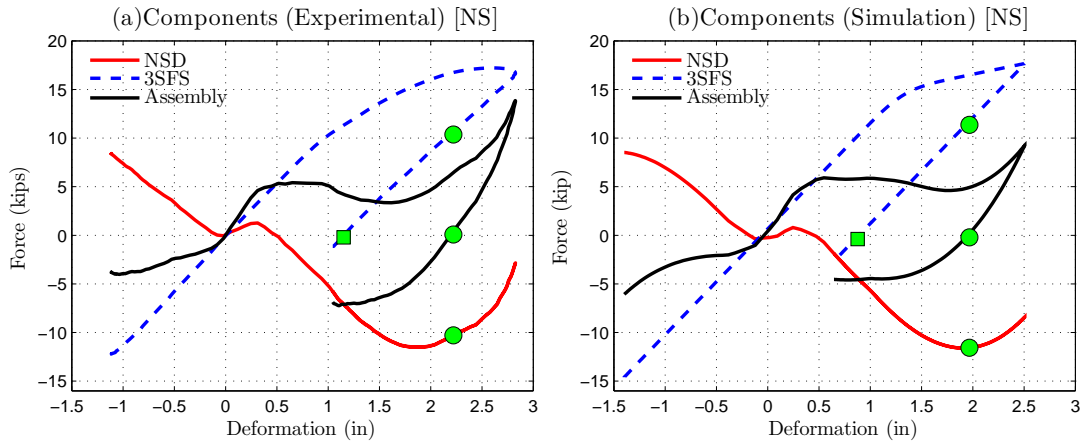


Figure 4.26: Trace of F-D behavior of NS with components in heavy-yielding structure (Pacoima GM; PGA=0.81g)

deformations in NS are similar to BS, the global collapse of the assembly is prevented in NS due to the stiffening in NSD.

By adding a viscous damper to the structure along with the NSD, the experimental force-deformation plots of the assembly and components are shown in Figure 4.27(d). With the addition of viscous damper, the excessive deformations caused due to the reduction in assembly stiffness are contained. From Figure 4.27, 4.28, 4.29 and Table 4.2, the peak deformation, acceleration and base shear of the AS are reduced to 1.39 *in.*, 0.58g and 13.7 *kips*, respectively. The response of 3SFS with the viscous damper (PS) is also calculated to demonstrate the role of NSD in the AS. Although the deformations are reduced with the addition of viscous damper, the acceleration and the base shear of the assembly will significantly shoot up due to the damper force, as shown in Figure 4.28(b,c), 4.29 and Table 4.2. The peak deformation, acceleration and base shear of the PS are 1.93 *in.*, 0.73g and 22.4 *kips*. Clearly, by adding the NSD along with the damper, the base shear and accelerations can be reduced. Assembly force-deformation loops of all the four systems, shown in Figure 4.29, confirms that by adding NSD and damper to the bilinear inelastic structure, the displacement, acceleration and base shear can be reduced.

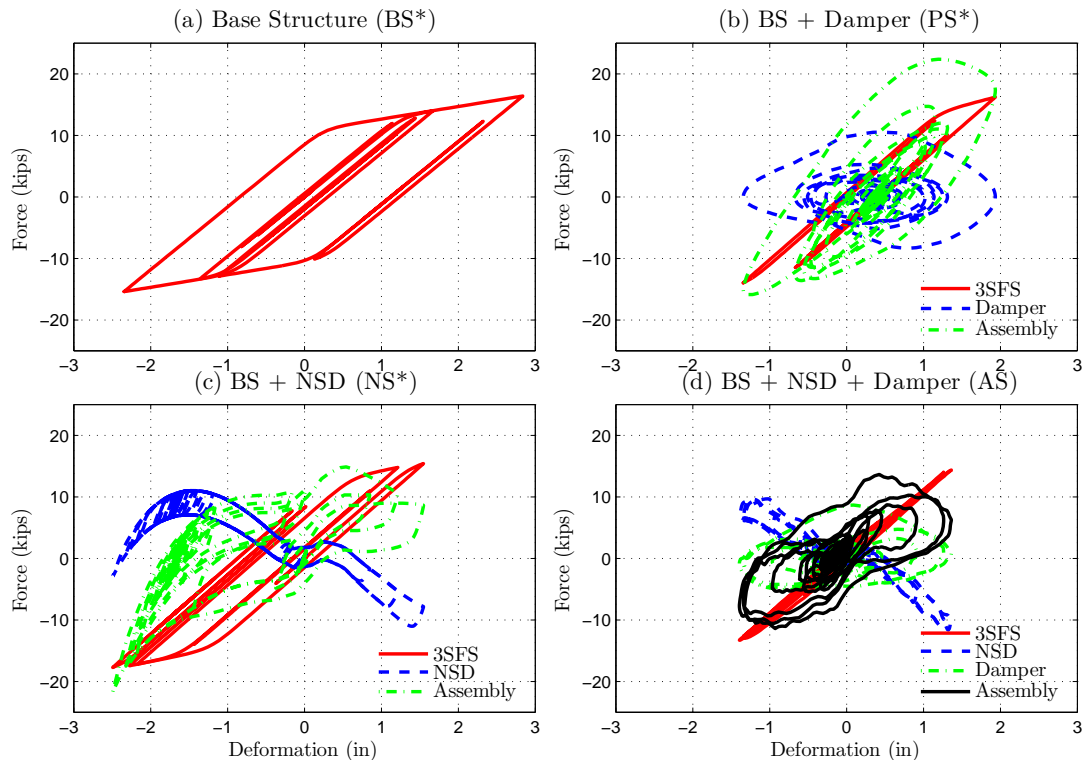


Figure 4.27: F-D behavior of BS, PS, NS and AS with components (Kobe GM; PGA=0.65g)

Table 4.2 and Figure 4.30 summarizes the peak response characteristics of all the four systems for four ground motions at higher PGA values so that the primary structure will yield. The key observations are:

1. Due to the presence of NSD, base shear of the NS and AS is consistently reduced up to 35% compared to the BS in the mild yielding cases. In the heavy yielding cases, the base shear in the assembly

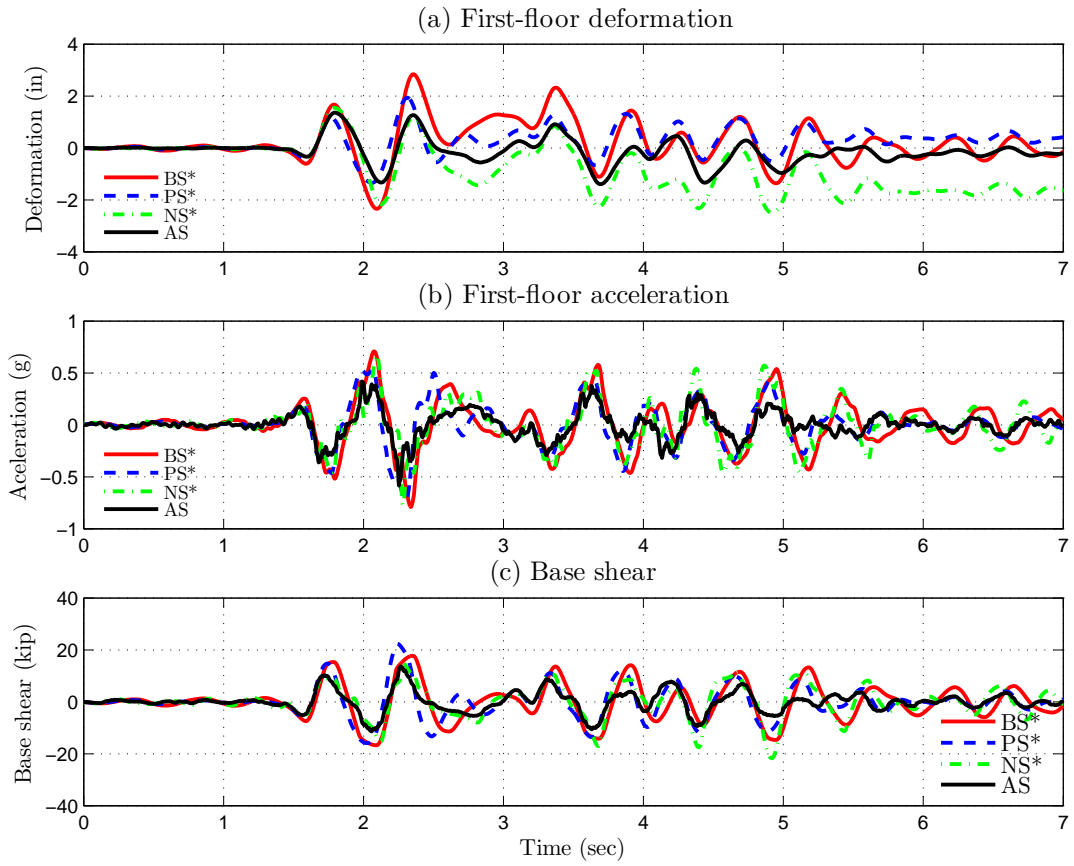


Figure 4.28: Comparison of first-floor displacement, acceleration and base-shear (Kobe GM; PGA=0.65g)

will be similar to the BS because of the stiffening. However, the structure can be prevented from collapse due to the high stiffness.

2. The addition of a viscous damper (PS) reduces the deformation of the assembly by more than 30% but the reduction in base shear less than 10%. In the case of Kobe ground motion, the base shear in PS has increased by 23%.
3. By adding the viscous damper in conjunction with NSD, the displacements, accelerations and base shears can be consistently reduced by more than 20%.
4. Permanent drift in the assembly after the ground motion is equal to the plastic deformation in the primary structure if the plastic-deformation is less than simulated yield displacement. If the plastic deformation in primary structure is larger than the simulated yield-displacement then the permanent drift in the assembly will be higher than the plastic deformation but the drift in excess of plastic-deformation is recoverable.

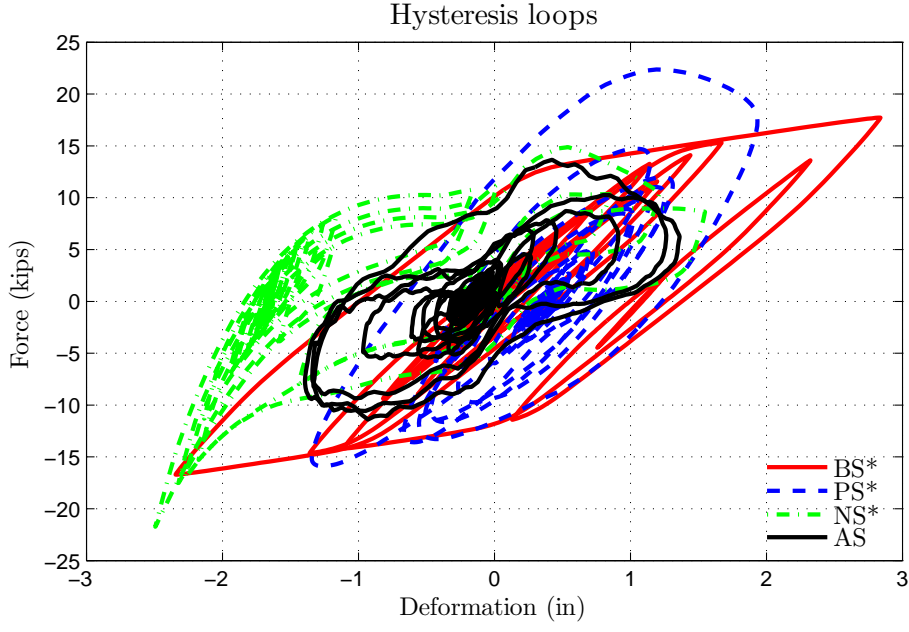


Figure 4.29: Comparison of assembly forces in SDOF structure (Kobe GM; PGA=0.65g)

5. The residual drift in AS is comparable with that of BS and PS. It should be noted that in the case of BS and PS the 3SFS is yielding in both the directions, so some of the plastic deformation is recovered. In the case of 3SFS and NSD assembly, since the force-deformation behavior of NSD is very asymmetric, the assembly has the tendency to remain in the region in which it has yielded first. However, simulation studies with a symmetric force-deformation of NSD have shown that the assembly can yield in both sides during the same ground motion (presented in chapter 1)

### 4.3 Summary

In this chapter, the concept of “apparent weakening” is analyzed in elastic and yielding structures. Comprehensive experimental and simulation studies have been carried on SDOF-3SFS yielding structure, to study the behavior of bilinear inelastic structure and NSD assembly during severe ground motions. Shake table studies carried on a SDOF-3SFS with the NSDs and damper installed in the first floor (AS) show that by adding NSD to the elastic structure, a bilinear elastic system can be emulated and as a result the base shear demands on the main structure during strong earthquakes can be reduced by 30%. The peak acceleration experienced by the structure is also reduced by more than 20%. However, the peak displacement of the NSD and structure assembly is increased due to the reduction in stiffness induced by the NSD. These increased deformations are controlled by adding a viscous damper. Consistent response reductions are observed for a suite of ground motions by the addition of the viscous fluid damper. The observed

Table 4.2: Summary of the peak responses from the shake table tests on braced structure [Yielding-tests]

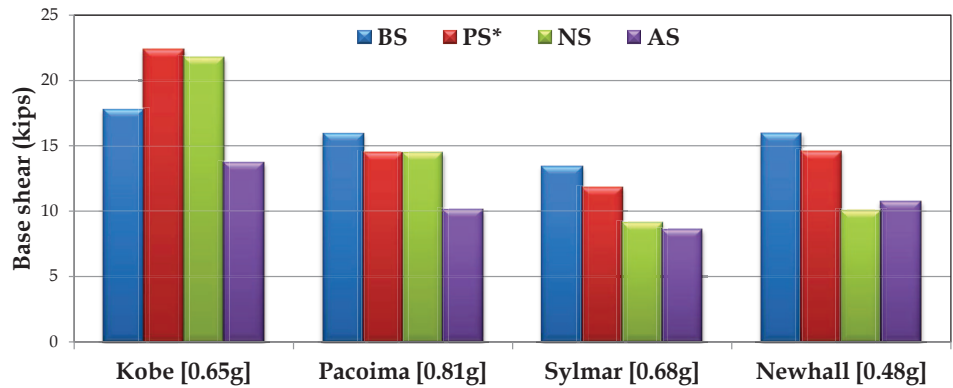
Sl. no.	Ground motion	Sys.	PGA (g)	First-floor response		Permanent drift			Base shear (kip)
				Deform. (in)	Accel. (g)	Tot.	Recov.	Resid.	
1	Kobe, 1995	BS*	0.65	2.84	0.79	0.05	-	0.05	17.72
2		PS*	0.65	1.93 (32%)	0.73 (7%)	0.36	-	0.36	22.36 (-26%)
3		NS*	0.65	2.49 (12%)	0.77 (2%)	1.67	0.80	0.87	21.74 (-23%)
4		AS	0.65	1.39 (51%)	0.58 (26%)	0.17	0.00	0.17	13.65 (23%)
5	Pacoima, 1997	BS	0.75	1.92	0.56	0.20	-	0.20	15.89
6		PS*	0.81	1.16 (40%)	0.49 (13%)	0.00	-	0.00	14.47 (9%)
7		NS	0.81	2.83 (-47%)	0.46 (18%)	2.11	0.97	1.14	14.45 (9%)
8		AS	0.75	1.65 (14%)	0.37 (35%)	0.32	0.12	0.20	10.10 (36%)
9	Sylmar, 1994	BS	0.68	1.29	0.47	0.00	-	0.00	13.37
10		PS*	0.68	0.87 (32%)	0.38 (19%)	0.02	-	0.02	11.78 (12%)
11		NS	0.63	1.71 (-32%)	0.34 (27%)	0.91	0.58	0.33	9.08 (32%)
12		AS	0.63	1.18 (8%)	0.34 (28%)	0.10	0.00	0.10	8.55 (36%)
13	Newhall, 1994	BS	0.44	1.72	0.50	0.03	-	0.03	15.91
14		PS*	0.48	1.16 (33%)	0.44 (13%)	0.00	-	0.00	14.56 (8%)
15		NS	0.48	1.36 (21%)	0.44 (12%)	0.43	0.30	0.13	10.02 (37%)
16		AS	0.44	1.30 (24%)	0.39 (22%)	0.16	0.00	0.16	10.71 (33%)

experimental behavior can be reproduced by the presented analytical models at the component level and also for the structure and device assembly.

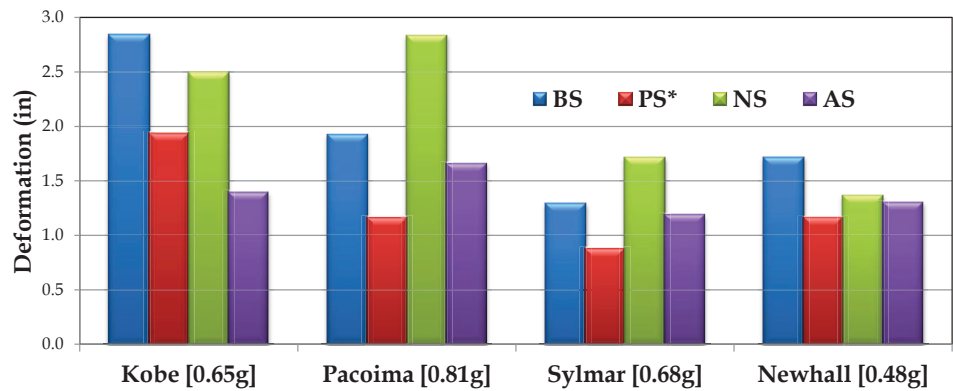
It has been shown through numerical studies that the addition of viscous damper will reduce the peak deformation by more than 20% but the structure will experience almost the same acceleration and base shear as the uncontrolled structure. The NSD in conjunction with a viscous damper is capable of simultaneously reducing the base shear, the acceleration and the displacement of the structure.

With the addition of NSD to the bilinear inelastic structure, the base shear and accelerations of the assembly are reduced by more than 30% for ground motions in which there is mild yielding in the primary structure. For more severe ground motions, the deformations of the assembly will be larger than the stiffening point of NSD; resulting in very high assembly stiffness, thereby increase in base shear and accelerations of the assembly. However, the high stiffness of the assembly will prevent the structure from collapsing. In the case where there is heavy yielding in the primary structure, the permanent drift in the assembly is larger than the plastic deformation in the primary structure. The permanent drift in excess of the plastic-deformation in the primary structure can be completely recovered by disengaging the NSD from the primary structure. It has also been demonstrated that the stiffening in NSD will prevent the structure from collapsing. Analogous to the inelastic design, the acceleration and base shear and deformation of the structure and NSD assembly can be reduced by more than 20% for moderate ground

### Base shear in the 3SFS



### Deformation of first-floor in the 3SFS



### Acceleration of first-floor in the 3SFS

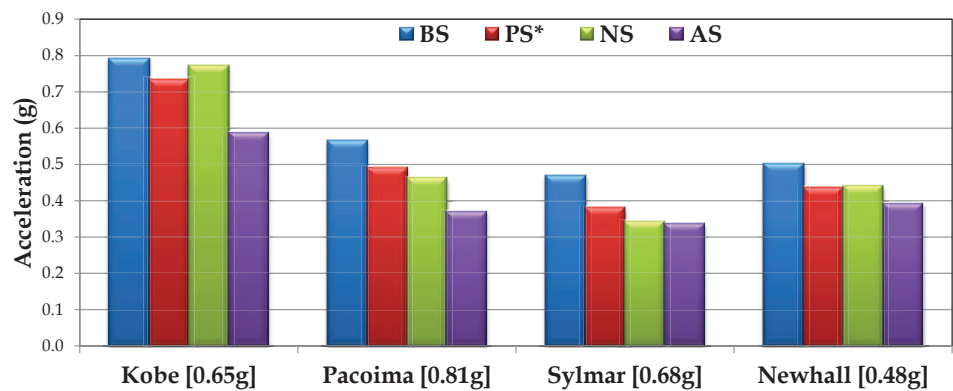


Figure 4.30: Summary of peak responses in yielding systems

motions and the collapse of structure can be prevented for severe ground motions. Additionally, part of the inelastic excursions incurred after a severe ground motion can be recovered by disconnecting the NSD.



## Chapter 5

# Apparent-Weakening in MDOF Structures

Experimental studies presented in previous chapter have confirmed that by adding the NSD to a SDOF system, the acceleration and base shear of the structure can be reduced significantly at the expense of increased deformations. The excessive deformations caused due to the reduction in “apparent stiffness” can be contained by adding a passive damper. So far, the focus and the application of NSD has only been on the response reduction of that story in which the NSD is installed. The impact of adding NSDs in one floor and multiple floors is the focus of study in this chapter. Because of the involved dynamics in the case of MDOF structures, the behavior of NSD in multi-story frames is studied in two different sections. First, the experimental results of 3SFS with NSDs in the first floor is studied to analyze the effect of NSDs on upper stories. Later, simulation studies on an inelastic nine-story multistoried shear building to demonstrate the effectiveness of placing NSDs and dampers at multiple locations along the height of the building is demonstrated (Pasala et al., 2012a).

The results reported in this chapter have demonstrated that by placing a NSD in a particular story the superstructure above that storey can be isolated from the effects of ground motion. Since the energy from ground motion is transmitted from bottom to top, the NSDs in the bottom floors will undergo large deformations. However, due to the reduction in assembly stiffness with the addition of NSDs, the bottom floors will undergo large deformations. To overcome this, a generalized scheme to incorporate NSDs with different properties is proposed in this study. To highlight the advantages of using NSDs and dampers in multiple stories, the response is compared with a passively controlled system and the uncontrolled primary structure for six standard ground motions. Large base deformations and permanent drifts which is common in base-isolating the structural systems are overcome by using NSDs in multiple stories, since the isolation is achieved over the height of the building and not confined to the base: referred as distributed isolation. It has been shown through the simulation studies that by placing the NSDs in the lower story’s the acceleration of the superstructure and base shear can be reduced significantly without affecting the drifts.

Rest of the chapter is organized as follows: First the shake table results on 3SFS (without braces in the

moment frame) with NSDs in the first floor are presented for moderate ground motions in section-5.1 and for severe ground motions in section-5.2. A nine-story 1:3 scale frame used to demonstrate the concept of distributed isolation is presented in section-5.3. Simulation results on the nine-story frame depicting the isolation capabilities of NSD and an optimization scheme to distribute isolation over the height of bottom few floors are presented in section-5.4 for a suite of ground motions.

## 5.1 Unbraced 3SFS Response to moderate ground motion

The beams in the 3SFS were yielding after the specimen is subjected to severe ground motion and to replace these beams, the whole structure has to be disassembled. Since it involves a great deal of money and time in order to do multiple yielding tests, the experimental tests were only performed on the 3SFS and NSD assembly. As mentioned earlier, to justify the importance of NSD, response of four systems have to be compared. So, the responses of 3SFS and 3SFS with damper have to be simulated using the analytical models. To ensure the consistency in modeling, first, the analytical models for the components developed in chapter 3 from first-principles and the unknown parameters in the models are obtained by calibrating with the experimental results of 3SFS and NSD assembly. Using the analytical models, the predicted behavior of the assembly is compared and they are in good agreement.

Elevation, actual photograph and the schematic of the 3SFS is shown in Figure 5.1; the elements in the schematic are color coded. In this section, experimental results of two tests (1) 3SFS, NSDs and damper assembly (AS) for Pacoima ground motion with a PGA of 0.62g and (2) 3SFS and NSDs assembly (NS) for Pacoima ground motion with a PGA of 0.78g are presented. Experimental results are compared with the simulation results to demonstrate the accuracy of analytical models used. Also, response of four different systems: (1) 3SFS or the base structure (BS); (2) 3SFS and NSD assembly (NS); (3) 3SFS, NSD and damper assembly (AS); (4) 3SFS and damper (PS) are generated using the analytical models and compared to highlight the advantages of apparent-weakening in multi-story building.

First, the impact of NSD in 3SFS for moderate ground motions is analyzed. Force-deformation (F-D) plots of all the three floors comparing the experimental and simulations results for Pacoima ground motion [PGA=0.62g] are separately shown in Figure 5.2. The force-deformation behavior of all the components (3SFS, NSD-East, NSD-West and damper) in the first floor is shown in Figure 5.3. From Figure 5.2(a), the overall behavior in the experiments and simulations of first-floor is similar but the maximum deformation in the experiments is 0.23 *in.* more than the simulations. This is due to the variable friction loop observed in the components, shown in Figure 5.3(b,c). The F-D behavior of 3SFS measured using load-cells, shown in Figure 5.3(a) has confirmed that the structure remains elastic. The F-D behavior of the damper measured using the uni-axial load cell is also in close agreement with the predicted behavior. As mentioned previously, the F-D behavior of the second and third floors, shown in Figure 5.2(b,c), is very noisy because the force in these storys is calculated using the accelerations of the steel slabs, however the average slope of the experimental results is closely matching with the simulation

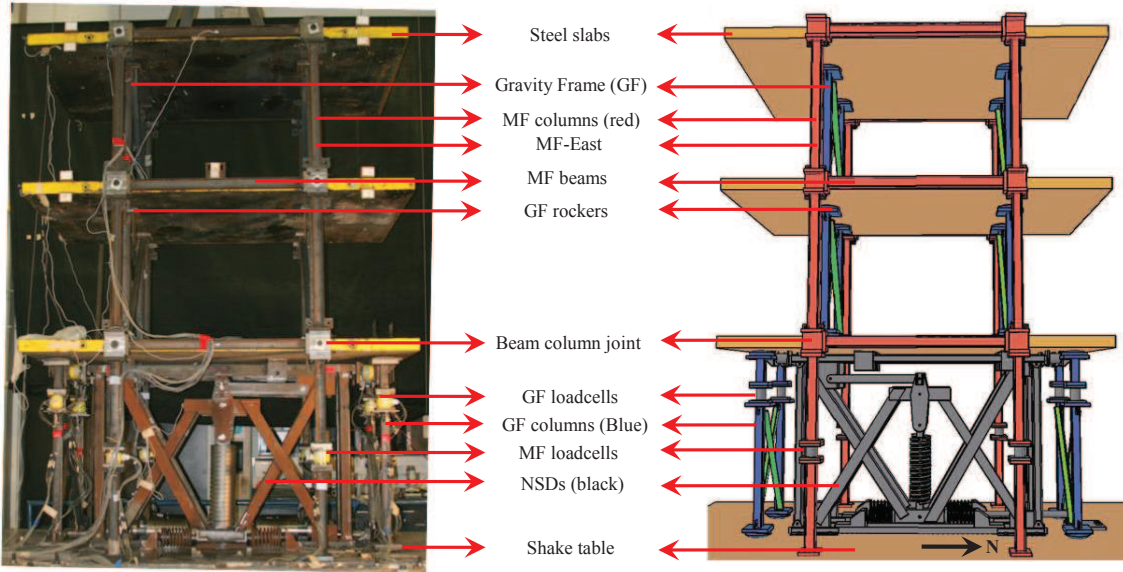


Figure 5.1: Schematic diagram and picture of unbraced 3SFS

results. Figure 5.2,5.3 confirm that the analytical models used for the components can be used to capture the experimentally observed behavior of the assembly reasonably well.

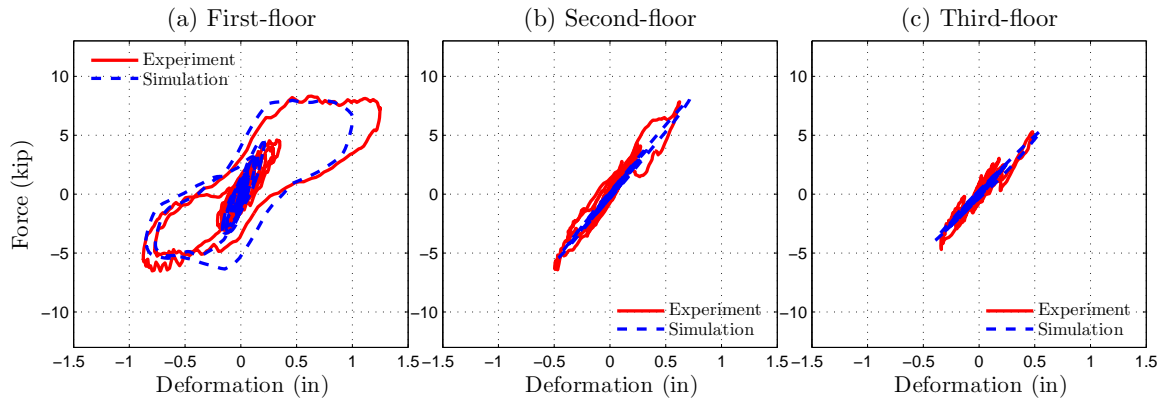


Figure 5.2: F-D behavior of individual floor in AS for Pacoima ground motion (PGA=0.62g)

The time-history response of first floor deformation, acceleration and base shear are compared in Figure 5.4. The F-D behavior of assembly and components in AS are shown separately for simulations and experiments in Figure 5.5. The comparisons of the results from shake-table tests and predicted results from the analytical models are in very good agreement.

Using the ground acceleration and the shake-table rocking data measured during the shake-table test, the behavior of BS, PS and NS is predicted and the F-D behavior of all the four systems is shown in Figure

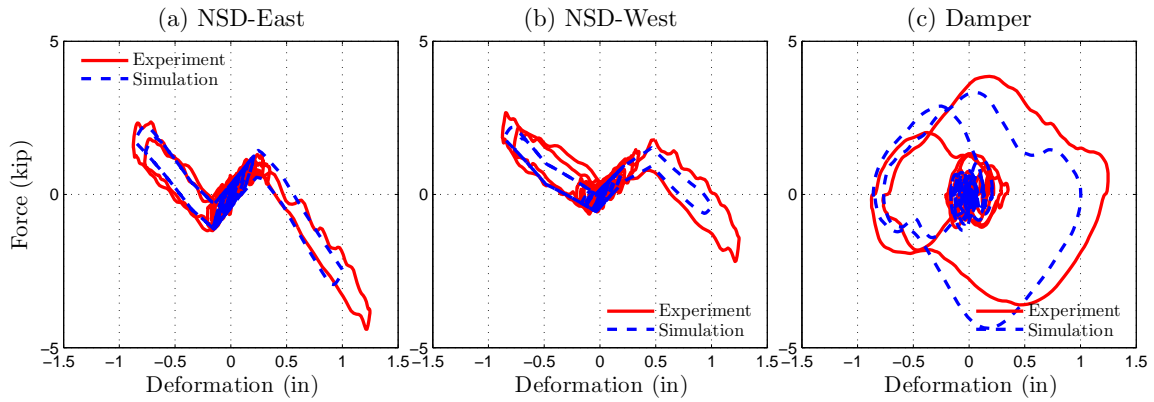


Figure 5.3: F-D behavior of NSD-East, NSD-West and damper in AS for Pacoima ground motion (PGA=0.62g)

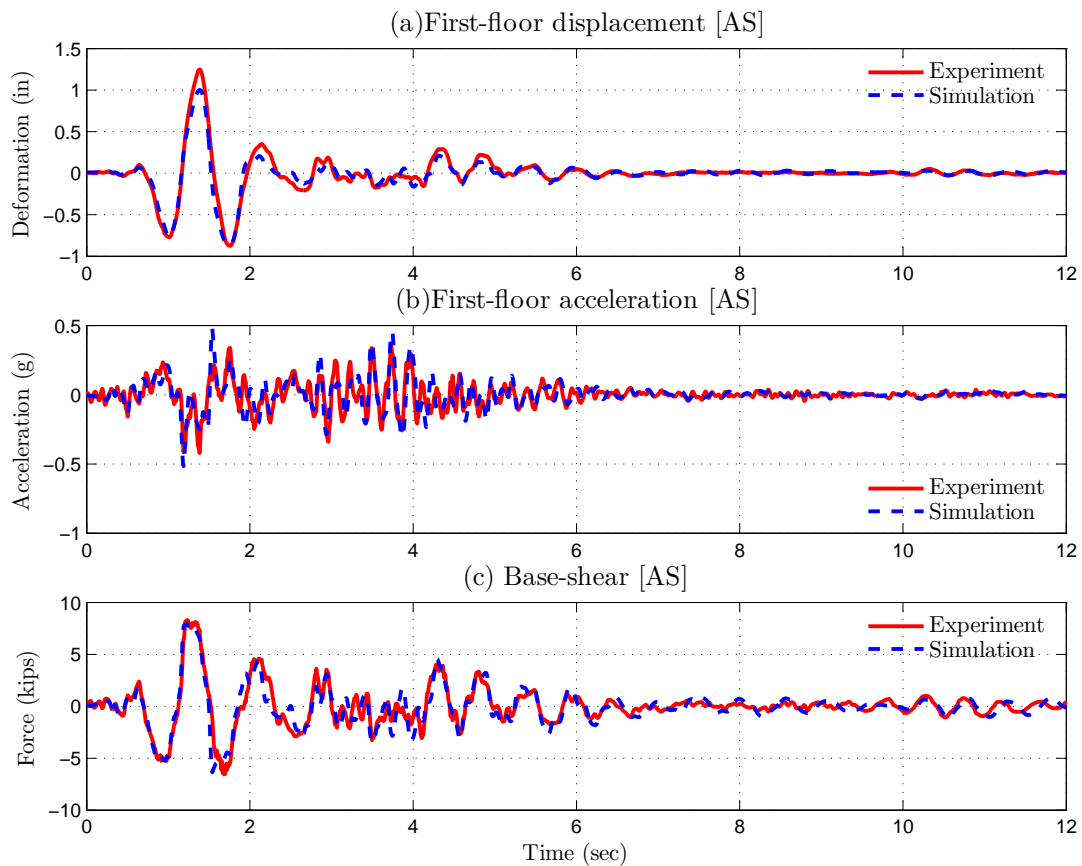


Figure 5.4: First floor response and base shear of AS (Pacoima GM; PGA=0.62g)

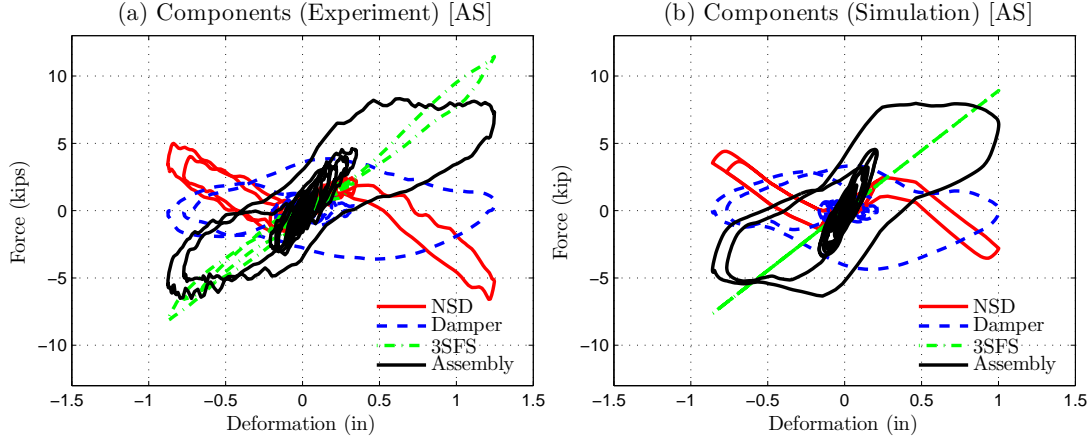


Figure 5.5: Comparison of F-D behavior of AS with components (Pacoima GM, PGA=0.62g)

5.6. F-D behavior of the first-floor in all the four systems are compared in Figure 5.7. First floor displacement, acceleration and base shear of all the four systems is compared in Figure 5.8. The superscript-“ $\ddagger$ ” in Figure 5.6-5.9 indicates that the results are obtained using the simulations. Figure 5.6 shows that the first and second floors of BS will yield for the Pacoima ground motion at a PGA of 0.62g. By adding damper to the base structure (PS), the input energy transferred to the second and third floors is reduced but the base shear experience by the first floor is same as in the BS, shown in Figure 5.6,5.7. If NSDs are connected in the first-floor instead of damper, shown as NS in Figure 5.6, the response of second and third floors and the base shear is reduced more than the BS and PS cases. However, the reduction in base-shear occurs at the expense of excessive displacement (50% more deformation in the first story compared to BS) due to the reduction in stiffness with the addition of NSD. By adding NSDs along with the damper, the inter-story response of the all the three floors are significantly reduced compared to BS, PS and NS, as shown in Figure 5.6,5.7,5.8.

The profile of maximum inter-story deformation, maximum floor displacement with respect to the shake-table and the maximum floor acceleration of all the three floors are shown in Figure 5.9. The inter-story deformation of the NS and AS is significantly reduced with the addition of NSDs in the second and third floor, shown in Figure 5.9(a). The relative deformation and acceleration of the first floor has increased with the addition of NSDs but the displacement and acceleration has increased marginally over the other two stories. As a result, the roof acceleration of AS is 30% less than BS, and the acceleration of NS is 15% smaller than the BS, shown in Figure 5.9(c). The roof displacement of AS is 30% less than the BS and 10% less than the NS. Although the inter-story drift in the first story of NS is 40% more than the other three systems, the roof deformation of NS is 15% less than the BS. Next, the behavior of NS and AS is analyzed for more sever ground motion [Pacoima ground motion with PGA of 0.78g].

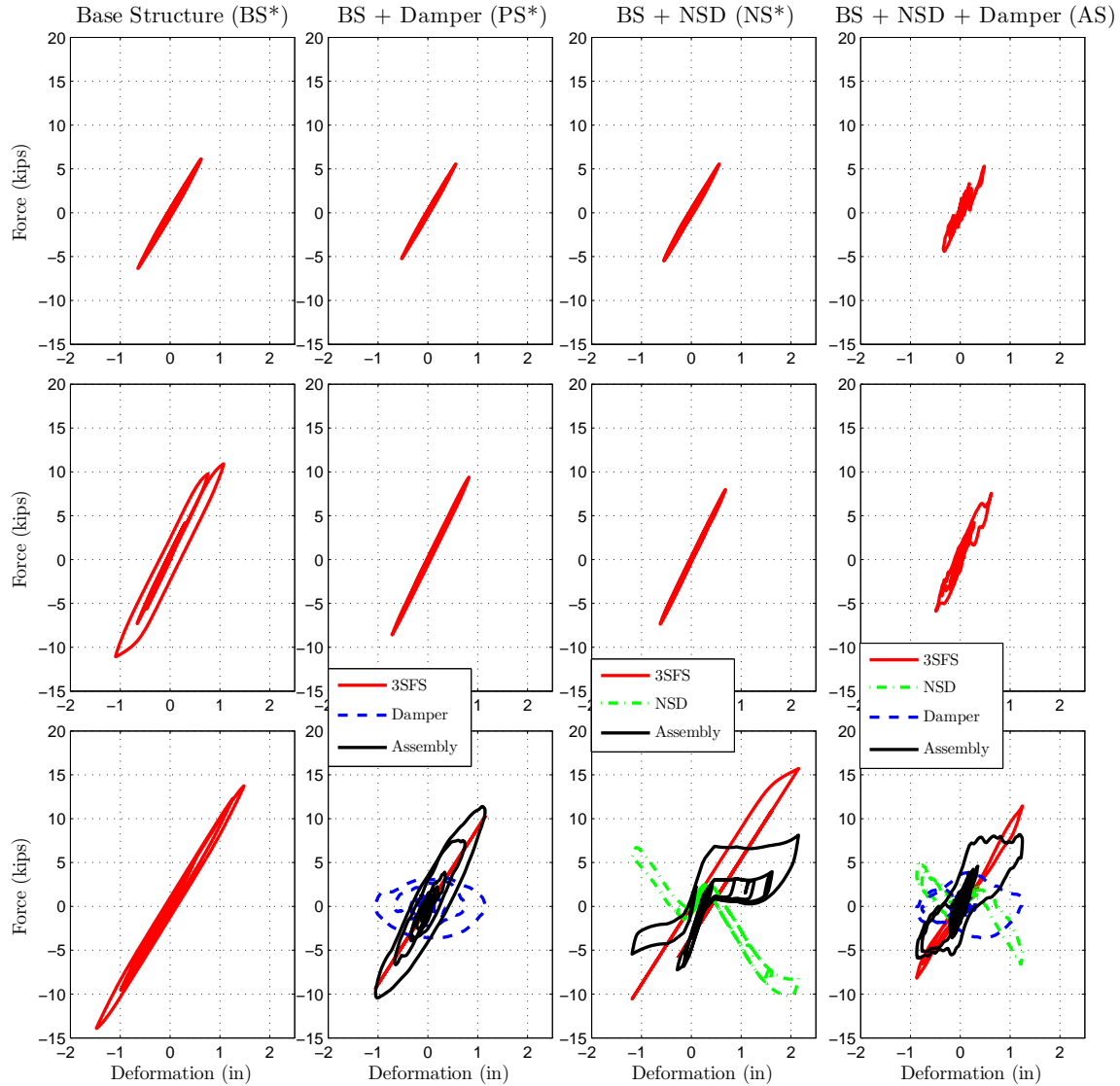


Figure 5.6: F-D behavior of all the floors in AS, BS, PS and AS with components (Pacoima GM; PGA=0.62g)

## 5.2 Unbraced 3SFS Response to severe ground motion

Shake-table test is performed on the 3SFS and NSDs assembly (NS) and the observed response of NS and components is compared with simulation results in Figure 5.10-5.13. Force-deformation (F-D) plots of all the three floors comparing the experimental and simulations results are separately shown in Figure 5.10. The force-deformation behavior of all the components (NSD-East and NSD-West) in the first floor

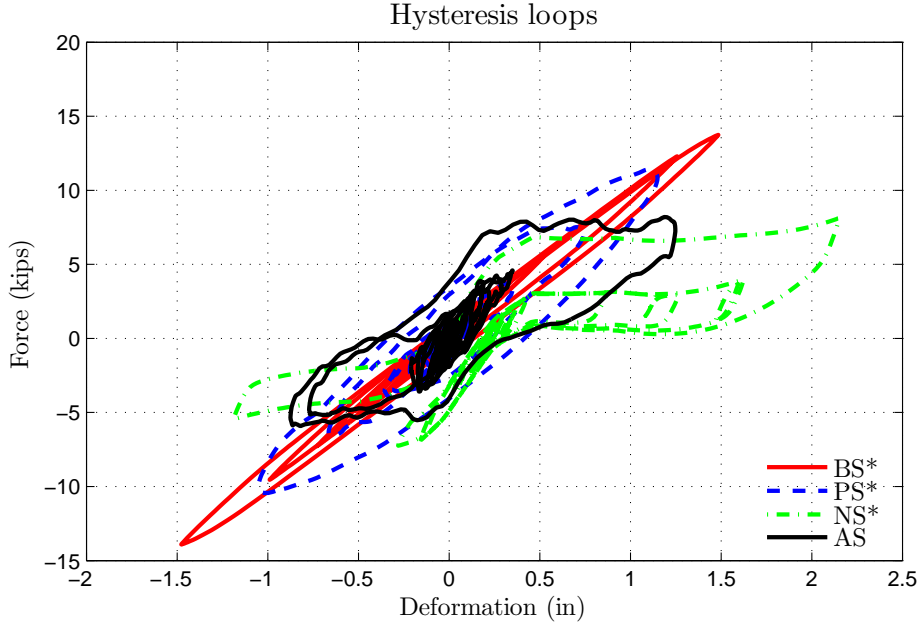


Figure 5.7: Comparison of F-D behavior of all the systems in first-floor (Pacoima GM; PGA=0.62g)

is shown in Figure 5.11. Similar to the results in Figure 5.2, the overall behavior in the experiments and simulations of first-floor, shown in Figure 5.10, is very similar. The first floor deformation, acceleration and base shear is shown in Figure 5.12. The F-D behavior of assembly and components in NS are shown separately for simulations and experiments in Figure 5.13.

The first-floor has deformed in the negative direction first with mild yielding and then it yielded in the positive direction (plastic deformation of more than 1 in.) as shown in Figure 5.13. Due to the permanent drift in the first-floor, there is slight rigid body rotation in the second and third floor, as a result, the F-D plots appear to have a permanent drift of 0.23 in. as shown in Figure 5.10(b,c). The measured and simulated F-D behavior of NSD-east and NSD-west are shown in 5.11 and it is clear from these plots that the NSDs enter the stiffening region. The stiffness of the assembly in the first floor reduces from 0.35 in. till 2 in. and beyond 2 in. it increases again. Overall, from Figure 5.10-5.13, the analytical models used were able to capture the observed experimental behavior reasonably well even when the primary structure has yielded significantly.

Using the ground acceleration and the shake-table rocking data measured during the shake-table test, the behavior of BS, PS and AS is predicted and the F-D behavior of all the four systems is shown separately in Figure 5.14. First-floor F-D behavior of all the four systems is compared in Figure 5.15, first floor displacement, acceleration and base shear is compared in Figure 5.16. Time-history trace of the roof displacement and acceleration of all the four systems is compared in Figure 5.17.

Figure 5.14 shows that the first and second floors of BS will yield for the Pacoima ground motion at a

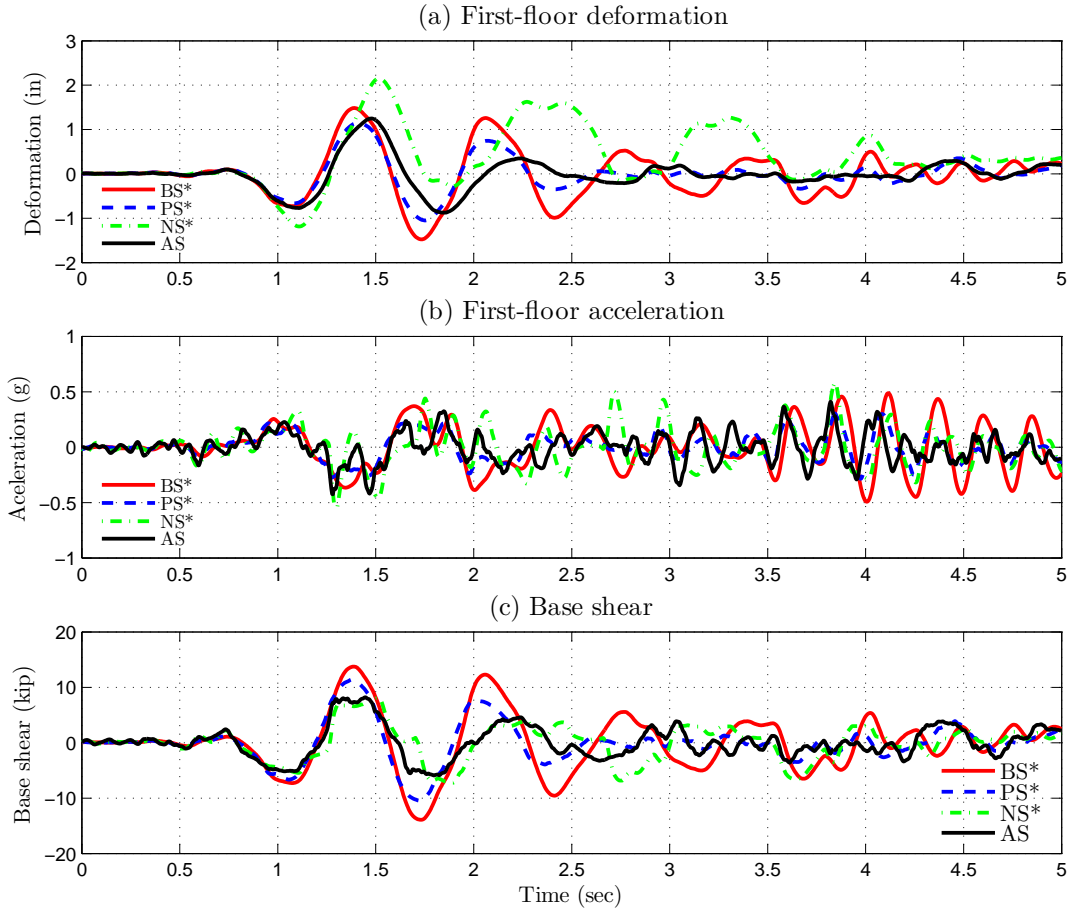


Figure 5.8: Comparison of the time-history of first floor response in all systems (Pacoima GM; PGA=0.62g)

PGA of 0.78g. With the addition of damper to the base structure (PS), the deformation in the first floor is reduced but the input energy transferred to the second and third floors is not reduced as a result the second floor has yielded, shown in Figure 5.14. Also, the base shear in PS is same as BS, shown in Figure 5.16. If NSDs are connected in the first-floor instead of damper, shown as NS in Figure 5.14, the response of second and third floors and the base shear is reduced more than the BS and PS cases and they remain elastic. The base shear of NS is reduced by more than 20% compared to BS and PS, shown in Figure 5.16. However, the reduction in base-shear occurs at the expense of large first-floor deformation (20% more deformation in the first story compared to BS) due to the reduction in stiffness with the addition of NSD, shown in Figure 5.15. By adding NSDs along with the damper, the inter-story response of the all the three floors are significantly reduced compared to BS, PS and NS, as shown in Figure 5.14 and Figure 5.17.

The profile of maximum inter-story deformation, maximum floor displacement with respect to the shake-table and the maximum floor acceleration of all the three floors are shown in Figure 5.18 for Pa-

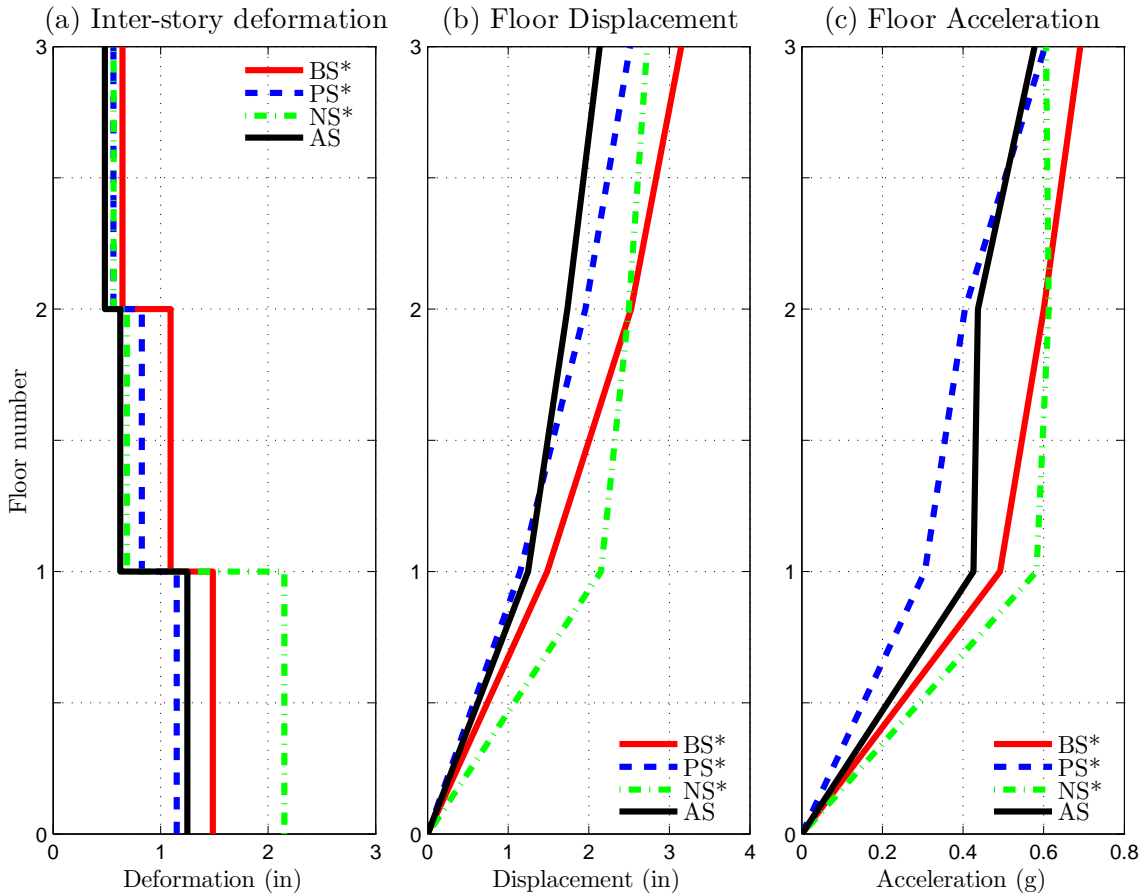


Figure 5.9: Comparison of response profile of all the systems in unbraced 3SFS (Pacoima GM; PGA=0.62g)

coima ground motion with PGA of 0.78g. The inter-story deformation of the NS and AS in the second and third floor is 30% less than the BS and PS due to the addition of NSDs, shown in Figure 5.18(a). The relative deformation and acceleration of the first floor has increased with the addition of just the NSDs, shown as NS in Figure 5.18(b,c), but the displacement and acceleration of the other two floors has not increased because the NSDs will prevent the transfer of input energy to the higher floors. As a result, the roof acceleration of NS is 20% less than BS and PS. By adding viscous damper along with the NSDs, all the responses i.e., the deformation in the first-floor, base shear, roof displacement and roof acceleration will be reduced compared to the other three systems, shown in Figure 5.18(a,b,c). Essentially, in the case of NS and AS, the NSDs are preventing the transmission of the input energy from the shake-table motion to the second and third floors by absorbing all the energy and viscous damper is dissipating the absorbed energy.

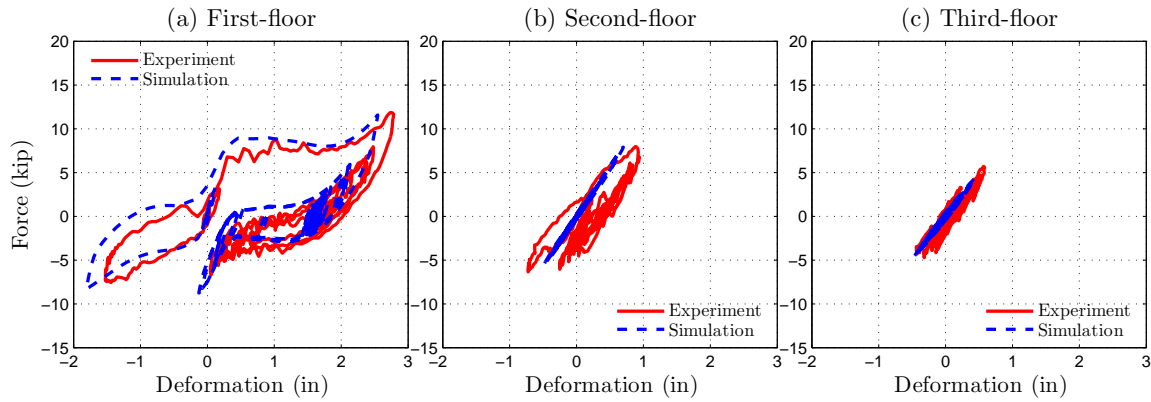


Figure 5.10: F-D behavior of individual floor in NS for Pacoima ground motion (PGA=0.78g)

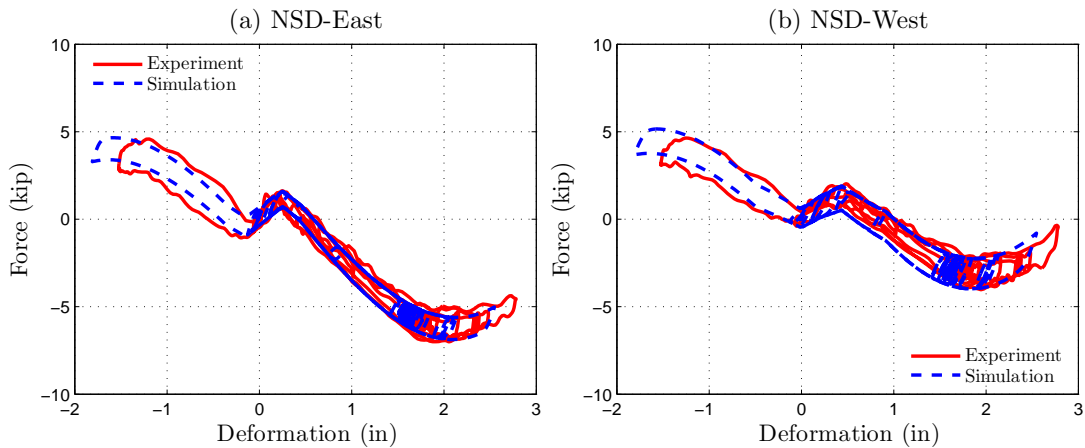


Figure 5.11: F-D behavior of NSD-East and NSD-West in NS for Pacoima ground motion (PGA=0.78g)

The viscous damper in the AS will also prevent the excessive deformation caused due to the reduction in stiffness. The peak response characteristics of all the four systems are summarized in Table 5.1 and also shown as bar-graphs in Figure 5.19 for three ground motions. The results are summarized below:

1. Addition of NSD in the first-floor will prevent the transfer of input energy from the ground motion to the second and third floors. Consequently, the inter-story deformation of the higher floors is significantly reduced, shown in Figure 5.19.
2. Addition of damper can control the deformations at the installation level, but the structure experiences same level of base-shear and the second and third floors will undergo the same level of inter-story deformations similar to the uncontrolled structure.
3. By incorporating NSDs and damper together in the structure, all the response characteristics can

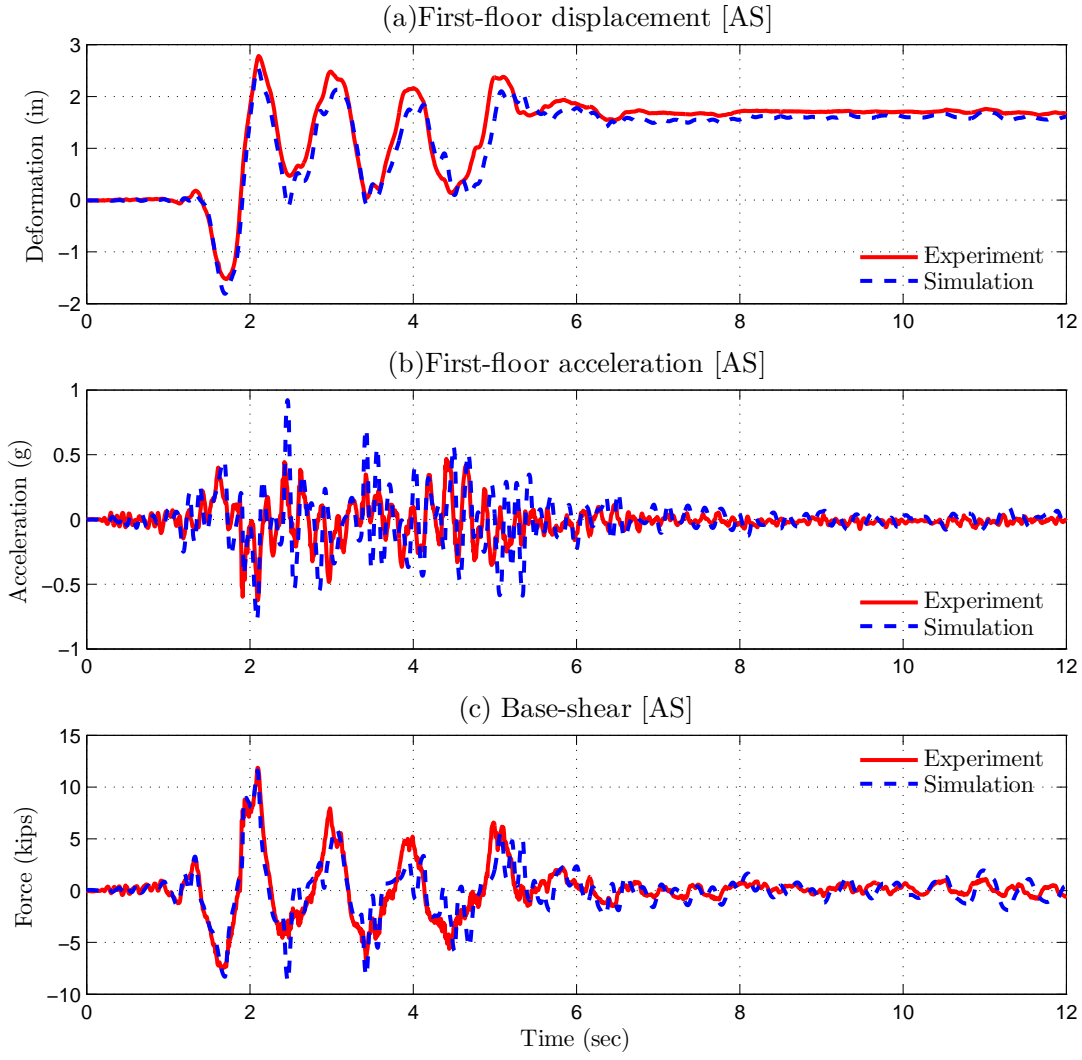


Figure 5.12: First floor response and base shear of NS (Pacoima GM; PGA=0.78g)

be consistently reduced.

### 5.3 Analytical modeling of nine-story frame

The advantages of installing NSDs and supplemental dampers in multiple stories is demonstrated through simulation studies on a nine-story, one-bay shear building (Pasala et al., 2012b). The story stiffness is assumed to be bilinear inelastic, inherent viscous damping of 1% is assumed for each story. Damping coefficient is calculated using the elastic stiffness of the structure, and maintained constant throughout the inelastic regime. Three dimensional drawing of the shear building with the NSDs installed in the walls

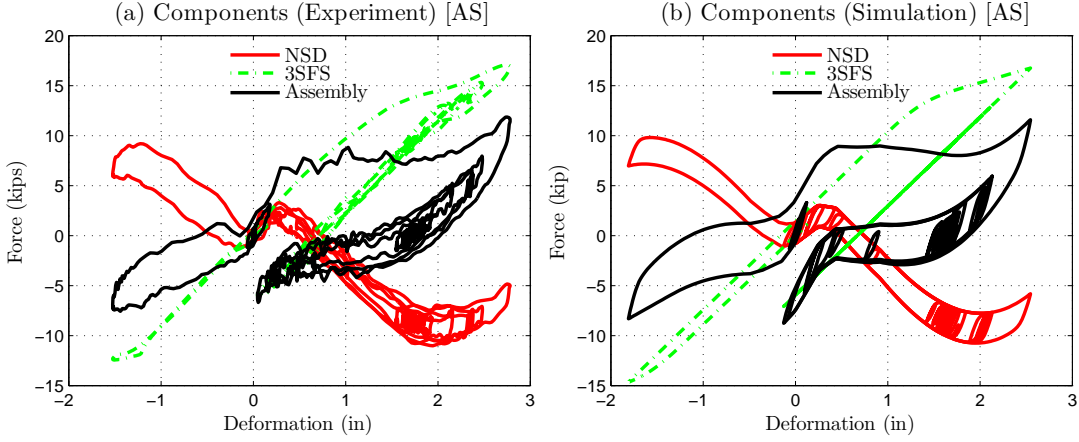


Figure 5.13: Comparison of F-D behavior of NS with components (Pacoima GM, PHA=0.78g)

at each story level is shown in Figure 5.20(left). Schematic diagram showing the equivalent components in each story, i.e. bilinear inelastic columns, supplemental passive damper and NSD is shown in Figure 5.20(Right). When connected, the NSDs will only transmit lateral forces and the device is self-contained in the vertical direction. The governing equation for the  $i^{th}$  floor is given by:

$$m_i \ddot{u}_i + F_{si}(u_{di}) + F_{NSDi}(u_{di}) + c_i(\dot{u}_{di}) - F_{si+1}(u_{di+1}) - F_{NSDi}(u_{di+1}) - c_{i+1}(\dot{u}_{di+1}) = 0 \quad (5.1)$$

where, subscripts  $i, i+1, i-1$  stands for the story number.  $m_i$  is the mass of  $i^{th}$  floor.  $u_{ri} = u_i - u_{i-1}$ , is the inter-story deformation of the  $i^{th}$  floor.  $u_i, \dot{u}_i$  and  $\ddot{u}_i$  are the displacement, velocity and acceleration of the  $i^{th}$  floor, respectively.  $F_{si}$  is the force exerted by the bilinear inelastic columns in the  $i^{th}$  floor and it is calculated using Sivaselvan-Reinhorn (SR) model (Sivaselvan and Reinhorn, 2000). The inelastic column force is given by

$$F_{si}(u_{di}) = \alpha_{si} K_{si} u_{di} + (1 - \alpha_{si}) K_{si} u_{syi} z_{si} \quad (5.2)$$

$$\left( \frac{dz_{si}}{du_{di}} \right) = \frac{1}{u_{syi}} (1 - |z_{si}|^{\eta_{si}} (\gamma_{si} \text{sgn}(z_{si} \times du_{di}) + \beta_{si})) \quad (5.3)$$

$K_{si}$  is the initial elastic stiffness of the floor,  $\alpha_{si}$  is the post-yielding stiffness ratio,  $u_{syi}$  is the yield displacement. The parameters  $\eta_{si}$ ,  $\gamma_{si}$ , and  $\beta_{si}$  are the constants in Sivaselvan-Reinhorn model for  $i^{th}$  story. The tangential stiffness of the hysteretic part is proportional to  $dz_{si}/du_{di}$ . The tangent stiffness of the system,  $K_{tsi}$ , can be then be represented by Eq. 5.4, which shows low stiffness after yielding ( $z \rightarrow 1$ ):

$$K_{tsi} = K_{si} (\alpha_{si} + (1 - \alpha_{si}) (1 - |z_{si}|^{\eta_{si}} (\gamma_{si} \text{sgn}(z_{si} \times du_{di}) + \beta_{si}))) \quad (5.4)$$

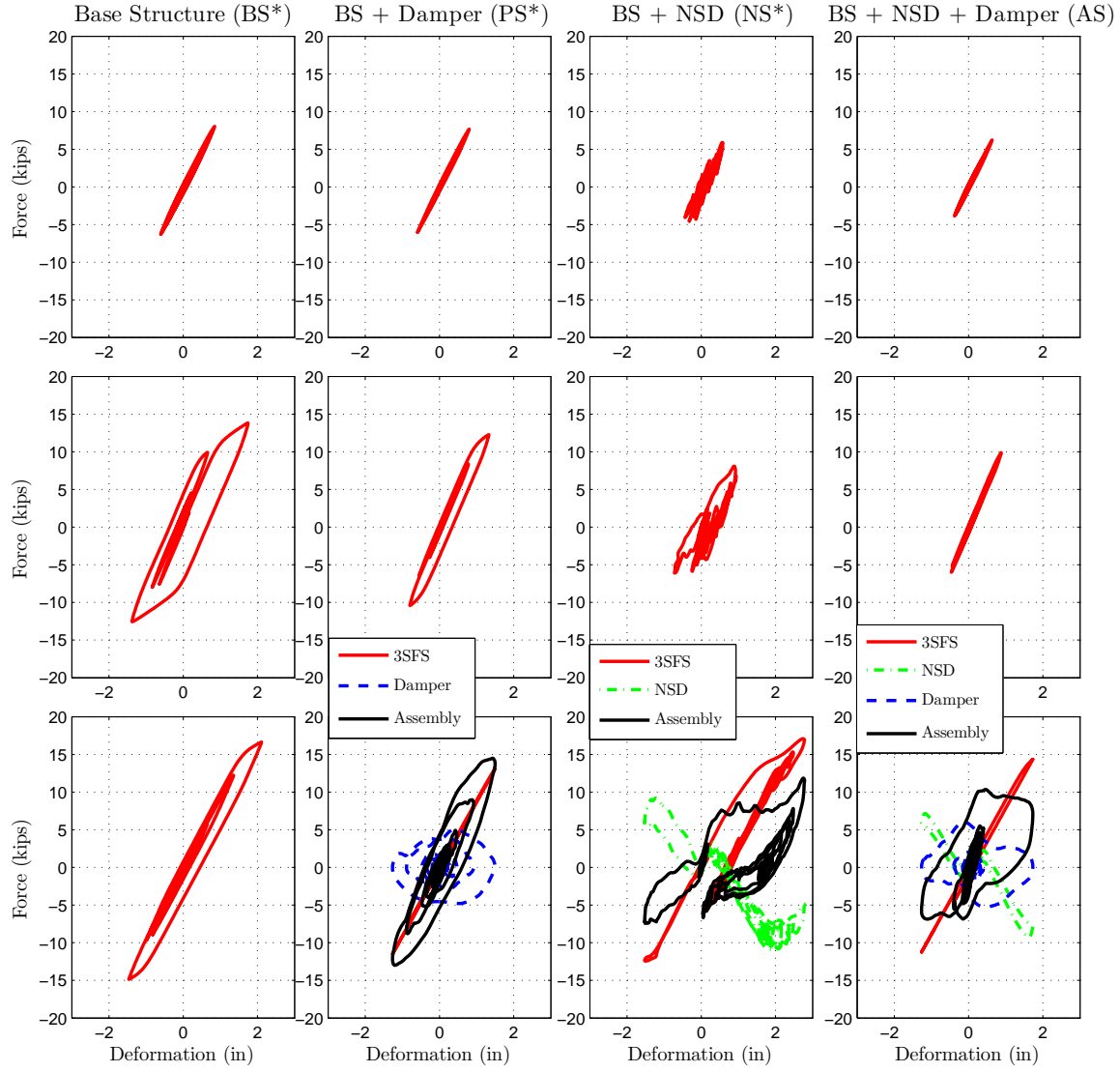


Figure 5.14: F-D behavior of all the floors in AS, BS, PS and AS with components (Pacoima GM; PGA=0.78g)

Mass, elastic-stiffness, yield displacement, damping values and the values of the SR model in the individual floor are obtained from the 3SFS presented in 3. The damping term consists of two components as shown in Eq. 5.5

$$F_{Di} = c_i (\dot{u}_i - \dot{u}_{i+1}) = 2(\xi_i + \xi_{sdi}) \sqrt{K_{si} m_i} (\dot{u}_i - \dot{u}_{i+1}) \quad (5.5)$$

$\xi_i$  is the inherent damping ratio of the  $i^{th}$  floor and  $\xi_{sdi}$  is the damping ratio of the supplemental damper added along with the NSD. In this study  $\xi_i = 1\%$  is used based on the experimental observations and

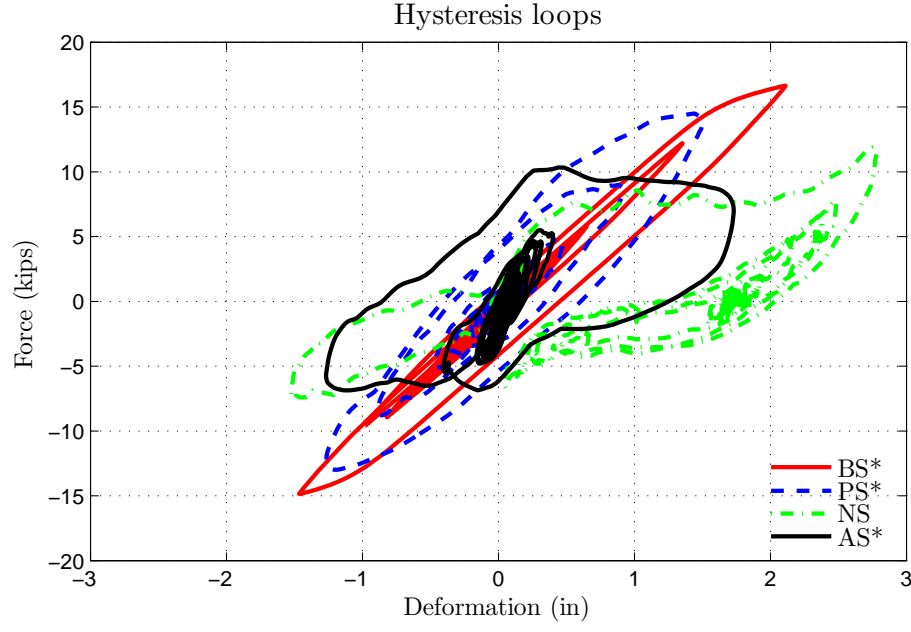


Figure 5.15: Comparison of F-D behavior of all the systems in first-floor (Pacoima GM; PGA=0.78g)

$\xi_{sdi}=20\%$  (initial) is adopted based on the results presented in chapter 1. The force exerted by the NSD,  $F_{NSDi}$  is given in Eq. 5.6 (also presented in Eq. 2.10).

$$F_{NSDi} = - \left( \frac{P_{in} + K_s l_p}{l_s} - K_s \right) \left( \frac{l_1}{l_2} \right) \left( 2 + \frac{l_2}{l_1} + \frac{l_p + l_1}{\sqrt{l_2^2 - u_{di}^2}} \right) u + K_g (u_{di}) u_{di} \quad (5.6)$$

The values of the parameters used for the simulations study are:  $P_{in}=8$  kips;  $K_s=1.6$  kip/in;  $l_p=30$  in;  $l_1=10$  in;  $l_2=5$  in and  $K_g$  has bilinear elastic behavior with initial stiffness of 5.9 kip/in and the stiffness becomes 0.15 kip/in for deformations larger than 0.3 in.  $K_g$  represents the behavior of gap-spring assembly; a two spring assembly connected in series to achieve zero stiffness in NSD for  $|u| < u'_y$ .

The height of each floor is 60 in. and the weight of each floor is 8.9 kips. The first three natural time-periods of the structure are 1.75 sec, 0.59 sec and 0.36 sec. Two NSDs are incorporated in each floor. Force deformation behavior the bilinear inelastic system (calculated using Eq. 5.2), supplemental viscous damper (calculated using Eq. 5.5), the NSD force (calculated using Eq. 5.6) and the assembly is shown in Figure 5.21. All the simulation results on nine-story frame are normalized and represented in dimensionless terms: force terms are normalized with respect to the yield force of the columns,  $F_y$ , floor displacement and inter-story deformations are normalized with respect to the yield displacement,  $u_y$ , of the columns.

The governing equation for the entire structure subjected to a ground motion with acceleration  $\ddot{u}_g(t)$

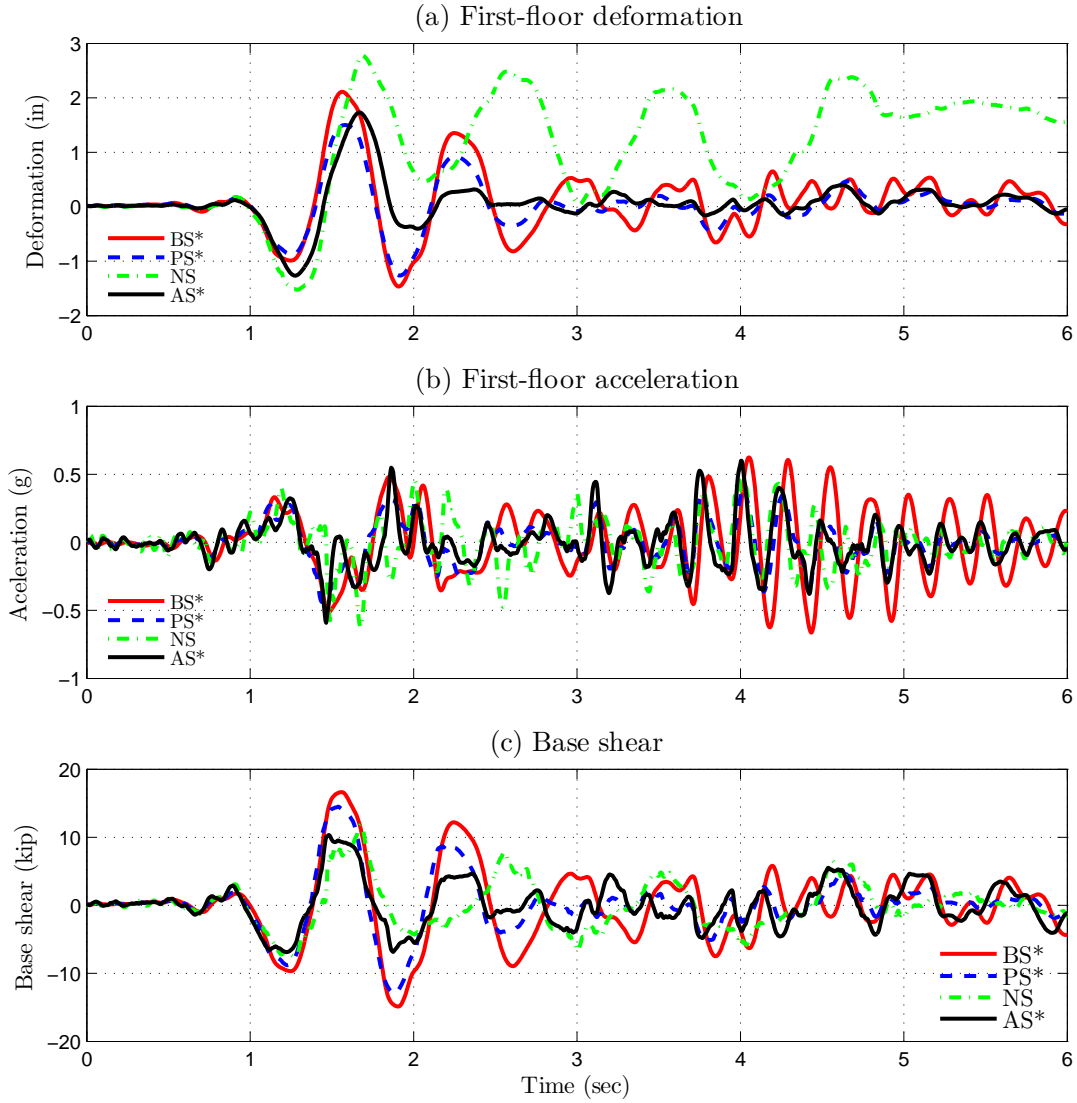


Figure 5.16: Comparison of the time-history of first floor response in all systems (Pacoima GM; PGA=0.78g)

is given by

$$\mathbf{M}\dot{\mathbf{u}}_r(t) + \mathbf{C}\mathbf{u}_r(t) + \mathbf{F}_s(\mathbf{u}_r) + \mathbf{F}_{NSD}(\mathbf{u}_r) = -\mathbf{M}\mathbf{I}\ddot{u}_g(t) \quad (5.7)$$

where,  $\mathbf{M}$  and  $\mathbf{C}$  are the mass and damping matrices of the structure.  $\mathbf{u}_r(t)$ ,  $\dot{\mathbf{u}}_r(t)$  and  $\ddot{\mathbf{u}}_r(t)$  are the displacement, velocity and acceleration vectors containing the floor response at each story with respect to the ground.  $\mathbf{F}_s$  and  $\mathbf{F}_{NSD}$  are the force vectors consisting of the nonlinear forces exerted on each mass due to the nonlinear stiffness of the structure and the NSD, respectively.  $\mathbf{I}$  is the influence coefficient vector

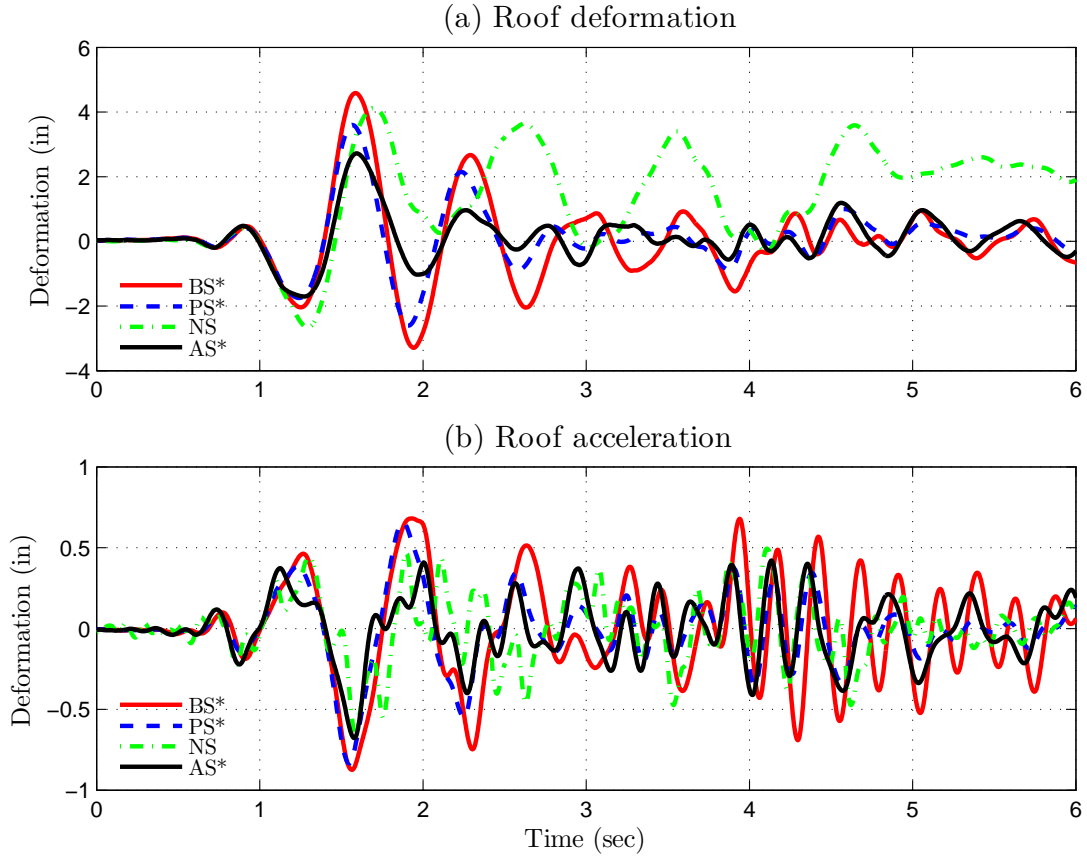


Figure 5.17: F-D behavior of all the systems and components shown separately (Pacoima GM; PGA=0.78g)

for ground acceleration. Two other force terms will be used in the simulation studies presented in the next section;  $F_i$  refers to assembly shear-force in the  $i^{th}$  story and  $F_b$  refers to the base shear (foundation force) of the structure. Using the analytical models described in this section, simulation studies demonstrating the advantages of using NSDs in multiple stories is demonstrated next.

The properties of NSD have to be chosen such that the strength reduction factor of bilinear structure and NSD assembly should comply with the values described in ASCE-07. The properties of the elastic structure, bilinear inelastic structure and assembly are shown in Figure 5.22. The strength reduction factor of the test frame used in this study,  $R_{oy} = F_o/F_y$ , is 1.25, but the suggested strength reduction factor in the design codes is 4.  $F_o$  is the maximum force in the elastic system for the suite of the ground motions used in this study and  $F_y$  is the yield force of the three-story structure. Since the columns of the test frame are conservative, the NSD is added to the system so that a strength reduction factor of 4 is achieved without altering the structure properties. After adding the NSD the strength reduction factor of the assembly,  $R_{yy'} = F_y/F'_y = 4$ . The strength reduction factor  $R_{yy'}$  should not be greater than 4 due to

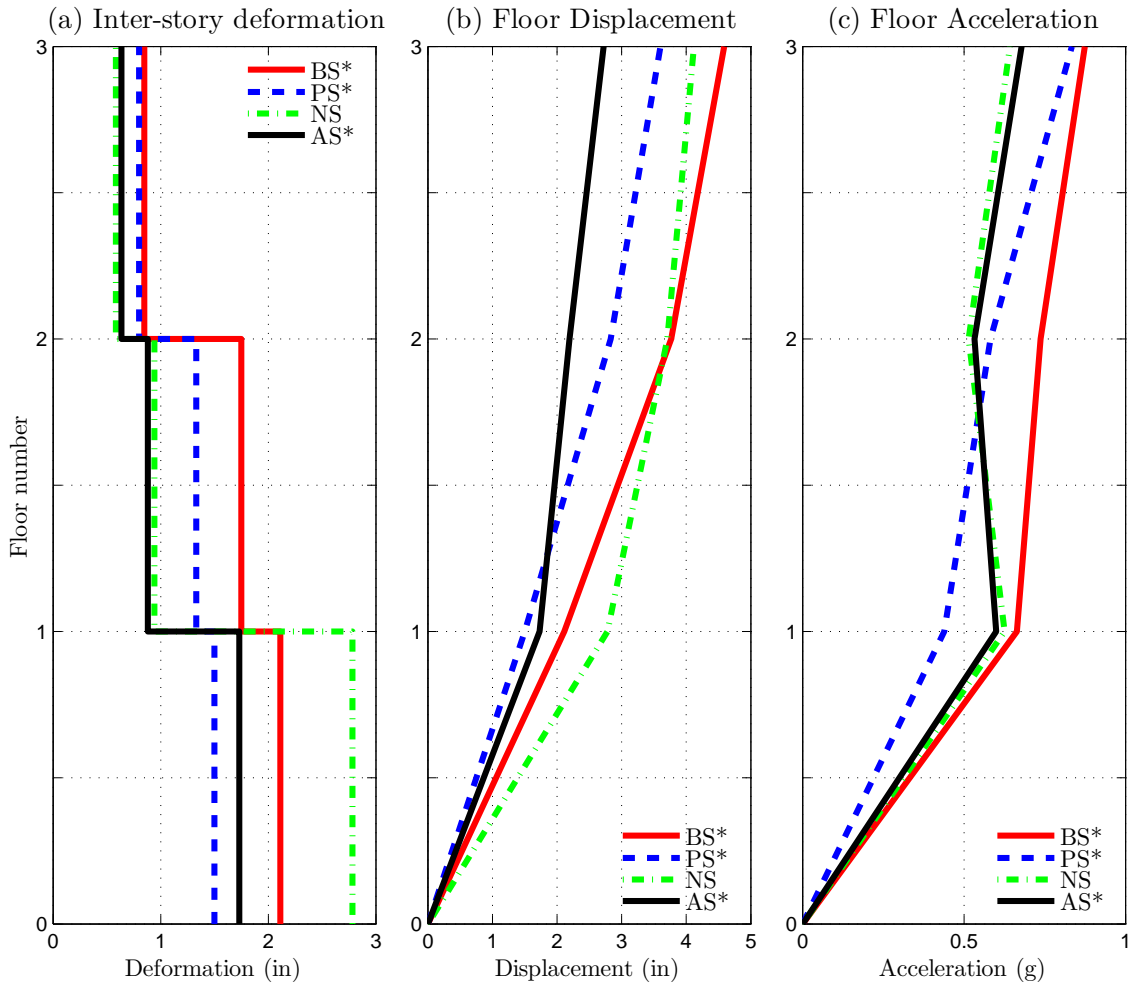


Figure 5.18: Comparison of response profile of all the systems in unbraced 3SFS (Pacoima GM; PGA=0.78g)

safety considerations.  $F'_y$  is the apparent-yield-strength (force in the NSD and structure assembly at  $u'_y$ ). Hence, the NSD and structure assembly has a strength reduction factor,  $R_{oy'} = F_o / F'_y$  of 5.

The ground movement during an earthquake will transmit energy to the structure. The peak response of the superstructure depends on the amount of energy transmitted from the ground motion. The impact of reducing the accelerations by adding the NSD is justified based on the amount on input energy transmitted to the structure. Using the governing equation developed in Eq. 5.7, the energy equation for the

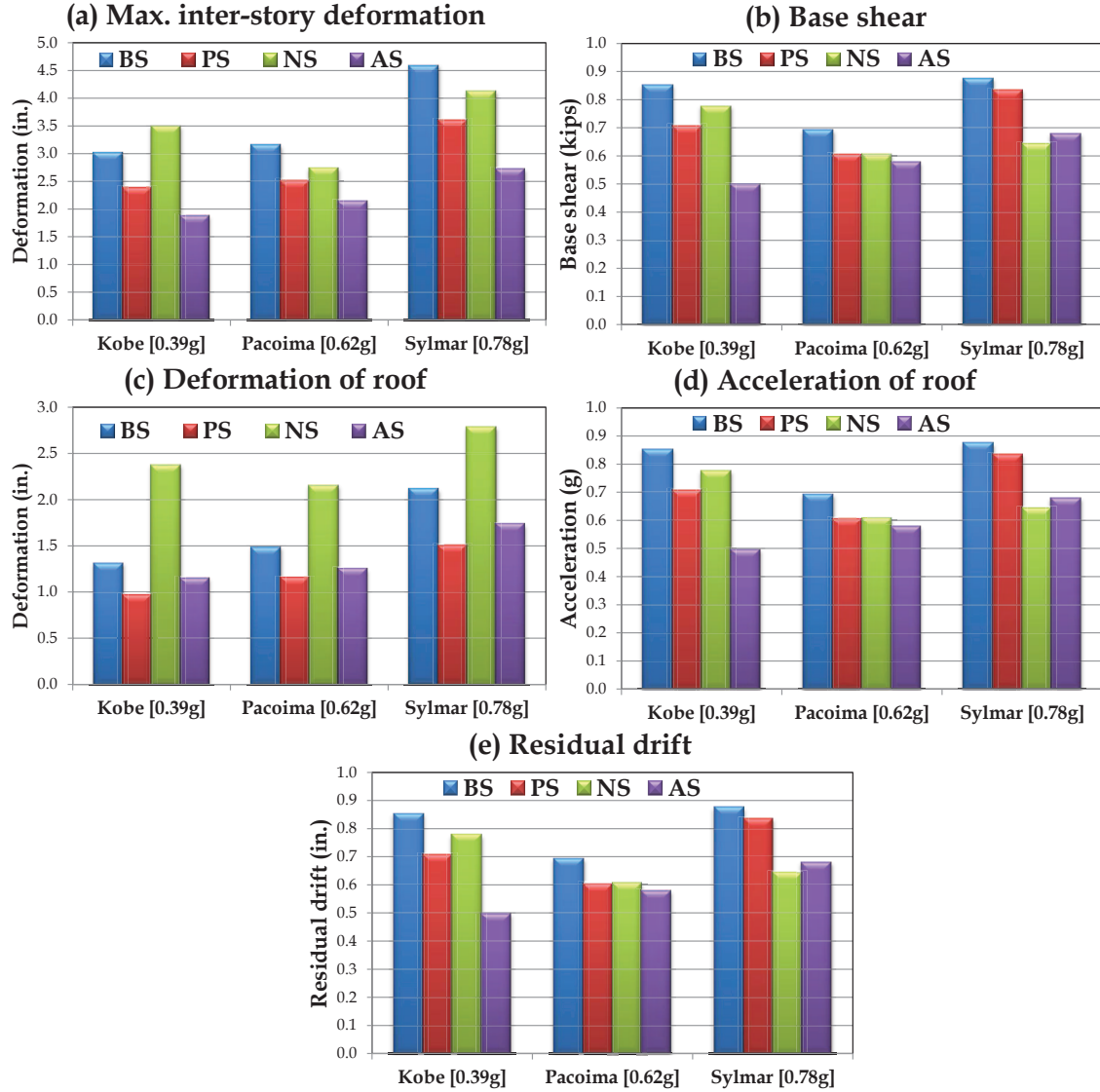


Figure 5.19: Bar graphs summarizing the shake-table results of unbraced 3SFs

structure will be (Chopra, 2007)

$$\underbrace{\frac{1}{2} \mathbf{u}_r^T \mathbf{M} \mathbf{u}_r}_{\text{Kinetic energy}} + \underbrace{\int_0^t (\mathbf{u}_r \mathbf{C}) d\mathbf{u}_r}_{\text{Damper dissipated energy}} + \underbrace{\int_0^t \mathbf{F}_{NSD}^T d\mathbf{u}_r}_{\text{Work done by NSD}} = \underbrace{\int_0^t \left[ \sum_{i=1}^n (\ddot{u}_i^T m_i) \right] d\mathbf{u}_g}_{\text{Input energy}} \quad (5.8)$$

In Eq. 5.8, the term on the right hand side represents the input energy transmitted to the structure due to the ground motion; it depends on the ground displacement,  $\mathbf{u}_g$ , and the acceleration of individual floor,

Table 5.1: Summary of the peak responses from the shake table tests on unbraced structure [Elastic-tests]

Sl. no.	Ground motion	System	Cmd. PGA (g)	First-floor response		Base shear (kip)
				Deform. (in)	Accel. (g)	
1	Kobe (Elastic) PGA:0.39g	BS*	1.31	3.00	0.85	0.68
2		PS*	0.96(27%)	2.38(21%)	0.71(17%)	0.25
3		NS*	2.38(-81%)	3.48(-16%)	0.78(9%)	0.55
4		AS	1.15(12%)	1.88(37%)	0.50(42%)	0.18
5	Pacoima (Elastic) PGA:0.62g	BS*	1.49	3.15	0.69	0.34
6		PS*	1.15(23%)	2.51(20%)	0.60(13%)	0.14
7		NS*	2.15(-45%)	2.73(13%)	0.61(12%)	0.31
8		AS	1.25(16%)	2.14(32%)	0.58(16%)	0.12
9	Pacoima (Yielding) PGA:0.78g	BS*	2.11	4.59	0.87	0.47
10		PS*	1.50(29%)	3.60(22%)	0.83(5%)	0.23
11		NS	2.78(-32%)	4.12(10%)	0.64(26%)	0.60
12		AS*	1.73(18%)	2.72(41%)	0.68(22%)	0.07

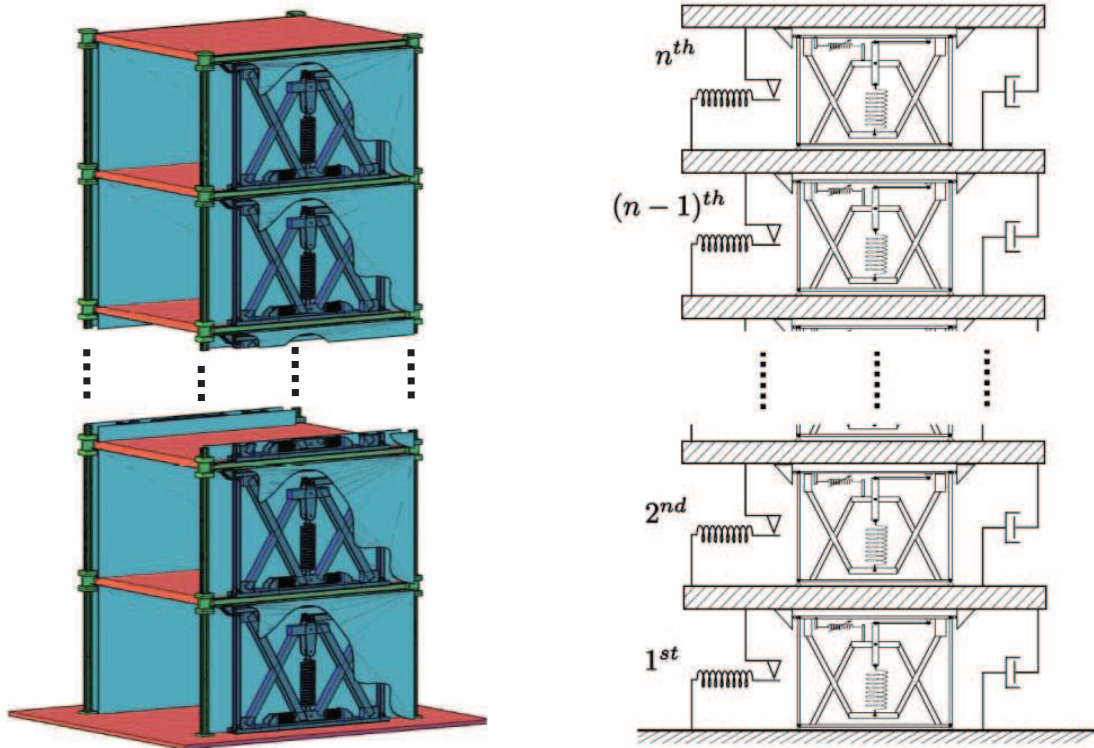


Figure 5.20: Schematic diagram of multi-story building with NSDs in every floor

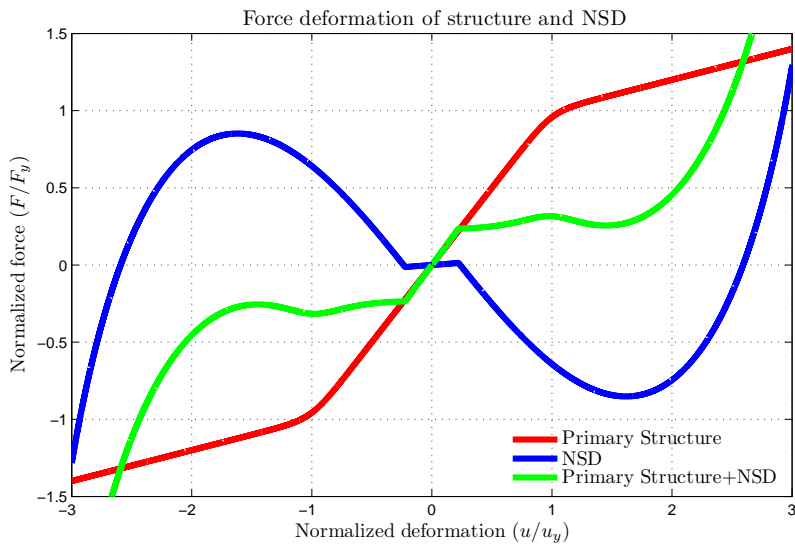


Figure 5.21: F-D plots depicting the strength reduction in single story

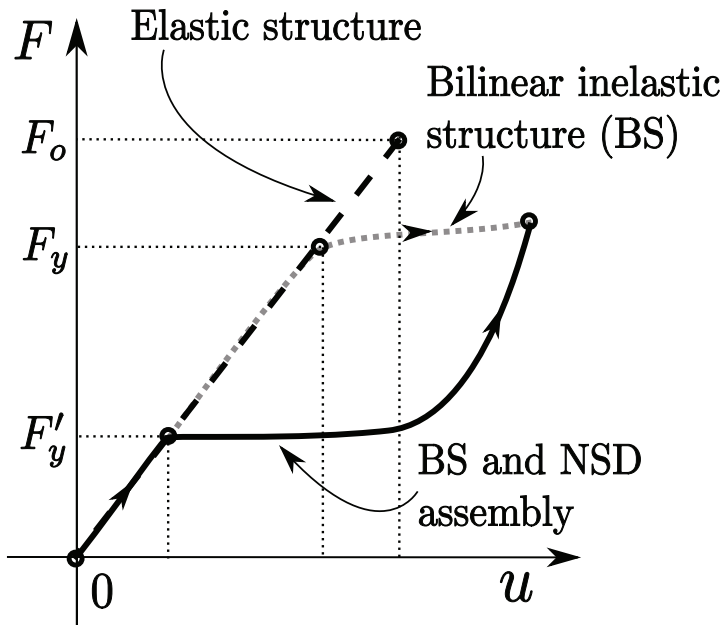


Figure 5.22: Schematic F-D plots depicting the strength reduction factor

$\ddot{u}_i$ . There is an additional term on the left hand side due to the addition of NSDs; work done by the NSD. Since the NSD exhibits nonlinear elastic behavior, the total work done by the NSD will be zero after the

ground motion if there is no permanent deformation in the primary structure. By comparing the response of a structure and NSD assembly with an uncontrolled structure; since the ground displacement remains the same for both the structures, reducing the acceleration of the structure is equivalent to reducing the amount of energy transmitted. This is further justified through simulation studies in the next section.

## 5.4 Vertically distributed isolation

To justify the addition of NSDs and also to highlight the role of NSDs, the response of three systems is compared in this study: base structure or primary structure (BS); primary structure with dampers or passively controlled system (PS); primary structure with NSDs and dampers or adaptive system (AS). As explained in the previous sections, adding the NSDs will reduce the acceleration of superstructure or in other words, the amount of energy transmitted to the super structure is decreased. The added supplemental damper will contain the excessive interstory deformations caused due to the reduction in the assembly stiffness. In the previous section, experimental results are presented with NSDs in the first floor of 3SFS. To exemplify the isolation attributes possessed by the NSD, the response of nine-story structure with a NSD and damper in the third-floor (randomly chosen) is analyzed next.

Nine-story structure (BS), nine-story structure with viscous damper in the third floor (PS-3) and nine-story structure with NSDs and viscous damper in the third floor (AS-3) are subjected to three cycles of sinusoidal ground motion. The time period of the input ground motion is equal to the fundamental period of the structure. The peak inter-story deformation,  $u_{di}$ , of all the floors is compared in Figure 5.23(a) for BS, PS-3 and AS-3. Inter-story deformations are normalized with the yield displacement of the floor-columns,  $u_y$ ; so,  $u_{di}/u_y > 1$  infers that the floor has undergone inelastic deformation. The floor displacement with respect to the ground is shown in Figure 5.23(b) and the floor acceleration is shown in Figure 5.23(c).

The force-deformation behavior of the three systems in third-floor is shown in Figure 5.24 and the response of the roof displacement, acceleration and base shear are shown in Figure 5.25. A vertical line is shown in Figure 5.25 at 5.75 sec marking the stop time of external input. From Figure 5.23-5.25, it is clear that the addition of damper in the third-floor (PS-3) resulted in very little reduction of the peak response characteristics. By adding two NSDs in the third floor along with the damper (AS-3), the response of the structure both above and below the third-floor is significantly reduced. For the AS-3, inter-story deformation in the first story and base shear (shown in Figure 5.25) is reduced by 50%, roof displacement is reduced by 15% and the roof acceleration (shown in Figure 5.25) is reduced by 30% compared to the BS and PS-3. Columns in all the floors of AS-3 remained elastic, except third floor, but the first three floors in BS and PS-3 have yielded. The reduction in response achieved in AS-3 is mainly attributed to two factors:

1. The energy transmitted to the floors four through nine is reduced due to the reduction in assembly stiffness of the third-floor. As explained previously in section-2, once the NSD engages, the assembly stiffness reduces and as a result the forces transferred to the floors above the third floor will be

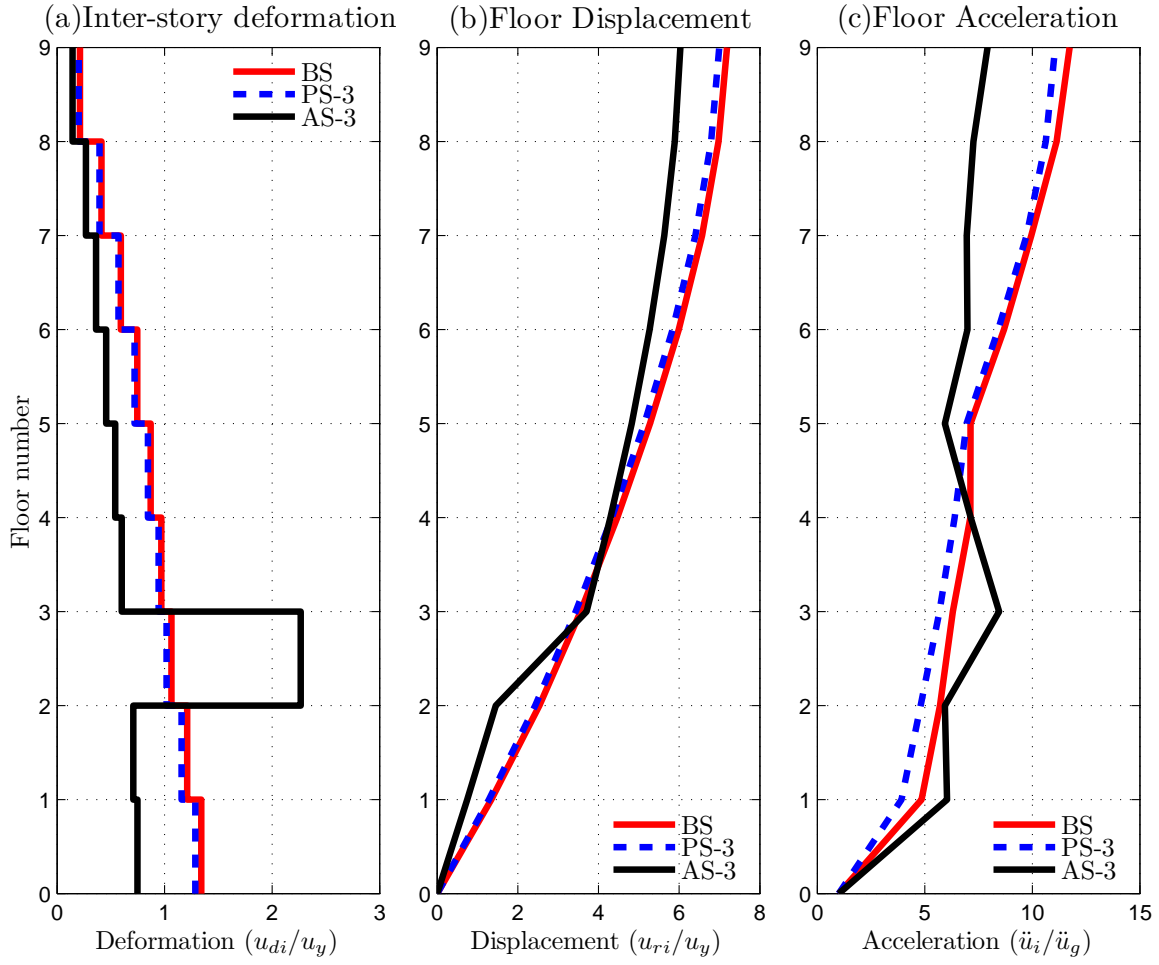


Figure 5.23: Comparison of the maximum response profile of the structure for periodic input. In AS-3, NSD and damper is placed in the third floor.

reduced.

2. By incorporating NSD, resonance in AS-3 can be avoided. Since the excitation frequency is matching with the natural frequency of BS and PS-3, they will resonate resulting in large deformations and accelerations. Whereas in the AS-3, after the NSDs are engaged (inter-story deformation of third floor exceeds the “apparent yield-displacement”,  $u'_y$ , of the NSDs), due to the bilinear-elastic behavior of the NSD and structure assembly, the natural frequency of the assembly changes and the assembly is prevented from resonating.

It is clear from Figure 5.23-5.25 that the addition of NSD in a particular floor results in reduction of

the response of the floors above that floor. Although the response of the superstructure and substructure of the third-floor in AS-3 is reduced, the third floor has undergone deformations twice that of BS and PS-3 due to the reduction in assembly stiffness. Also, the third floor in AS-3 has undergone large permanent drift where as the other systems remained elastic, shown in Figure 5.24. Although a passive damper is present in the third floor of AS-3 along with the NSDs, it is not enough to prevent the primary structure from undergoing inelastic deformations. Subsequent sections in this chapter discuss various approaches to prevent these large localized deformations.

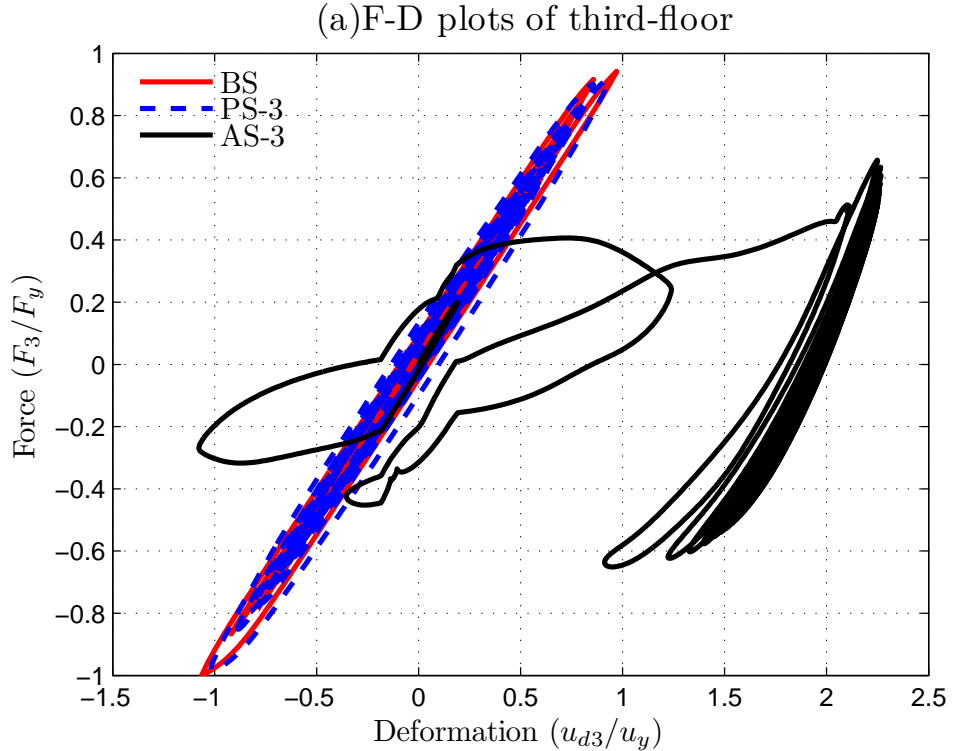


Figure 5.24: Comparison roof acceleration and base shear experienced by the BS, PS-3 and AS-3 for periodic input. In the case of AS-3, NSD and damper are placed in the third-floor and only damper in the case of PS-3.

Further, two NSDs and a viscous damper are placed in every floor for AS and a damper is placed in every floor for PS. The peak inter-story deformation, floor displacement and floor acceleration are shown in Figure 5.26. The force-deformation behavior of the three systems in first-floor is shown in Figure 5.27, response of the roof acceleration and base shear are shown in Figure 5.28. Adding viscous dampers in all the floors to the primary structure (PS) will result in the reduction of inter-story deformation of first floor by 35%, roof deformation by 20% and roof acceleration by 35% compared to BS (shown in Figure 5.26), but the base shear of the structure is same as the BS, shown in Figure 5.28(c). With the addition of NSDs in every floor (AS), all the responses are further reduced by 20% and the base shear is also reduced

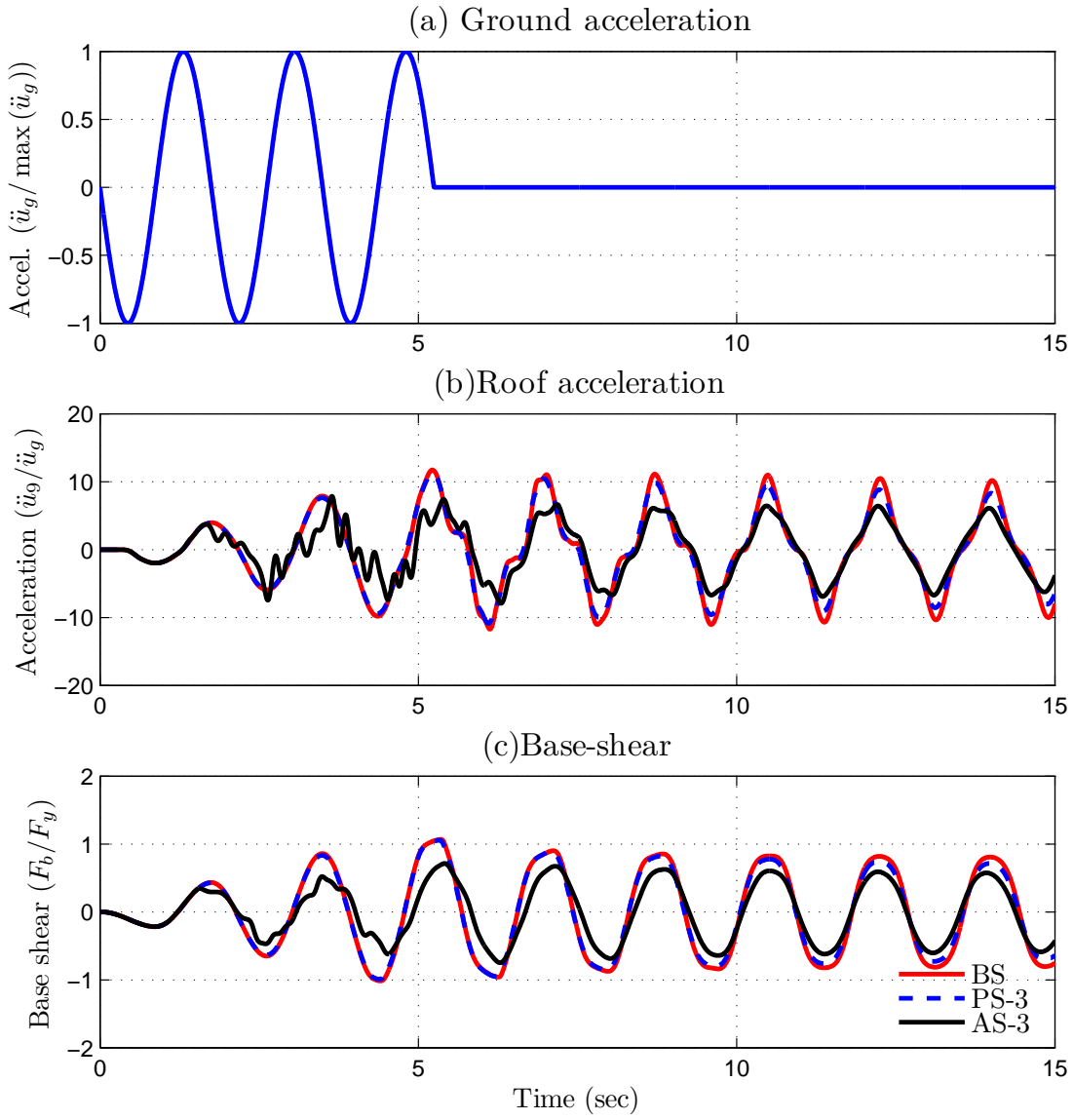


Figure 5.25: F-D behavior of third-floor for periodic input. In the case of AS-3, NSD and damper are placed in the third-floor and only damper in the case of PS-3.

by more than 50%. The reduction in response is again due to the reduction in the force transmitted to the superstructure due to the addition of NSDs and avoiding the resonance state. Unlike the results with NSDs only in third-floor (shown in Figure 5.23-5.25), by adding NSDs in all the floors, the response is consistently reduced in all the floors without any excessive localized deformations.

Preliminary analysis has revealed that even with the NSDs and dampers in every floor (AS), large inter-story deformations in the bottom three floors is common for six ground motions used in this study.

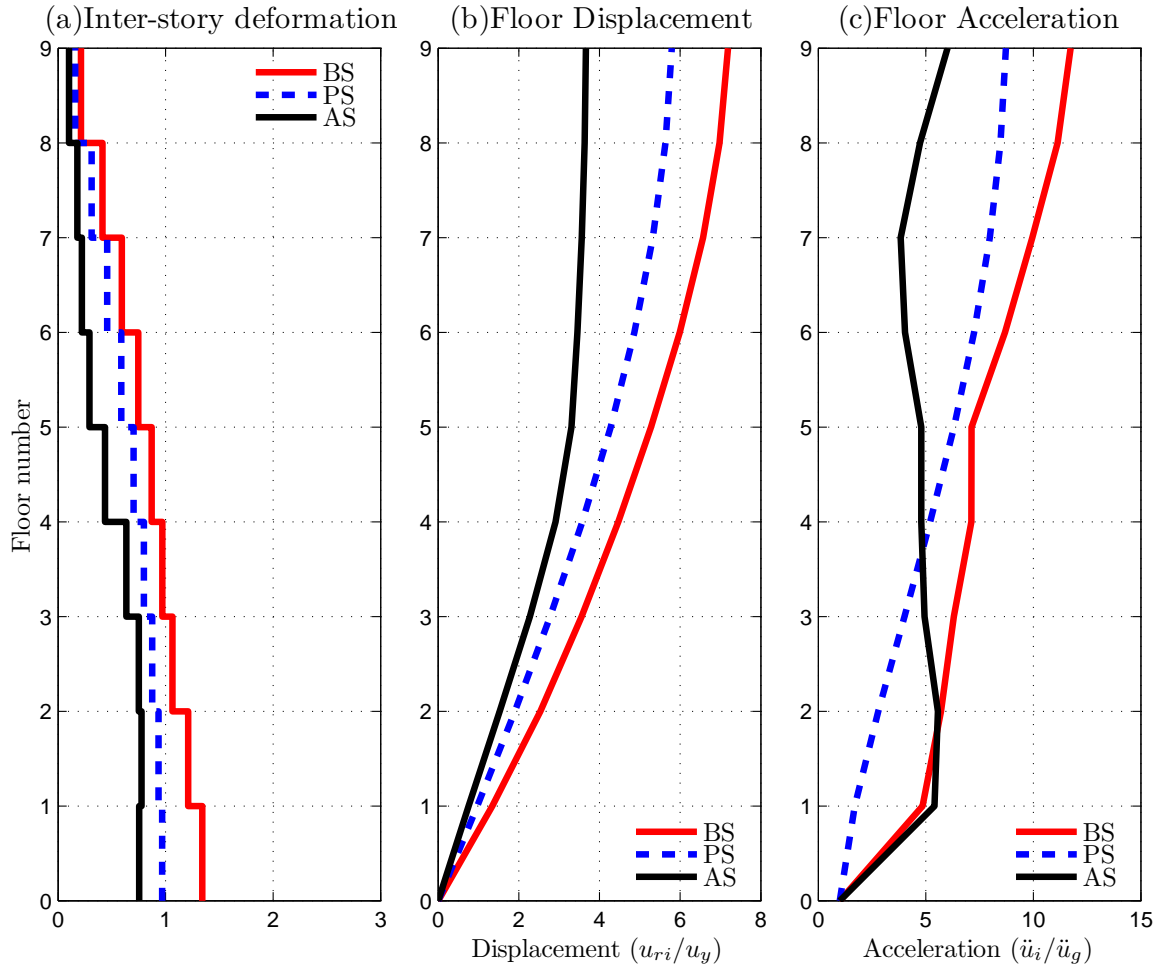


Figure 5.26: Comparison of the maximum response profile of the structure for periodic input. In AS-3, NSD and damper is placed in the third floor.

The peak interstory deformation, floor displacement and floor acceleration are shown in Figure 5.29 for Kobe-JMA (NS component) ground motion with PGA of 0.84g. From Figure 5.29, although the floor accelerations and floor displacements of AS are substantially reduced, the inter-story deformation in the first floor is very high ( $u_{di}/u_y=1.65$ ). This is due to the fact that during a ground motion, the forces are transmitted from bottom to top in multi-story structure, so the bottom stories always yield first. Since the magnitude of all the ground motions used in this study is high, the columns in first floor have yielded significantly in all the test cases.

However, the results presented in Figure 5.23-5.25 are an exception because of the time-period of

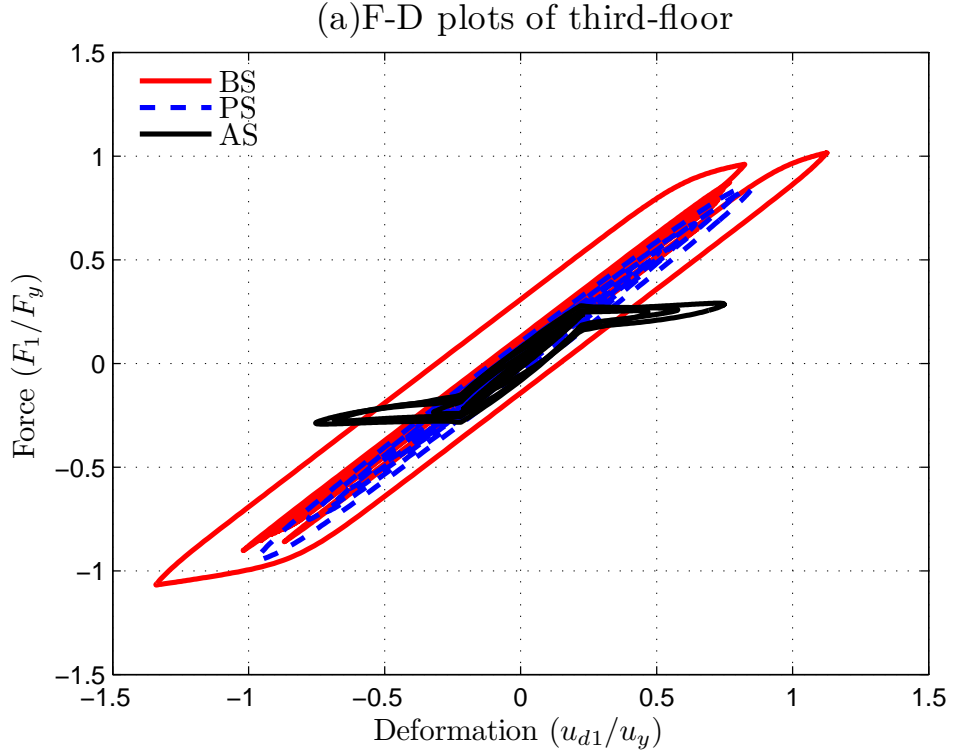


Figure 5.27: Comparison roof acceleration and base shear experienced by the BS, PS and AS for periodic input. In the case of AS, NSDs with dampers are placed in all the floors and dampers are placed in the case of PS.

the input ground motion. If the time-period of the ground input is large (greater than or equal to the fundamental period of the structure), then all the NSDs in the higher floors also engage as a result the response reduction is achieved over multiple floors. For short period pulses like the ground motion data, only the NSDs in the first-floor engage as a result the columns in the first floor will always undergo large inelastic deformation. To overcome this limitation, the properties of NSDs in different floors are modified such that NSDs in all the floors engage to prevent excessive inter-story deformation in the first-floor.

“Apparent yield-displacement”,  $u'_y$ , of NSDs in different stories is modified to achieve the desired objective. Using an optimization algorithm, the desired set of apparent yield-displacements of NSDs in all the floors is calculated by minimizing the peak responses of all the floors. Constrained nonlinear optimization algorithm is used to find the optimal NSD properties. The objective function is a weighted sum of individual story drifts and story acceleration as shown in Eq. 5.9.

$$\Pi = \sum_{i=1}^9 (\lambda_d |u_{di}| + \lambda_a |\ddot{u}_i|) \quad (5.9)$$

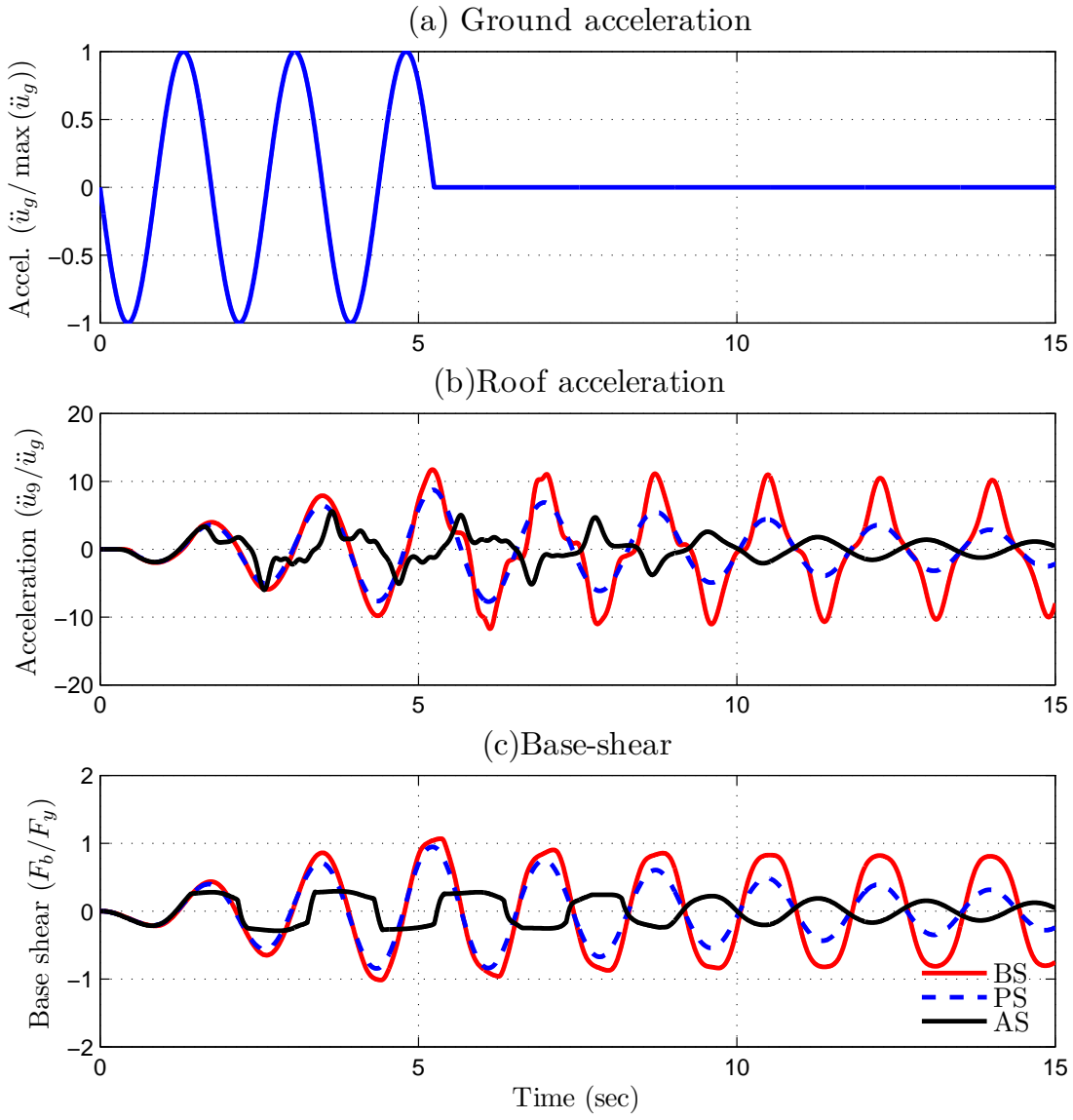


Figure 5.28: F-D behavior of first-floor for periodic input. In the case of AS, NSD and damper are placed in all floors and only damper in the case of PS.

$\lambda_d$  and  $\lambda_a$  the weighting functions used in calculating the objective function. The goal of optimization is to minimize  $\Pi$ , subject to the constraints that the strength reduction factor of individual story  $R'_{yy_i}$  should be less than 4, shown in Eq. 5.10.

$$\min_{\ddot{u}_g} \Pi(\ddot{u}_g) \quad (5.10)$$

$$\text{subject } R'_{yy_i} \leq 4 \quad (5.11)$$

Table 5.2: Optimized apparent yield displacements (normalized) in each story for all ground motions

Floor No.	Kobe	Sylmar	Newhall	Chi-Chi	Rinaldi	Erzikan
1	1.00	1.00	1.00	1.00	1.00	1.00
2	0.86	0.76	0.83	1.00	0.75	0.94
3	0.79	0.71	0.67	0.93	0.60	0.90
4	0.71	0.67	0.67	0.86	0.55	0.90
5	0.71	0.71	0.67	1.04	0.50	0.90
6	0.71	0.71	0.67	1.07	0.50	0.90

The damper properties remain unchanged i.e., viscous damper with 20% damping ratio. Response of the structure with different NSD properties in every floor is referred as AS-optimal.

Since the primary structure is inelastic system and the NSD is nonlinear, the optimization problem is nonconvex and will have no unique solution. For each ground motion, several solutions were obtained from the optimization tool (MATLAB, *fmincon* (MATLAB, 2010)) by changing the starting seed. The solutions that follow a certain trend are picked as the acceptable solutions. Obtaining a generalized solution given the structure properties and design ground motion will be the focus of future study.

The optimal NSD parameters obtained from the optimization has revealed that the  $u'_y$  of the second floor should be lower than the  $u'_y$  of first floor so that NSDs in both the floors will engage at the same time and prevent excessive deformation in the first-floor. By extending this idea to higher floors,  $u'_y$  should decrease from bottom floor to top floor. The values of  $u'_y$  in AS-optimal are listed in Table 5.2 for six ground motions; values are normalized with the first-floor  $u'_y$ . It should be noted that there are multiple solutions to the optimization problem and the results that suit the general pattern are chosen and reported in this study. After the NSDs in the bottom five floors are engaged the upper four floors have undergone very little deformation so the  $u'_y$  of floors six to nine have no impact on the overall behavior.

The peak inter-story deformation of all the floors is compared in Figure 5.29(a) for BS, PS, AS and AS-optimal for Kobe-NS ground motion [PGA=0.84g]. The floor displacement with respect to the ground is shown in Figure 5.29(b) and the floor acceleration is shown in Figure 5.29(c). The force-deformation behavior of BS, PS and AS-optimal in first-floor is shown in Figure 5.30 and the response of the roof displacement, acceleration and base shear are shown in Figure 5.31. It is clear from the response profiles in Figure 5.29(a) that the peak inter-story deformation of all the floors is reduced in the case of AS-optimal. The floor deformation of the roof is reduced by more than 15%, the roof acceleration is reduced by 30% and base shear is reduced by more than 30% compared to BS and PS, shown in Figure 5.29-5.31 and Table 5.3. In the case of inter-story deformation and floor acceleration the achieved reduction in all the floors should also be a criterion. To take this into account the average of response in all the floors is calculated and used as a performance index. The profiles of story drift, story acceleration and inter-story deformation of the nine-story frame for all the six ground motions comparing the BS, PS and AS-optimal

are shown in Figure 5.32, 5.33 and 5.34, respectively. Bar-graphs summarizing the results from all the six ground motions are shown in Figure 5.35 and tabulated in Table 5.3. AS in Figures 5.32-5.35 and Table 5.3 refers to AS-optimal.

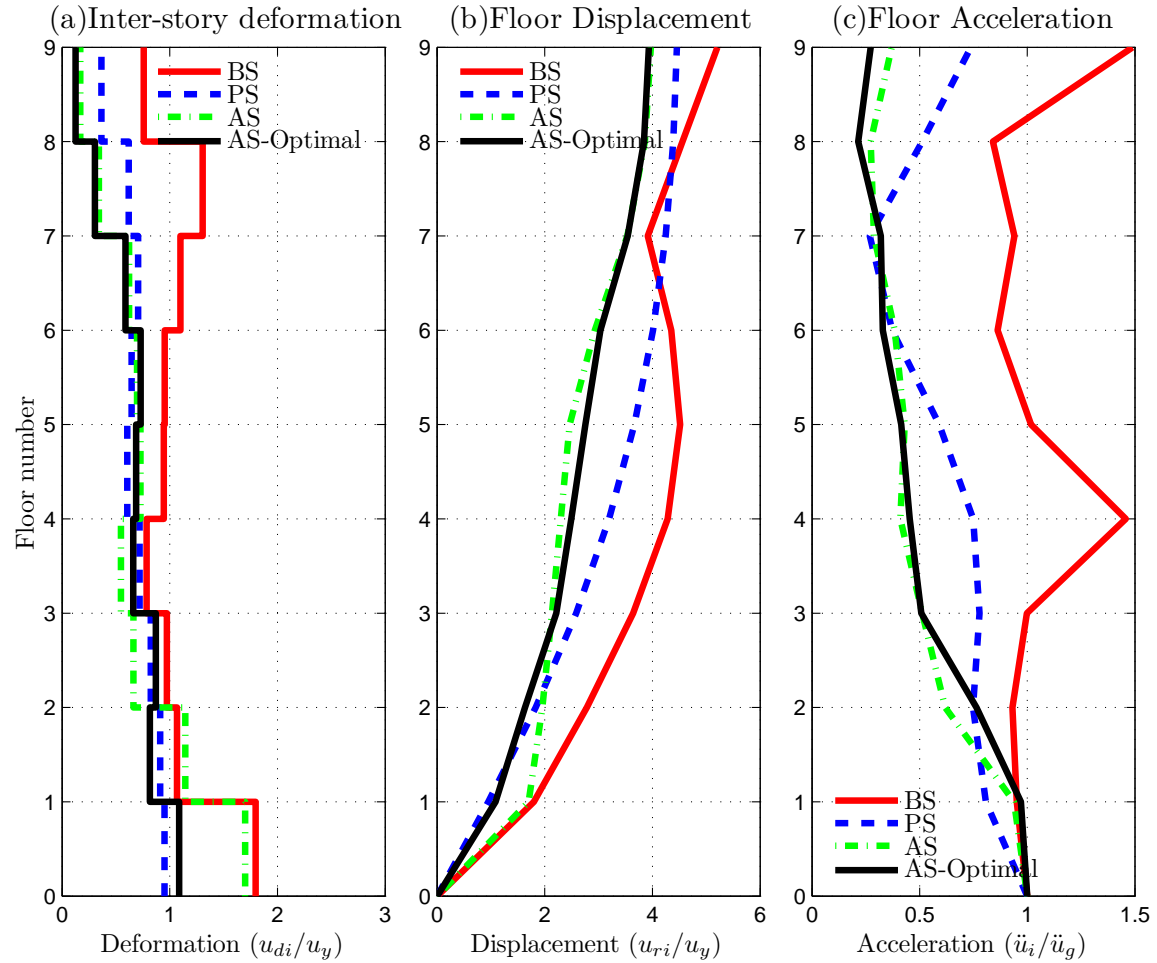


Figure 5.29: Comparison of the maximum response profile of the structure for Kobe-NS ground motion [PGA=0.84g])

The story drift profiles shown in Figure 5.32, confirms that the addition of dampers (BS and AS-optimal) will reduce the story drifts compared to BS. With the addition of NSDs in all the floors along with dampers, the drift is localized to the first three or four floors and the higher stories undergo rigid body motion, from Figure 5.32 and Figure 5.34. The inter-story deformation in the bottom three floors of NS is higher than the PS in case of Chi-Chi and Rinaldi ground motions, but is consistently less than the BS by more than 20%. Although the inter-story drifts of AS-optimal is higher than PS for few ground

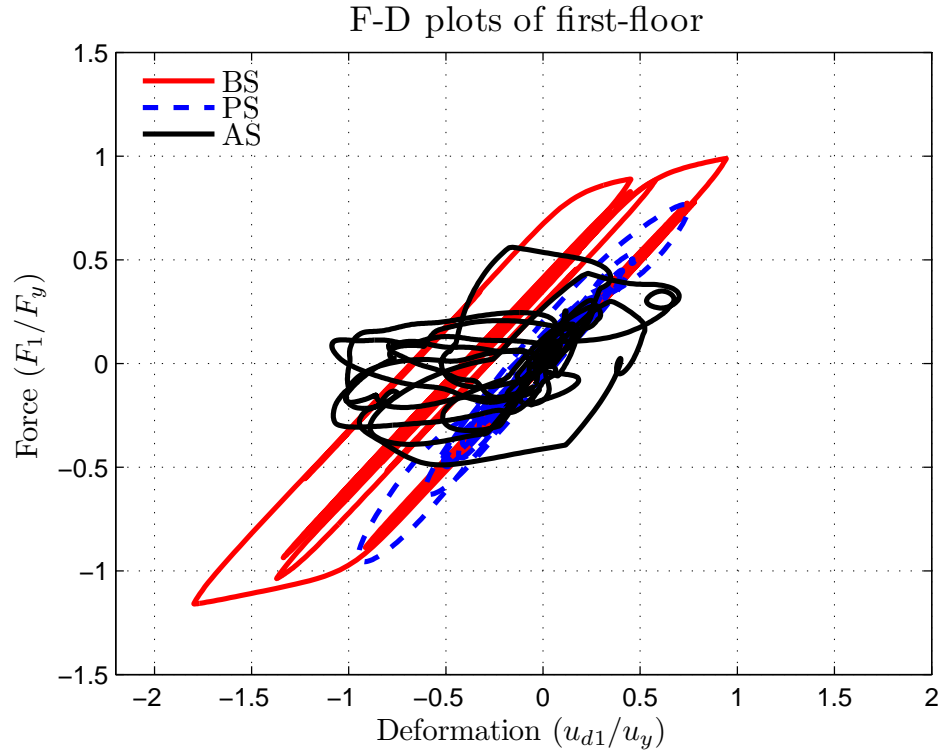


Figure 5.30: F-D behavior of the 1st floor in BS, PS and AS-optimal for Kobe-NS ground motion [PGA=0.84g]

motions, the average drift is less than PS, shown in Figure 5.35 and the Table 5.3. This shows that the inter-story deformation is localized in the bottom floors, essentially isolating the higher floors. The acceleration profiles shown in Figure 5.33 for all the ground motions shows the acceleration reductions in all the floors. The bar-graphs shown in Figure 5.35 and the Table 5.3 can be summarized as follows:

1. The floor acceleration, roof displacement and base shear of AS-optimal is consistently less than BS and PS by more than 20% for all the ground motions.
2. Peak inter-story deformation of AS-optimal for some ground motions is higher than PS but it always less than BS. Although the maximum inter-story deformation of AS-optimal, which generally occurs in the bottom three floors, is larger than PS, it should be noted that the inter-story deformation in all other floors is less than BS and PS.
3. Adding the NSDs will result in consistent reduction of floor accelerations, floor deformations of all the floors (average values in Table 5.3 and Figure 5.35) and base shear as compared to BS.

Table 5.3: Summary of the peak responses from the shake table tests on unbraced structure [Yielding-tests]

Sl. no.	Ground motion	Sys tem	PGA (g)	Drift $u_g/H$	Inter-defor $\mu_{di}/u_y$		Accel. $\ddot{u}_i/\ddot{u}_g$		Base shear $F_b/F_y$
					Max.	Mean	Max.	Mean	
1	Kobe- NS,1995	BS	0.84	1.30	1.80	1.08	1.49	1.05	1.16
2		PS	0.84	1.11(14)	0.95(47)	0.70(34)	0.74(50)	0.62(41)	0.96(18)
3		AS	0.84	0.93(29)	1.07(41)	0.54(50)	0.35(77)	0.39(63)	0.56(52)
4	Erzikan- NS (1992)	BS	0.36	1.66	1.24	0.84	1.72	1.09	1.05
5		PS	0.36	1.41(15)	0.93(25)	0.67(20)	1.07(38)	0.73(33)	0.92(13)
6		AS	0.36	1.19(28)	0.87(30)	0.60(29)	0.64(63)	0.58(47)	0.34(68)
7	Rinaldi-FN (1994)	BS	0.63	1.55	1.77	1.11	1.72	1.10	1.15
8		PS	0.63	1.35(13)	1.09(38)	0.82(26)	0.96(44)	0.72(35)	1.05(9)
9		AS	0.63	1.40(10)	1.62(8)	0.76(31)	0.26(85)	0.34(69)	0.50(56)
10	Newhall- FN (1994)	BS	0.55	1.37	1.25	0.91	1.93	1.39	1.05
11		PS	0.55	1.02(26)	1.01(19)	0.65(28)	0.96(50)	0.82(41)	1.00(5)
12		AS	0.55	1.24(10)	1.35(-8)	0.74(19)	0.34(83)	0.45(67)	0.54(48)
13	Chi-Chi NS (1999)	BS	0.20	1.83	1.86	0.88	2.09	1.51	1.17
14		PS	0.20	1.59(13)	1.21(35)	0.71(19)	1.33(37)	1.08(29)	1.05(11)
15		AS	0.20	1.31(28)	1.88(-1)	0.88(-1)	0.83(60)	0.66(56)	0.59(49)
16	Sylmar-FN (1994)	BS	0.61	1.98	1.39	0.99	1.48	1.05	1.08
17		PS	0.61	1.77(10)	1.10(21)	0.80(19)	0.65(56)	0.52(51)	1.04(3)
18		AS	0.61	1.07(46)	1.18(15)	0.59(40)	0.24(84)	0.31(71)	0.45(58)

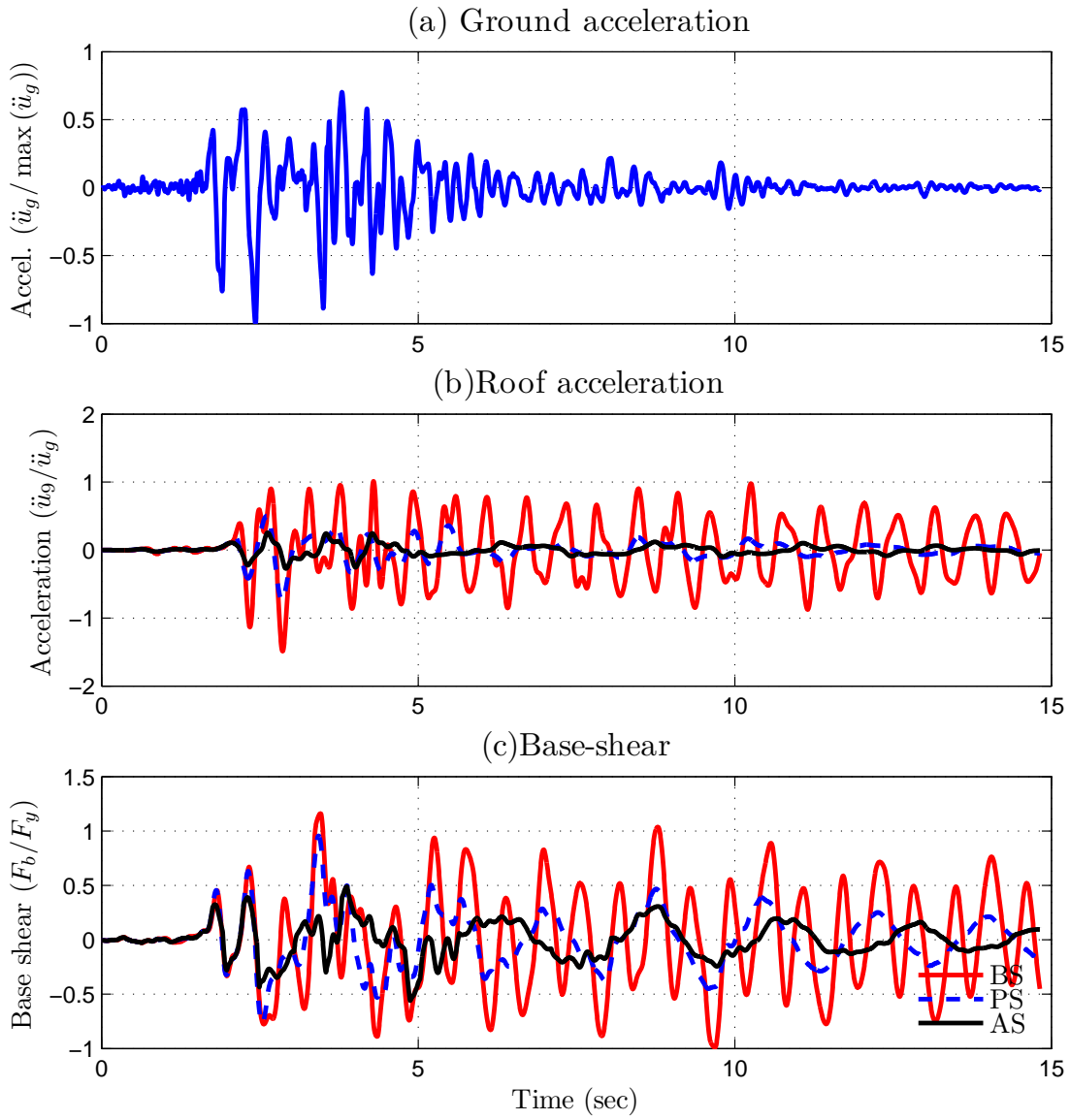


Figure 5.31: Comparison of roof acceleration and base shear experienced by the BS, PS and AS-optimal for Kobe-NS ground motion [PGA=0.84g]

## 5.5 Summary

In this chapter, the advantages of using NSDs in multi-story structures are demonstrated through experimental and simulation studies. Shake-table studies have been performed on three-story fixed base structure with two NSDs and a viscous damper in the first floor. Experimental results have proved that the addition of NSDs in the first-floor will screen the input energy transmitted to the super structure. However, the first-floor is subjected to large inter-story deformation due to the reduction in stiffness with the

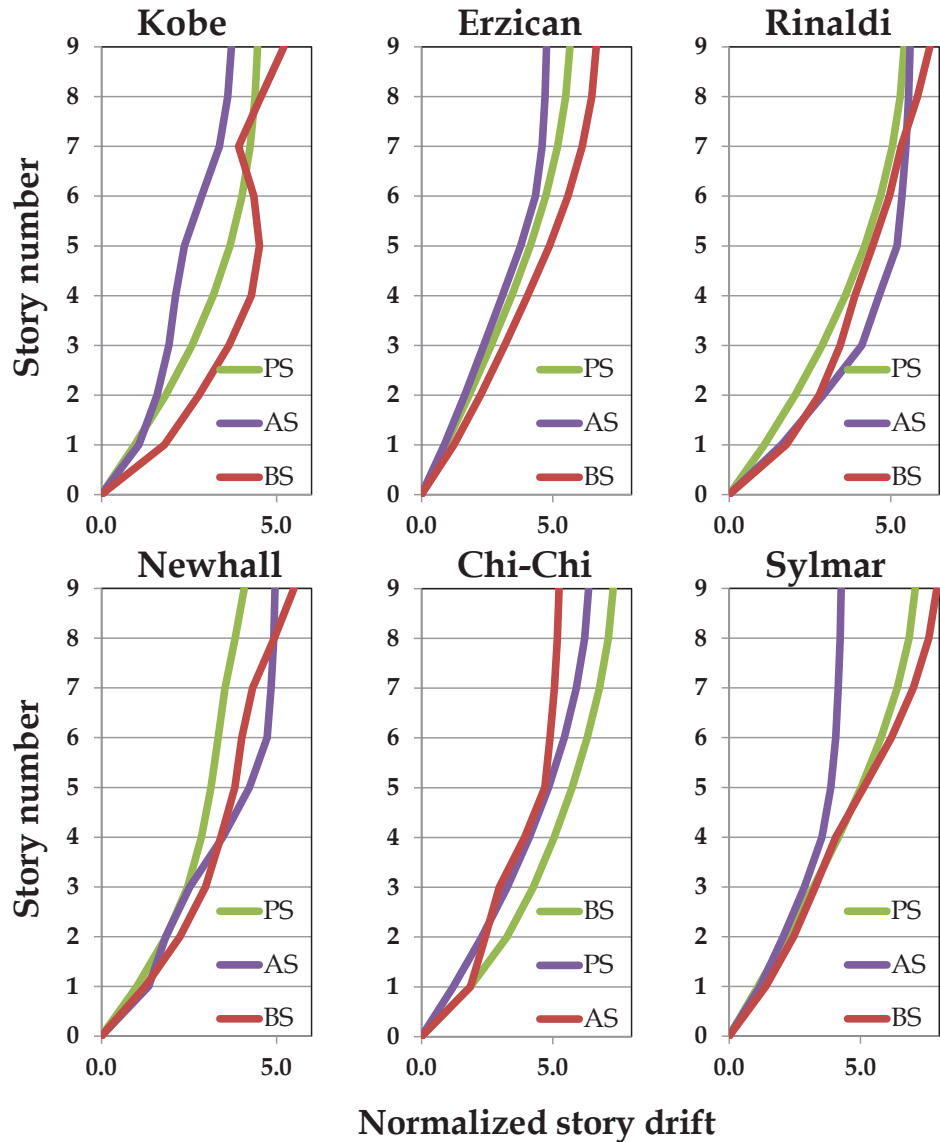


Figure 5.32: Comparison of the story drift profiles of BS, PS and AS

addition of NSDs. By adding a viscous damper along with the NSDs, the deformations can be contained without increasing the base shear and roof accelerations.

Experimental results on the unbraced 3SFS have confirmed that the inter-story deformations, roof accelerations and base shear of the AS will be consistently reduced by more than 15%, 20% and 40%, respectively, compared to the BS, PS. NSDs are capable of absorbing most of the input energy and dissipate it through the viscous damper thus preventing the structural and non-structural components of the superstructure from experiencing large accelerations and preserve the integrity of the structure. Also, the huge

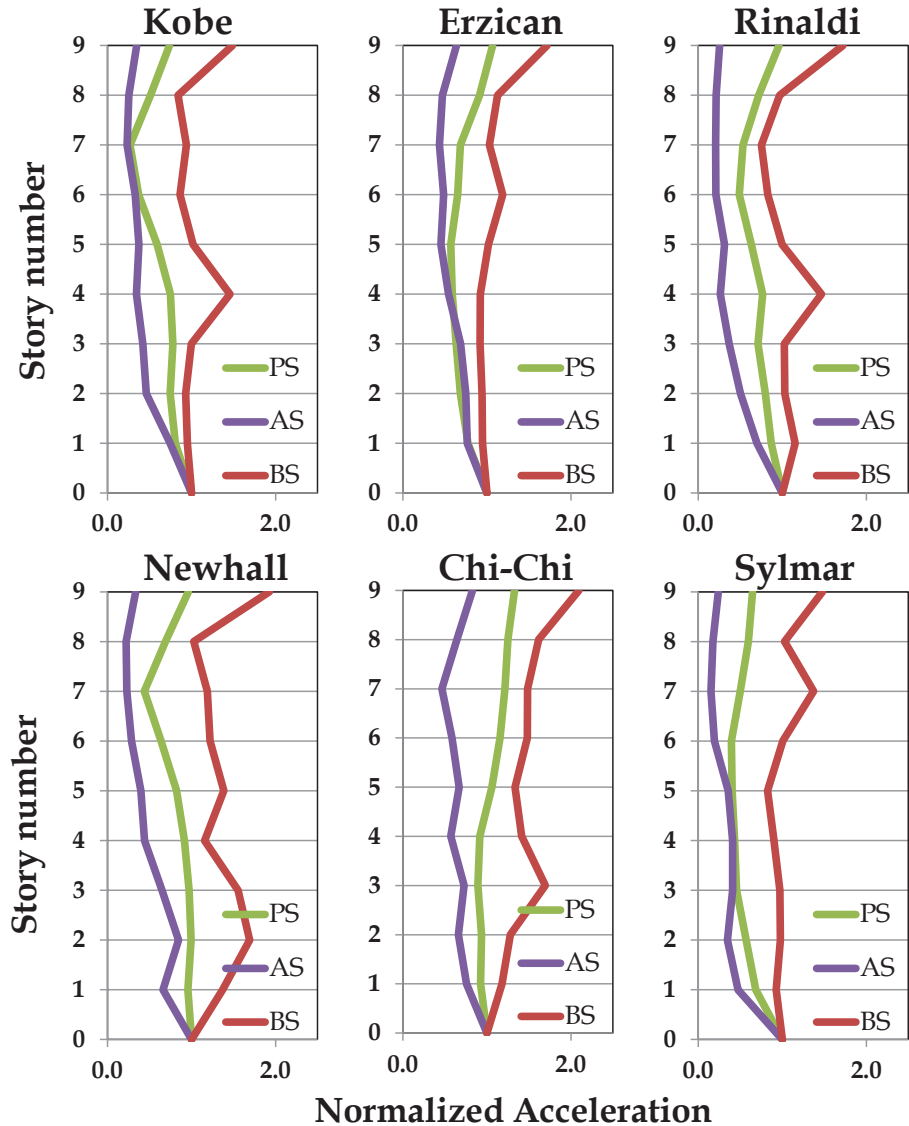


Figure 5.33: Comparison of the story acceleration profiles of BS, PS and AS

reductions in base shear will avoid the large foundation forces experienced otherwise. Generic numerical models are also developed and calibrated to replicate the experimental results at component level and assembly level. These models can be used to study the sensitivity of the design parameters for the structure and the NSD. Given the nonlinear behavior of the components and the complexity of the assembly, the close agreement between the experimental results and the analytical predictions shows that developed models are representative of the actual structures.

Comprehensive simulation studies have also been carried on 1:3 scale nine-story yielding structure, to

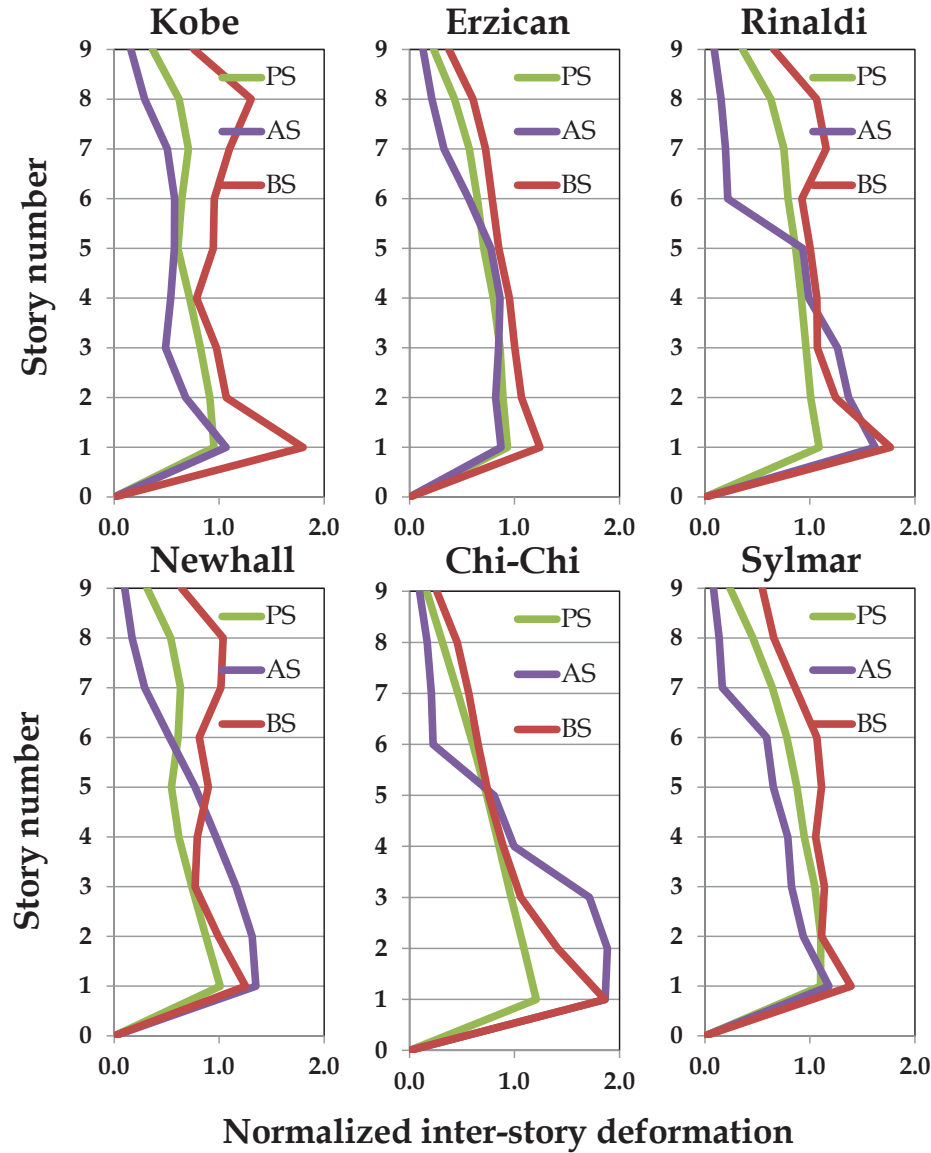


Figure 5.34: Comparison of the inter-story deformation profiles of BS, PS and AS

analyze the role of NSDs in multistory buildings and also to find the desired configuration of NSDs to achieve response reduction during severe ground motions. Results presented herein have confirmed that the addition of NSD in a particular story will prevent the transfer of the input energy from ground motion to the super structure and also the resonance state of the primary structure can be avoided. However, the inter-story deformations in the installed floor will be significantly larger compared to uncontrolled structure. These excessive localized deformations can be prevented by placing NSDs (having different properties) in multiple stories and letting them engage at the same time.

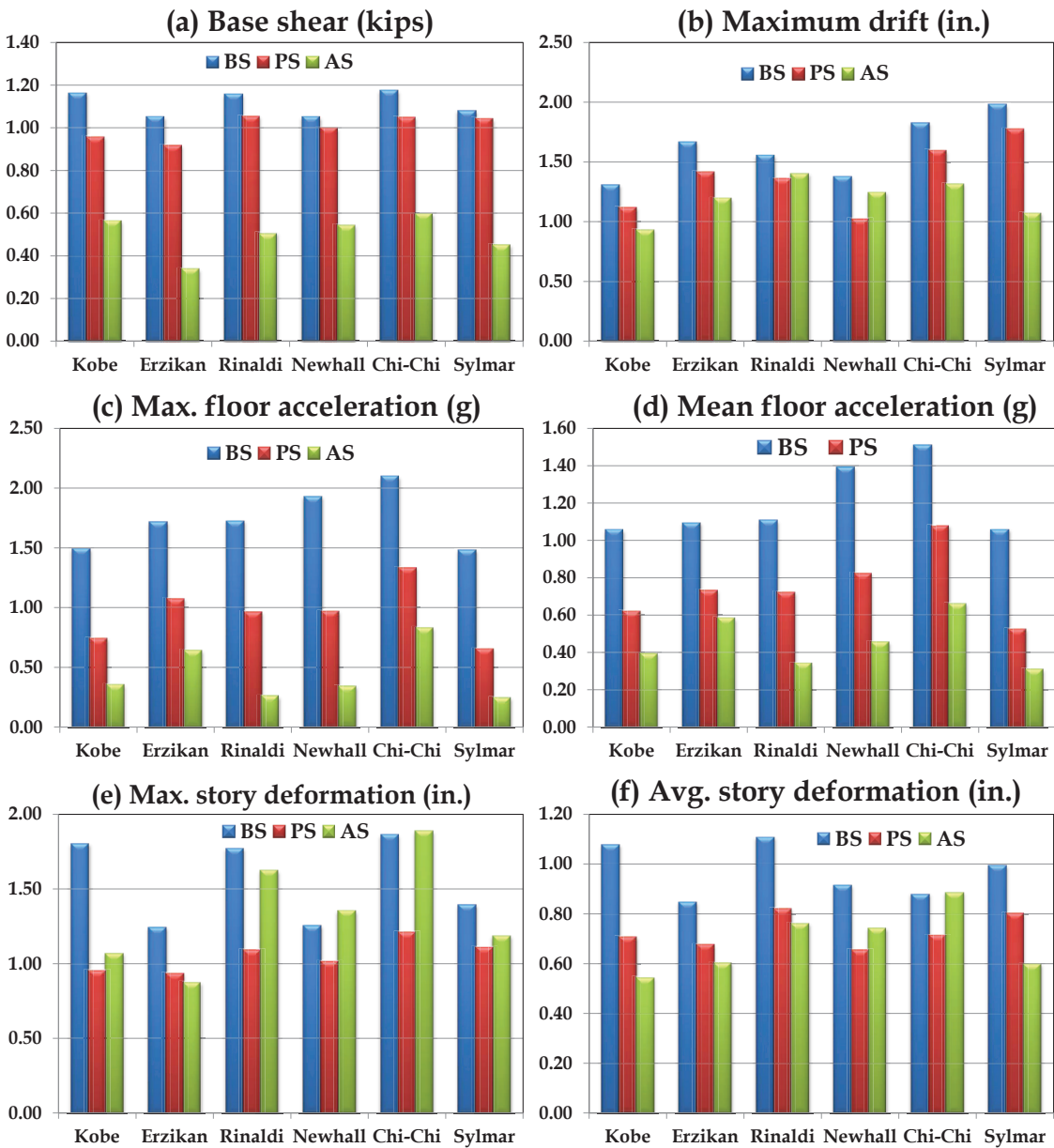


Figure 5.35: Bar graphs summarizing the normalized response of BS, PS and AS for six ground motions

An optimization study has been carried to find the desired properties of NSD as a function of the story height for six ground motions. The “apparent yield-displacement” of the NSDs should decrease from bottom to top to prevent large inelastic deformations in the first story. The optimal properties of NSDs for a given structure and a target response reduction can be calculated based on the site specific spectra. Response has demonstrated that the base shear and maximum floor accelerations of the AS-optimal is reduced by more than 40% and 20%, respectively for all the ground motions tested. In all the test cases, the

top four floors of the nine-story frame have undergone very little deformation confirming that the input energy is dissipated in the bottom five floors, unlike the base-isolation system where all the deformations and energy dissipation occurs at the base of structure. This study has revealed that installing NSDs and dampers in multiple stories can overcome some of the limitations posed by the passive control devices and base-isolation systems. However, from the practical point of view, the proposed approach and the NSD needs to be enhanced further because they are sensitive to the design ground motion, the estimated force-deformation behavior and the excessive permanent deformations observed for severe ground motions.



# Chapter 6

## Conclusions

For a new concept to get accepted and materialize in the structural engineering community, implementation-lag is about two to three decades. Complexity of the control device and uncertainty over its reliable in-situ performance plays a major role in getting an approval from the practicing engineers. Taking these factors into consideration, in this research, we attempted to develop novel adaptive control devices and new control strategies to mitigate the excessive structural responses during strong earthquake motions. The key emphasis is on developing an adaptive control device capable of being implemented in a real-life structure. The key contributions of this study are summarized next.

### 6.1 “Apparent weakening” in elastic SDOF structure

Comprehensive experimental and simulation studies have been carried on SDOF-3SFS structure, to study the behavior in elastic structure and negative stiffness device (NSD) assembly for a suite of ground motions. Five ground motions are used for shake table tests and seven ground motion are used for simulation studies; the ground motions chosen are representative of both near-fault and far-field earthquakes. Shake table studies carried on a SDOF-3SFS with the NSDs and damper installed in the first floor (AS) show that by adding NSD to the elastic structure, a bilinear elastic system can be emulated and as a result the base shear demands on the main structure during strong earthquakes can be reduced by 30%. The peak acceleration experienced by the structure is also reduced by more than 20%. However, the peak displacement of the NSD and structure assembly is increased due to the reduction in stiffness induced by the NSD. These increased deformations are controlled by adding a viscous damper. Consistent response reductions are observed for a suite of ground motions by the addition of the viscous fluid damper. The observed experimental behavior can be reproduced by the presented analytical models at the component level and also for the structure and device assembly.

It has been shown through the numerical studies that the addition of viscous damper will reduce the peak deformation by more than 20% but the structure will experience almost the same acceleration and

base shear as the uncontrolled structure. The NSD in conjunction with a viscous damper is capable of simultaneously reducing the base shear, the acceleration and the displacement of the structure.

## 6.2 “Apparent weakening” in yielding SDOF structure

With the addition of NSD to the bilinear inelastic structure, the base shear and accelerations of the assembly are reduced by more than 30% for ground motions in which there is mild yielding in the primary structure. For more severe ground motions, the deformations of the assembly will be larger than the stiffening point of NSD; resulting in very high assembly stiffness thereby increase in base shear and accelerations of the assembly. However, the high stiffness of the assembly will prevent the structure from collapsing. In the case where there is heavy yielding in the primary structure, the permanent drift in the assembly is larger than the plastic deformation in the primary structure. The permanent drift in excess of the plastic-deformation in the primary structure can be completely recovered by disengaging the NSD from the primary structure. It has also been demonstrated that the stiffening in NSD will prevent the structure from collapsing. Analogous to the inelastic design, the acceleration and base shear and deformation of the structure and NSD assembly can be reduced by more than 20% for moderate ground motions and the collapse of structure can be prevented for severe ground motions. Additionally, part of the inelastic excursions incurred after a severe ground motion can be recovered by disconnecting the NSD.

## 6.3 Distributed isolation in MDOF structure using NSD

The advantages of using NSDs in multi-story structures are demonstrated through experimental and simulation studies. Shake-table studies performed on three-story fixed base structure have proved that the addition of NSDs in the first-floor will screen the input energy transmitted to the super structure. Experimental results on the unbraced 3SFS have confirmed that the inter-story deformations, roof accelerations and base shear of the AS will be consistently reduced by more than 15%, 20% and 40%, respectively, compared to the primary structure (BS) and primary structure with passive damper (PS). NSDs are capable of preventing the transmission of input energy thus preventing the structural and non-structural components of the super-structure from experiencing large accelerations and preserve the integrity of the structure.

Also, reductions more than 30% in base shear will avoid the large foundation forces experienced otherwise. Generic numerical models are also developed and calibrated to replicate the experimental results at component level and assembly level. These models can be used to study the sensitivity of the design parameters for the structure and the NSD. Given the nonlinear behavior of the components and the complexity of the assembly, the close agreement between the experimental results and the analytical predictions shows that developed models are representative of the actual structures.

Comprehensive simulation studies carried on 1:3 scale nine-story yielding structure, demonstrated the role of NSDs in multistory buildings and also to find the desired configuration of NSDs to achieve response reduction during severe ground motions. Addition of NSD in a particular story will prevent the transfer of the input energy from ground motion to the super structure and also the resonance state of the primary structure can be avoided. However, the inter-story deformations in the installed floor will be significantly larger compared to uncontrolled structure. These excessive localized deformations can be prevented by placing NSDs (having different properties) in multiple stories and letting them engage at the same time. The “apparent yield-displacement” of the NSDs should decrease from bottom to top to prevent large inelastic deformations in the first story. The optimal properties of NSDs for a given structure and a target response reduction can be calculated based on the site specific spectra. Numerical studies have demonstrated that the base shear and maximum floor accelerations of the AS with optimal NSD properties are reduced by more than 40% and 20%, respectively for all the ground motions tested. In all the test cases, the top four floors of the nine-story frame have undergone very little deformation confirming that the input energy is dissipated in the bottom five floors, unlike the base-isolation system where all the deformations and energy dissipation occurs at the base of structure.



# Chapter 7

## References

- Preventing earthquake disasters: The grand challenge in earthquake engineering: A research agenda for the network for earthquake engineering simulation (NEES). [http://www.nap.edu/openbook.php?record\\_id=10799&page=156](http://www.nap.edu/openbook.php?record_id=10799&page=156). URL [http://www.nap.edu/openbook.php?record\\_id=10799&page=156](http://www.nap.edu/openbook.php?record_id=10799&page=156).
- USGS: Largest and deadliest earthquakes by year. <http://earthquake.usgs.gov/earthquakes/eqarchives/year/byyear.php>. URL <http://earthquake.usgs.gov/>.
- A. K. Chopra. *Dynamics of structures: Theory and applications to earthquake engineering*. Prentice-Hall international series in civil engineering and engineering mechanics. Pearson/Prentice Hall, 2007.
- G. P. Cimellaro, O. Lavan, and A. M. Reinhorn. Design of passive systems for control of inelastic structures. *Earthquake Engineering & Structural Dynamics*, 38(6):783–804, 2009.
- M. C. Constantinou and M. D. Symans. Experimental study of seismic response of buildings with supplemental fluid dampers. *The Structural Design of Tall Buildings*, 2(2):93–132, 1993.
- D. M. Fenz and M. C. Constantinou. Spherical sliding isolation bearings with adaptive behavior: Experimental verification. *Earthquake Engineering & Structural Dynamics*, 37(2):185–205, 2007.
- D. M. Fenz and M. C. Constantinou. Spherical sliding isolation bearings with adaptive behavior: Theory. *Earthquake Engineering & Structural Dynamics*, 37(2):163–183, 2008.
- N. Gluck, A. M. Reinhorn, J. Gluck, and R. Levy. Design of supplemental dampers for control of structures. *Journal of Structural Engineering, ASCE*, 122(12):1394–1399, 1996.
- H. Iemura and M. H. Pradono. Advances in the development of pseudo-negative-stiffness dampers for seismic response control. *Structural Control and Health Monitoring*, 16(7-8):784–799, 2009.

- D. K. Kusumastuti, A. M. Reinhorn, and A. Rutenberg. A versatile experimentation model for study of structures near collapse applied to seismic evaluation of irregular structures. Technical report, University at Buffalo, SUNY, 2005.
- N. Makris and C. J. Black. Dimensional analysis of bilinear oscillators under pulse-type excitations. *Journal of Engineering Mechanics*, 130(9):1019–1031, 2004a.
- N. Makris and C. J. Black. Dimensional analysis of rigid-plastic and elastoplastic structures under pulse-type excitations. *Journal of Engineering Mechanics*, 130(9):1006–1018, 2004b.
- MATLAB. *version 7.10.0 (R2010a)*. The MathWorks Inc., Natick, Massachusetts, 2010.
- W. G. Molyneaux. Supports for vibration isolation. Technical Report ARC/CP-322, Aeronautical Research Council, Great Britain, 1957.
- S. Nagarajaiah. Adaptive passive, semiactive, smart tuned mass dampers: identification and control using empirical mode decomposition, hilbert transform, and short-term fourier transform. *Structural Control and Health Monitoring*, 16(7-8):800–841, 2009.
- S. Nagarajaiah and A. M. Reinhorn. Applicability of pseudo-force method to highly nonlinear dynamic problems. In *Proceedings of Structures Congress*, pages 165–172. ASCE, 1994.
- S. Nagarajaiah, A. M. Reinhorn, and M. C. Constantinou. Nonlinear dynamic analysis of 3d base-isolated structures. *Journal of Structural Engineering, ASCE*, 117(7):2035–2054, 1991.
- Y. Ohtori, R. E. Christenson, B. F. Spencer, and S. J. Dyke. Benchmark control problems for seismically excited nonlinear buildings. *Journal of Engineering Mechanics*, 130(4):366–385, 2004.
- D. T. R. Pasala, A. A. Sarlis, S. Nagarajaiah, A. M. Reinhorn, M. C. Constantinou, and D. Taylor. Negative stiffness device for seismic response control of multi-story buildings: Experimental study. *Earthquake Engineering and Structural Dynamics (under review)*, 2012a.
- D. T. R. Pasala, A. A. Sarlis, S. Nagarajaiah, A. M. Reinhorn, M. C. Constantinou, and D. Taylor. Negative stiffness device for seismic response control of multi-story buildings: Distributed isolation. *Earthquake Engineering and Structural Dynamics (under review)*, 2012b.
- D. T. R. Pasala, A. A. Sarlis, A. M. Reinhorn, S. Nagarajaiah, M. C. Constantinou, and D. Taylor. Simulated bilinear-elastic behavior in a SDOF elastic structure using negative stiffness device: Experimental and analytical study. *Journal of Structural Engineering, ASCE (under review)*, 2012c.
- D. T. R. Pasala, A. A. Sarlis, A. M. Reinhorn, S. Nagarajaiah, M. C. Constantinou, and D. Taylor. Apparent-weakening in SDOF yielding structure using negative stiffness device: Experimental and analytical study. *Earthquake Engineering and Structural Dynamics (under review)*, 2012d.

- D. T. R. Pasala, A. A. Sarlis, M. C. Constantinou, A. M. Reinhorn, S. Nagarajaiah, and D. Taylor. Negative stiffness device for seismic protection of structures. *Journal of Structural Engineering, ASCE*, DOI:10.1061/(ASCE)ST.1943-541X.0000616, April, 2012a.
- D. T. R. Pasala, A. A. Sarlis, S. Nagarajaiah, A. M. Reinhorn, M. C. Constantinou, and D. Taylor. Adaptive negative stiffness: A new structural modification approach for seismic protection. *Journal of Structural Engineering, ASCE*, DOI:10.1061/(ASCE)ST.1943-541X.0000615, April, 2012b.
- D. L. Platus. Negative-stiffness-mechanism vibration isolation systems. In *Proceedings of SPIE*, pages 44–54, San Jose, CA, USA, 1992.
- D. L. Platus. Vibration isolation system, 2004. URL <http://www.google.at/patents/US6676101>. U.S. Classification: 248/603; International Classification: F16F/1300.
- A. M. Reinhorn, S. Viti, and A. S. Whittaker. Retrofit of structures: Strength reduction with damping enhancement. In *Proceedings, KEERC-MCEER Joint Seminar on Contributions to Earthquake Engineering, Multi-disciplinary Center for Earthquake Engineering Research*, 2002.
- A. M. Reinhorn, S. Viti, and G. P. Cimellaro. Retrofit of structures: Strength reduction with damping enhancement. In *Proceedings of the 37th UJNR panel meeting on wind and seismic effects*, pages 16–21, 2005.
- A. M. Reinhorn, O. Lavan, and G. Cimellaro. Design of controlled elastic and inelastic structures. *Earthquake Engineering and Engineering Vibration*, 8:469–479, 2009. ISSN 1671-3664.
- A. A. Sarlis. *Adaptive seismic protection of systems*. PhD thesis, University at Buffalo, SUNY, Buffalo, New York, July 2012.
- M. V. Sivaselvan and A. M. Reinhorn. Hysteretic models for deteriorating inelastic structures. *Journal of Engineering Mechanics*, 126(6):633–640, 2000.
- T. T. Soong. Experimental simulation of degrading structures through active control. *Earthquake Engineering & Structural Dynamics*, 27(2):143–154, 1998.
- B. F. Spencer and S. Nagarajaiah. State of the art of structural control. *Journal of Structural Engineering, ASCE*, 129(7):845–856, 2003.
- S. Viti, G. P. Cimellaro, and A. M. Reinhorn. Retrofit of a hospital through strength reduction and enhanced damping. *Smart Structures and Systems*, 2(4):339–355, 2006.



## MCEER Technical Reports

MCEER publishes technical reports on a variety of subjects written by authors funded through MCEER. These reports are available from both MCEER Publications and the National Technical Information Service (NTIS). Requests for reports should be directed to MCEER Publications, MCEER, University at Buffalo, State University of New York, 133A Ketter Hall, Buffalo, New York 14260. Reports can also be requested through NTIS, P.O. Box 1425, Springfield, Virginia 22151. NTIS accession numbers are shown in parenthesis, if available.

- NCEER-87-0001 "First-Year Program in Research, Education and Technology Transfer," 3/5/87, (PB88-134275, A04, MF-A01).
- NCEER-87-0002 "Experimental Evaluation of Instantaneous Optimal Algorithms for Structural Control," by R.C. Lin, T.T. Soong and A.M. Reinhorn, 4/20/87, (PB88-134341, A04, MF-A01).
- NCEER-87-0003 "Experimentation Using the Earthquake Simulation Facilities at University at Buffalo," by A.M. Reinhorn and R.L. Ketter, not available.
- NCEER-87-0004 "The System Characteristics and Performance of a Shaking Table," by J.S. Hwang, K.C. Chang and G.C. Lee, 6/1/87, (PB88-134259, A03, MF-A01). This report is available only through NTIS (see address given above).
- NCEER-87-0005 "A Finite Element Formulation for Nonlinear Viscoplastic Material Using a Q Model," by O. Gyebi and G. Dasgupta, 11/2/87, (PB88-213764, A08, MF-A01).
- NCEER-87-0006 "Symbolic Manipulation Program (SMP) - Algebraic Codes for Two and Three Dimensional Finite Element Formulations," by X. Lee and G. Dasgupta, 11/9/87, (PB88-218522, A05, MF-A01).
- NCEER-87-0007 "Instantaneous Optimal Control Laws for Tall Buildings Under Seismic Excitations," by J.N. Yang, A. Akbarpour and P. Ghaemmaghami, 6/10/87, (PB88-134333, A06, MF-A01). This report is only available through NTIS (see address given above).
- NCEER-87-0008 "IDARC: Inelastic Damage Analysis of Reinforced Concrete Frame - Shear-Wall Structures," by Y.J. Park, A.M. Reinhorn and S.K. Kunath, 7/20/87, (PB88-134325, A09, MF-A01). This report is only available through NTIS (see address given above).
- NCEER-87-0009 "Liquefaction Potential for New York State: A Preliminary Report on Sites in Manhattan and Buffalo," by M. Budhu, V. Vijayakumar, R.F. Giese and L. Baumgras, 8/31/87, (PB88-163704, A03, MF-A01). This report is available only through NTIS (see address given above).
- NCEER-87-0010 "Vertical and Torsional Vibration of Foundations in Inhomogeneous Media," by A.S. Veletsos and K.W. Dotson, 6/1/87, (PB88-134291, A03, MF-A01). This report is only available through NTIS (see address given above).
- NCEER-87-0011 "Seismic Probabilistic Risk Assessment and Seismic Margins Studies for Nuclear Power Plants," by Howard H.M. Hwang, 6/15/87, (PB88-134267, A03, MF-A01). This report is only available through NTIS (see address given above).
- NCEER-87-0012 "Parametric Studies of Frequency Response of Secondary Systems Under Ground-Acceleration Excitations," by Y. Yong and Y.K. Lin, 6/10/87, (PB88-134309, A03, MF-A01). This report is only available through NTIS (see address given above).
- NCEER-87-0013 "Frequency Response of Secondary Systems Under Seismic Excitation," by J.A. HoLung, J. Cai and Y.K. Lin, 7/31/87, (PB88-134317, A05, MF-A01). This report is only available through NTIS (see address given above).
- NCEER-87-0014 "Modelling Earthquake Ground Motions in Seismically Active Regions Using Parametric Time Series Methods," by G.W. Ellis and A.S. Cakmak, 8/25/87, (PB88-134283, A08, MF-A01). This report is only available through NTIS (see address given above).
- NCEER-87-0015 "Detection and Assessment of Seismic Structural Damage," by E. DiPasquale and A.S. Cakmak, 8/25/87, (PB88-163712, A05, MF-A01). This report is only available through NTIS (see address given above).

- NCEER-87-0016 "Pipeline Experiment at Parkfield, California," by J. Isenberg and E. Richardson, 9/15/87, (PB88-163720, A03, MF-A01). This report is available only through NTIS (see address given above).
- NCEER-87-0017 "Digital Simulation of Seismic Ground Motion," by M. Shinozuka, G. Deodatis and T. Harada, 8/31/87, (PB88-155197, A04, MF-A01). This report is available only through NTIS (see address given above).
- NCEER-87-0018 "Practical Considerations for Structural Control: System Uncertainty, System Time Delay and Truncation of Small Control Forces," J.N. Yang and A. Akbarpour, 8/10/87, (PB88-163738, A08, MF-A01). This report is only available through NTIS (see address given above).
- NCEER-87-0019 "Modal Analysis of Nonclassically Damped Structural Systems Using Canonical Transformation," by J.N. Yang, S. Sarkani and F.X. Long, 9/27/87, (PB88-187851, A04, MF-A01).
- NCEER-87-0020 "A Nonstationary Solution in Random Vibration Theory," by J.R. Red-Horse and P.D. Spanos, 11/3/87, (PB88-163746, A03, MF-A01).
- NCEER-87-0021 "Horizontal Impedances for Radially Inhomogeneous Viscoelastic Soil Layers," by A.S. Veletsos and K.W. Dotson, 10/15/87, (PB88-150859, A04, MF-A01).
- NCEER-87-0022 "Seismic Damage Assessment of Reinforced Concrete Members," by Y.S. Chung, C. Meyer and M. Shinozuka, 10/9/87, (PB88-150867, A05, MF-A01). This report is available only through NTIS (see address given above).
- NCEER-87-0023 "Active Structural Control in Civil Engineering," by T.T. Soong, 11/11/87, (PB88-187778, A03, MF-A01).
- NCEER-87-0024 "Vertical and Torsional Impedances for Radially Inhomogeneous Viscoelastic Soil Layers," by K.W. Dotson and A.S. Veletsos, 12/87, (PB88-187786, A03, MF-A01).
- NCEER-87-0025 "Proceedings from the Symposium on Seismic Hazards, Ground Motions, Soil-Liquefaction and Engineering Practice in Eastern North America," October 20-22, 1987, edited by K.H. Jacob, 12/87, (PB88-188115, A23, MF-A01). This report is available only through NTIS (see address given above).
- NCEER-87-0026 "Report on the Whittier-Narrows, California, Earthquake of October 1, 1987," by J. Pantelic and A. Reinhorn, 11/87, (PB88-187752, A03, MF-A01). This report is available only through NTIS (see address given above).
- NCEER-87-0027 "Design of a Modular Program for Transient Nonlinear Analysis of Large 3-D Building Structures," by S. Srivastav and J.F. Abel, 12/30/87, (PB88-187950, A05, MF-A01). This report is only available through NTIS (see address given above).
- NCEER-87-0028 "Second-Year Program in Research, Education and Technology Transfer," 3/8/88, (PB88-219480, A04, MF-A01).
- NCEER-88-0001 "Workshop on Seismic Computer Analysis and Design of Buildings With Interactive Graphics," by W. McGuire, J.F. Abel and C.H. Conley, 1/18/88, (PB88-187760, A03, MF-A01). This report is only available through NTIS (see address given above).
- NCEER-88-0002 "Optimal Control of Nonlinear Flexible Structures," by J.N. Yang, F.X. Long and D. Wong, 1/22/88, (PB88-213772, A06, MF-A01).
- NCEER-88-0003 "Substructuring Techniques in the Time Domain for Primary-Secondary Structural Systems," by G.D. Manolis and G. Juhn, 2/10/88, (PB88-213780, A04, MF-A01).
- NCEER-88-0004 "Iterative Seismic Analysis of Primary-Secondary Systems," by A. Singhal, L.D. Lutes and P.D. Spanos, 2/23/88, (PB88-213798, A04, MF-A01).
- NCEER-88-0005 "Stochastic Finite Element Expansion for Random Media," by P.D. Spanos and R. Ghanem, 3/14/88, (PB88-213806, A03, MF-A01).

- NCEER-88-0006 "Combining Structural Optimization and Structural Control," by F.Y. Cheng and C.P. Pantelides, 1/10/88, (PB88-213814, A05, MF-A01).
- NCEER-88-0007 "Seismic Performance Assessment of Code-Designed Structures," by H.H-M. Hwang, J-W. Jaw and H-J. Shau, 3/20/88, (PB88-219423, A04, MF-A01). This report is only available through NTIS (see address given above).
- NCEER-88-0008 "Reliability Analysis of Code-Designed Structures Under Natural Hazards," by H.H-M. Hwang, H. Ushiba and M. Shinohara, 2/29/88, (PB88-229471, A07, MF-A01). This report is only available through NTIS (see address given above).
- NCEER-88-0009 "Seismic Fragility Analysis of Shear Wall Structures," by J-W Jaw and H.H-M. Hwang, 4/30/88, (PB89-102867, A04, MF-A01).
- NCEER-88-0010 "Base Isolation of a Multi-Story Building Under a Harmonic Ground Motion - A Comparison of Performances of Various Systems," by F-G Fan, G. Ahmadi and I.G. Tadjbakhsh, 5/18/88, (PB89-122238, A06, MF-A01). This report is only available through NTIS (see address given above).
- NCEER-88-0011 "Seismic Floor Response Spectra for a Combined System by Green's Functions," by F.M. Lavelle, L.A. Bergman and P.D. Spanos, 5/1/88, (PB89-102875, A03, MF-A01).
- NCEER-88-0012 "A New Solution Technique for Randomly Excited Hysteretic Structures," by G.Q. Cai and Y.K. Lin, 5/16/88, (PB89-102883, A03, MF-A01).
- NCEER-88-0013 "A Study of Radiation Damping and Soil-Structure Interaction Effects in the Centrifuge," by K. Weissman, supervised by J.H. Prevost, 5/24/88, (PB89-144703, A06, MF-A01).
- NCEER-88-0014 "Parameter Identification and Implementation of a Kinematic Plasticity Model for Frictional Soils," by J.H. Prevost and D.V. Griffiths, not available.
- NCEER-88-0015 "Two- and Three- Dimensional Dynamic Finite Element Analyses of the Long Valley Dam," by D.V. Griffiths and J.H. Prevost, 6/17/88, (PB89-144711, A04, MF-A01).
- NCEER-88-0016 "Damage Assessment of Reinforced Concrete Structures in Eastern United States," by A.M. Reinhorn, M.J. Seidel, S.K. Kunzath and Y.J. Park, 6/15/88, (PB89-122220, A04, MF-A01). This report is only available through NTIS (see address given above).
- NCEER-88-0017 "Dynamic Compliance of Vertically Loaded Strip Foundations in Multilayered Viscoelastic Soils," by S. Ahmad and A.S.M. Israil, 6/17/88, (PB89-102891, A04, MF-A01).
- NCEER-88-0018 "An Experimental Study of Seismic Structural Response With Added Viscoelastic Dampers," by R.C. Lin, Z. Liang, T.T. Soong and R.H. Zhang, 6/30/88, (PB89-122212, A05, MF-A01). This report is available only through NTIS (see address given above).
- NCEER-88-0019 "Experimental Investigation of Primary - Secondary System Interaction," by G.D. Manolis, G. Juhn and A.M. Reinhorn, 5/27/88, (PB89-122204, A04, MF-A01).
- NCEER-88-0020 "A Response Spectrum Approach For Analysis of Nonclassically Damped Structures," by J.N. Yang, S. Sarkani and F.X. Long, 4/22/88, (PB89-102909, A04, MF-A01).
- NCEER-88-0021 "Seismic Interaction of Structures and Soils: Stochastic Approach," by A.S. Veletsos and A.M. Prasad, 7/21/88, (PB89-122196, A04, MF-A01). This report is only available through NTIS (see address given above).
- NCEER-88-0022 "Identification of the Serviceability Limit State and Detection of Seismic Structural Damage," by E. DiPasquale and A.S. Cakmak, 6/15/88, (PB89-122188, A05, MF-A01). This report is available only through NTIS (see address given above).
- NCEER-88-0023 "Multi-Hazard Risk Analysis: Case of a Simple Offshore Structure," by B.K. Bhartia and E.H. Vanmarcke, 7/21/88, (PB89-145213, A05, MF-A01).

- NCEER-88-0024 "Automated Seismic Design of Reinforced Concrete Buildings," by Y.S. Chung, C. Meyer and M. Shinozuka, 7/5/88, (PB89-122170, A06, MF-A01). This report is available only through NTIS (see address given above).
- NCEER-88-0025 "Experimental Study of Active Control of MDOF Structures Under Seismic Excitations," by L.L. Chung, R.C. Lin, T.T. Soong and A.M. Reinhorn, 7/10/88, (PB89-122600, A04, MF-A01).
- NCEER-88-0026 "Earthquake Simulation Tests of a Low-Rise Metal Structure," by J.S. Hwang, K.C. Chang, G.C. Lee and R.L. Ketter, 8/1/88, (PB89-102917, A04, MF-A01).
- NCEER-88-0027 "Systems Study of Urban Response and Reconstruction Due to Catastrophic Earthquakes," by F. Kozin and H.K. Zhou, 9/22/88, (PB90-162348, A04, MF-A01).
- NCEER-88-0028 "Seismic Fragility Analysis of Plane Frame Structures," by H.H-M. Hwang and Y.K. Low, 7/31/88, (PB89-131445, A06, MF-A01).
- NCEER-88-0029 "Response Analysis of Stochastic Structures," by A. Kardara, C. Bucher and M. Shinozuka, 9/22/88, (PB89-174429, A04, MF-A01).
- NCEER-88-0030 "Nonnormal Accelerations Due to Yielding in a Primary Structure," by D.C.K. Chen and L.D. Lutes, 9/19/88, (PB89-131437, A04, MF-A01).
- NCEER-88-0031 "Design Approaches for Soil-Structure Interaction," by A.S. Veletsos, A.M. Prasad and Y. Tang, 12/30/88, (PB89-174437, A03, MF-A01). This report is available only through NTIS (see address given above).
- NCEER-88-0032 "A Re-evaluation of Design Spectra for Seismic Damage Control," by C.J. Turkstra and A.G. Tallin, 11/7/88, (PB89-145221, A05, MF-A01).
- NCEER-88-0033 "The Behavior and Design of Noncontact Lap Splices Subjected to Repeated Inelastic Tensile Loading," by V.E. Sagan, P. Gergely and R.N. White, 12/8/88, (PB89-163737, A08, MF-A01).
- NCEER-88-0034 "Seismic Response of Pile Foundations," by S.M. Mamoon, P.K. Banerjee and S. Ahmad, 11/1/88, (PB89-145239, A04, MF-A01).
- NCEER-88-0035 "Modeling of R/C Building Structures With Flexible Floor Diaphragms (IDARC2)," by A.M. Reinhorn, S.K. Kunath and N. Panahshahi, 9/7/88, (PB89-207153, A07, MF-A01).
- NCEER-88-0036 "Solution of the Dam-Reservoir Interaction Problem Using a Combination of FEM, BEM with Particular Integrals, Modal Analysis, and Substructuring," by C-S. Tsai, G.C. Lee and R.L. Ketter, 12/31/88, (PB89-207146, A04, MF-A01).
- NCEER-88-0037 "Optimal Placement of Actuators for Structural Control," by F.Y. Cheng and C.P. Pantelides, 8/15/88, (PB89-162846, A05, MF-A01).
- NCEER-88-0038 "Teflon Bearings in Aseismic Base Isolation: Experimental Studies and Mathematical Modeling," by A. Mokha, M.C. Constantinou and A.M. Reinhorn, 12/5/88, (PB89-218457, A10, MF-A01). This report is available only through NTIS (see address given above).
- NCEER-88-0039 "Seismic Behavior of Flat Slab High-Rise Buildings in the New York City Area," by P. Weidlinger and M. Ettouney, 10/15/88, (PB90-145681, A04, MF-A01).
- NCEER-88-0040 "Evaluation of the Earthquake Resistance of Existing Buildings in New York City," by P. Weidlinger and M. Ettouney, 10/15/88, not available.
- NCEER-88-0041 "Small-Scale Modeling Techniques for Reinforced Concrete Structures Subjected to Seismic Loads," by W. Kim, A. El-Attar and R.N. White, 11/22/88, (PB89-189625, A05, MF-A01).
- NCEER-88-0042 "Modeling Strong Ground Motion from Multiple Event Earthquakes," by G.W. Ellis and A.S. Cakmak, 10/15/88, (PB89-174445, A03, MF-A01).

- NCEER-88-0043 "Nonstationary Models of Seismic Ground Acceleration," by M. Grigoriu, S.E. Ruiz and E. Rosenblueth, 7/15/88, (PB89-189617, A04, MF-A01).
- NCEER-88-0044 "SARCF User's Guide: Seismic Analysis of Reinforced Concrete Frames," by Y.S. Chung, C. Meyer and M. Shinouzuka, 11/9/88, (PB89-174452, A08, MF-A01).
- NCEER-88-0045 "First Expert Panel Meeting on Disaster Research and Planning," edited by J. Pantelic and J. Stoyle, 9/15/88, (PB89-174460, A05, MF-A01).
- NCEER-88-0046 "Preliminary Studies of the Effect of Degrading Infill Walls on the Nonlinear Seismic Response of Steel Frames," by C.Z. Chrysostomou, P. Gergely and J.F. Abel, 12/19/88, (PB89-208383, A05, MF-A01).
- NCEER-88-0047 "Reinforced Concrete Frame Component Testing Facility - Design, Construction, Instrumentation and Operation," by S.P. Pessiki, C. Conley, T. Bond, P. Gergely and R.N. White, 12/16/88, (PB89-174478, A04, MF-A01).
- NCEER-89-0001 "Effects of Protective Cushion and Soil Compliancy on the Response of Equipment Within a Seismically Excited Building," by J.A. HoLung, 2/16/89, (PB89-207179, A04, MF-A01).
- NCEER-89-0002 "Statistical Evaluation of Response Modification Factors for Reinforced Concrete Structures," by H.H-M. Hwang and J-W. Jaw, 2/17/89, (PB89-207187, A05, MF-A01).
- NCEER-89-0003 "Hysteretic Columns Under Random Excitation," by G-Q. Cai and Y.K. Lin, 1/9/89, (PB89-196513, A03, MF-A01).
- NCEER-89-0004 "Experimental Study of 'Elephant Foot Bulge' Instability of Thin-Walled Metal Tanks," by Z-H. Jia and R.L. Ketter, 2/22/89, (PB89-207195, A03, MF-A01).
- NCEER-89-0005 "Experiment on Performance of Buried Pipelines Across San Andreas Fault," by J. Isenberg, E. Richardson and T.D. O'Rourke, 3/10/89, (PB89-218440, A04, MF-A01). This report is available only through NTIS (see address given above).
- NCEER-89-0006 "A Knowledge-Based Approach to Structural Design of Earthquake-Resistant Buildings," by M. Subramani, P. Gergely, C.H. Conley, J.F. Abel and A.H. Zaghw, 1/15/89, (PB89-218465, A06, MF-A01).
- NCEER-89-0007 "Liquefaction Hazards and Their Effects on Buried Pipelines," by T.D. O'Rourke and P.A. Lane, 2/1/89, (PB89-218481, A09, MF-A01).
- NCEER-89-0008 "Fundamentals of System Identification in Structural Dynamics," by H. Imai, C-B. Yun, O. Maruyama and M. Shinouzuka, 1/26/89, (PB89-207211, A04, MF-A01).
- NCEER-89-0009 "Effects of the 1985 Michoacan Earthquake on Water Systems and Other Buried Lifelines in Mexico," by A.G. Ayala and M.J. O'Rourke, 3/8/89, (PB89-207229, A06, MF-A01).
- NCEER-89-R010 "NCEER Bibliography of Earthquake Education Materials," by K.E.K. Ross, Second Revision, 9/1/89, (PB90-125352, A05, MF-A01). This report is replaced by NCEER-92-0018.
- NCEER-89-0011 "Inelastic Three-Dimensional Response Analysis of Reinforced Concrete Building Structures (IDARC-3D), Part I - Modeling," by S.K. Kunnath and A.M. Reinhorn, 4/17/89, (PB90-114612, A07, MF-A01). This report is available only through NTIS (see address given above).
- NCEER-89-0012 "Recommended Modifications to ATC-14," by C.D. Poland and J.O. Malley, 4/12/89, (PB90-108648, A15, MF-A01).
- NCEER-89-0013 "Repair and Strengthening of Beam-to-Column Connections Subjected to Earthquake Loading," by M. Corazao and A.J. Durrani, 2/28/89, (PB90-109885, A06, MF-A01).
- NCEER-89-0014 "Program EXKAL2 for Identification of Structural Dynamic Systems," by O. Maruyama, C-B. Yun, M. Hoshiya and M. Shinouzuka, 5/19/89, (PB90-109877, A09, MF-A01).

- NCEER-89-0015 "Response of Frames With Bolted Semi-Rigid Connections, Part I - Experimental Study and Analytical Predictions," by P.J. DiCorso, A.M. Reinhorn, J.R. Dickerson, J.B. Radziminski and W.L. Harper, 6/1/89, not available.
- NCEER-89-0016 "ARMA Monte Carlo Simulation in Probabilistic Structural Analysis," by P.D. Spanos and M.P. Mignolet, 7/10/89, (PB90-109893, A03, MF-A01).
- NCEER-89-P017 "Preliminary Proceedings from the Conference on Disaster Preparedness - The Place of Earthquake Education in Our Schools," Edited by K.E.K. Ross, 6/23/89, (PB90-108606, A03, MF-A01).
- NCEER-89-0017 "Proceedings from the Conference on Disaster Preparedness - The Place of Earthquake Education in Our Schools," Edited by K.E.K. Ross, 12/31/89, (PB90-207895, A012, MF-A02). This report is available only through NTIS (see address given above).
- NCEER-89-0018 "Multidimensional Models of Hysteretic Material Behavior for Vibration Analysis of Shape Memory Energy Absorbing Devices, by E.J. Graesser and F.A. Cozzarelli, 6/7/89, (PB90-164146, A04, MF-A01).
- NCEER-89-0019 "Nonlinear Dynamic Analysis of Three-Dimensional Base Isolated Structures (3D-BASIS)," by S. Nagarajaiah, A.M. Reinhorn and M.C. Constantinou, 8/3/89, (PB90-161936, A06, MF-A01). This report has been replaced by NCEER-93-0011.
- NCEER-89-0020 "Structural Control Considering Time-Rate of Control Forces and Control Rate Constraints," by F.Y. Cheng and C.P. Pantelides, 8/3/89, (PB90-120445, A04, MF-A01).
- NCEER-89-0021 "Subsurface Conditions of Memphis and Shelby County," by K.W. Ng, T-S. Chang and H-H.M. Hwang, 7/26/89, (PB90-120437, A03, MF-A01).
- NCEER-89-0022 "Seismic Wave Propagation Effects on Straight Jointed Buried Pipelines," by K. Elhmadi and M.J. O'Rourke, 8/24/89, (PB90-162322, A10, MF-A02).
- NCEER-89-0023 "Workshop on Serviceability Analysis of Water Delivery Systems," edited by M. Grigoriu, 3/6/89, (PB90-127424, A03, MF-A01).
- NCEER-89-0024 "Shaking Table Study of a 1/5 Scale Steel Frame Composed of Tapered Members," by K.C. Chang, J.S. Hwang and G.C. Lee, 9/18/89, (PB90-160169, A04, MF-A01).
- NCEER-89-0025 "DYNA1D: A Computer Program for Nonlinear Seismic Site Response Analysis - Technical Documentation," by Jean H. Prevost, 9/14/89, (PB90-161944, A07, MF-A01). This report is available only through NTIS (see address given above).
- NCEER-89-0026 "1:4 Scale Model Studies of Active Tendon Systems and Active Mass Dampers for Aseismic Protection," by A.M. Reinhorn, T.T. Soong, R.C. Lin, Y.P. Yang, Y. Fukao, H. Abe and M. Nakai, 9/15/89, (PB90-173246, A10, MF-A02). This report is available only through NTIS (see address given above).
- NCEER-89-0027 "Scattering of Waves by Inclusions in a Nonhomogeneous Elastic Half Space Solved by Boundary Element Methods," by P.K. Hadley, A. Askar and A.S. Cakmak, 6/15/89, (PB90-145699, A07, MF-A01).
- NCEER-89-0028 "Statistical Evaluation of Deflection Amplification Factors for Reinforced Concrete Structures," by H.H.M. Hwang, J-W. Jaw and A.L. Ch'ng, 8/31/89, (PB90-164633, A05, MF-A01).
- NCEER-89-0029 "Bedrock Accelerations in Memphis Area Due to Large New Madrid Earthquakes," by H.H.M. Hwang, C.H.S. Chen and G. Yu, 11/7/89, (PB90-162330, A04, MF-A01).
- NCEER-89-0030 "Seismic Behavior and Response Sensitivity of Secondary Structural Systems," by Y.Q. Chen and T.T. Soong, 10/23/89, (PB90-164658, A08, MF-A01).
- NCEER-89-0031 "Random Vibration and Reliability Analysis of Primary-Secondary Structural Systems," by Y. Ibrahim, M. Grigoriu and T.T. Soong, 11/10/89, (PB90-161951, A04, MF-A01).

- NCEER-89-0032 "Proceedings from the Second U.S. - Japan Workshop on Liquefaction, Large Ground Deformation and Their Effects on Lifelines, September 26-29, 1989," Edited by T.D. O'Rourke and M. Hamada, 12/1/89, (PB90-209388, A22, MF-A03).
- NCEER-89-0033 "Deterministic Model for Seismic Damage Evaluation of Reinforced Concrete Structures," by J.M. Bracci, A.M. Reinhorn, J.B. Mander and S.K. Kunnath, 9/27/89, (PB91-108803, A06, MF-A01).
- NCEER-89-0034 "On the Relation Between Local and Global Damage Indices," by E. DiPasquale and A.S. Cakmak, 8/15/89, (PB90-173865, A05, MF-A01).
- NCEER-89-0035 "Cyclic Undrained Behavior of Nonplastic and Low Plasticity Silts," by A.J. Walker and H.E. Stewart, 7/26/89, (PB90-183518, A10, MF-A01).
- NCEER-89-0036 "Liquefaction Potential of Surficial Deposits in the City of Buffalo, New York," by M. Budhu, R. Giese and L. Baumgrass, 1/17/89, (PB90-208455, A04, MF-A01).
- NCEER-89-0037 "A Deterministic Assessment of Effects of Ground Motion Incoherence," by A.S. Veletsos and Y. Tang, 7/15/89, (PB90-164294, A03, MF-A01).
- NCEER-89-0038 "Workshop on Ground Motion Parameters for Seismic Hazard Mapping," July 17-18, 1989, edited by R.V. Whitman, 12/1/89, (PB90-173923, A04, MF-A01).
- NCEER-89-0039 "Seismic Effects on Elevated Transit Lines of the New York City Transit Authority," by C.J. Costantino, C.A. Miller and E. Heymsfield, 12/26/89, (PB90-207887, A06, MF-A01).
- NCEER-89-0040 "Centrifugal Modeling of Dynamic Soil-Structure Interaction," by K. Weissman, Supervised by J.H. Prevost, 5/10/89, (PB90-207879, A07, MF-A01).
- NCEER-89-0041 "Linearized Identification of Buildings With Cores for Seismic Vulnerability Assessment," by I-K. Ho and A.E. Aktan, 11/1/89, (PB90-251943, A07, MF-A01).
- NCEER-90-0001 "Geotechnical and Lifeline Aspects of the October 17, 1989 Loma Prieta Earthquake in San Francisco," by T.D. O'Rourke, H.E. Stewart, F.T. Blackburn and T.S. Dickerman, 1/90, (PB90-208596, A05, MF-A01).
- NCEER-90-0002 "Nonnormal Secondary Response Due to Yielding in a Primary Structure," by D.C.K. Chen and L.D. Lutes, 2/28/90, (PB90-251976, A07, MF-A01).
- NCEER-90-0003 "Earthquake Education Materials for Grades K-12," by K.E.K. Ross, 4/16/90, (PB91-251984, A05, MF-A05). This report has been replaced by NCEER-92-0018.
- NCEER-90-0004 "Catalog of Strong Motion Stations in Eastern North America," by R.W. Busby, 4/3/90, (PB90-251984, A05, MF-A01).
- NCEER-90-0005 "NCEER Strong-Motion Data Base: A User Manual for the GeoBase Release (Version 1.0 for the Sun3)," by P. Friberg and K. Jacob, 3/31/90 (PB90-258062, A04, MF-A01).
- NCEER-90-0006 "Seismic Hazard Along a Crude Oil Pipeline in the Event of an 1811-1812 Type New Madrid Earthquake," by H.H.M. Hwang and C-H.S. Chen, 4/16/90, (PB90-258054, A04, MF-A01).
- NCEER-90-0007 "Site-Specific Response Spectra for Memphis Sheahan Pumping Station," by H.H.M. Hwang and C.S. Lee, 5/15/90, (PB91-108811, A05, MF-A01).
- NCEER-90-0008 "Pilot Study on Seismic Vulnerability of Crude Oil Transmission Systems," by T. Ariman, R. Dobry, M. Grigoriu, F. Kozin, M. O'Rourke, T. O'Rourke and M. Shinozuka, 5/25/90, (PB91-108837, A06, MF-A01).
- NCEER-90-0009 "A Program to Generate Site Dependent Time Histories: EQGEN," by G.W. Ellis, M. Srinivasan and A.S. Cakmak, 1/30/90, (PB91-108829, A04, MF-A01).
- NCEER-90-0010 "Active Isolation for Seismic Protection of Operating Rooms," by M.E. Talbott, Supervised by M. Shinozuka, 6/8/9, (PB91-110205, A05, MF-A01).

- NCEER-90-0011 "Program LINEARID for Identification of Linear Structural Dynamic Systems," by C-B. Yun and M. Shinozuka, 6/25/90, (PB91-110312, A08, MF-A01).
- NCEER-90-0012 "Two-Dimensional Two-Phase Elasto-Plastic Seismic Response of Earth Dams," by A.N. Yiagos, Supervised by J.H. Prevost, 6/20/90, (PB91-110197, A13, MF-A02).
- NCEER-90-0013 "Secondary Systems in Base-Isolated Structures: Experimental Investigation, Stochastic Response and Stochastic Sensitivity," by G.D. Manolis, G. Juhn, M.C. Constantinou and A.M. Reinhorn, 7/1/90, (PB91-110320, A08, MF-A01).
- NCEER-90-0014 "Seismic Behavior of Lightly-Reinforced Concrete Column and Beam-Column Joint Details," by S.P. Pessiki, C.H. Conley, P. Gergely and R.N. White, 8/22/90, (PB91-108795, A11, MF-A02).
- NCEER-90-0015 "Two Hybrid Control Systems for Building Structures Under Strong Earthquakes," by J.N. Yang and A. Danielians, 6/29/90, (PB91-125393, A04, MF-A01).
- NCEER-90-0016 "Instantaneous Optimal Control with Acceleration and Velocity Feedback," by J.N. Yang and Z. Li, 6/29/90, (PB91-125401, A03, MF-A01).
- NCEER-90-0017 "Reconnaissance Report on the Northern Iran Earthquake of June 21, 1990," by M. Mehrain, 10/4/90, (PB91-125377, A03, MF-A01).
- NCEER-90-0018 "Evaluation of Liquefaction Potential in Memphis and Shelby County," by T.S. Chang, P.S. Tang, C.S. Lee and H. Hwang, 8/10/90, (PB91-125427, A09, MF-A01).
- NCEER-90-0019 "Experimental and Analytical Study of a Combined Sliding Disc Bearing and Helical Steel Spring Isolation System," by M.C. Constantinou, A.S. Mokha and A.M. Reinhorn, 10/4/90, (PB91-125385, A06, MF-A01). This report is available only through NTIS (see address given above).
- NCEER-90-0020 "Experimental Study and Analytical Prediction of Earthquake Response of a Sliding Isolation System with a Spherical Surface," by A.S. Mokha, M.C. Constantinou and A.M. Reinhorn, 10/11/90, (PB91-125419, A05, MF-A01).
- NCEER-90-0021 "Dynamic Interaction Factors for Floating Pile Groups," by G. Gazetas, K. Fan, A. Kaynia and E. Kausel, 9/10/90, (PB91-170381, A05, MF-A01).
- NCEER-90-0022 "Evaluation of Seismic Damage Indices for Reinforced Concrete Structures," by S. Rodriguez-Gomez and A.S. Cakmak, 9/30/90, PB91-171322, A06, MF-A01).
- NCEER-90-0023 "Study of Site Response at a Selected Memphis Site," by H. Desai, S. Ahmad, E.S. Gazetas and M.R. Oh, 10/11/90, (PB91-196857, A03, MF-A01).
- NCEER-90-0024 "A User's Guide to Strongmo: Version 1.0 of NCEER's Strong-Motion Data Access Tool for PCs and Terminals," by P.A. Friberg and C.A.T. Susch, 11/15/90, (PB91-171272, A03, MF-A01).
- NCEER-90-0025 "A Three-Dimensional Analytical Study of Spatial Variability of Seismic Ground Motions," by L-L. Hong and A.H.-S. Ang, 10/30/90, (PB91-170399, A09, MF-A01).
- NCEER-90-0026 "MUMOID User's Guide - A Program for the Identification of Modal Parameters," by S. Rodriguez-Gomez and E. DiPasquale, 9/30/90, (PB91-171298, A04, MF-A01).
- NCEER-90-0027 "SARCF-II User's Guide - Seismic Analysis of Reinforced Concrete Frames," by S. Rodriguez-Gomez, Y.S. Chung and C. Meyer, 9/30/90, (PB91-171280, A05, MF-A01).
- NCEER-90-0028 "Viscous Dampers: Testing, Modeling and Application in Vibration and Seismic Isolation," by N. Makris and M.C. Constantinou, 12/20/90 (PB91-190561, A06, MF-A01).
- NCEER-90-0029 "Soil Effects on Earthquake Ground Motions in the Memphis Area," by H. Hwang, C.S. Lee, K.W. Ng and T.S. Chang, 8/2/90, (PB91-190751, A05, MF-A01).

- NCEER-91-0001 "Proceedings from the Third Japan-U.S. Workshop on Earthquake Resistant Design of Lifeline Facilities and Countermeasures for Soil Liquefaction, December 17-19, 1990," edited by T.D. O'Rourke and M. Hamada, 2/1/91, (PB91-179259, A99, MF-A04).
- NCEER-91-0002 "Physical Space Solutions of Non-Proportionally Damped Systems," by M. Tong, Z. Liang and G.C. Lee, 1/15/91, (PB91-179242, A04, MF-A01).
- NCEER-91-0003 "Seismic Response of Single Piles and Pile Groups," by K. Fan and G. Gazetas, 1/10/91, (PB92-174994, A04, MF-A01).
- NCEER-91-0004 "Damping of Structures: Part 1 - Theory of Complex Damping," by Z. Liang and G. Lee, 10/10/91, (PB92-197235, A12, MF-A03).
- NCEER-91-0005 "3D-BASIS - Nonlinear Dynamic Analysis of Three Dimensional Base Isolated Structures: Part II," by S. Nagarajaiah, A.M. Reinhorn and M.C. Constantinou, 2/28/91, (PB91-190553, A07, MF-A01). This report has been replaced by NCEER-93-0011.
- NCEER-91-0006 "A Multidimensional Hysteretic Model for Plasticity Deforming Metals in Energy Absorbing Devices," by E.J. Graesser and F.A. Cozzarelli, 4/9/91, (PB92-108364, A04, MF-A01).
- NCEER-91-0007 "A Framework for Customizable Knowledge-Based Expert Systems with an Application to a KBES for Evaluating the Seismic Resistance of Existing Buildings," by E.G. Ibarra-Anaya and S.J. Fenves, 4/9/91, (PB91-210930, A08, MF-A01).
- NCEER-91-0008 "Nonlinear Analysis of Steel Frames with Semi-Rigid Connections Using the Capacity Spectrum Method," by G.G. Deierlein, S-H. Hsieh, Y-J. Shen and J.F. Abel, 7/2/91, (PB92-113828, A05, MF-A01).
- NCEER-91-0009 "Earthquake Education Materials for Grades K-12," by K.E.K. Ross, 4/30/91, (PB91-212142, A06, MF-A01). This report has been replaced by NCEER-92-0018.
- NCEER-91-0010 "Phase Wave Velocities and Displacement Phase Differences in a Harmonically Oscillating Pile," by N. Makris and G. Gazetas, 7/8/91, (PB92-108356, A04, MF-A01).
- NCEER-91-0011 "Dynamic Characteristics of a Full-Size Five-Story Steel Structure and a 2/5 Scale Model," by K.C. Chang, G.C. Yao, G.C. Lee, D.S. Hao and Y.C. Yeh, 7/2/91, (PB93-116648, A06, MF-A02).
- NCEER-91-0012 "Seismic Response of a 2/5 Scale Steel Structure with Added Viscoelastic Dampers," by K.C. Chang, T.T. Soong, S-T. Oh and M.L. Lai, 5/17/91, (PB92-110816, A05, MF-A01).
- NCEER-91-0013 "Earthquake Response of Retaining Walls; Full-Scale Testing and Computational Modeling," by S. Alampalli and A-W.M. Elgamal, 6/20/91, not available.
- NCEER-91-0014 "3D-BASIS-M: Nonlinear Dynamic Analysis of Multiple Building Base Isolated Structures," by P.C. Tsopelas, S. Nagarajaiah, M.C. Constantinou and A.M. Reinhorn, 5/28/91, (PB92-113885, A09, MF-A02).
- NCEER-91-0015 "Evaluation of SEAOC Design Requirements for Sliding Isolated Structures," by D. Theodossiou and M.C. Constantinou, 6/10/91, (PB92-114602, A11, MF-A03).
- NCEER-91-0016 "Closed-Loop Modal Testing of a 27-Story Reinforced Concrete Flat Plate-Core Building," by H.R. Somaprasad, T. Toksoy, H. Yoshiyuki and A.E. Aktan, 7/15/91, (PB92-129980, A07, MF-A02).
- NCEER-91-0017 "Shake Table Test of a 1/6 Scale Two-Story Lightly Reinforced Concrete Building," by A.G. El-Attar, R.N. White and P. Gergely, 2/28/91, (PB92-222447, A06, MF-A02).
- NCEER-91-0018 "Shake Table Test of a 1/8 Scale Three-Story Lightly Reinforced Concrete Building," by A.G. El-Attar, R.N. White and P. Gergely, 2/28/91, (PB93-116630, A08, MF-A02).
- NCEER-91-0019 "Transfer Functions for Rigid Rectangular Foundations," by A.S. Veletsos, A.M. Prasad and W.H. Wu, 7/31/91, not available.

- NCEER-91-0020 "Hybrid Control of Seismic-Excited Nonlinear and Inelastic Structural Systems," by J.N. Yang, Z. Li and A. Danielians, 8/1/91, (PB92-143171, A06, MF-A02).
- NCEER-91-0021 "The NCEER-91 Earthquake Catalog: Improved Intensity-Based Magnitudes and Recurrence Relations for U.S. Earthquakes East of New Madrid," by L. Seeber and J.G. Armbruster, 8/28/91, (PB92-176742, A06, MF-A02).
- NCEER-91-0022 "Proceedings from the Implementation of Earthquake Planning and Education in Schools: The Need for Change - The Roles of the Changemakers," by K.E.K. Ross and F. Winslow, 7/23/91, (PB92-129998, A12, MF-A03).
- NCEER-91-0023 "A Study of Reliability-Based Criteria for Seismic Design of Reinforced Concrete Frame Buildings," by H.H.M. Hwang and H-M. Hsu, 8/10/91, (PB92-140235, A09, MF-A02).
- NCEER-91-0024 "Experimental Verification of a Number of Structural System Identification Algorithms," by R.G. Ghanem, H. Gavin and M. Shinozuka, 9/18/91, (PB92-176577, A18, MF-A04).
- NCEER-91-0025 "Probabilistic Evaluation of Liquefaction Potential," by H.H.M. Hwang and C.S. Lee," 11/25/91, (PB92-143429, A05, MF-A01).
- NCEER-91-0026 "Instantaneous Optimal Control for Linear, Nonlinear and Hysteretic Structures - Stable Controllers," by J.N. Yang and Z. Li, 11/15/91, (PB92-163807, A04, MF-A01).
- NCEER-91-0027 "Experimental and Theoretical Study of a Sliding Isolation System for Bridges," by M.C. Constantinou, A. Kartoum, A.M. Reinhorn and P. Bradford, 11/15/91, (PB92-176973, A10, MF-A03).
- NCEER-92-0001 "Case Studies of Liquefaction and Lifeline Performance During Past Earthquakes, Volume 1: Japanese Case Studies," Edited by M. Hamada and T. O'Rourke, 2/17/92, (PB92-197243, A18, MF-A04).
- NCEER-92-0002 "Case Studies of Liquefaction and Lifeline Performance During Past Earthquakes, Volume 2: United States Case Studies," Edited by T. O'Rourke and M. Hamada, 2/17/92, (PB92-197250, A20, MF-A04).
- NCEER-92-0003 "Issues in Earthquake Education," Edited by K. Ross, 2/3/92, (PB92-222389, A07, MF-A02).
- NCEER-92-0004 "Proceedings from the First U.S. - Japan Workshop on Earthquake Protective Systems for Bridges," Edited by I.G. Buckle, 2/4/92, (PB94-142239, A99, MF-A06).
- NCEER-92-0005 "Seismic Ground Motion from a Haskell-Type Source in a Multiple-Layered Half-Space," A.P. Theoharis, G. Deodatis and M. Shinozuka, 1/2/92, not available.
- NCEER-92-0006 "Proceedings from the Site Effects Workshop," Edited by R. Whitman, 2/29/92, (PB92-197201, A04, MF-A01).
- NCEER-92-0007 "Engineering Evaluation of Permanent Ground Deformations Due to Seismically-Induced Liquefaction," by M.H. Baziar, R. Dobry and A-W.M. Elgamal, 3/24/92, (PB92-222421, A13, MF-A03).
- NCEER-92-0008 "A Procedure for the Seismic Evaluation of Buildings in the Central and Eastern United States," by C.D. Poland and J.O. Malley, 4/2/92, (PB92-222439, A20, MF-A04).
- NCEER-92-0009 "Experimental and Analytical Study of a Hybrid Isolation System Using Friction Controllable Sliding Bearings," by M.Q. Feng, S. Fujii and M. Shinozuka, 5/15/92, (PB93-150282, A06, MF-A02).
- NCEER-92-0010 "Seismic Resistance of Slab-Column Connections in Existing Non-Ductile Flat-Plate Buildings," by A.J. Durrani and Y. Du, 5/18/92, (PB93-116812, A06, MF-A02).
- NCEER-92-0011 "The Hysteretic and Dynamic Behavior of Brick Masonry Walls Upgraded by Ferrocement Coatings Under Cyclic Loading and Strong Simulated Ground Motion," by H. Lee and S.P. Prawel, 5/11/92, not available.
- NCEER-92-0012 "Study of Wire Rope Systems for Seismic Protection of Equipment in Buildings," by G.F. Demetriades, M.C. Constantinou and A.M. Reinhorn, 5/20/92, (PB93-116655, A08, MF-A02).

- NCEER-92-0013 "Shape Memory Structural Dampers: Material Properties, Design and Seismic Testing," by P.R. Witting and F.A. Cozzarelli, 5/26/92, (PB93-116663, A05, MF-A01).
- NCEER-92-0014 "Longitudinal Permanent Ground Deformation Effects on Buried Continuous Pipelines," by M.J. O'Rourke, and C. Nordberg, 6/15/92, (PB93-116671, A08, MF-A02).
- NCEER-92-0015 "A Simulation Method for Stationary Gaussian Random Functions Based on the Sampling Theorem," by M. Grigoriu and S. Balopoulou, 6/11/92, (PB93-127496, A05, MF-A01).
- NCEER-92-0016 "Gravity-Load-Designed Reinforced Concrete Buildings: Seismic Evaluation of Existing Construction and Detailing Strategies for Improved Seismic Resistance," by G.W. Hoffmann, S.K. Kunnath, A.M. Reinhorn and J.B. Mander, 7/15/92, (PB94-142007, A08, MF-A02).
- NCEER-92-0017 "Observations on Water System and Pipeline Performance in the Limón Area of Costa Rica Due to the April 22, 1991 Earthquake," by M. O'Rourke and D. Ballantyne, 6/30/92, (PB93-126811, A06, MF-A02).
- NCEER-92-0018 "Fourth Edition of Earthquake Education Materials for Grades K-12," Edited by K.E.K. Ross, 8/10/92, (PB93-114023, A07, MF-A02).
- NCEER-92-0019 "Proceedings from the Fourth Japan-U.S. Workshop on Earthquake Resistant Design of Lifeline Facilities and Countermeasures for Soil Liquefaction," Edited by M. Hamada and T.D. O'Rourke, 8/12/92, (PB93-163939, A99, MF-E11).
- NCEER-92-0020 "Active Bracing System: A Full Scale Implementation of Active Control," by A.M. Reinhorn, T.T. Soong, R.C. Lin, M.A. Riley, Y.P. Wang, S. Aizawa and M. Higashino, 8/14/92, (PB93-127512, A06, MF-A02).
- NCEER-92-0021 "Empirical Analysis of Horizontal Ground Displacement Generated by Liquefaction-Induced Lateral Spreads," by S.F. Bartlett and T.L. Youd, 8/17/92, (PB93-188241, A06, MF-A02).
- NCEER-92-0022 "IDARC Version 3.0: Inelastic Damage Analysis of Reinforced Concrete Structures," by S.K. Kunnath, A.M. Reinhorn and R.F. Lobo, 8/31/92, (PB93-227502, A07, MF-A02).
- NCEER-92-0023 "A Semi-Empirical Analysis of Strong-Motion Peaks in Terms of Seismic Source, Propagation Path and Local Site Conditions, by M. Kamiyama, M.J. O'Rourke and R. Flores-Berrones, 9/9/92, (PB93-150266, A08, MF-A02).
- NCEER-92-0024 "Seismic Behavior of Reinforced Concrete Frame Structures with Nonductile Details, Part I: Summary of Experimental Findings of Full Scale Beam-Column Joint Tests," by A. Beres, R.N. White and P. Gergely, 9/30/92, (PB93-227783, A05, MF-A01).
- NCEER-92-0025 "Experimental Results of Repaired and Retrofitted Beam-Column Joint Tests in Lightly Reinforced Concrete Frame Buildings," by A. Beres, S. El-Borgi, R.N. White and P. Gergely, 10/29/92, (PB93-227791, A05, MF-A01).
- NCEER-92-0026 "A Generalization of Optimal Control Theory: Linear and Nonlinear Structures," by J.N. Yang, Z. Li and S. Vongchavalitkul, 11/2/92, (PB93-188621, A05, MF-A01).
- NCEER-92-0027 "Seismic Resistance of Reinforced Concrete Frame Structures Designed Only for Gravity Loads: Part I - Design and Properties of a One-Third Scale Model Structure," by J.M. Bracci, A.M. Reinhorn and J.B. Mander, 12/1/92, (PB94-104502, A08, MF-A02).
- NCEER-92-0028 "Seismic Resistance of Reinforced Concrete Frame Structures Designed Only for Gravity Loads: Part II - Experimental Performance of Subassemblages," by L.E. Aycardi, J.B. Mander and A.M. Reinhorn, 12/1/92, (PB94-104510, A08, MF-A02).
- NCEER-92-0029 "Seismic Resistance of Reinforced Concrete Frame Structures Designed Only for Gravity Loads: Part III - Experimental Performance and Analytical Study of a Structural Model," by J.M. Bracci, A.M. Reinhorn and J.B. Mander, 12/1/92, (PB93-227528, A09, MF-A01).

- NCEER-92-0030 "Evaluation of Seismic Retrofit of Reinforced Concrete Frame Structures: Part I - Experimental Performance of Retrofitted Subassemblages," by D. Choudhuri, J.B. Mander and A.M. Reinhorn, 12/8/92, (PB93-198307, A07, MF-A02).
- NCEER-92-0031 "Evaluation of Seismic Retrofit of Reinforced Concrete Frame Structures: Part II - Experimental Performance and Analytical Study of a Retrofitted Structural Model," by J.M. Bracci, A.M. Reinhorn and J.B. Mander, 12/8/92, (PB93-198315, A09, MF-A03).
- NCEER-92-0032 "Experimental and Analytical Investigation of Seismic Response of Structures with Supplemental Fluid Viscous Dampers," by M.C. Constantinou and M.D. Symans, 12/21/92, (PB93-191435, A10, MF-A03). This report is available only through NTIS (see address given above).
- NCEER-92-0033 "Reconnaissance Report on the Cairo, Egypt Earthquake of October 12, 1992," by M. Khater, 12/23/92, (PB93-188621, A03, MF-A01).
- NCEER-92-0034 "Low-Level Dynamic Characteristics of Four Tall Flat-Plate Buildings in New York City," by H. Gavin, S. Yuan, J. Grossman, E. Pekelis and K. Jacob, 12/28/92, (PB93-188217, A07, MF-A02).
- NCEER-93-0001 "An Experimental Study on the Seismic Performance of Brick-Infilled Steel Frames With and Without Retrofit," by J.B. Mander, B. Nair, K. Wojtkowski and J. Ma, 1/29/93, (PB93-227510, A07, MF-A02).
- NCEER-93-0002 "Social Accounting for Disaster Preparedness and Recovery Planning," by S. Cole, E. Pantoja and V. Razak, 2/22/93, (PB94-142114, A12, MF-A03).
- NCEER-93-0003 "Assessment of 1991 NEHRP Provisions for Nonstructural Components and Recommended Revisions," by T.T. Soong, G. Chen, Z. Wu, R-H. Zhang and M. Grigoriu, 3/1/93, (PB93-188639, A06, MF-A02).
- NCEER-93-0004 "Evaluation of Static and Response Spectrum Analysis Procedures of SEAOC/UBC for Seismic Isolated Structures," by C.W. Winters and M.C. Constantinou, 3/23/93, (PB93-198299, A10, MF-A03).
- NCEER-93-0005 "Earthquakes in the Northeast - Are We Ignoring the Hazard? A Workshop on Earthquake Science and Safety for Educators," edited by K.E.K. Ross, 4/2/93, (PB94-103066, A09, MF-A02).
- NCEER-93-0006 "Inelastic Response of Reinforced Concrete Structures with Viscoelastic Braces," by R.F. Lobo, J.M. Bracci, K.L. Shen, A.M. Reinhorn and T.T. Soong, 4/5/93, (PB93-227486, A05, MF-A02).
- NCEER-93-0007 "Seismic Testing of Installation Methods for Computers and Data Processing Equipment," by K. Kosar, T.T. Soong, K.L. Shen, J.A. HoLung and Y.K. Lin, 4/12/93, (PB93-198299, A07, MF-A02).
- NCEER-93-0008 "Retrofit of Reinforced Concrete Frames Using Added Dampers," by A. Reinhorn, M. Constantinou and C. Li, not available.
- NCEER-93-0009 "Seismic Behavior and Design Guidelines for Steel Frame Structures with Added Viscoelastic Dampers," by K.C. Chang, M.L. Lai, T.T. Soong, D.S. Hao and Y.C. Yeh, 5/1/93, (PB94-141959, A07, MF-A02).
- NCEER-93-0010 "Seismic Performance of Shear-Critical Reinforced Concrete Bridge Piers," by J.B. Mander, S.M. Waheed, M.T.A. Chaudhary and S.S. Chen, 5/12/93, (PB93-227494, A08, MF-A02).
- NCEER-93-0011 "3D-BASIS-TABS: Computer Program for Nonlinear Dynamic Analysis of Three Dimensional Base Isolated Structures," by S. Nagarajaiah, C. Li, A.M. Reinhorn and M.C. Constantinou, 8/2/93, (PB94-141819, A09, MF-A02).
- NCEER-93-0012 "Effects of Hydrocarbon Spills from an Oil Pipeline Break on Ground Water," by O.J. Helweg and H.H.M. Hwang, 8/3/93, (PB94-141942, A06, MF-A02).
- NCEER-93-0013 "Simplified Procedures for Seismic Design of Nonstructural Components and Assessment of Current Code Provisions," by M.P. Singh, L.E. Suarez, E.E. Matheu and G.O. Maldonado, 8/4/93, (PB94-141827, A09, MF-A02).
- NCEER-93-0014 "An Energy Approach to Seismic Analysis and Design of Secondary Systems," by G. Chen and T.T. Soong, 8/6/93, (PB94-142767, A11, MF-A03).

- NCEER-93-0015 "Proceedings from School Sites: Becoming Prepared for Earthquakes - Commemorating the Third Anniversary of the Loma Prieta Earthquake," Edited by F.E. Winslow and K.E.K. Ross, 8/16/93, (PB94-154275, A16, MF-A02).
- NCEER-93-0016 "Reconnaissance Report of Damage to Historic Monuments in Cairo, Egypt Following the October 12, 1992 Dahshur Earthquake," by D. Sykora, D. Look, G. Croci, E. Karaesmen and E. Karaesmen, 8/19/93, (PB94-142221, A08, MF-A02).
- NCEER-93-0017 "The Island of Guam Earthquake of August 8, 1993," by S.W. Swan and S.K. Harris, 9/30/93, (PB94-141843, A04, MF-A01).
- NCEER-93-0018 "Engineering Aspects of the October 12, 1992 Egyptian Earthquake," by A.W. Elgamal, M. Amer, K. Adalier and A. Abul-Fadl, 10/7/93, (PB94-141983, A05, MF-A01).
- NCEER-93-0019 "Development of an Earthquake Motion Simulator and its Application in Dynamic Centrifuge Testing," by I. Krstelj, Supervised by J.H. Prevost, 10/23/93, (PB94-181773, A-10, MF-A03).
- NCEER-93-0020 "NCEER-Taisei Corporation Research Program on Sliding Seismic Isolation Systems for Bridges: Experimental and Analytical Study of a Friction Pendulum System (FPS)," by M.C. Constantinou, P. Tsopelas, Y-S. Kim and S. Okamoto, 11/1/93, (PB94-142775, A08, MF-A02).
- NCEER-93-0021 "Finite Element Modeling of Elastomeric Seismic Isolation Bearings," by L.J. Billings, Supervised by R. Shepherd, 11/8/93, not available.
- NCEER-93-0022 "Seismic Vulnerability of Equipment in Critical Facilities: Life-Safety and Operational Consequences," by K. Porter, G.S. Johnson, M.M. Zadeh, C. Scawthorn and S. Eder, 11/24/93, (PB94-181765, A16, MF-A03).
- NCEER-93-0023 "Hokkaido Nansei-oki, Japan Earthquake of July 12, 1993, by P.I. Yanev and C.R. Scawthorn, 12/23/93, (PB94-181500, A07, MF-A01).
- NCEER-94-0001 "An Evaluation of Seismic Serviceability of Water Supply Networks with Application to the San Francisco Auxiliary Water Supply System," by I. Markov, Supervised by M. Grigoriu and T. O'Rourke, 1/21/94, (PB94-204013, A07, MF-A02).
- NCEER-94-0002 "NCEER-Taisei Corporation Research Program on Sliding Seismic Isolation Systems for Bridges: Experimental and Analytical Study of Systems Consisting of Sliding Bearings, Rubber Restoring Force Devices and Fluid Dampers," Volumes I and II, by P. Tsopelas, S. Okamoto, M.C. Constantinou, D. Ozaki and S. Fujii, 2/4/94, (PB94-181740, A09, MF-A02 and PB94-181757, A12, MF-A03).
- NCEER-94-0003 "A Markov Model for Local and Global Damage Indices in Seismic Analysis," by S. Rahman and M. Grigoriu, 2/18/94, (PB94-206000, A12, MF-A03).
- NCEER-94-0004 "Proceedings from the NCEER Workshop on Seismic Response of Masonry Infills," edited by D.P. Abrams, 3/1/94, (PB94-180783, A07, MF-A02).
- NCEER-94-0005 "The Northridge, California Earthquake of January 17, 1994: General Reconnaissance Report," edited by J.D. Goltz, 3/11/94, (PB94-193943, A10, MF-A03).
- NCEER-94-0006 "Seismic Energy Based Fatigue Damage Analysis of Bridge Columns: Part I - Evaluation of Seismic Capacity," by G.A. Chang and J.B. Mander, 3/14/94, (PB94-219185, A11, MF-A03).
- NCEER-94-0007 "Seismic Isolation of Multi-Story Frame Structures Using Spherical Sliding Isolation Systems," by T.M. Al-Hussaini, V.A. Zayas and M.C. Constantinou, 3/17/94, (PB94-193745, A09, MF-A02).
- NCEER-94-0008 "The Northridge, California Earthquake of January 17, 1994: Performance of Highway Bridges," edited by I.G. Buckle, 3/24/94, (PB94-193851, A06, MF-A02).
- NCEER-94-0009 "Proceedings of the Third U.S.-Japan Workshop on Earthquake Protective Systems for Bridges," edited by I.G. Buckle and I. Friedland, 3/31/94, (PB94-195815, A99, MF-A06).

- NCEER-94-0010 "3D-BASIS-ME: Computer Program for Nonlinear Dynamic Analysis of Seismically Isolated Single and Multiple Structures and Liquid Storage Tanks," by P.C. Tsopelas, M.C. Constantinou and A.M. Reinhorn, 4/12/94, (PB94-204922, A09, MF-A02).
- NCEER-94-0011 "The Northridge, California Earthquake of January 17, 1994: Performance of Gas Transmission Pipelines," by T.D. O'Rourke and M.C. Palmer, 5/16/94, (PB94-204989, A05, MF-A01).
- NCEER-94-0012 "Feasibility Study of Replacement Procedures and Earthquake Performance Related to Gas Transmission Pipelines," by T.D. O'Rourke and M.C. Palmer, 5/25/94, (PB94-206638, A09, MF-A02).
- NCEER-94-0013 "Seismic Energy Based Fatigue Damage Analysis of Bridge Columns: Part II - Evaluation of Seismic Demand," by G.A. Chang and J.B. Mander, 6/1/94, (PB95-18106, A08, MF-A02).
- NCEER-94-0014 "NCEER-Taisei Corporation Research Program on Sliding Seismic Isolation Systems for Bridges: Experimental and Analytical Study of a System Consisting of Sliding Bearings and Fluid Restoring Force/Damping Devices," by P. Tsopelas and M.C. Constantinou, 6/13/94, (PB94-219144, A10, MF-A03).
- NCEER-94-0015 "Generation of Hazard-Consistent Fragility Curves for Seismic Loss Estimation Studies," by H. Hwang and J-R. Huo, 6/14/94, (PB95-181996, A09, MF-A02).
- NCEER-94-0016 "Seismic Study of Building Frames with Added Energy-Absorbing Devices," by W.S. Pong, C.S. Tsai and G.C. Lee, 6/20/94, (PB94-219136, A10, A03).
- NCEER-94-0017 "Sliding Mode Control for Seismic-Excited Linear and Nonlinear Civil Engineering Structures," by J. Yang, J. Wu, A. Agrawal and Z. Li, 6/21/94, (PB95-138483, A06, MF-A02).
- NCEER-94-0018 "3D-BASIS-TABS Version 2.0: Computer Program for Nonlinear Dynamic Analysis of Three Dimensional Base Isolated Structures," by A.M. Reinhorn, S. Nagarajaiah, M.C. Constantinou, P. Tsopelas and R. Li, 6/22/94, (PB95-182176, A08, MF-A02).
- NCEER-94-0019 "Proceedings of the International Workshop on Civil Infrastructure Systems: Application of Intelligent Systems and Advanced Materials on Bridge Systems," Edited by G.C. Lee and K.C. Chang, 7/18/94, (PB95-252474, A20, MF-A04).
- NCEER-94-0020 "Study of Seismic Isolation Systems for Computer Floors," by V. Lambrou and M.C. Constantinou, 7/19/94, (PB95-138533, A10, MF-A03).
- NCEER-94-0021 "Proceedings of the U.S.-Italian Workshop on Guidelines for Seismic Evaluation and Rehabilitation of Unreinforced Masonry Buildings," Edited by D.P. Abrams and G.M. Calvi, 7/20/94, (PB95-138749, A13, MF-A03).
- NCEER-94-0022 "NCEER-Taisei Corporation Research Program on Sliding Seismic Isolation Systems for Bridges: Experimental and Analytical Study of a System Consisting of Lubricated PTFE Sliding Bearings and Mild Steel Dampers," by P. Tsopelas and M.C. Constantinou, 7/22/94, (PB95-182184, A08, MF-A02).
- NCEER-94-0023 "Development of Reliability-Based Design Criteria for Buildings Under Seismic Load," by Y.K. Wen, H. Hwang and M. Shinozuka, 8/1/94, (PB95-211934, A08, MF-A02).
- NCEER-94-0024 "Experimental Verification of Acceleration Feedback Control Strategies for an Active Tendon System," by S.J. Dyke, B.F. Spencer, Jr., P. Quast, M.K. Sain, D.C. Kaspari, Jr. and T.T. Soong, 8/29/94, (PB95-212320, A05, MF-A01).
- NCEER-94-0025 "Seismic Retrofitting Manual for Highway Bridges," Edited by I.G. Buckle and I.F. Friedland, published by the Federal Highway Administration (PB95-212676, A15, MF-A03).
- NCEER-94-0026 "Proceedings from the Fifth U.S.-Japan Workshop on Earthquake Resistant Design of Lifeline Facilities and Countermeasures Against Soil Liquefaction," Edited by T.D. O'Rourke and M. Hamada, 11/7/94, (PB95-220802, A99, MF-E08).

- NCEER-95-0001 "Experimental and Analytical Investigation of Seismic Retrofit of Structures with Supplemental Damping: Part 1 - Fluid Viscous Damping Devices," by A.M. Reinhorn, C. Li and M.C. Constantinou, 1/3/95, (PB95-266599, A09, MF-A02).
- NCEER-95-0002 "Experimental and Analytical Study of Low-Cycle Fatigue Behavior of Semi-Rigid Top-And-Sear Angle Connections," by G. Pekcan, J.B. Mander and S.S. Chen, 1/5/95, (PB95-220042, A07, MF-A02).
- NCEER-95-0003 "NCEER-ATC Joint Study on Fragility of Buildings," by T. Anagnos, C. Rojahn and A.S. Kiremidjian, 1/20/95, (PB95-220026, A06, MF-A02).
- NCEER-95-0004 "Nonlinear Control Algorithms for Peak Response Reduction," by Z. Wu, T.T. Soong, V. Gattulli and R.C. Lin, 2/16/95, (PB95-220349, A05, MF-A01).
- NCEER-95-0005 "Pipeline Replacement Feasibility Study: A Methodology for Minimizing Seismic and Corrosion Risks to Underground Natural Gas Pipelines," by R.T. Eguchi, H.A. Seligson and D.G. Honegger, 3/2/95, (PB95-252326, A06, MF-A02).
- NCEER-95-0006 "Evaluation of Seismic Performance of an 11-Story Frame Building During the 1994 Northridge Earthquake," by F. Naeim, R. DiSilio, K. Benuska, A. Reinhorn and C. Li, not available.
- NCEER-95-0007 "Prioritization of Bridges for Seismic Retrofitting," by N. Basöz and A.S. Kiremidjian, 4/24/95, (PB95-252300, A08, MF-A02).
- NCEER-95-0008 "Method for Developing Motion Damage Relationships for Reinforced Concrete Frames," by A. Singhal and A.S. Kiremidjian, 5/11/95, (PB95-266607, A06, MF-A02).
- NCEER-95-0009 "Experimental and Analytical Investigation of Seismic Retrofit of Structures with Supplemental Damping: Part II - Friction Devices," by C. Li and A.M. Reinhorn, 7/6/95, (PB96-128087, A11, MF-A03).
- NCEER-95-0010 "Experimental Performance and Analytical Study of a Non-Ductile Reinforced Concrete Frame Structure Retrofitted with Elastomeric Spring Dampers," by G. Pekcan, J.B. Mander and S.S. Chen, 7/14/95, (PB96-137161, A08, MF-A02).
- NCEER-95-0011 "Development and Experimental Study of Semi-Active Fluid Damping Devices for Seismic Protection of Structures," by M.D. Symans and M.C. Constantinou, 8/3/95, (PB96-136940, A23, MF-A04).
- NCEER-95-0012 "Real-Time Structural Parameter Modification (RSPM): Development of Innervated Structures," by Z. Liang, M. Tong and G.C. Lee, 4/11/95, (PB96-137153, A06, MF-A01).
- NCEER-95-0013 "Experimental and Analytical Investigation of Seismic Retrofit of Structures with Supplemental Damping: Part III - Viscous Damping Walls," by A.M. Reinhorn and C. Li, 10/1/95, (PB96-176409, A11, MF-A03).
- NCEER-95-0014 "Seismic Fragility Analysis of Equipment and Structures in a Memphis Electric Substation," by J-R. Huo and H.H.M. Hwang, 8/10/95, (PB96-128087, A09, MF-A02).
- NCEER-95-0015 "The Hanshin-Awaji Earthquake of January 17, 1995: Performance of Lifelines," Edited by M. Shinozuka, 11/3/95, (PB96-176383, A15, MF-A03).
- NCEER-95-0016 "Highway Culvert Performance During Earthquakes," by T.L. Youd and C.J. Beckman, available as NCEER-96-0015.
- NCEER-95-0017 "The Hanshin-Awaji Earthquake of January 17, 1995: Performance of Highway Bridges," Edited by I.G. Buckle, 12/1/95, not available.
- NCEER-95-0018 "Modeling of Masonry Infill Panels for Structural Analysis," by A.M. Reinhorn, A. Madan, R.E. Valles, Y. Reichmann and J.B. Mander, 12/8/95, (PB97-110886, MF-A01, A06).
- NCEER-95-0019 "Optimal Polynomial Control for Linear and Nonlinear Structures," by A.K. Agrawal and J.N. Yang, 12/11/95, (PB96-168737, A07, MF-A02).

- NCEER-95-0020 "Retrofit of Non-Ductile Reinforced Concrete Frames Using Friction Dampers," by R.S. Rao, P. Gergely and R.N. White, 12/22/95, (PB97-133508, A10, MF-A02).
- NCEER-95-0021 "Parametric Results for Seismic Response of Pile-Supported Bridge Bents," by G. Mylonakis, A. Nikolaou and G. Gazetas, 12/22/95, (PB97-100242, A12, MF-A03).
- NCEER-95-0022 "Kinematic Bending Moments in Seismically Stressed Piles," by A. Nikolaou, G. Mylonakis and G. Gazetas, 12/23/95, (PB97-113914, MF-A03, A13).
- NCEER-96-0001 "Dynamic Response of Unreinforced Masonry Buildings with Flexible Diaphragms," by A.C. Costley and D.P. Abrams," 10/10/96, (PB97-133573, MF-A03, A15).
- NCEER-96-0002 "State of the Art Review: Foundations and Retaining Structures," by I. Po Lam, not available.
- NCEER-96-0003 "Ductility of Rectangular Reinforced Concrete Bridge Columns with Moderate Confinement," by N. Wehbe, M. Saidi, D. Sanders and B. Douglas, 11/7/96, (PB97-133557, A06, MF-A02).
- NCEER-96-0004 "Proceedings of the Long-Span Bridge Seismic Research Workshop," edited by I.G. Buckle and I.M. Friedland, not available.
- NCEER-96-0005 "Establish Representative Pier Types for Comprehensive Study: Eastern United States," by J. Kulicki and Z. Prucz, 5/28/96, (PB98-119217, A07, MF-A02).
- NCEER-96-0006 "Establish Representative Pier Types for Comprehensive Study: Western United States," by R. Imbsen, R.A. Schamber and T.A. Osterkamp, 5/28/96, (PB98-118607, A07, MF-A02).
- NCEER-96-0007 "Nonlinear Control Techniques for Dynamical Systems with Uncertain Parameters," by R.G. Ghanem and M.I. Bujakow, 5/27/96, (PB97-100259, A17, MF-A03).
- NCEER-96-0008 "Seismic Evaluation of a 30-Year Old Non-Ductile Highway Bridge Pier and Its Retrofit," by J.B. Mander, B. Mahmoodzadegan, S. Bhadra and S.S. Chen, 5/31/96, (PB97-110902, MF-A03, A10).
- NCEER-96-0009 "Seismic Performance of a Model Reinforced Concrete Bridge Pier Before and After Retrofit," by J.B. Mander, J.H. Kim and C.A. Ligozio, 5/31/96, (PB97-110910, MF-A02, A10).
- NCEER-96-0010 "IDARC2D Version 4.0: A Computer Program for the Inelastic Damage Analysis of Buildings," by R.E. Valles, A.M. Reinhorn, S.K. Kunnath, C. Li and A. Madan, 6/3/96, (PB97-100234, A17, MF-A03).
- NCEER-96-0011 "Estimation of the Economic Impact of Multiple Lifeline Disruption: Memphis Light, Gas and Water Division Case Study," by S.E. Chang, H.A. Seligson and R.T. Eguchi, 8/16/96, (PB97-133490, A11, MF-A03).
- NCEER-96-0012 "Proceedings from the Sixth Japan-U.S. Workshop on Earthquake Resistant Design of Lifeline Facilities and Countermeasures Against Soil Liquefaction, Edited by M. Hamada and T. O'Rourke, 9/11/96, (PB97-133581, A99, MF-A06).
- NCEER-96-0013 "Chemical Hazards, Mitigation and Preparedness in Areas of High Seismic Risk: A Methodology for Estimating the Risk of Post-Earthquake Hazardous Materials Release," by H.A. Seligson, R.T. Eguchi, K.J. Tierney and K. Richmond, 11/7/96, (PB97-133565, MF-A02, A08).
- NCEER-96-0014 "Response of Steel Bridge Bearings to Reversed Cyclic Loading," by J.B. Mander, D-K. Kim, S.S. Chen and G.J. Premus, 11/13/96, (PB97-140735, A12, MF-A03).
- NCEER-96-0015 "Highway Culvert Performance During Past Earthquakes," by T.L. Youd and C.J. Beckman, 11/25/96, (PB97-133532, A06, MF-A01).
- NCEER-97-0001 "Evaluation, Prevention and Mitigation of Pounding Effects in Building Structures," by R.E. Valles and A.M. Reinhorn, 2/20/97, (PB97-159552, A14, MF-A03).
- NCEER-97-0002 "Seismic Design Criteria for Bridges and Other Highway Structures," by C. Rojahn, R. Mayes, D.G. Anderson, J. Clark, J.H. Hom, R.V. Nutt and M.J. O'Rourke, 4/30/97, (PB97-194658, A06, MF-A03).

- NCEER-97-0003 "Proceedings of the U.S.-Italian Workshop on Seismic Evaluation and Retrofit," Edited by D.P. Abrams and G.M. Calvi, 3/19/97, (PB97-194666, A13, MF-A03).
- NCEER-97-0004 "Investigation of Seismic Response of Buildings with Linear and Nonlinear Fluid Viscous Dampers," by A.A. Seleemah and M.C. Constantinou, 5/21/97, (PB98-109002, A15, MF-A03).
- NCEER-97-0005 "Proceedings of the Workshop on Earthquake Engineering Frontiers in Transportation Facilities," edited by G.C. Lee and I.M. Friedland, 8/29/97, (PB98-128911, A25, MR-A04).
- NCEER-97-0006 "Cumulative Seismic Damage of Reinforced Concrete Bridge Piers," by S.K. Kunnath, A. El-Bahy, A. Taylor and W. Stone, 9/2/97, (PB98-108814, A11, MF-A03).
- NCEER-97-0007 "Structural Details to Accommodate Seismic Movements of Highway Bridges and Retaining Walls," by R.A. Imbsen, R.A. Schamber, E. Thorkildsen, A. Kartoum, B.T. Martin, T.N. Rosser and J.M. Kulicki, 9/3/97, (PB98-108996, A09, MF-A02).
- NCEER-97-0008 "A Method for Earthquake Motion-Damage Relationships with Application to Reinforced Concrete Frames," by A. Singhal and A.S. Kiremidjian, 9/10/97, (PB98-108988, A13, MF-A03).
- NCEER-97-0009 "Seismic Analysis and Design of Bridge Abutments Considering Sliding and Rotation," by K. Fishman and R. Richards, Jr., 9/15/97, (PB98-108897, A06, MF-A02).
- NCEER-97-0010 "Proceedings of the FHWA/NCEER Workshop on the National Representation of Seismic Ground Motion for New and Existing Highway Facilities," edited by I.M. Friedland, M.S. Power and R.L. Mayes, 9/22/97, (PB98-128903, A21, MF-A04).
- NCEER-97-0011 "Seismic Analysis for Design or Retrofit of Gravity Bridge Abutments," by K.L. Fishman, R. Richards, Jr. and R.C. Divito, 10/2/97, (PB98-128937, A08, MF-A02).
- NCEER-97-0012 "Evaluation of Simplified Methods of Analysis for Yielding Structures," by P. Tsopelas, M.C. Constantinou, C.A. Kircher and A.S. Whittaker, 10/31/97, (PB98-128929, A10, MF-A03).
- NCEER-97-0013 "Seismic Design of Bridge Columns Based on Control and Repairability of Damage," by C-T. Cheng and J.B. Mander, 12/8/97, (PB98-144249, A11, MF-A03).
- NCEER-97-0014 "Seismic Resistance of Bridge Piers Based on Damage Avoidance Design," by J.B. Mander and C-T. Cheng, 12/10/97, (PB98-144223, A09, MF-A02).
- NCEER-97-0015 "Seismic Response of Nominally Symmetric Systems with Strength Uncertainty," by S. Balopoulos and M. Grigoriu, 12/23/97, (PB98-153422, A11, MF-A03).
- NCEER-97-0016 "Evaluation of Seismic Retrofit Methods for Reinforced Concrete Bridge Columns," by T.J. Wipf, F.W. Klaiber and F.M. Russo, 12/28/97, (PB98-144215, A12, MF-A03).
- NCEER-97-0017 "Seismic Fragility of Existing Conventional Reinforced Concrete Highway Bridges," by C.L. Mullen and A.S. Cakmak, 12/30/97, (PB98-153406, A08, MF-A02).
- NCEER-97-0018 "Loss Assessment of Memphis Buildings," edited by D.P. Abrams and M. Shinozuka, 12/31/97, (PB98-144231, A13, MF-A03).
- NCEER-97-0019 "Seismic Evaluation of Frames with Infill Walls Using Quasi-static Experiments," by K.M. Mosalam, R.N. White and P. Gergely, 12/31/97, (PB98-153455, A07, MF-A02).
- NCEER-97-0020 "Seismic Evaluation of Frames with Infill Walls Using Pseudo-dynamic Experiments," by K.M. Mosalam, R.N. White and P. Gergely, 12/31/97, (PB98-153430, A07, MF-A02).
- NCEER-97-0021 "Computational Strategies for Frames with Infill Walls: Discrete and Smeared Crack Analyses and Seismic Fragility," by K.M. Mosalam, R.N. White and P. Gergely, 12/31/97, (PB98-153414, A10, MF-A02).

- NCEER-97-0022 "Proceedings of the NCEER Workshop on Evaluation of Liquefaction Resistance of Soils," edited by T.L. Youd and I.M. Idriss, 12/31/97, (PB98-155617, A15, MF-A03).
- MCEER-98-0001 "Extraction of Nonlinear Hysteretic Properties of Seismically Isolated Bridges from Quick-Release Field Tests," by Q. Chen, B.M. Douglas, E.M. Maragakis and I.G. Buckle, 5/26/98, (PB99-118838, A06, MF-A01).
- MCEER-98-0002 "Methodologies for Evaluating the Importance of Highway Bridges," by A. Thomas, S. Eshenaur and J. Kulicki, 5/29/98, (PB99-118846, A10, MF-A02).
- MCEER-98-0003 "Capacity Design of Bridge Piers and the Analysis of Overstrength," by J.B. Mander, A. Dutta and P. Goel, 6/1/98, (PB99-118853, A09, MF-A02).
- MCEER-98-0004 "Evaluation of Bridge Damage Data from the Loma Prieta and Northridge, California Earthquakes," by N. Basoz and A. Kiremidjian, 6/2/98, (PB99-118861, A15, MF-A03).
- MCEER-98-0005 "Screening Guide for Rapid Assessment of Liquefaction Hazard at Highway Bridge Sites," by T. L. Youd, 6/16/98, (PB99-118879, A06, not available on microfiche).
- MCEER-98-0006 "Structural Steel and Steel/Concrete Interface Details for Bridges," by P. Ritchie, N. Kauhl and J. Kulicki, 7/13/98, (PB99-118945, A06, MF-A01).
- MCEER-98-0007 "Capacity Design and Fatigue Analysis of Confined Concrete Columns," by A. Dutta and J.B. Mander, 7/14/98, (PB99-118960, A14, MF-A03).
- MCEER-98-0008 "Proceedings of the Workshop on Performance Criteria for Telecommunication Services Under Earthquake Conditions," edited by A.J. Schiff, 7/15/98, (PB99-118952, A08, MF-A02).
- MCEER-98-0009 "Fatigue Analysis of Unconfined Concrete Columns," by J.B. Mander, A. Dutta and J.H. Kim, 9/12/98, (PB99-123655, A10, MF-A02).
- MCEER-98-0010 "Centrifuge Modeling of Cyclic Lateral Response of Pile-Cap Systems and Seat-Type Abutments in Dry Sands," by A.D. Gadre and R. Dobry, 10/2/98, (PB99-123606, A13, MF-A03).
- MCEER-98-0011 "IDARC-BRIDGE: A Computational Platform for Seismic Damage Assessment of Bridge Structures," by A.M. Reinhorn, V. Simeonov, G. Mylonakis and Y. Reichman, 10/2/98, (PB99-162919, A15, MF-A03).
- MCEER-98-0012 "Experimental Investigation of the Dynamic Response of Two Bridges Before and After Retrofitting with Elastomeric Bearings," by D.A. Wendichansky, S.S. Chen and J.B. Mander, 10/2/98, (PB99-162927, A15, MF-A03).
- MCEER-98-0013 "Design Procedures for Hinge Restrainers and Hinge Sear Width for Multiple-Frame Bridges," by R. Des Roches and G.L. Fenves, 11/3/98, (PB99-140477, A13, MF-A03).
- MCEER-98-0014 "Response Modification Factors for Seismically Isolated Bridges," by M.C. Constantinou and J.K. Quarshie, 11/3/98, (PB99-140485, A14, MF-A03).
- MCEER-98-0015 "Proceedings of the U.S.-Italy Workshop on Seismic Protective Systems for Bridges," edited by I.M. Friedland and M.C. Constantinou, 11/3/98, (PB2000-101711, A22, MF-A04).
- MCEER-98-0016 "Appropriate Seismic Reliability for Critical Equipment Systems: Recommendations Based on Regional Analysis of Financial and Life Loss," by K. Porter, C. Scawthorn, C. Taylor and N. Blais, 11/10/98, (PB99-157265, A08, MF-A02).
- MCEER-98-0017 "Proceedings of the U.S. Japan Joint Seminar on Civil Infrastructure Systems Research," edited by M. Shinozuka and A. Rose, 11/12/98, (PB99-156713, A16, MF-A03).
- MCEER-98-0018 "Modeling of Pile Footings and Drilled Shafts for Seismic Design," by I. PoLam, M. Kapuskar and D. Chaudhuri, 12/21/98, (PB99-157257, A09, MF-A02).

- MCEER-99-0001 "Seismic Evaluation of a Masonry Infilled Reinforced Concrete Frame by Pseudodynamic Testing," by S.G. Buonopane and R.N. White, 2/16/99, (PB99-162851, A09, MF-A02).
- MCEER-99-0002 "Response History Analysis of Structures with Seismic Isolation and Energy Dissipation Systems: Verification Examples for Program SAP2000," by J. Scheller and M.C. Constantinou, 2/22/99, (PB99-162869, A08, MF-A02).
- MCEER-99-0003 "Experimental Study on the Seismic Design and Retrofit of Bridge Columns Including Axial Load Effects," by A. Dutta, T. Kokorina and J.B. Mander, 2/22/99, (PB99-162877, A09, MF-A02).
- MCEER-99-0004 "Experimental Study of Bridge Elastomeric and Other Isolation and Energy Dissipation Systems with Emphasis on Uplift Prevention and High Velocity Near-source Seismic Excitation," by A. Kasalanati and M. C. Constantinou, 2/26/99, (PB99-162885, A12, MF-A03).
- MCEER-99-0005 "Truss Modeling of Reinforced Concrete Shear-flexure Behavior," by J.H. Kim and J.B. Mander, 3/8/99, (PB99-163693, A12, MF-A03).
- MCEER-99-0006 "Experimental Investigation and Computational Modeling of Seismic Response of a 1:4 Scale Model Steel Structure with a Load Balancing Supplemental Damping System," by G. Pekcan, J.B. Mander and S.S. Chen, 4/2/99, (PB99-162893, A11, MF-A03).
- MCEER-99-0007 "Effect of Vertical Ground Motions on the Structural Response of Highway Bridges," by M.R. Button, C.J. Cronin and R.L. Mayes, 4/10/99, (PB2000-101411, A10, MF-A03).
- MCEER-99-0008 "Seismic Reliability Assessment of Critical Facilities: A Handbook, Supporting Documentation, and Model Code Provisions," by G.S. Johnson, R.E. Sheppard, M.D. Quilici, S.J. Eder and C.R. Scawthorn, 4/12/99, (PB2000-101701, A18, MF-A04).
- MCEER-99-0009 "Impact Assessment of Selected MCEER Highway Project Research on the Seismic Design of Highway Structures," by C. Rojahn, R. Mayes, D.G. Anderson, J.H. Clark, D'Appolonia Engineering, S. Gloyd and R.V. Nutt, 4/14/99, (PB99-162901, A10, MF-A02).
- MCEER-99-0010 "Site Factors and Site Categories in Seismic Codes," by R. Dobry, R. Ramos and M.S. Power, 7/19/99, (PB2000-101705, A08, MF-A02).
- MCEER-99-0011 "Restrainer Design Procedures for Multi-Span Simply-Supported Bridges," by M.J. Randall, M. Saiidi, E. Maragakis and T. Isakovic, 7/20/99, (PB2000-101702, A10, MF-A02).
- MCEER-99-0012 "Property Modification Factors for Seismic Isolation Bearings," by M.C. Constantinou, P. Tsopelas, A. Kasalanati and E. Wolff, 7/20/99, (PB2000-103387, A11, MF-A03).
- MCEER-99-0013 "Critical Seismic Issues for Existing Steel Bridges," by P. Ritchie, N. Kauhl and J. Kulicki, 7/20/99, (PB2000-101697, A09, MF-A02).
- MCEER-99-0014 "Nonstructural Damage Database," by A. Kao, T.T. Soong and A. Vender, 7/24/99, (PB2000-101407, A06, MF-A01).
- MCEER-99-0015 "Guide to Remedial Measures for Liquefaction Mitigation at Existing Highway Bridge Sites," by H.G. Cooke and J. K. Mitchell, 7/26/99, (PB2000-101703, A11, MF-A03).
- MCEER-99-0016 "Proceedings of the MCEER Workshop on Ground Motion Methodologies for the Eastern United States," edited by N. Abrahamson and A. Becker, 8/11/99, (PB2000-103385, A07, MF-A02).
- MCEER-99-0017 "Quindío, Colombia Earthquake of January 25, 1999: Reconnaissance Report," by A.P. Asfura and P.J. Flores, 10/4/99, (PB2000-106893, A06, MF-A01).
- MCEER-99-0018 "Hysteretic Models for Cyclic Behavior of Deteriorating Inelastic Structures," by M.V. Sivaselvan and A.M. Reinhorn, 11/5/99, (PB2000-103386, A08, MF-A02).

- MCEER-99-0019 "Proceedings of the 7<sup>th</sup> U.S.- Japan Workshop on Earthquake Resistant Design of Lifeline Facilities and Countermeasures Against Soil Liquefaction," edited by T.D. O'Rourke, J.P. Bardet and M. Hamada, 11/19/99, (PB2000-103354, A99, MF-A06).
- MCEER-99-0020 "Development of Measurement Capability for Micro-Vibration Evaluations with Application to Chip Fabrication Facilities," by G.C. Lee, Z. Liang, J.W. Song, J.D. Shen and W.C. Liu, 12/1/99, (PB2000-105993, A08, MF-A02).
- MCEER-99-0021 "Design and Retrofit Methodology for Building Structures with Supplemental Energy Dissipating Systems," by G. Pekcan, J.B. Mander and S.S. Chen, 12/31/99, (PB2000-105994, A11, MF-A03).
- MCEER-00-0001 "The Marmara, Turkey Earthquake of August 17, 1999: Reconnaissance Report," edited by C. Scawthorn; with major contributions by M. Bruneau, R. Eguchi, T. Holzer, G. Johnson, J. Mander, J. Mitchell, W. Mitchell, A. Papageorgiou, C. Scaethorn, and G. Webb, 3/23/00, (PB2000-106200, A11, MF-A03).
- MCEER-00-0002 "Proceedings of the MCEER Workshop for Seismic Hazard Mitigation of Health Care Facilities," edited by G.C. Lee, M. Ettouney, M. Grigoriu, J. Hauer and J. Nigg, 3/29/00, (PB2000-106892, A08, MF-A02).
- MCEER-00-0003 "The Chi-Chi, Taiwan Earthquake of September 21, 1999: Reconnaissance Report," edited by G.C. Lee and C.H. Loh, with major contributions by G.C. Lee, M. Bruneau, I.G. Buckle, S.E. Chang, P.J. Flores, T.D. O'Rourke, M. Shinozuka, T.T. Soong, C-H. Loh, K-C. Chang, Z-J. Chen, J-S. Hwang, M-L. Lin, G-Y. Liu, K-C. Tsai, G.C. Yao and C-L. Yen, 4/30/00, (PB2001-100980, A10, MF-A02).
- MCEER-00-0004 "Seismic Retrofit of End-Sway Frames of Steel Deck-Truss Bridges with a Supplemental Tendon System: Experimental and Analytical Investigation," by G. Pekcan, J.B. Mander and S.S. Chen, 7/1/00, (PB2001-100982, A10, MF-A02).
- MCEER-00-0005 "Sliding Fragility of Unrestrained Equipment in Critical Facilities," by W.H. Chong and T.T. Soong, 7/5/00, (PB2001-100983, A08, MF-A02).
- MCEER-00-0006 "Seismic Response of Reinforced Concrete Bridge Pier Walls in the Weak Direction," by N. Abo-Shadi, M. Saiidi and D. Sanders, 7/17/00, (PB2001-100981, A17, MF-A03).
- MCEER-00-0007 "Low-Cycle Fatigue Behavior of Longitudinal Reinforcement in Reinforced Concrete Bridge Columns," by J. Brown and S.K. Kunath, 7/23/00, (PB2001-104392, A08, MF-A02).
- MCEER-00-0008 "Soil Structure Interaction of Bridges for Seismic Analysis," I. PoLam and H. Law, 9/25/00, (PB2001-105397, A08, MF-A02).
- MCEER-00-0009 "Proceedings of the First MCEER Workshop on Mitigation of Earthquake Disaster by Advanced Technologies (MEDAT-1), edited by M. Shinozuka, D.J. Inman and T.D. O'Rourke, 11/10/00, (PB2001-105399, A14, MF-A03).
- MCEER-00-0010 "Development and Evaluation of Simplified Procedures for Analysis and Design of Buildings with Passive Energy Dissipation Systems, Revision 01," by O.M. Ramirez, M.C. Constantinou, C.A. Kircher, A.S. Whittaker, M.W. Johnson, J.D. Gomez and C. Chrysostomou, 11/16/01, (PB2001-105523, A23, MF-A04).
- MCEER-00-0011 "Dynamic Soil-Foundation-Structure Interaction Analyses of Large Caissons," by C-Y. Chang, C-M. Mok, Z-L. Wang, R. Settgast, F. Waggoner, M.A. Ketchum, H.M. Gonnermann and C-C. Chin, 12/30/00, (PB2001-104373, A07, MF-A02).
- MCEER-00-0012 "Experimental Evaluation of Seismic Performance of Bridge Restrainers," by A.G. Vlassis, E.M. Maragakis and M. Saiid Saiidi, 12/30/00, (PB2001-104354, A09, MF-A02).
- MCEER-00-0013 "Effect of Spatial Variation of Ground Motion on Highway Structures," by M. Shinozuka, V. Saxena and G. Deodatis, 12/31/00, (PB2001-108755, A13, MF-A03).
- MCEER-00-0014 "A Risk-Based Methodology for Assessing the Seismic Performance of Highway Systems," by S.D. Werner, C.E. Taylor, J.E. Moore, II, J.S. Walton and S. Cho, 12/31/00, (PB2001-108756, A14, MF-A03).

- MCEER-01-0001 "Experimental Investigation of P-Delta Effects to Collapse During Earthquakes," by D. Vian and M. Bruneau, 6/25/01, (PB2002-100534, A17, MF-A03).
- MCEER-01-0002 "Proceedings of the Second MCEER Workshop on Mitigation of Earthquake Disaster by Advanced Technologies (MEDAT-2)," edited by M. Bruneau and D.J. Inman, 7/23/01, (PB2002-100434, A16, MF-A03).
- MCEER-01-0003 "Sensitivity Analysis of Dynamic Systems Subjected to Seismic Loads," by C. Roth and M. Grigoriu, 9/18/01, (PB2003-100884, A12, MF-A03).
- MCEER-01-0004 "Overcoming Obstacles to Implementing Earthquake Hazard Mitigation Policies: Stage 1 Report," by D.J. Alesch and W.J. Petak, 12/17/01, (PB2002-107949, A07, MF-A02).
- MCEER-01-0005 "Updating Real-Time Earthquake Loss Estimates: Methods, Problems and Insights," by C.E. Taylor, S.E. Chang and R.T. Eguchi, 12/17/01, (PB2002-107948, A05, MF-A01).
- MCEER-01-0006 "Experimental Investigation and Retrofit of Steel Pile Foundations and Pile Bents Under Cyclic Lateral Loadings," by A. Shama, J. Mander, B. Blabac and S. Chen, 12/31/01, (PB2002-107950, A13, MF-A03).
- MCEER-02-0001 "Assessment of Performance of Bolu Viaduct in the 1999 Duzce Earthquake in Turkey" by P.C. Roussis, M.C. Constantinou, M. Erdik, E. Durukal and M. Dicleli, 5/8/02, (PB2003-100883, A08, MF-A02).
- MCEER-02-0002 "Seismic Behavior of Rail Counterweight Systems of Elevators in Buildings," by M.P. Singh, Rildova and L.E. Suarez, 5/27/02. (PB2003-100882, A11, MF-A03).
- MCEER-02-0003 "Development of Analysis and Design Procedures for Spread Footings," by G. Mylonakis, G. Gazetas, S. Nikolaou and A. Chauncey, 10/02/02, (PB2004-101636, A13, MF-A03, CD-A13).
- MCEER-02-0004 "Bare-Earth Algorithms for Use with SAR and LIDAR Digital Elevation Models," by C.K. Huyck, R.T. Eguchi and B. Houshmand, 10/16/02, (PB2004-101637, A07, CD-A07).
- MCEER-02-0005 "Review of Energy Dissipation of Compression Members in Concentrically Braced Frames," by K.Lee and M. Bruneau, 10/18/02, (PB2004-101638, A10, CD-A10).
- MCEER-03-0001 "Experimental Investigation of Light-Gauge Steel Plate Shear Walls for the Seismic Retrofit of Buildings" by J. Berman and M. Bruneau, 5/2/03, (PB2004-101622, A10, MF-A03, CD-A10).
- MCEER-03-0002 "Statistical Analysis of Fragility Curves," by M. Shinotuka, M.Q. Feng, H. Kim, T. Uzawa and T. Ueda, 6/16/03, (PB2004-101849, A09, CD-A09).
- MCEER-03-0003 "Proceedings of the Eighth U.S.-Japan Workshop on Earthquake Resistant Design f Lifeline Facilities and Countermeasures Against Liquefaction," edited by M. Hamada, J.P. Bardet and T.D. O'Rourke, 6/30/03, (PB2004-104386, A99, CD-A99).
- MCEER-03-0004 "Proceedings of the PRC-US Workshop on Seismic Analysis and Design of Special Bridges," edited by L.C. Fan and G.C. Lee, 7/15/03, (PB2004-104387, A14, CD-A14).
- MCEER-03-0005 "Urban Disaster Recovery: A Framework and Simulation Model," by S.B. Miles and S.E. Chang, 7/25/03, (PB2004-104388, A07, CD-A07).
- MCEER-03-0006 "Behavior of Underground Piping Joints Due to Static and Dynamic Loading," by R.D. Meis, M. Maragakis and R. Siddharthan, 11/17/03, (PB2005-102194, A13, MF-A03, CD-A00).
- MCEER-04-0001 "Experimental Study of Seismic Isolation Systems with Emphasis on Secondary System Response and Verification of Accuracy of Dynamic Response History Analysis Methods," by E. Wolff and M. Constantinou, 1/16/04 (PB2005-102195, A99, MF-E08, CD-A00).
- MCEER-04-0002 "Tension, Compression and Cyclic Testing of Engineered Cementitious Composite Materials," by K. Kesner and S.L. Billington, 3/1/04, (PB2005-102196, A08, CD-A08).

- MCEER-04-0003 "Cyclic Testing of Braces Laterally Restrained by Steel Studs to Enhance Performance During Earthquakes," by O.C. Celik, J.W. Berman and M. Bruneau, 3/16/04, (PB2005-102197, A13, MF-A03, CD-A00).
- MCEER-04-0004 "Methodologies for Post Earthquake Building Damage Detection Using SAR and Optical Remote Sensing: Application to the August 17, 1999 Marmara, Turkey Earthquake," by C.K. Huyck, B.J. Adams, S. Cho, R.T. Eguchi, B. Mansouri and B. Houshmand, 6/15/04, (PB2005-104888, A10, CD-A00).
- MCEER-04-0005 "Nonlinear Structural Analysis Towards Collapse Simulation: A Dynamical Systems Approach," by M.V. Sivaselvan and A.M. Reinhorn, 6/16/04, (PB2005-104889, A11, MF-A03, CD-A00).
- MCEER-04-0006 "Proceedings of the Second PRC-US Workshop on Seismic Analysis and Design of Special Bridges," edited by G.C. Lee and L.C. Fan, 6/25/04, (PB2005-104890, A16, CD-A00).
- MCEER-04-0007 "Seismic Vulnerability Evaluation of Axially Loaded Steel Built-up Laced Members," by K. Lee and M. Bruneau, 6/30/04, (PB2005-104891, A16, CD-A00).
- MCEER-04-0008 "Evaluation of Accuracy of Simplified Methods of Analysis and Design of Buildings with Damping Systems for Near-Fault and for Soft-Soil Seismic Motions," by E.A. Pavlou and M.C. Constantinou, 8/16/04, (PB2005-104892, A08, MF-A02, CD-A00).
- MCEER-04-0009 "Assessment of Geotechnical Issues in Acute Care Facilities in California," by M. Lew, T.D. O'Rourke, R. Dobry and M. Koch, 9/15/04, (PB2005-104893, A08, CD-A00).
- MCEER-04-0010 "Scissor-Jack-Damper Energy Dissipation System," by A.N. Sigaher-Boyle and M.C. Constantinou, 12/1/04 (PB2005-108221).
- MCEER-04-0011 "Seismic Retrofit of Bridge Steel Truss Piers Using a Controlled Rocking Approach," by M. Pollino and M. Bruneau, 12/20/04 (PB2006-105795).
- MCEER-05-0001 "Experimental and Analytical Studies of Structures Seismically Isolated with an Uplift-Restraint Isolation System," by P.C. Roussis and M.C. Constantinou, 1/10/05 (PB2005-108222).
- MCEER-05-0002 "A Versatile Experimentation Model for Study of Structures Near Collapse Applied to Seismic Evaluation of Irregular Structures," by D. Kusumastuti, A.M. Reinhorn and A. Rutenberg, 3/31/05 (PB2006-101523).
- MCEER-05-0003 "Proceedings of the Third PRC-US Workshop on Seismic Analysis and Design of Special Bridges," edited by L.C. Fan and G.C. Lee, 4/20/05, (PB2006-105796).
- MCEER-05-0004 "Approaches for the Seismic Retrofit of Braced Steel Bridge Piers and Proof-of-Concept Testing of an Eccentrically Braced Frame with Tubular Link," by J.W. Berman and M. Bruneau, 4/21/05 (PB2006-101524).
- MCEER-05-0005 "Simulation of Strong Ground Motions for Seismic Fragility Evaluation of Nonstructural Components in Hospitals," by A. Wanitkorkul and A. Filiatrault, 5/26/05 (PB2006-500027).
- MCEER-05-0006 "Seismic Safety in California Hospitals: Assessing an Attempt to Accelerate the Replacement or Seismic Retrofit of Older Hospital Facilities," by D.J. Alesch, L.A. Arendt and W.J. Petak, 6/6/05 (PB2006-105794).
- MCEER-05-0007 "Development of Seismic Strengthening and Retrofit Strategies for Critical Facilities Using Engineered Cementitious Composite Materials," by K. Kesner and S.L. Billington, 8/29/05 (PB2006-111701).
- MCEER-05-0008 "Experimental and Analytical Studies of Base Isolation Systems for Seismic Protection of Power Transformers," by N. Murota, M.Q. Feng and G-Y. Liu, 9/30/05 (PB2006-111702).
- MCEER-05-0009 "3D-BASIS-ME-MB: Computer Program for Nonlinear Dynamic Analysis of Seismically Isolated Structures," by P.C. Tsopelas, P.C. Roussis, M.C. Constantinou, R. Buchanan and A.M. Reinhorn, 10/3/05 (PB2006-111703).
- MCEER-05-0010 "Steel Plate Shear Walls for Seismic Design and Retrofit of Building Structures," by D. Vian and M. Bruneau, 12/15/05 (PB2006-111704).

- MCEER-05-0011 "The Performance-Based Design Paradigm," by M.J. Astrella and A. Whittaker, 12/15/05 (PB2006-111705).
- MCEER-06-0001 "Seismic Fragility of Suspended Ceiling Systems," H. Badillo-Almaraz, A.S. Whittaker, A.M. Reinhorn and G.P. Cimellaro, 2/4/06 (PB2006-111706).
- MCEER-06-0002 "Multi-Dimensional Fragility of Structures," by G.P. Cimellaro, A.M. Reinhorn and M. Bruneau, 3/1/06 (PB2007-106974, A09, MF-A02, CD A00).
- MCEER-06-0003 "Built-Up Shear Links as Energy Dissipators for Seismic Protection of Bridges," by P. Dusicka, A.M. Itani and I.G. Buckle, 3/15/06 (PB2006-111708).
- MCEER-06-0004 "Analytical Investigation of the Structural Fuse Concept," by R.E. Vargas and M. Bruneau, 3/16/06 (PB2006-111709).
- MCEER-06-0005 "Experimental Investigation of the Structural Fuse Concept," by R.E. Vargas and M. Bruneau, 3/17/06 (PB2006-111710).
- MCEER-06-0006 "Further Development of Tubular Eccentrically Braced Frame Links for the Seismic Retrofit of Braced Steel Truss Bridge Piers," by J.W. Berman and M. Bruneau, 3/27/06 (PB2007-105147).
- MCEER-06-0007 "REDARS Validation Report," by S. Cho, C.K. Huyck, S. Ghosh and R.T. Eguchi, 8/8/06 (PB2007-106983).
- MCEER-06-0008 "Review of Current NDE Technologies for Post-Earthquake Assessment of Retrofitted Bridge Columns," by J.W. Song, Z. Liang and G.C. Lee, 8/21/06 (PB2007-106984).
- MCEER-06-0009 "Liquefaction Remediation in Silty Soils Using Dynamic Compaction and Stone Columns," by S. Thevanayagam, G.R. Martin, R. Nashed, T. Shenthal, T. Kanagalingam and N. Ecemis, 8/28/06 (PB2007-106985).
- MCEER-06-0010 "Conceptual Design and Experimental Investigation of Polymer Matrix Composite Infill Panels for Seismic Retrofitting," by W. Jung, M. Chiewanichakorn and A.J. Aref, 9/21/06 (PB2007-106986).
- MCEER-06-0011 "A Study of the Coupled Horizontal-Vertical Behavior of Elastomeric and Lead-Rubber Seismic Isolation Bearings," by G.P. Warn and A.S. Whittaker, 9/22/06 (PB2007-108679).
- MCEER-06-0012 "Proceedings of the Fourth PRC-US Workshop on Seismic Analysis and Design of Special Bridges: Advancing Bridge Technologies in Research, Design, Construction and Preservation," Edited by L.C. Fan, G.C. Lee and L. Ziang, 10/12/06 (PB2007-109042).
- MCEER-06-0013 "Cyclic Response and Low Cycle Fatigue Characteristics of Plate Steels," by P. Dusicka, A.M. Itani and I.G. Buckle, 11/1/06 06 (PB2007-106987).
- MCEER-06-0014 "Proceedings of the Second US-Taiwan Bridge Engineering Workshop," edited by W.P. Yen, J. Shen, J-Y. Chen and M. Wang, 11/15/06 (PB2008-500041).
- MCEER-06-0015 "User Manual and Technical Documentation for the REDARS™ Import Wizard," by S. Cho, S. Ghosh, C.K. Huyck and S.D. Werner, 11/30/06 (PB2007-114766).
- MCEER-06-0016 "Hazard Mitigation Strategy and Monitoring Technologies for Urban and Infrastructure Public Buildings: Proceedings of the China-US Workshops," edited by X.Y. Zhou, A.L. Zhang, G.C. Lee and M. Tong, 12/12/06 (PB2008-500018).
- MCEER-07-0001 "Static and Kinetic Coefficients of Friction for Rigid Blocks," by C. Kafali, S. Fathali, M. Grigoriu and A.S. Whittaker, 3/20/07 (PB2007-114767).
- MCEER-07-0002 "Hazard Mitigation Investment Decision Making: Organizational Response to Legislative Mandate," by L.A. Arendt, D.J. Alesch and W.J. Petak, 4/9/07 (PB2007-114768).
- MCEER-07-0003 "Seismic Behavior of Bidirectional-Resistant Ductile End Diaphragms with Unbonded Braces in Straight or Skewed Steel Bridges," by O. Celik and M. Bruneau, 4/11/07 (PB2008-105141).

- MCEER-07-0004 "Modeling Pile Behavior in Large Pile Groups Under Lateral Loading," by A.M. Dodds and G.R. Martin, 4/16/07 (PB2008-105142).
- MCEER-07-0005 "Experimental Investigation of Blast Performance of Seismically Resistant Concrete-Filled Steel Tube Bridge Piers," by S. Fujikura, M. Bruneau and D. Lopez-Garcia, 4/20/07 (PB2008-105143).
- MCEER-07-0006 "Seismic Analysis of Conventional and Isolated Liquefied Natural Gas Tanks Using Mechanical Analogs," by I.P. Christovasilis and A.S. Whittaker, 5/1/07, not available.
- MCEER-07-0007 "Experimental Seismic Performance Evaluation of Isolation/Restrain Systems for Mechanical Equipment – Part 1: Heavy Equipment Study," by S. Fathali and A. Filiatral, 6/6/07 (PB2008-105144).
- MCEER-07-0008 "Seismic Vulnerability of Timber Bridges and Timber Substructures," by A.A. Sharma, J.B. Mander, I.M. Friedland and D.R. Allicock, 6/7/07 (PB2008-105145).
- MCEER-07-0009 "Experimental and Analytical Study of the XY-Friction Pendulum (XY-FP) Bearing for Bridge Applications," by C.C. Marin-Artieda, A.S. Whittaker and M.C. Constantinou, 6/7/07 (PB2008-105191).
- MCEER-07-0010 "Proceedings of the PRC-US Earthquake Engineering Forum for Young Researchers," Edited by G.C. Lee and X.Z. Qi, 6/8/07 (PB2008-500058).
- MCEER-07-0011 "Design Recommendations for Perforated Steel Plate Shear Walls," by R. Purba and M. Bruneau, 6/18/07, (PB2008-105192).
- MCEER-07-0012 "Performance of Seismic Isolation Hardware Under Service and Seismic Loading," by M.C. Constantinou, A.S. Whittaker, Y. Kalpakidis, D.M. Fenz and G.P. Warn, 8/27/07, (PB2008-105193).
- MCEER-07-0013 "Experimental Evaluation of the Seismic Performance of Hospital Piping Subassemblies," by E.R. Goodwin, E. Maragakis and A.M. Itani, 9/4/07, (PB2008-105194).
- MCEER-07-0014 "A Simulation Model of Urban Disaster Recovery and Resilience: Implementation for the 1994 Northridge Earthquake," by S. Miles and S.E. Chang, 9/7/07, (PB2008-106426).
- MCEER-07-0015 "Statistical and Mechanistic Fragility Analysis of Concrete Bridges," by M. Shinozuka, S. Banerjee and S-H. Kim, 9/10/07, (PB2008-106427).
- MCEER-07-0016 "Three-Dimensional Modeling of Inelastic Buckling in Frame Structures," by M. Schachter and AM. Reinhorn, 9/13/07, (PB2008-108125).
- MCEER-07-0017 "Modeling of Seismic Wave Scattering on Pile Groups and Caissons," by I. Po Lam, H. Law and C.T. Yang, 9/17/07 (PB2008-108150).
- MCEER-07-0018 "Bridge Foundations: Modeling Large Pile Groups and Caissons for Seismic Design," by I. Po Lam, H. Law and G.R. Martin (Coordinating Author), 12/1/07 (PB2008-111190).
- MCEER-07-0019 "Principles and Performance of Roller Seismic Isolation Bearings for Highway Bridges," by G.C. Lee, Y.C. Ou, Z. Liang, T.C. Niu and J. Song, 12/10/07 (PB2009-110466).
- MCEER-07-0020 "Centrifuge Modeling of Permeability and Pinning Reinforcement Effects on Pile Response to Lateral Spreading," by L.L Gonzalez-Lagos, T. Abdoun and R. Dobry, 12/10/07 (PB2008-111191).
- MCEER-07-0021 "Damage to the Highway System from the Pisco, Perú Earthquake of August 15, 2007," by J.S. O'Connor, L. Mesa and M. Nykamp, 12/10/07, (PB2008-108126).
- MCEER-07-0022 "Experimental Seismic Performance Evaluation of Isolation/Restrain Systems for Mechanical Equipment – Part 2: Light Equipment Study," by S. Fathali and A. Filiatral, 12/13/07 (PB2008-111192).
- MCEER-07-0023 "Fragility Considerations in Highway Bridge Design," by M. Shinozuka, S. Banerjee and S.H. Kim, 12/14/07 (PB2008-111193).

- MCEER-07-0024 "Performance Estimates for Seismically Isolated Bridges," by G.P. Warn and A.S. Whittaker, 12/30/07 (PB2008-112230).
- MCEER-08-0001 "Seismic Performance of Steel Girder Bridge Superstructures with Conventional Cross Frames," by L.P. Carden, A.M. Itani and I.G. Buckle, 1/7/08, (PB2008-112231).
- MCEER-08-0002 "Seismic Performance of Steel Girder Bridge Superstructures with Ductile End Cross Frames with Seismic Isolators," by L.P. Carden, A.M. Itani and I.G. Buckle, 1/7/08 (PB2008-112232).
- MCEER-08-0003 "Analytical and Experimental Investigation of a Controlled Rocking Approach for Seismic Protection of Bridge Steel Truss Piers," by M. Pollino and M. Bruneau, 1/21/08 (PB2008-112233).
- MCEER-08-0004 "Linking Lifeline Infrastructure Performance and Community Disaster Resilience: Models and Multi-Stakeholder Processes," by S.E. Chang, C. Pasion, K. Tatebe and R. Ahmad, 3/3/08 (PB2008-112234).
- MCEER-08-0005 "Modal Analysis of Generally Damped Linear Structures Subjected to Seismic Excitations," by J. Song, Y-L. Chu, Z. Liang and G.C. Lee, 3/4/08 (PB2009-102311).
- MCEER-08-0006 "System Performance Under Multi-Hazard Environments," by C. Kafali and M. Grigoriu, 3/4/08 (PB2008-112235).
- MCEER-08-0007 "Mechanical Behavior of Multi-Spherical Sliding Bearings," by D.M. Fenz and M.C. Constantinou, 3/6/08 (PB2008-112236).
- MCEER-08-0008 "Post-Earthquake Restoration of the Los Angeles Water Supply System," by T.H.P. Tabucchi and R.A. Davidson, 3/7/08 (PB2008-112237).
- MCEER-08-0009 "Fragility Analysis of Water Supply Systems," by A. Jacobson and M. Grigoriu, 3/10/08 (PB2009-105545).
- MCEER-08-0010 "Experimental Investigation of Full-Scale Two-Story Steel Plate Shear Walls with Reduced Beam Section Connections," by B. Qu, M. Bruneau, C-H. Lin and K-C. Tsai, 3/17/08 (PB2009-106368).
- MCEER-08-0011 "Seismic Evaluation and Rehabilitation of Critical Components of Electrical Power Systems," S. Ersoy, B. Feizi, A. Ashrafi and M. Ala Saadeghvaziri, 3/17/08 (PB2009-105546).
- MCEER-08-0012 "Seismic Behavior and Design of Boundary Frame Members of Steel Plate Shear Walls," by B. Qu and M. Bruneau, 4/26/08 . (PB2009-106744).
- MCEER-08-0013 "Development and Appraisal of a Numerical Cyclic Loading Protocol for Quantifying Building System Performance," by A. Filiatralt, A. Wanitkorkul and M. Constantinou, 4/27/08 (PB2009-107906).
- MCEER-08-0014 "Structural and Nonstructural Earthquake Design: The Challenge of Integrating Specialty Areas in Designing Complex, Critical Facilities," by W.J. Petak and D.J. Alesch, 4/30/08 (PB2009-107907).
- MCEER-08-0015 "Seismic Performance Evaluation of Water Systems," by Y. Wang and T.D. O'Rourke, 5/5/08 (PB2009-107908).
- MCEER-08-0016 "Seismic Response Modeling of Water Supply Systems," by P. Shi and T.D. O'Rourke, 5/5/08 (PB2009-107910).
- MCEER-08-0017 "Numerical and Experimental Studies of Self-Centering Post-Tensioned Steel Frames," by D. Wang and A. Filiatralt, 5/12/08 (PB2009-110479).
- MCEER-08-0018 "Development, Implementation and Verification of Dynamic Analysis Models for Multi-Spherical Sliding Bearings," by D.M. Fenz and M.C. Constantinou, 8/15/08 (PB2009-107911).
- MCEER-08-0019 "Performance Assessment of Conventional and Base Isolated Nuclear Power Plants for Earthquake Blast Loadings," by Y.N. Huang, A.S. Whittaker and N. Luco, 10/28/08 (PB2009-107912).

- MCEER-08-0020 "Remote Sensing for Resilient Multi-Hazard Disaster Response – Volume I: Introduction to Damage Assessment Methodologies," by B.J. Adams and R.T. Eguchi, 11/17/08 (PB2010-102695).
- MCEER-08-0021 "Remote Sensing for Resilient Multi-Hazard Disaster Response – Volume II: Counting the Number of Collapsed Buildings Using an Object-Oriented Analysis: Case Study of the 2003 Bam Earthquake," by L. Gusella, C.K. Huyck and B.J. Adams, 11/17/08 (PB2010-100925).
- MCEER-08-0022 "Remote Sensing for Resilient Multi-Hazard Disaster Response – Volume III: Multi-Sensor Image Fusion Techniques for Robust Neighborhood-Scale Urban Damage Assessment," by B.J. Adams and A. McMillan, 11/17/08 (PB2010-100926).
- MCEER-08-0023 "Remote Sensing for Resilient Multi-Hazard Disaster Response – Volume IV: A Study of Multi-Temporal and Multi-Resolution SAR Imagery for Post-Katrina Flood Monitoring in New Orleans," by A. McMillan, J.G. Morley, B.J. Adams and S. Chesworth, 11/17/08 (PB2010-100927).
- MCEER-08-0024 "Remote Sensing for Resilient Multi-Hazard Disaster Response – Volume V: Integration of Remote Sensing Imagery and VIEWS<sup>TM</sup> Field Data for Post-Hurricane Charley Building Damage Assessment," by J.A. Womble, K. Mehta and B.J. Adams, 11/17/08 (PB2009-115532).
- MCEER-08-0025 "Building Inventory Compilation for Disaster Management: Application of Remote Sensing and Statistical Modeling," by P. Sarabandi, A.S. Kiremidjian, R.T. Eguchi and B. J. Adams, 11/20/08 (PB2009-110484).
- MCEER-08-0026 "New Experimental Capabilities and Loading Protocols for Seismic Qualification and Fragility Assessment of Nonstructural Systems," by R. Retamales, G. Mosqueda, A. Filiatral and A. Reinhorn, 11/24/08 (PB2009-110485).
- MCEER-08-0027 "Effects of Heating and Load History on the Behavior of Lead-Rubber Bearings," by I.V. Kalpakidis and M.C. Constantinou, 12/1/08 (PB2009-115533).
- MCEER-08-0028 "Experimental and Analytical Investigation of Blast Performance of Seismically Resistant Bridge Piers," by S.Fujikura and M. Bruneau, 12/8/08 (PB2009-115534).
- MCEER-08-0029 "Evolutionary Methodology for Aseismic Decision Support," by Y. Hu and G. Dargush, 12/15/08.
- MCEER-08-0030 "Development of a Steel Plate Shear Wall Bridge Pier System Conceived from a Multi-Hazard Perspective," by D. Keller and M. Bruneau, 12/19/08 (PB2010-102696).
- MCEER-09-0001 "Modal Analysis of Arbitrarily Damped Three-Dimensional Linear Structures Subjected to Seismic Excitations," by Y.L. Chu, J. Song and G.C. Lee, 1/31/09 (PB2010-100922).
- MCEER-09-0002 "Air-Blast Effects on Structural Shapes," by G. Ballantyne, A.S. Whittaker, A.J. Aref and G.F. Dargush, 2/2/09 (PB2010-102697).
- MCEER-09-0003 "Water Supply Performance During Earthquakes and Extreme Events," by A.L. Bonneau and T.D. O'Rourke, 2/16/09 (PB2010-100923).
- MCEER-09-0004 "Generalized Linear (Mixed) Models of Post-Earthquake Ignitions," by R.A. Davidson, 7/20/09 (PB2010-102698).
- MCEER-09-0005 "Seismic Testing of a Full-Scale Two-Story Light-Frame Wood Building: NEESWood Benchmark Test," by I.P. Christovasilis, A. Filiatral and A. Wanitkorkul, 7/22/09 (PB2012-102401).
- MCEER-09-0006 "IDARC2D Version 7.0: A Program for the Inelastic Damage Analysis of Structures," by A.M. Reinhorn, H. Roh, M. Sivaselvan, S.K. Kunnath, R.E. Valles, A. Madan, C. Li, R. Lobo and Y.J. Park, 7/28/09 (PB2010-103199).
- MCEER-09-0007 "Enhancements to Hospital Resiliency: Improving Emergency Planning for and Response to Hurricanes," by D.B. Hess and L.A. Arendt, 7/30/09 (PB2010-100924).

- MCEER-09-0008 "Assessment of Base-Isolated Nuclear Structures for Design and Beyond-Design Basis Earthquake Shaking," by Y.N. Huang, A.S. Whittaker, R.P. Kennedy and R.L. Mayes, 8/20/09 (PB2010-102699).
- MCEER-09-0009 "Quantification of Disaster Resilience of Health Care Facilities," by G.P. Cimellaro, C. Fumo, A.M Reinhorn and M. Bruneau, 9/14/09 (PB2010-105384).
- MCEER-09-0010 "Performance-Based Assessment and Design of Squat Reinforced Concrete Shear Walls," by C.K. Gulec and A.S. Whittaker, 9/15/09 (PB2010-102700).
- MCEER-09-0011 "Proceedings of the Fourth US-Taiwan Bridge Engineering Workshop," edited by W.P. Yen, J.J. Shen, T.M. Lee and R.B. Zheng, 10/27/09 (PB2010-500009).
- MCEER-09-0012 "Proceedings of the Special International Workshop on Seismic Connection Details for Segmental Bridge Construction," edited by W. Phillip Yen and George C. Lee, 12/21/09 (PB2012-102402).
- MCEER-10-0001 "Direct Displacement Procedure for Performance-Based Seismic Design of Multistory Woodframe Structures," by W. Pang and D. Rosowsky, 4/26/10 (PB2012-102403).
- MCEER-10-0002 "Simplified Direct Displacement Design of Six-Story NEESWood Capstone Building and Pre-Test Seismic Performance Assessment," by W. Pang, D. Rosowsky, J. van de Lindt and S. Pei, 5/28/10 (PB2012-102404).
- MCEER-10-0003 "Integration of Seismic Protection Systems in Performance-Based Seismic Design of Woodframed Structures," by J.K. Shinde and M.D. Symans, 6/18/10 (PB2012-102405).
- MCEER-10-0004 "Modeling and Seismic Evaluation of Nonstructural Components: Testing Frame for Experimental Evaluation of Suspended Ceiling Systems," by A.M. Reinhorn, K.P. Ryu and G. Maddaloni, 6/30/10 (PB2012-102406).
- MCEER-10-0005 "Analytical Development and Experimental Validation of a Structural-Fuse Bridge Pier Concept," by S. El-Bahey and M. Bruneau, 10/1/10 (PB2012-102407).
- MCEER-10-0006 "A Framework for Defining and Measuring Resilience at the Community Scale: The PEOPLES Resilience Framework," by C.S. Renschler, A.E. Frazier, L.A. Arendt, G.P. Cimellaro, A.M. Reinhorn and M. Bruneau, 10/8/10 (PB2012-102408).
- MCEER-10-0007 "Impact of Horizontal Boundary Elements Design on Seismic Behavior of Steel Plate Shear Walls," by R. Purba and M. Bruneau, 11/14/10 (PB2012-102409).
- MCEER-10-0008 "Seismic Testing of a Full-Scale Mid-Rise Building: The NEESWood Capstone Test," by S. Pei, J.W. van de Lindt, S.E. Pryor, H. Shimizu, H. Isoda and D.R. Rammer, 12/1/10 (PB2012-102410).
- MCEER-10-0009 "Modeling the Effects of Detonations of High Explosives to Inform Blast-Resistant Design," by P. Sherkar, A.S. Whittaker and A.J. Aref, 12/1/10 (PB2012-102411).
- MCEER-10-0010 "L'Aquila Earthquake of April 6, 2009 in Italy: Rebuilding a Resilient City to Withstand Multiple Hazards," by G.P. Cimellaro, I.P. Christovasilis, A.M. Reinhorn, A. De Stefano and T. Kirova, 12/29/10.
- MCEER-11-0001 "Numerical and Experimental Investigation of the Seismic Response of Light-Frame Wood Structures," by I.P. Christovasilis and A. Filiatrault, 8/8/11 (PB2012-102412).
- MCEER-11-0002 "Seismic Design and Analysis of a Precast Segmental Concrete Bridge Model," by M. Anagnostopoulou, A. Filiatrault and A. Aref, 9/15/11.
- MCEER-11-0003 "Proceedings of the Workshop on Improving Earthquake Response of Substation Equipment," Edited by A.M. Reinhorn, 9/19/11 (PB2012-102413).
- MCEER-11-0004 "LRFD-Based Analysis and Design Procedures for Bridge Bearings and Seismic Isolators," by M.C. Constantinou, I. Kalpakidis, A. Filiatrault and R.A. Ecker Lay, 9/26/11.

- MCEER-11-0005 "Experimental Seismic Evaluation, Model Parameterization, and Effects of Cold-Formed Steel-Framed Gypsum Partition Walls on the Seismic Performance of an Essential Facility," by R. Davies, R. Retamales, G. Mosqueda and A. Filiatralut, 10/12/11.
- MCEER-11-0006 "Modeling and Seismic Performance Evaluation of High Voltage Transformers and Bushings," by A.M. Reinhorn, K. Oikonomou, H. Roh, A. Schiff and L. Kempner, Jr., 10/3/11.
- MCEER-11-0007 "Extreme Load Combinations: A Survey of State Bridge Engineers," by G.C. Lee, Z. Liang, J.J. Shen and J.S. O'Connor, 10/14/11.
- MCEER-12-0001 "Simplified Analysis Procedures in Support of Performance Based Seismic Design," by Y.N. Huang and A.S. Whittaker.
- MCEER-12-0002 "Seismic Protection of Electrical Transformer Bushing Systems by Stiffening Techniques," by M. Koliou, A. Filiatralut, A.M. Reinhorn and N. Oliveto, 6/1/12.
- MCEER-12-0003 "Post-Earthquake Bridge Inspection Guidelines," by J.S. O'Connor and S. Alampalli, 6/8/12.
- MCEER-12-0004 "Integrated Design Methodology for Isolated Floor Systems in Single-Degree-of-Freedom Structural Fuse Systems," by S. Cui, M. Bruneau and M.C. Constantinou, 6/13/12.
- MCEER-12-0005 "Characterizing the Rotational Components of Earthquake Ground Motion," by D. Basu, A.S. Whittaker and M.C. Constantinou, 6/15/12.
- MCEER-12-0006 "Bayesian Fragility for Nonstructural Systems," by C.H. Lee and M.D. Grigoriu, 9/12/12.
- MCEER-12-0007 "A Numerical Model for Capturing the In-Plane Seismic Response of Interior Metal Stud Partition Walls," by R.L. Wood and T.C. Hutchinson, 9/12/12.
- MCEER-12-0008 "Assessment of Floor Accelerations in Yielding Buildings," by J.D. Wieser, G. Pekcan, A.E. Zaghi, A.M. Itani and E. Maragakis, 10/5/12.
- MCEER-13-0001 "Experimental Seismic Study of Pressurized Fire Sprinkler Piping Systems," by Y. Tian, A. Filiatralut and G. Mosqueda, 4/8/13.
- MCEER-13-0002 "Enhancing Resource Coordination for Multi-Modal Evacuation Planning," by D.B. Hess, B.W. Conley and C.M. Farrell, 2/8/13.
- MCEER-13-0003 "Seismic Response of Base Isolated Buildings Considering Pounding to Moat Walls," by A. Masroor and G. Mosqueda, 2/26/13.
- MCEER-13-0004 "Seismic Response Control of Structures Using a Novel Adaptive Passive Negative Stiffness Device," by D.T.R. Pasala, A.A. Sarlis, S. Nagarajaiah, A.M. Reinhorn, M.C. Constantinou and D.P. Taylor, 6/10/13.